



Dedeo, Domonkos (2023) *Novel pharmacological tools for investigating the pharmacology of free fatty acid receptor 2*. PhD thesis.

<http://theses.gla.ac.uk/83550/>

Copyright and moral rights for this work are retained by the author

A copy can be downloaded for personal non-commercial research or study, without prior permission or charge

This work cannot be reproduced or quoted extensively from without first obtaining permission in writing from the author

The content must not be changed in any way or sold commercially in any format or medium without the formal permission of the author

When referring to this work, full bibliographic details including the author, title, awarding institution and date of the thesis must be given

Enlighten: Theses

<https://theses.gla.ac.uk/>
research-enlighten@glasgow.ac.uk

Novel Pharmacological Tools for Investigating the Pharmacology of Free Fatty Acid Receptor 2

Domonkos Dedeo

BSc (Hons), AFHEA

Submitted in fulfilment of the requirements for the Degree of
Doctor of Philosophy

Centre for Translational Pharmacology
Institute of Molecular, Cell and Systems Biology
College of Medical, Veterinary and Life Sciences
University of Glasgow

September 2022



University
of Glasgow

ABSTRACT

The G protein-coupled receptor FFA2 acts as a receptor for short chain fatty acids produced by commensal bacteria through the fermentation of dietary fibre. While FFA2 is implicated in several disease conditions, such as obesity and ulcerative colitis, the receptor has so far not been successfully exploited therapeutically. This may reflect marked species selectivity of antagonists for the human receptor, which hinder pre-clinical *in vivo* studies in rodent models of disease. Herein a novel transgenic mouse strain expressing human FFA2 with an integrated HA epitope tag (hFFA2-HA) was characterised as a novel animal model. To assess the expression of hFFA2-HA at the messenger RNA and protein levels, quantitative reverse-transcription PCR and immunohistochemistry approaches were utilised. hFFA2-HA was found to be expressed in adipose, colon, spleen and bone marrow-derived neutrophils, at equivalent levels as mouse FFA2 in C57BL/6N mice. In addition, hFFA2-HA expression was confirmed in subsets of enteroendocrine and haematopoietic cells in the intestine and spleen, respectively. Following immunocytochemical confirmation of hFFA2-HA protein expression in bone marrow-derived neutrophils, these were used in functional studies *ex vivo*. The functionality of hFFA2-HA on neutrophils was established with the use of the hFFA2-selective radioligand [³H]GLPG0974, which was found to specifically bind membranes from hFFA2-HA mouse neutrophils, and with the use of the endogenous ligand propionate in [³⁵S]GTPγS incorporation assays, where a concentration-dependent response was observed. Importantly, hFFA2-selective antagonists were able to inhibit C3-induced [³⁵S]GTPγS incorporation and chemotaxis in hFFA2-HA-expressing, but not in C57BL/6N neutrophils. For the investigation of hFFA2 phosphorylation, novel, potentially phosphosite-specific antisera were evaluated through Western Blot and immunocytochemistry methods. Here, residues Thr³⁰⁶ and Thr³¹⁰ were observed to be phosphorylated in an agonist-dependent manner, while residues Ser²⁹⁶ and Ser²⁹⁷ appeared to be constitutively phosphorylated. Replacement of these residues with alanine abolished antiserum binding but did not fully ablate β-arrestin-2 interactions. The development of novel pharmacological research tools, here in the form of transgenic mouse models and phosphosite-specific antisera, can not only aid understanding of FFA2 signalling and pharmacology but can also bridge the translational gap between *in vitro* and clinical studies.

TABLE OF CONTENTS

ABSTRACT	II
TABLE OF CONTENTS	III
LIST OF FIGURES	VIII
LIST OF TABLES	XII
LIST OF PUBLICATIONS	XIII
ACKNOWLEDGEMENTS	XIV
AUTHOR'S DECLARATION.....	XV
ABBREVIATIONS	XVI
CHAPTER 1 - INTRODUCTION	1
1.1 G protein-coupled receptors.....	1
1.1.1 GPCR structure and families	1
1.1.2 Canonical GPCR signalling.....	4
1.1.3 GPCR ligand pharmacology.....	7
1.2 Free fatty acid receptors.....	12
1.2.1 Metabolites as signalling molecules.....	12
1.2.2 Deorphanisation of the free fatty acid receptor family	13
1.3 SCFA receptors.....	16
1.3.1 SCFAs as endogenous ligands	16
1.3.2 Physiological functions and therapeutic implications	20
1.3.2.1 Enteroendocrine functions	20
1.3.2.2 Roles in adipose tissue homeostasis.....	20
1.3.2.3 Roles in the pancreas and glucose homeostasis	20
1.3.2.4 Roles in the peripheral nervous system	20
1.3.2.5 Immune functions	20
1.3.3 Drug development efforts for SCFA receptors	29
1.4 Aims	39

CHAPTER 2 - MATERIALS AND METHODS	41
2.1 Reagents	41
2.1.1 Pharmacological compounds	41
2.1.2 Primers	41
2.1.3 Antibodies	42
2.1.4 Enzymes	43
2.1.5 Other reagents	43
2.1.6 Media, buffers and solutions	45
2.2 Molecular biology	47
2.2.1 Site-directed mutagenesis - generation of hFFA2 PD mutants	47
2.2.2 Bacterial cloning strategy	48
2.2.3 Plasmid DNA purification	48
2.2.4 Sequencing	50
2.3 Cell culture	50
2.3.1 Mammalian cell line maintenance	50
2.3.2 Generation of stably transfected Flp-In T-REx 293 cell lines	51
2.3.3 Generation of transiently transfected cell lines	52
2.4 Animals	52
2.4.1 Source	52
2.4.2 Mouse maintenance	53
2.4.3 Ethics statement	53
2.5 Gene expression analysis	53
2.5.1 RNA extraction	53
2.5.2 Agarose gel electrophoresis	54
2.5.3 Reverse transcription	54
2.5.4 Quantitative reverse transcription polymerase chain reaction	55
2.6 <i>Ex vivo</i> pharmacological assays	56
2.6.1 Neutrophil isolation	56

2.6.2 Neutrophil chemotaxis (ATPlite assay)	57
2.6.3 Neutrophil extracellular trap quantification	58
2.7 <i>In vitro</i> functional assays.....	59
2.7.1 Membrane preparation	59
2.7.2 Determination of protein concentration (BCA Assay)	59
2.7.3 [³⁵ S]-GTPγS incorporation assay	60
2.7.4 Heterologous [³ H] radioligand binding assay	61
2.7.5 BRET-based β-arrestin-2 recruitment assay	62
2.8 Histology.....	63
2.8.1 Immunocytochemistry (ICC)	63
2.8.2 Immunohistochemistry (IHC).....	65
2.9 Immunoblotting.....	67
2.9.1 Lysate preparation	67
2.9.2 Immunoprecipitation.....	67
2.9.3 Western blotting.....	68
2.10 Data analysis and curve fitting.....	69
2.10.1 Tissue expression analysis	69
2.10.2 Fluorescence intensity analysis	70
2.10.3 Binding parameter analysis	70
2.10.4 Functional agonist and antagonist assay analysis	71
2.10.5 Allosteric operational model	71
2.10.6 Statistical analysis	72
CHAPTER 3 - CHARACTERISATION OF HFFA2-HA-EXPRESSING MICE	73
3.1 Introduction	73
3.2 Results	77
3.2.1 Quantitative reverse transcription PCR of mouse tissues	77
3.2.2 Immunohistochemical investigation of transgenic mouse intestine....	80
3.2.3 Immunohistochemical investigation of transgenic mouse spleen	104

3.2.4 Immunocytochemical investigation of transgenic mouse neutrophils	116
3.3 Discussion.....	120
3.3.1 The transgenic hFFA2-HA mouse expresses hFFA2 mRNA in a number of tissues.....	120
3.3.2 The hFFA2-HA protein is expressed in enteroendocrine and immune cells of hFFA2-HA mice	123
CHAPTER 4 - FUNCTIONAL CHARACTERISATION OF HFFA2-HA NEUTROPHILS	
.....	129
4.1 Introduction	129
4.2 Results	133
4.2.1 <i>In vitro</i> evaluation of ligand binding and efficacy in transgenic mouse-derived neutrophils	133
4.2.2 Evaluation of transgenic mouse-derived neutrophil function <i>ex vivo</i>	139
4.3 Discussion.....	145
4.3.1 Human orthologue-specific FFA2 ligands bind to and affect activation of hFFA2-HA in mouse-derived neutrophils.....	145
4.3.2 Whole cell responses are mediated by hFFA2-HA in the transgenic hFFA2-HA mouse-derived neutrophils	150
CHAPTER 5 - NON-G PROTEIN-MEDIATED SIGNALLING IN FFA2	154
5.1 Introduction	154
5.2 Results	160
5.2.1 Evaluation of phosphosite-specific antisera for FFA2	160
5.2.2 Characterisation of phosphodeficient mutants of hFFA2	176
5.2.3 β -arrestin-2 recruitment in phosphodeficient mutants of hFFA2.....	183
5.2.4 Phosphorylation of hFFA2-HA in mouse-derived neutrophils.....	187
5.3 Discussion.....	213
5.3.1 Phosphosite-specific antisera selectively recognise activated hFFA2 and hFFA2-DREADD	213
5.3.2 Mutational alteration of phosphorylation sites affects antiserum binding and hFFA2 receptor function.....	217

5.3.3 Phosphosite-specific antisera can track receptor phosphorylation *in vitro* and *ex vivo*.....221

CHAPTER 6 - FINAL DISCUSSION..... 227

REFERENCES 235

LIST OF FIGURES

Figure 1.1. GPCR families and their structural features	3
Figure 1.2. GPCR signal transduction pathways	5
Figure 1.3. Pharmacology of orthosteric GPCR ligands	8
Figure 1.4. Pharmacology of GPCR Positive Allosteric Modulators (PAMs)	10
Figure 1.5. Pharmacology of GPCR Negative Allosteric Modulators (NAMs) and Mixed-effect modulators	11
Figure 1.6. Biased signalling through GPCRs	12
Figure 1.7. Signalling pathways through SCFA receptors.....	19
Figure 1.8. DREADD variant of human FFA2	21
Figure 1.9. Physiological functions of SCFA receptors	26
Figure 1.10. Immune functions of FFA2	28
Figure 1.11. SCFA receptor ligands	30
Figure 3.1. qRT-PCR amplification plot of hFFA2-HA colon dilutions	77
Figure 3.2. Standard curves for qRT-PCR primers in mouse colon	78
Figure 3.3. qRT-PCR quantification of hFFA2 and mFFA2 in mouse tissues ..	79
Figure 3.4. Immunocytochemical detection of hFFA2-HA in overexpressing cells	81
Figure 3.5. Immunohistochemical detection of hFFA2-HA in mouse ileum and colon (No primary antibody control).....	82
Figure 3.6. Immunohistochemical detection of hFFA2-HA in mouse ileum (Chromogranin A).....	83
Figure 3.7. Immunohistochemical detection of hFFA2-HA in mouse colon (Chromogranin A).....	84
Figure 3.8. Immunohistochemical detection of hFFA2-HA in mouse ileum (Glucagon-like peptide 1)	86
Figure 3.9. Immunohistochemical detection of hFFA2-HA in mouse colon (Glucagon-like peptide 1)	87
Figure 3.10. Immunohistochemical detection of hFFA2-HA in mouse ileum (Peptide YY)	89
Figure 3.11. Immunohistochemical detection of hFFA2-HA in mouse colon (Peptide YY)	90
Figure 3.12. Distribution of hFFA2 and cellular markers in hFFA2-HA mouse enteroendocrine cells (EECs).....	91

Figure 3.13. Immunohistochemical detection of hFFA2-HA in mouse duodenum (CD45)	93
Figure 3.14. Immunohistochemical detection of hFFA2-HA in mouse ileum (CD45)	94
Figure 3.15. Immunohistochemical detection of hFFA2-HA in mouse duodenum (CD3).....	96
Figure 3.16. Immunohistochemical detection of hFFA2-HA in mouse ileum (CD3)	97
Figure 3.17. Immunohistochemical detection of hFFA2-HA in mouse duodenum (CD11b).....	99
Figure 3.18. Immunohistochemical detection of hFFA2-HA in mouse ileum (CD11b).....	100
Figure 3.19. Immunohistochemical detection of hFFA2-HA in mouse duodenum (CD11c).....	102
Figure 3.20. Immunohistochemical detection of hFFA2-HA in mouse ileum (CD11c)	103
Figure 3.21. Distribution of hFFA2 and cellular markers in hFFA2-HA mouse intestinal immune cells.....	104
Figure 3.22. Immunohistochemical detection of erythrocytes in mouse spleen (No primary antibody control)	105
Figure 3.23. Immunohistochemical detection of hFFA2-HA in mouse spleen white pulp and marginal zone (CD45)	106
Figure 3.24. Immunohistochemical detection of hFFA2-HA in mouse spleen red pulp (CD45)	107
Figure 3.25. Immunohistochemical detection of hFFA2-HA in mouse spleen white pulp and marginal zone (CD11b)	109
Figure 3.26. Immunohistochemical detection of hFFA2-HA in mouse spleen red pulp (CD11b)	110
Figure 3.27. Immunohistochemical detection of hFFA2-HA in mouse spleen white pulp and marginal zone (CD11c).....	112
Figure 3.28. Immunohistochemical detection of hFFA2-HA in mouse spleen red pulp (CD11c).....	113
Figure 3.29. Distribution of hFFA2 and cellular markers in hFFA2-HA mouse spleen.....	114

Figure 3.30. Immunohistochemical detection of hFFA2-HA in mouse spleen (4× magnification)	115
Figure 3.31. Immunohistochemical detection of hFFA2-HA in mouse spleen (40× magnification)	116
Figure 3.32. Immunocytochemical detection of hFFA2-HA in mouse neutrophils (CD11b).....	118
Figure 3.33. Immunocytochemical detection of hFFA2-HA in mouse neutrophils (CD11c).....	119
Figure 3.34. Immunocytochemical detection of hFFA2-HA in mouse neutrophils (Fluorescence intensity)	120
Figure 4.1. Heterologous radioligand binding in mouse neutrophils	134
Figure 4.2. Agonist-induced [³⁵ S]GTPγS incorporation	136
Figure 4.3. PAM effect on agonist-induced [³⁵ S]GTPγS incorporation	138
Figure 4.4. Antagonist effect on agonist-induced [³⁵ S]GTPγS incorporation	139
Figure 4.5. Agonist effects on mouse neutrophil chemotaxis	141
Figure 4.6. Antagonist effects on mouse neutrophil chemotaxis	143
Figure 4.7. Neutrophil extracellular trap formation	145
Figure 5.1. Putative phosphorylation sites on human and mouse FFA2.....	156
Figure 5.2. Western Blot analysis of hFFA2-eYFP phosphorylation	161
Figure 5.3. Western Blot analysis of mFFA2-eYFP phosphorylation.....	162
Figure 5.4. Western Blot analysis of hFFA2-DREADD-eYFP phosphorylation	163
Figure 5.5. Western Blot analysis of hFFA2-eYFP phosphorylation in the presence of λ-protein phosphatase	164
Figure 5.6. Western Blot analysis of CATPB effect on hFFA2-eYFP phosphorylation.....	165
Figure 5.7. Western Blot analysis of CATPB effect on hFFA2-DREADD-eYFP phosphorylation.....	166
Figure 5.8. Immunocytochemical staining of Flp-In T-REx 293 parental cells (Phosphosite-specific antisera)	167
Figure 5.9. Immunocytochemical detection of hFFA2-eYFP phosphorylation in overexpressing cells (pSer ²⁹⁶ /pSer ²⁹⁷)	168
Figure 5.10. Immunocytochemical detection of hFFA2-eYFP phosphorylation in overexpressing cells (pThr ³⁰⁶ /pThr ³¹⁰)	169
Figure 5.11. Immunocytochemical detection of hFFA2-DREADD-eYFP phosphorylation in overexpressing cells (pSer ²⁹⁶ /pSer ²⁹⁷)	171

Figure 5.12. Immunocytochemical detection of hFFA2-DREADD-eYFP phosphorylation in overexpressing cells (pThr ³⁰⁶ /pThr ³¹⁰).....	172
Figure 5.13. Immunocytochemical detection of mFFA2-eYFP phosphorylation in overexpressing cells (pSer ²⁹⁶ /pSer ²⁹⁷).....	174
Figure 5.14. Immunocytochemical detection of mFFA2-eYFP phosphorylation in overexpressing cells (pThr ³⁰⁶ /pThr ³¹⁰)	175
Figure 5.15. Western Blot analysis of phosphorylation in phosphodeficient hFFA2-eYFP mutants	177
Figure 5.16. Immunocytochemical detection of hFFA2-PD1 phosphorylation in overexpressing cells (pSer ²⁹⁶ /pSer ²⁹⁷)	178
Figure 5.17. Immunocytochemical detection of hFFA2-PD1 phosphorylation in overexpressing cells (pThr ³⁰⁶ /pThr ³¹⁰)	179
Figure 5.18. Immunocytochemical detection of hFFA2-PD2 phosphorylation in overexpressing cells (pSer ²⁹⁶ /pSer ²⁹⁷)	181
Figure 5.19. Immunocytochemical detection of hFFA2-PD2 phosphorylation in overexpressing cells (pThr ³⁰⁶ /pThr ³¹⁰)	182
Figure 5.20. Agonist-induced β -arrestin-2 recruitment	183
Figure 5.21. Agonist-induced β -arrestin-2 recruitment in phosphodeficient hFFA2-eYFP mutants	185
Figure 5.22. Agonist-induced [³⁵ S]GTP γ S incorporation in phosphodeficient hFFA2-eYFP mutants	187
Figure 5.23. Western Blot analysis of hFFA2-HA and hFFA2-DREADD-HA phosphorylation.....	188
Figure 5.24. Immunocytochemical staining of Flp-In T-REx 293 parental cells (Phosphosite-specific antisera and HA)	189
Figure 5.25. Immunocytochemical detection of hFFA2-HA phosphorylation in overexpressing cells (pSer ²⁹⁶ /pSer ²⁹⁷)	191
Figure 5.26. Immunocytochemical detection of hFFA2-HA phosphorylation in overexpressing cells (pThr ³⁰⁶ /pThr ³¹⁰)	192
Figure 5.27. Immunocytochemical detection of the effect of CATPB on hFFA2-HA phosphorylation in overexpressing cells.....	193
Figure 5.28. Immunocytochemical detection of hFFA2-DREADD-HA phosphorylation in overexpressing cells (pSer ²⁹⁶ /pSer ²⁹⁷)	195
Figure 5.29. Immunocytochemical detection of hFFA2-DREADD-HA phosphorylation in overexpressing cells (pThr ³⁰⁶ /pThr ³¹⁰).....	196

Figure 5.30. Immunocytochemical detection of the effect of CATPB on hFFA2-DREADD-HA phosphorylation in overexpressing cells 197

Figure 5.31. Immunocytochemical staining of minus-CRE mouse neutrophils 199

Figure 5.32. Immunocytochemical detection of hFFA2-HA phosphorylation in mouse neutrophils (pSer²⁹⁶/pSer²⁹⁷) 201

Figure 5.33. Immunocytochemical detection of hFFA2-HA phosphorylation in mouse neutrophils (pThr³⁰⁶/pThr³¹⁰) 202

Figure 5.34. Immunocytochemical detection of the effect of CATPB on hFFA2-HA phosphorylation in mouse neutrophils..... 203

Figure 5.35. Immunocytochemical detection of hFFA2-DREADD-HA phosphorylation in mouse neutrophils (pSer²⁹⁶/pSer²⁹⁷) 205

Figure 5.36. Immunocytochemical detection of hFFA2-DREADD-HA phosphorylation in mouse neutrophils (pThr³⁰⁶/pThr³¹⁰) 206

Figure 5.37. Immunocytochemical detection of the effect of CATPB on hFFA2-DREADD-HA phosphorylation in mouse neutrophils..... 207

Figure 5.38. Immunocytochemical detection of hFFA2-HA and hFFA2-DREADD-HA phosphorylation in mouse neutrophils (Fluorescence intensity) 211

Figure 5.39. Fluorescence ratios of immunocytochemical staining of mouse neutrophils..... 212

LIST OF TABLES

Table 5.1. Potency (pEC₅₀), basal and maximum efficacy (E_{max}) of propionate (C3) at hFFA2-eYFP phosphodeficient mutants in BRET-based β-arrestin-2 recruitment assays 186

Table 5.2. Potency (pEC₅₀), basal and maximum efficacy (E_{max}) of propionate (C3) at hFFA2-eYFP phosphodeficient mutants in [³⁵S]GTPγS incorporation assays 186

LIST OF PUBLICATIONS

Bolognini, D., Dedeo, D. & Milligan, G. 2021. Metabolic and inflammatory functions of short-chain fatty acid receptors. *Current opinion in endocrine and metabolic research*, 16, 1-9.

Hansen, A. H., Christensen, H. B., Pandey, S. K., Sergeev, E., Valentini, A., Dunlop, J., Dedeo, D., Fratta, S., Hudson, B. D., Milligan, G., Ulven, T. & Rexen Ulven, E. 2021. Structure-Activity Relationship Explorations and Discovery of a Potent Antagonist for the Free Fatty Acid Receptor 2. *ChemMedChem*, 16, 3326-3341.

ACKNOWLEDGEMENTS

First and foremost, I would like to thank Professor Graeme Milligan for his continuing guidance throughout my academic career. In fact, my interest and love for molecular pharmacology was sparked by Professor Milligan's lectures during my undergraduate studies, so I am incredibly lucky to have been able to work with and learn from him. His ideas and insight were invaluable for both this project and for my professional development.

I would also like to extend my gratitude to current and former members of the Centre for Translational Pharmacology. First, Dr Daniele Bolognini, who shared with me his experience on FFA2, and aided me in my fledgling attempts at working with animals. Dr Sara Marsango, who introduced me to the beauties of molecular biology and would always find ways to help me troubleshoot my experiments. Dr Natasja Barki, who taught me the art (well, science) of immunohistochemistry and gave great advice on how to improve experiments. And Laura Jenkins, who always found time to help me with experimental design and optimisation. I would also like to thank all other members of the Centre, past and present, to whom I could always turn when needing help, advice, or even just a nice conversation.

I could not have completed my work, were it not for the unfailing support of my family. Our conversations have provided me with a different perspective, allowing me to re-evaluate my own work. Above all, I am extremely grateful to my partner, Lee, who has been my main source of emotional support over the course of this project, and who reassured me whenever I was having doubts about my abilities.

My final acknowledgement goes to my beautiful son (read: cat), Fahéj. Not only was he able to force me to take breaks by stealing my pens, but he also has a unique ability to cheer me up even on my worst days.

AUTHOR'S DECLARATION

I declare that, except where explicit reference is made to the contribution of others, that this thesis is the result of my own work and has not previously been submitted for a degree or diploma at the University of Glasgow or at any other institution.

Signature:

Name: Domonkos Dedeo

Date: 06/09/2022

ABBREVIATIONS

AP2	Adaptor protein 2
ANOVA	Analysis of Variance
ATP	Adenosine triphosphate
BRET	Bioluminescence resonance energy transfer
BSA	Bovine serum albumin
cAMP	Cyclic adenosine monophosphate
CD	Cluster of differentiation
cDNA	Complementary deoxyribonucleic acid
CNS	Central Nervous System
CPM	Counts per minute
C_T	Cycle threshold
DAG	<i>sn</i> -1,2-diacylglycerol
DAPI	4',6-diamidino-2-phenylindole
DC	Dendritic cell
DMSO	Dimethyl sulfoxide
DOX	Doxycycline
DPM	Disintegrations per minute
DREADD	Designer Receptors Exclusively Activated by Designer Drugs
dsDNA	Double-stranded DNA
ECL	Extracellular loop
EEC	Enteroendocrine cell
eYFP	Enhanced yellow fluorescent protein
FA	Fatty acid
FBS	Foetal bovine serum
FFA	Free fatty acid
FFA2	Free fatty acid receptor 2
G protein	Guanine nucleotide-binding protein
GDP	Guanosine diphosphate
GF	Germ-free

GFP	Green fluorescent protein
GLP-1	Glucagon-like peptide 1
GPCR	G protein-coupled receptor
GRK	G protein-coupled receptor kinase
GSIS	Glucose-stimulated insulin secretion
GTP	Guanosine-5'-triphosphate
GTPase	Guanine nucleotide triphosphatase
HA	Haemagglutinin
HEK293	Human embryonic kidney cell line 293
HFD	High-fat diet
HTRF	Homogeneous time-resolved fluorescence
ICC	Immunocytochemistry
ICL	Intracellular loop
ILF	Isolated lymphoid follicle
Ig	Immunoglobulin
IHC	Immunohistochemistry
IL	Interleukin
ILC3	Type 3 innate lymphoid cell
IP3	Inositol 1,4,5-triphosphate
K_d	Dissociation constant
KO	Knock-out
λPP	λ-Protein phosphatase
mRNA	Messenger ribonucleic acid
NAM	Negative allosteric modulator
NET	Neutrophil extracellular trap
NLuc	Nanoluciferase
PAM	Positive allosteric modulator
PD	Phosphorylation-deficient
PTX	Pertussis toxin
PYY	Peptide YY

qRT-PCR	Quantitative reverse transcription polymerase chain reaction
RT	Room-temperature
SA	Sorbic acid
SAR	Structure-activity relationship
SCA	Small carboxylic acid
SCFA	Short chain fatty acid
SDS-PAGE	Sodium dodecyl sulphate polyacrylamide gel electrophoresis
TGFα	Transforming growth factor α
TM	Transmembrane domain
TNFα	Tumour necrosis factor α
WB	Western blot
WT	Wild type

CHAPTER 1 - INTRODUCTION

1.1 G protein-coupled receptors

1.1.1 GPCR structure and families

G protein-coupled receptors (GPCRs) are a superfamily of cell surface proteins with some 800 members in humans. Their name derives from heterotrimeric G proteins (guanine nucleotide-binding proteins) through which they initiate downstream signalling cascades in response to extracellular stimuli. As all tissues in vertebrates express various GPCRs, it is not surprising that they are one of the most commonly targeted class of proteins by small molecule drugs. Indeed, about 350 non-olfactory GPCRs are considered druggable, 165 of which are established targets and make up approximately 20% of targets exploited by current small molecule drugs (Rask-Andersen et al., 2014, Yang et al., 2021).

Structurally, all GPCRs share the same basic structure, made up of seven trans-membrane (TM) α -helices (hence the alternative terminology, 7-transmembrane receptors), with an extracellular N-terminus and an intracellular C-terminus. The helices are also connected by 3 intracellular loops (ICLs) and 3 extracellular loops (ECLs). Intracellular segments, while not necessarily conserved, are similar in structure throughout all GPCRs. The diversity found in the structure of the N-terminus, however, has implications on ligand binding and thus gave rise to the initial classification of GPCRs into 5 classes. With information guided by genomic studies, these have been adapted into the current classification system of 5 families: Rhodopsin (class A), Secretin (class B), Adhesion (class B), Glutamate (class C) and Frizzled/Taste2 (class F) families (Fredriksson et al., 2003b, Schioth and Fredriksson, 2005).

The vast majority of GPCRs are members of the Rhodopsin family (Class A; *Figure 1.1A*). In addition to about 380 olfactory class A receptors, around 284 are potentially druggable. As such, they also make up the majority of druggable GPCR targets. They show the highest diversity in the types of endogenous ligands, including nucleotides, steroids, peptides, proteins, and lipids (Yang et al., 2021). For this class, the N-terminus is relatively short, and as such it is rarely involved in ligand binding. Endogenous ligands tend to bind in the pockets formed by the TM domains, which varies depending on the endogenous ligand,

with potential interactions with the ECLs. In addition, receptors of this family contain highly conserved residues that constitute the DRY motif (Rovati et al., 2007) and the NPxxY motif (Urizar et al., 2005), which are believed to stabilise various activation states, and thus diverse downstream signalling.

The Secretin family (Class B; *Figure 1.1B*) contains 15 members activated by various peptide hormones, including corticotropin-releasing hormone, parathyroid peptide hormone and growth hormone-releasing hormone. Conserved cysteine (Cys) residues on the N-terminus and ECLs of receptors allow stabilisation by disulphide bonds. Thus, the peptide ligands bind through interactions with the N-terminus and the pocket of the TM domains (Miller et al., 2012).

In the case of Adhesion receptors (Class B; *Figure 1.1C*), the extended N-terminus contains a GPCR autoproteolysis-inducing (GAIN) domain, where the adhesion-motif-containing N-terminal binds non-covalently through the GPCR proteolytic site (GPS). The adhesion motif itself contains residues which are readily glycosylated, and thus attach to extracellular matrix proteins (ECM). Upon mechanical movement through the ECM, the N-terminal segment detaches at the GAIN domain, which in turn induces the conformational changes necessary to initiate downstream signalling (Olaniru and Persaud, 2019). The 33 members in this family can be categorised into 9 subgroups based on the unique N-terminal motifs (Hamann et al., 2015). They are distinct in their role in migration and cell adhesion.

Glutamate family receptor (Class C; *Figure 1.1D*) N-termini contain a Venus fly trap domain (VFT): a bilobular structure which acts as the ligand binding site. The segment below the VFT also contains a Cys-rich domain, which aids structural stability during the dimerisation necessary for receptor activation (Kunishima et al., 2000). This family is composed of 22 members, including 8 metabotropic glutamate receptors and 2 γ -aminobutyric acid b (GABA_b) receptors (Fredriksson et al., 2003b, Lagerström and Schiöth, 2008).

The Frizzled/Taste2 (Class F) family is made up of 10 Frizzled and 1 Smoothened receptor. In Frizzled receptors (*Figure 1.1E*), a Cys-rich domain (CRD) serves as

the primary ligand-binding site, where a hydrophobic groove allows the binding of WNT proteins via their palmitoleate moiety (Macdonald and He, 2012). There is some evidence that the ECLs may also be involved in ligand binding (Dann et al., 2001). The classification of the 25 Taste2 receptors in the same family has been contentious, since their sequence identity is less than 20% and they are architecturally more similar to rhodopsin family GPCRs (Alfonso-Prieto et al., 2019).

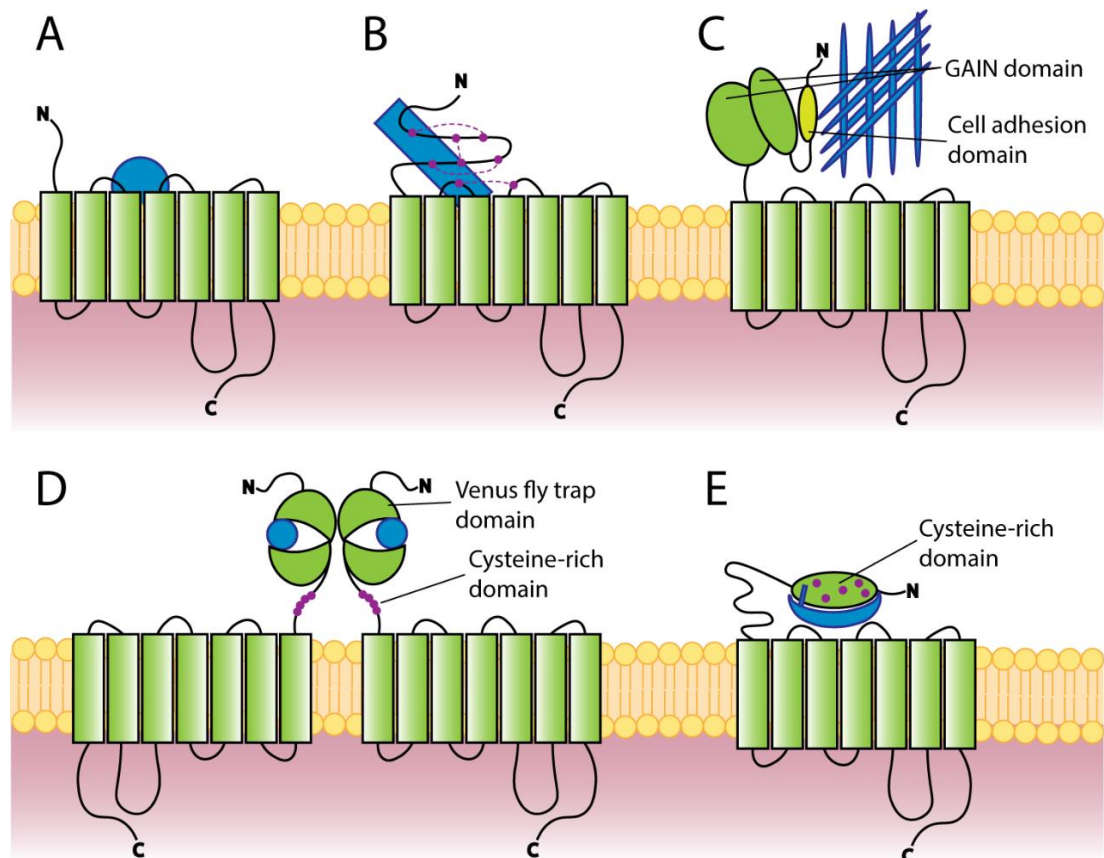


Figure 1.1. GPCR families and their structural features. All G protein-coupled receptor (GPCR) families share the same basic arrangement of 7 trans-membrane helices, with an intracellular C-terminus and an extracellular N-terminus. Despite these shared characteristics, the families N termini vary significantly between families, thus demonstrating a range of ligand binding modes (ligands show in blue). A) In comparison with other families, Rhodopsin family (Class A) receptors possess a relatively short N terminus, which is generally not involved in ligand binding. Endogenous ligands bind in the pocket formed by the TM regions. B) Secretin family (Class B) receptors are characterised by conserved cysteine (Cys) residues (shown in purple) which stabilise the N-terminus and extracellular loops for ligand binding. C) Adhesion family (Class B) receptors possess a GPCR autoproteolysis-inducing (GAIN) domain responsible for the cleavage of the N-terminus, allowing the separation of the adhesion domain, and thus interaction with extracellular matrix proteins. D) Glutamate family (Class C) receptors contain Cys-rich domains for dimer stabilisation and bilobular Venus fly trap domains for ligand binding. E) Frizzled (Class F) family receptors contain a conserved Cys-rich domain. WNT glycoproteins bind this domain with the aid of its palmitoleate moiety, alongside potential further interactions with the extracellular loops.

1.1.2 Canonical GPCR signalling

Upon activation by an extracellular stimulus, GPCRs undergo conformational changes which initiate the intracellular signalling cascade. Specifically, the eponymous heterotrimeric G proteins are recruited to the intracellular surface of the receptor, where interactions trigger the exchange of guanosine diphosphate (GDP) for guanosine triphosphate (GTP) on the G protein α -subunit. G proteins thus activated dissociate, allowing the α -subunit and the $\beta\gamma$ -heterodimer to trigger specific downstream responses (Simon et al., 1991).

What downstream pathways are activated is determined by the identity of each G protein subunit. There are 16 distinct α subunits, categorised into 4 families based on sequence similarities and downstream signalling effectors: $G\alpha_s$ ($G\alpha_s$ and $G\alpha_{olf}$), $G\alpha_i$ ($G\alpha_{i1}$, $G\alpha_{i2}$, $G\alpha_{i3}$, $G\alpha_{oA}$, $G\alpha_{oB}$, $G\alpha_{t1}$, $G\alpha_{t2}$ and $G\alpha_z$), $G\alpha_q$ ($G\alpha_q$, $G\alpha_{11}$, $G\alpha_{14}$, $G\alpha_{15}$ and $G\alpha_{16}$) and $G\alpha_{12}$ ($G\alpha_{12}$ and $G\alpha_{13}$) (Simon et al., 1991). There is also a level of diversity in the $G\beta$ and $G\gamma$ subunits (5 and 12 subtypes, respectively) (Smrcka and Fisher, 2019). Such diversity can give rise to complex downstream effects and physiological responses.

Members of the $G\alpha_s$ family activate adenylyl cyclase (AC), thus causing an increase in intracellular cyclic adenosine monophosphate (cAMP) levels. In turn, cAMP binds and activates protein kinase A (PKA), leading to phosphorylation of further downstream proteins. By contrast, members of the $G\alpha_i$ family inhibit AC, opposing the downstream effects of $G\alpha_s$. $G\alpha_q$ family proteins are able to activate phospholipase C β (PLC β), which catalyses the production of inositol-1,4,5-triphosphate (IP3) and *sn*-1,2-diacylglycerol (DAG). By signalling through the IP3 receptors on the endoplasmic reticulum, IP3 can induce the release of Ca^{2+} from intracellular storage, while DAG activates protein kinase C (PKC) (Simon et al., 1991). Signalling through $G\alpha_{12}$ has been fairly poorly characterised until recently. Rho guanine nucleotide exchange factors (RhoGEFs) activated by $G\alpha_{12/13}$ regulate the Ras homolog family member A (RhoA)-Rho-associated, coiled-coil containing protein kinase (ROCK) pathway (Patel et al., 2014). Canonically, $G\alpha$ subunits were believed to be the primary determinants of receptor signalling, however it has become increasingly clear that the $\beta\gamma$ -heterodimers can mediate cellular responses in their own right (Ford et al., 1998).

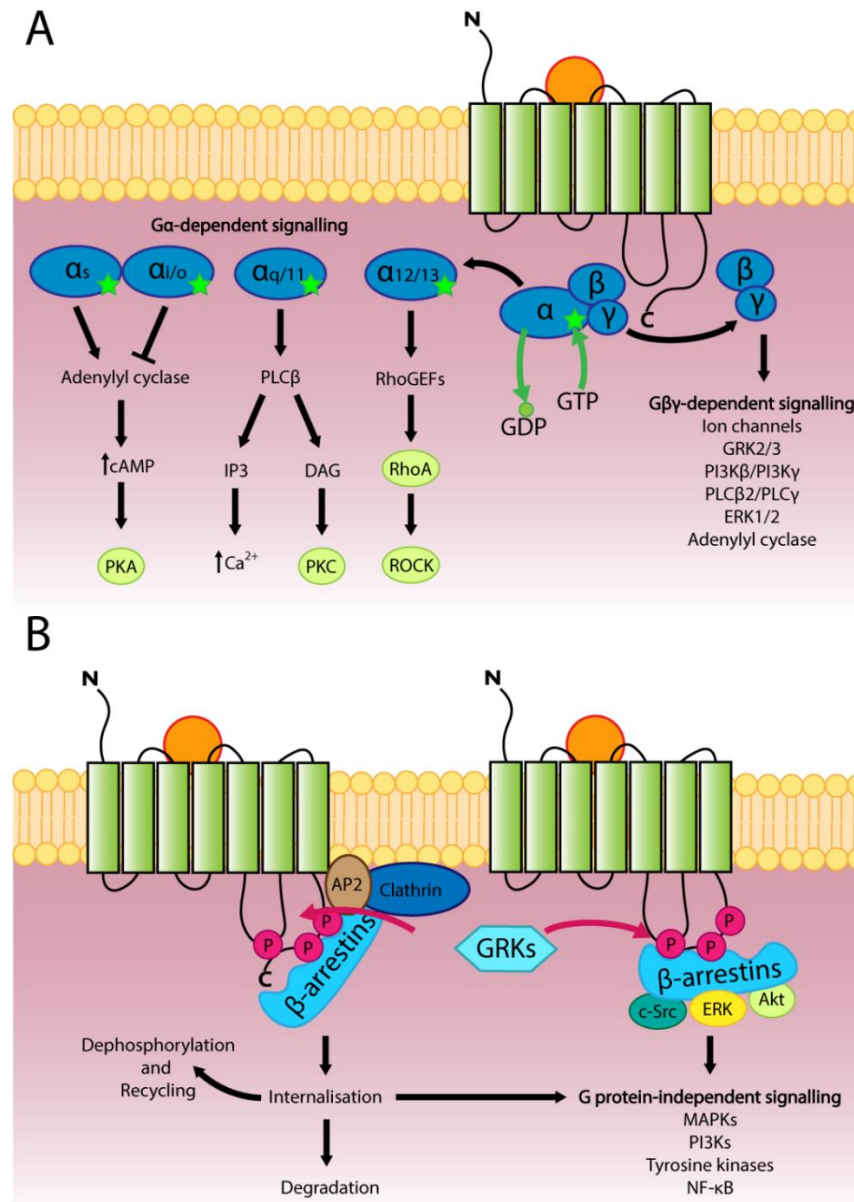


Figure 1.2. GPCR signal transduction pathways. A) Ligand binding (in orange) induces conformational changes in GPCR, allowing the binding of the heterotrimeric G proteins. This interaction facilitates the exchange of GDP (green circle) for GTP (green star) on the $G\alpha$ subunit, and the subsequent dissociation of the $G\alpha$ subunit from the $G\beta\gamma$ dimer. Signalling pathways engaged are dependent on the identity of the $G\alpha$ subunit. $G\alpha_s$ stimulates, while $G\alpha_{i/o}$ inhibits adenylyl cyclase, resulting in increased or decreased levels of intracellular cAMP, respectively, thus regulating protein kinase A (PKA) activity. $G\alpha_{q/11}$ mediates signalling through phospholipase C β (PLC β), leading to increased intracellular Ca $^{2+}$ levels through inositol 1,4,5-triphosphate (IP $_3$), and protein kinase C (PKC) activation through *sn*-1,2-diacylglycerol (DAG). $G\alpha_{12/13}$ regulates the RhoA/ROCK (Ras homolog family member A/Rho-associated, coiled-coil containing protein kinase) pathway via Rho guanine nucleotide exchange factors (RhoGEFs). $G\beta\gamma$ subunits are also able to mediate a range of responses. The inherent GTPase activity of $G\alpha$ hydrolyses GTP to GDP, thus terminating signalling and allowing re-association of the G protein subunits. B) Residues on the intracellular loops and C-terminus of activated GPCRs are phosphorylated (in magenta) by GPCR kinases (GRKs), which in turn leads to the recruitment of β -arrestins. β -arrestin interactions with clathrin leads to GPCR downregulation through internalisation. Internalised GPCRs may be dephosphorylated and recycled to the cell surface, degraded in lysosomes, or they could induce further signalling cascades. β -arrestins are also able to interact with a range of kinases, allowing numerous downstream signals. PI3K - phosphatidylinositol 3-kinase; PLC γ - phospholipase C γ ; ERK - extracellular signal-regulated kinase; AP2 - adaptor protein complex 2; c-Src - Proto-oncogene tyrosine-protein kinase Src; Akt - Protein kinase B; MAPK - mitogen-activated protein kinase; NF- κ B - nuclear factor kappa-light-chain-enhancer of activated B cells.

Despite the fairly straightforward concept of G protein activation (*Figure 1.2A*), complexity is added by a number of factors. As described above, there are numerous subtypes of each subunit of the heterotrimer. This allows for incredibly diverse combinations, each with potentially differential cellular effects. This of course depends on both the coupling preference of the GPCRs, and the expression levels of each subunit variant. Additionally, GPCRs can activate multiple G proteins (and also multiple subtypes) while activated, which in turn are able to activate multiple downstream effectors, resulting in a vastly amplified signalling cascade.

As GTP is hydrolysed to GDP by the Ras-like guanine nucleotide triphosphatase (GTPase) domain of $G\alpha$, subunits reassociate, thus returning to the inactive state (Lambright et al., 1996). GPCRs themselves are inactivated through the employment of GPCR kinases (GRKs), which are recruited to the intracellular segments of the receptor (*Figure 1.2B*). GRKs catalyse the phosphorylation of serine (Ser) and threonine (Thr) residues on ICLs and the C-terminus in specific patterns, which in turn allows the recruitment of β -arrestins. Through their interaction with clathrin (with the aid of adaptor protein complex 2; AP2), β -arrestins mediate the downregulation of GPCRs through internalisation (Goodman et al., 1996). Internalised receptors are subsequently degraded in lysosomes or dephosphorylated and recycled. In spite of the traditional view, β -arrestin binding and receptor internalisation may not be the final step in GPCR signalling. Sustained or reactivated G-protein-mediated signalling from endosomes has been demonstrated in several receptors (Irannejad et al., 2013, Thomsen et al., 2016). While β -arrestins themselves were not initially considered signalling molecules, in recent decades it has become increasingly clear that they are able to mediate downstream signalling in their own right. Thus, they are able to interact with kinases, ubiquitin ligases and calmodulin, among others (Latorraca et al., 2020). Although in literature this is often referred to “G-protein-independent” signalling (Gesty-Palmer et al., 2009), current evidence suggests that β -arrestin-mediated signalling is dependent on functional G-proteins (Grundmann et al., 2018). The functions of β -arrestins are discussed in more detail in **Chapter 5**.

1.1.3 GPCR ligand pharmacology

The primary defining factors of GPCR ligands are affinity and efficacy (Kenakin, 2002, Kenakin et al., 2006). Affinity refers to the ability of the ligand to bind the receptor, generally expressed as the equilibrium dissociation constant (K_d). In order to obtain these values, saturation or competition binding assays can be employed using radiolabelled ligands. More recently, the same assay principles have been applied in bioluminescence resonance energy transfer (BRET)-based assays using fluorescent ligands and luciferase-tagged receptors (Christiansen et al., 2016, Hansen et al., 2017). Through competition binding assays it can also be determined whether ligands share a binding site with the endogenous ligand (orthosteric site) or bind at a distinct region on the receptor (allosteric site). Ligand efficacy, expressed as E_{max} , is the ability of a ligand to elicit a molecular or physiological response through the receptor, by inducing conformational changes which allow interactions with G proteins and other effectors.

Early models describe this conformational change as a 2-state (inactive and active) model however this has been largely discredited by knowledge gained over the past decades. Perhaps the most influential of these developments has been the increased availability of high-resolution GPCR structures. Since the deciphering of the structure of agonist-activated β_2 -adrenoceptor in complex with $G\alpha_s$ over a decade ago (Rasmussen et al., 2011), both the number of available structures and the methods utilised to obtain them have multiplied. While X-ray diffraction studies require artificial receptor stabilisation (Magnani et al., 2016), more recent cryo-electron microscopy (cryo-EM) methods are able to capture the range of GPCR activation states, in complex with various ligands and G-proteins (Liang et al., 2017, Zhang et al., 2017). As a result, currently nearly 1000 structures (active, inactive and intermediate) are available through GPCRdb (<https://gpcrdb.org/structure>), more than half of which were identified through cryo-EM. The availability of such structures is of interest not only for our understanding of fundamental receptor mechanisms, but also for future rational drug design to stabilise certain conformations.

The range of different structures for an individual receptor are representative of the continuum of activation states, the energy states of which are influenced by ligand binding and association of G proteins (Kenakin, 2019b). In the absence of

ligands, the majority of GPCRs have a preference for the inactive conformations, with a minority of receptors assuming conformations which are able to induce cellular responses in a ligand-independent manner (also called constitutive activity). Upon binding by an agonist, a shift occurs in the proportion of receptors assuming a signalling conformation, thus generating ligand-dependent signalling (Latorraca et al., 2017). Depending on the efficacy of this activation, agonists can be categorised as full, partial or super-agonists. Full agonists produce responses equivalent to the maximum efficacy of the endogenous ligands, while partial and super-agonists produce efficacies lower or higher than this, respectively (*Figure 1.3A-C*). On the other hand, neutral antagonists stabilise the non-signalling conformations of the receptors, thus preventing receptor activation while simultaneously maintaining constitutive receptor signalling (*Figure 1.3D*). Inverse agonists, however, push the equilibrium of receptor states further towards inactivation, thus ablating constitutive receptor signalling (*Figure 1.3E*) (Kenakin, 2001, Kenakin, 2002).

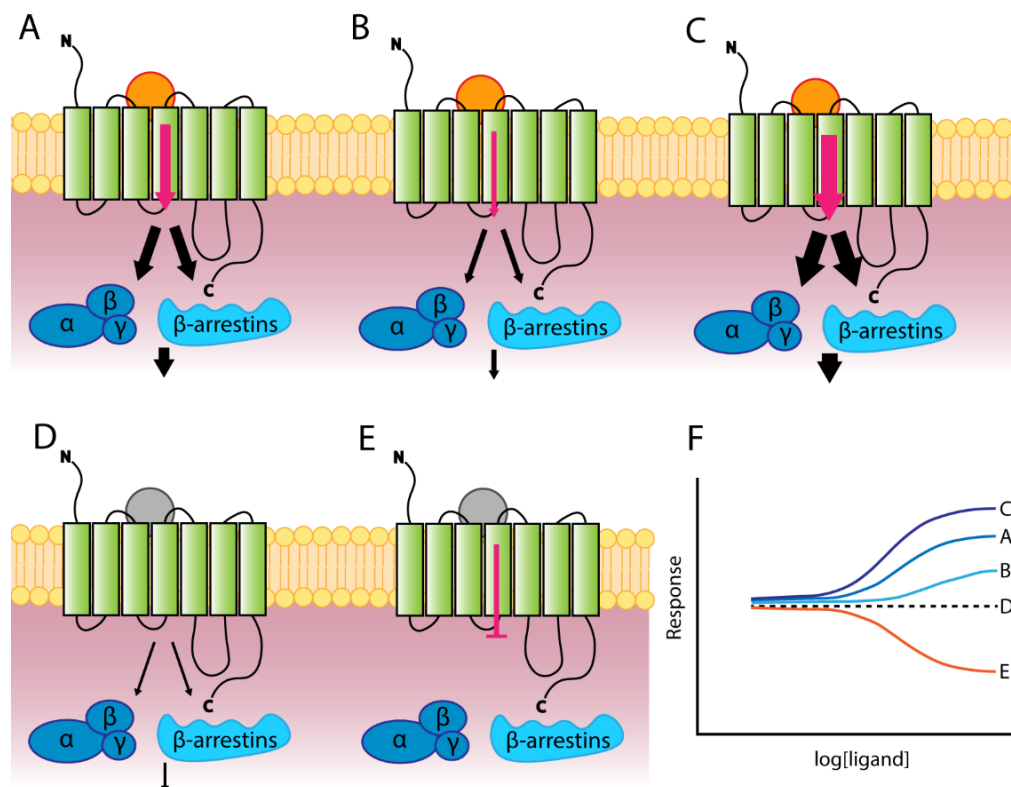


Figure 1.3. Pharmacology of orthosteric GPCR ligands. Binding of agonists (orange circles) to the orthosteric ligand binding site of GPCRs may result in various degrees of activation (magenta arrows): A) full agonism, B) partial agonism or C) superagonism (where the maximum efficacy exceeds that of endogenous ligands). Alternatively, binding of D) neutral antagonists and E) inverse agonists (grey circles) prevent receptor activation by agonists, meanwhile maintaining or inhibiting basal activity, respectively. E) Representative concentration-response curves for each type of orthosteric ligand.

The landscape of GPCR ligand pharmacology is complicated even further by ligands which bind allosteric sites of the receptor. On the one hand, allosteric ligands can act as agonists in their own right. Perhaps more interestingly, allosteric ligands may change the way in which orthosteric agonists interact with the receptor. The ability of an allosteric ligand to influence the affinity and/or maximum efficacy of the orthosteric ligand is expressed as the affinity cooperativity factor (α) and the activation cooperativity factor (β). Ligands which modulate either of these factors in a positive manner are termed positive allosteric modulators (PAMs) (*Figure 1.4*). PAMs may modulate either α or β , or both, resulting a leftward shift and/or increased maximum of the orthosteric agonist concentration-response curves (Kenakin, 2007). These have particular therapeutic interest, as they would maintain the spatiotemporal characteristics of signalling in conditions where there is a reduction in the endogenous ligands, such as in Alzheimer's Disease (Bradley et al., 2016a). By contrast, ago-allosteric modulators have agonist properties, thus allowing increased efficacies at non-activating concentrations of the orthosteric ligand (Kenakin and Miller, 2010).

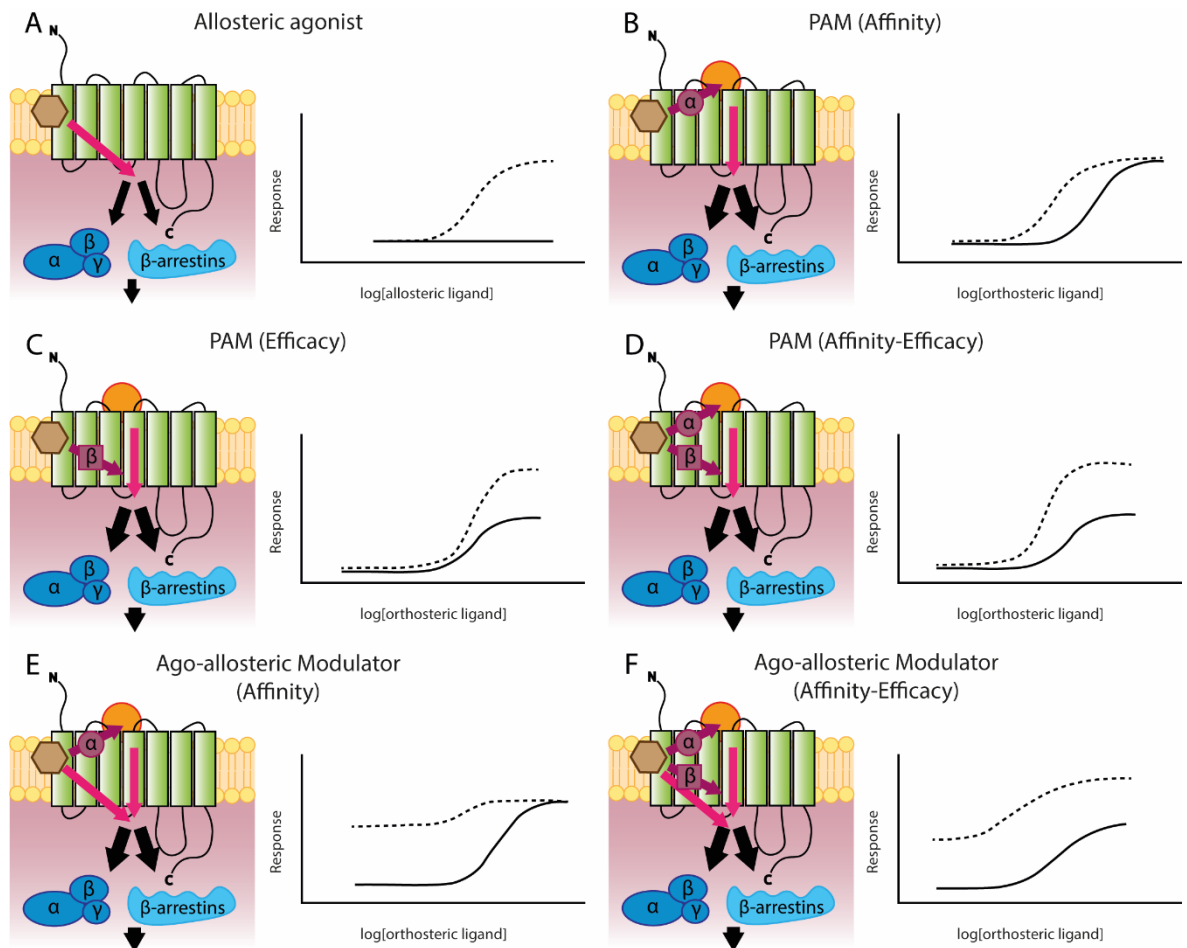


Figure 1.4. Pharmacology of GPCR Positive Allosteric Modulators (PAMs). Ligands binding to sites other than the orthosteric site (brown hexagon) may exert agonistic effects in their own right (magenta arrows) and/or modulate the affinity (α) and/or efficacy (β) (burgundy arrows) of orthosteric ligands (orange circles). Representative concentration-response curves show effects in the absence (solid line) or presence (dashed line) of allosteric ligands. A) Allosteric agonists can induce receptor activation in the absence of an orthosteric ligand. PAMs may positively modulate orthosteric agonist B) affinity, C) efficacy, or D) both, without having agonist effects by themselves. Ago-allosteric modulators, on the other hand, have agonistic effects in addition to modulating orthosteric agonist E) affinity, or F) affinity and efficacy.

Allosteric ligands are not restricted to various PAM types. In fact, allosteric ligands can act as antagonists, as well as negative allosteric modulators (NAM), exerting a negative effect on α or β (Figure 1.5). Such modulation would lead to a rightward shift or a lowered maximum efficacy in orthosteric agonist concentration-response curves (Jazayeri et al., 2016, Keov et al., 2011). Interestingly, negative modulation of β can be accompanied by PAM and/or agonist effects exerted by the allosteric ligand. Thus, NAM-agonists which possess agonist activity show higher efficacy at non-activating concentrations of the orthosteric ligand, while simultaneously lowering the maximum efficacy. On the other hand, PAM-antagonists positively modulate α , while negatively modulating β , thus producing a leftward shift in the orthosteric agonist curve,

alongside lowered maximum efficacy (Kenakin and Strachan, 2018). PAM/NAMs possess a combination of these effects. With such an intricate system of possible effects, it is not surprising that allosteric ligands have attracted the attention of drug development efforts.

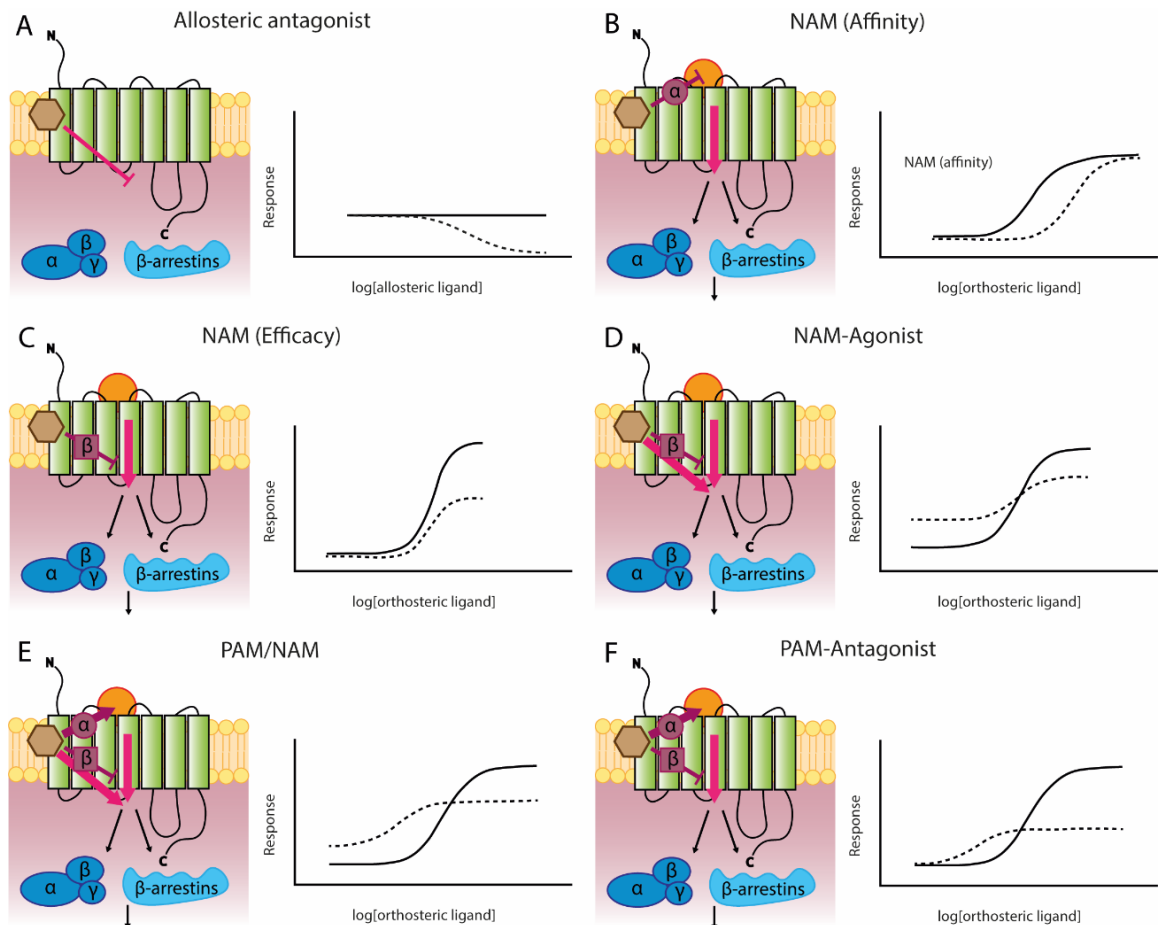


Figure 1.5. Pharmacology of GPCR Negative Allosteric Modulators (NAMs) and Mixed-effect modulators. Ligands binding to sites other than the orthosteric site (brown hexagon) may exert agonistic or antagonistic effects in their own right (magenta arrows) and/or modulate the affinity (α) and/or efficacy (β) (burgundy arrows) of orthosteric ligands (orange circles). Representative concentration-response curves show effects in the absence (solid line) or presence (dashed line) of allosteric ligands. A) Allosteric antagonists may inhibit receptor signalling in their own right. NAMs may negatively modulate the B) affinity or C) efficacy of orthosteric agonists. D) NAM-agonists can negatively modulate orthosteric agonist efficacy, while exerting agonistic effects in their own right. On the other hand, E) PAM/NAMs and F) PAM-antagonists both positively modulate orthosteric agonist affinity, while negatively modulating efficacy. PAM/NAMs also have inherent agonist activity, which PAM-antagonists do not.

Having discussed much of GPCR ligand pharmacology, it is perhaps not surprising, that even further levels of complexity can be explored with regards to signalling pathways. Most ligands are regarded as “balanced”, referring to the fact that all effectors to which the target receptor is coupled are affected equally. A balanced agonist of a receptor would therefore activate all possible coupling responses (both G protein- and β -arrestin-mediated). For therapeutic

purposes, however, it may be desirable to activate one signalling pathway with a beneficial physiological response, while not affecting another, which may lead to detrimental effects. Thus, ligands which preferentially activate/inhibit one signalling pathway over another are termed “biased” ligands (*Figure 1.6*). Allosteric ligands may also modify the signalling of a balanced orthosteric agonist to produce biased signalling (Kenakin, 2019a, Bolognini et al., 2016).

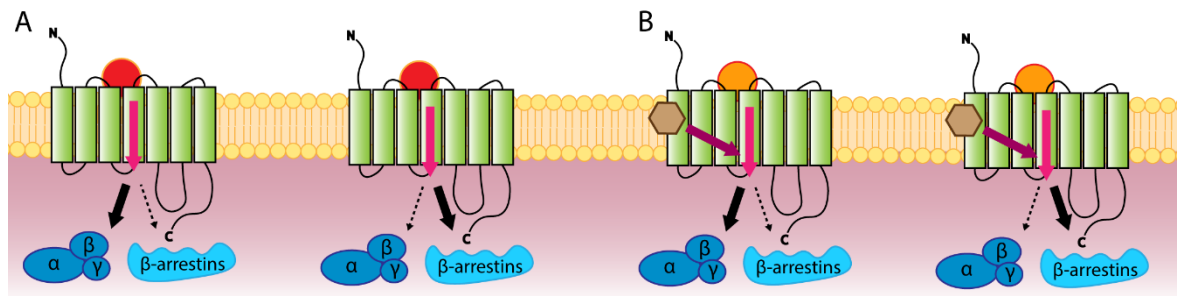


Figure 1.6. Biased signalling through GPCRs. A) Biased orthosteric agonists (red circles) may promote responses either through G proteins (or specific G protein subtypes) or through β -arrestins. B) Biased allosteric ligands (brown hexagon) may push signalling by balanced orthosteric agonists (orange circles) towards biased signalling through either G proteins or β -arrestins.

1.2 Free fatty acid receptors

1.2.1 Metabolites as signalling molecules

For a long time, metabolites have been known to have diverse roles, both as sources of energy and as key factors in intracellular signalling (Milligan et al., 2017). It is only fairly recently, however, that their roles as extracellular signalling molecules has been explored. In particular in easily accessible tissues, metabolites are able to signal through GPCRs. Of particular interest have been a group of GPCRs which respond to free fatty acids (FFAs). Fatty acids (FAs) are composed of a carboxylic acid moiety and an aliphatic carbon chain, the length of which allows categorisation into three groups: short chain fatty acids (SCFAs; 1-6 carbons), medium chain fatty acids (MCFAs; 7-12 carbons) and long chain fatty acids (LCFAs; 12+ carbons). Especially in the case of MCFAs and LCFAs, the position of unsaturated carbons may be important in imparting protective effects. The negative effect of saturated fatty acids (SFAs) on cardiovascular disease risk has been widely researched (Wang and Hu, 2017), leading to dietary recommendations emphasising the benefits of polyunsaturated fatty acids (PUFAs). ω -3 FAs have enjoyed special attention by the public as potential

dietary supplements, due to their anti-inflammatory effects (Oh et al., 2010, Oh and Olefsky, 2012).

SCFAs differ from MCFAs and LCFAs not only in chain length, but also in their source. MCFAs and LCFAs are mainly derived from dietary fats or *de novo* synthesis by the liver. Similarly, the SCFA butyrate can be obtained through dietary sources such as fermented soy products (Qiao et al., 2022) and cheeses (Haddad et al., 2022), and the oxidation of both alcohol (Lundquist et al., 1962) and fatty acids (Yamashita et al., 2001) in the liver leads to the production of acetate. While some acetate and propionate is produced via fermentation of amino acids (Morrison and Preston, 2016), SCFAs are primarily products of dietary fibre fermentation by commensal bacteria (Milligan et al., 2017). Certain species of microbiota preferentially produce specific SCFAs which, in addition to the amount of fibre consumed, can influence physiological effects exerted by these compounds. For example, through the production of the SCFA propionate, *Akkermansia muciniphila* can partially counteract obesity-associated inflammation by normalising intestinal permeability (Everard et al., 2013, El Hage et al., 2019). In addition to metabolic diseases, microbiota have been implicated in cardiovascular (Witkowski et al., 2020), liver (Albillos et al., 2020) and neuropsychiatric (Generoso et al., 2021) diseases. Modulation of the composition of the microbiota - either by anti- and/or probiotics or by faecal transplants - has therefore been considered as a strategy for combatting metabolic diseases (Jia et al., 2008, Kootte et al., 2012, Smits et al., 2013).

1.2.2 Deorphanisation of the free fatty acid receptor family

Considering the wide array of roles associated with SCFAs, it is of paramount importance to understand the signalling pathways which they regulate. The identification of a group of GPCRs which are activated by FAs has opened up new avenues for potential interventions. The FFA receptor family consists of four members: FFA1 (formerly GPR40), FFA2 (GPR43), FFA3 (GPR41) and FFA4 (GPR120). While both FFA1 and FFA4 are activated by LCFAs, FFA1 also responds to MCFAs. FFA2 and FFA3, on the other hand, respond to SCFAs. FFA1-FFA3 share the same chromosomal location (19q13.1 in humans) and show a high degree of sequence identity (29-41%) (Sawzdargo et al., 1997). Another receptor, GPR42,

which shares 98% homology with FFA3 is also encoded in this region. To date, only a single study explored signalling through GPR42, contradicting the consensus about its pseudogene status (Puhl III et al., 2015). Unlike other members of the family, FFA4 is encoded on chromosome 10 (10q23.33 in humans) and has merely 18-23% homology with the other members of the family.

Following initial identification of the receptors, the endogenous ligands of each member of the FFA receptor family were identified in deorphanisation efforts. FFA1-3 were all identified by a single study through database analysis (Sawzdargo et al., 1997), and were also the first to be deorphanised by multiple independent studies in 2003. Firstly, MCFAs and LCFAs were identified as ligands for FFA1 via Ca^{2+} -assay based ligand fishing screens using over 1,000 putative agonist compounds (Briscoe et al., 2003, Itoh et al., 2003). Additionally, FFA1 was also identified as the target of LCFAs when these compounds were tested against a complement of 10 orphan GPCRs (Kotarsky et al., 2003). In a similar vein, endogenous ligands for FFA2 were also identified by three independent groups. Compound libraries were again tested against FFA2 and FFA3, leading to the identification of SCFAs as activating ligands for both receptors (Brown et al., 2003, Le Poul et al., 2003). The same conclusion was reached by the final study, which employed a more targeted approach based on the knowledge of the effect of SCFAs on leukocytes, in combination with the high expression of FFA2 on these cells (Nilsson et al., 2003).

While other members of the FFA family were being deorphanised, FFA4 had only just been identified, again via genomic data base analysis (Fredriksson et al., 2003a). Similar to FFA1-3, an extensive library of compounds was tested against FFA4 in order to identify endogenous ligands. During initial deorphanisation, PUFAs (including ω -3 FAs) were identified as the endogenous ligands (Hirasawa et al., 2005, Oh et al., 2010, Davenport et al., 2013). However, SFAs were later shown to activate FFA4 with similar potency, albeit with lower efficacy than PUFAs (Christiansen et al., 2015).

In addition to the FFA receptor family, 3 additional GPCRs have been described as receptors for FFAs: GPR84, Olf78 and HCA₂. First identified two decades ago (Wittenberger et al., 2001), GPR84 remains to this day an orphan receptor - one

whose endogenous ligand has not been identified. Although the receptor has been shown to be activated by MCFAs, these are not present in the relevant tissues at appropriate concentrations (Wang et al., 2006b, Davenport et al., 2013). Nevertheless, due to its expression in immune cell populations and its upregulation in response to inflammatory stimuli, GPR84 has been the focus of avid research as a potential target for inflammatory conditions such as ulcerative colitis (Marsango et al., 2022a, Nagasaki et al., 2012). Indeed, there is an ongoing effort to produce selective ligands for GPR84 (Pillaiyar et al., 2017, Jenkins et al., 2021, Mahindra et al., 2022), with one antagonist entering but subsequently failing to meet anticipated endpoints in clinical trials (Vermeire et al., 2017).

As briefly mentioned in *Section 1.1.1*, olfactory GPCRs are traditionally not considered druggable. In recent years, however, potential roles beyond olfaction have been suggested. This arose in response to olfactory receptors being discovered in the mouse kidney, where they were found to contribute to physiological functions (Pluznick et al., 2009). Among these was Olfr78 (or OR51E2 in humans), which was later reported to be activated by SCFAs to modulate blood pressure and renin release (Pluznick, 2014). Olfr78 has also been shown to be expressed in enteroendocrine cells (EECs) in the colon, and it is downregulated in mouse models of colitis (Fleischer et al., 2015, Kotlo et al., 2020).

HCA₂ (formerly GPR109A) is a member of the hydroxy-carboxylic acid (HCA) receptor family. Although deorphanisation eventually led to β -hydroxy-butyrate (β -OHB) being identified as the endogenous ligand (Offermanns et al., 2011), initial studies also showed activation by FAs 4-8 carbons in length (Taggart et al., 2005). While butyrate (and other SCFAs) may not be the most potent endogenous ligands, in the colon where its levels are sufficient, it can activate HCA₂ with tumour suppressing effects (Thangaraju et al., 2009). Although recent research focuses on the inflammatory (Carretta et al., 2020) and anti-inflammatory (Graff et al., 2016) roles of HCA₂, focus has been on ligands other than SCFAs. As such, the future of HCA₂ as a SCFA receptor is unclear.

1.3 SCFA receptors

1.3.1 SCFAs as endogenous ligands

Although a number of metabolites have now been established as signalling molecules, SCFAs have received particular attention due to their source. As they are dependent on dietary fibre fermentation by the commensal bacteria, SCFAs show a unique interaction between the microbiome and the host (Cook and Sellin, 1998). Even prior to the discovery of metabolite-sensing receptors, the various physiological functions of SCFAs were appreciated. The primary SCFAs produced by fermentation are acetic (C2), propionic (C3) and butyric (C4) acid, although formic (C1), pentanoic (C5), hexanoic (C6), iso-butyric and iso-pentanoic acid are also produced in small quantities. Even though the composition of intestinal SCFAs can vary due to the type of fermenting bacteria present or the substrates available to them, C2 is by far the most abundant (with C2:C3:C4 present in a ratio of 1:0.31:0.15) (Soergel, 1994). The normal luminal concentration for these ranges between 50-100mM, however they are significantly and differentially diluted as they move away from the gut lumen. As a result, uptake by the gut epithelium, the concentration of C4 in the hepatic portal vein may be as low as 30 μ M, while C2 and C3 maintain higher concentrations (260 μ M and 90 μ M, respectively). The majority of C3 is sequestered within the liver, resulting in low peripheral C3 and C4 concentrations (around 5 μ M each). As a result, C2 is the predominant SCFA species in the circulation at around 70 μ M (Cummings et al., 1987), and the most likely to exert effect through FFA2 and FFA3 in target tissues beyond the gut. Local concentrations of C2 might be further augmented in these target tissues, specifically via production by pancreatic β -cells (Tang et al., 2015) and subpopulations of adipocytes (Sun et al., 2020) thus mediating auto- and paracrine signalling.

Since the highest concentration of each SCFA can be found in the intestinal lumen, it is not surprising that SCFAs primarily affect EECs of the intestinal lumen, although resident macrophages and circulating neutrophils are also affected (Husted et al., 2017). The balance in the concentration of each SCFA, and therefore the effects they exert both in the gut and systemically, can be disrupted by high-fat diets (HFD). HFD has a multimodal effect on the circulating

FA levels. The presence of lipids in the duodenum stimulates cholecystokinin release from I-cells, which in turn triggers the release of bile from the gall bladder. The chronically high levels of hydrophobic bile acids triggered by HFD may increase the permeability of the intestinal wall indirectly by affecting the composition of the gut microbiota (Stenman, 2012, Cani et al., 2008). As such, there is a transient reduction in microbes which promote gut barrier integrity (such as *Bifidobacterium* spp.) (Cani et al., 2007), accompanied by an augmentation of species which reduce it (such as *Desulfovibrio* spp.). Of the latter category, *Bilophila wadsworthia* utilises sulphur from taurine-containing bile salts, producing hydrogen sulphide as a genotoxic by-product (Devkota et al., 2012). The resulting hyperpermeability of the intestinal wall, in combination with a concomitant degeneration of the luminal mucus layer, leads to the leakage of luminal toxins and FAs other than C2 into the circulation (Raybould, 2012). In particular, the presence of bacterial lipopolysaccharides (LPS) in the circulation is believed to be the underlying cause of the systemic low-grade inflammation present in obesity (Cani et al., 2008). In addition, infiltration by leukocytes and the release of proinflammatory cytokines are hallmarks of inflammatory bowel disease (IBD).

Given the importance of the microbiome in SCFA production, modifying, or completely ablating it can be used to further reveal the physiological functions of SCFAs. By administering SCFAs or, alternatively, knocking out (KO) SCFA receptors in combination with germ-free (GF) maintenance of mouse models allows the unravelling of the links between SCFAs and SCFA receptors (Milligan et al., 2017). The first of such studies demonstrated that wild type (WT) animals raised as GF and conventionally raised FFA2-KO mice both displayed exacerbated inflammatory responses in models of colitis, arthritis, and asthma. While GF responses could be rescued by C2 administration, this was not the case for FFA2-KO mice (Maslowski et al., 2009). In GF mice, a reduction in intestinal regulatory T-lymphocyte populations was also observed, which could be rescued by SCFA administration in WT but not in FFA2-KO animals (Smith et al., 2013). By contrast, in a gout model, FFA2-KO and GF raising or antibiotic treatment of WT mice both resulted in decreased production of pro-inflammatory interleukin (IL)-1 β and CXCL1, accompanied by decreased ROS production and inflammasome assembly by macrophages. Exogenous C2 and gut recolonisation were both able

to restore inflammatory responses in GF but not in FFA2-KO mice (Vieira et al., 2015). Beyond the roles in inflammatory processes, FFA2 was also found to influence adiposity. Under normal conditions, while FFA2-KO mice were obese on a normal chow diet, mice overexpressing FFA2 specifically in adipose were lean even when fed a HFD. When raised as GF, both strains displayed normal phenotypes (Kimura et al., 2013). On the other hand, KO of FFA3 resulted in decreased adiposity in comparison to WT mice; a difference which was not present when animals were raised as GF. These differences were associated with reduced expression of the anorexigenic hormone peptide YY (PYY) in FFA3-KO mice (Samuel et al., 2008). Feeding mice a diet with a high fibre content was found to alter microbiota in not only the gut but also in the lung, thus increasing SCFA levels and reducing lung inflammation. Although administration of C3 produced similar protective effects in WT and FFA2-KO, it did not do so in FFA3-KO mice (Trompette et al., 2014). With these studies, a causative link between microbiome-derived SCFAs and the SCFA receptors could be clearly established.

While the same SCFAs are able to activate both FFA2 and FFA3, their potency in doing so differs between the two receptors. At human (h)FFA2, SCFAs display the following rank order: C2 = C3 = C4 > C5 > C6 = C1. By contrast, at hFFA3 the order of potency is C3 = C5 = C4 > C2 > C1 (Brown et al., 2003). Not only are SCFA potencies different between the two receptors, but the signalling pathways to which they couple also differ (*Figure 1.7*). Both receptors can activate the pertussis toxin (PTX)-sensitive $G\alpha_{i/o}$ pathways, however FFA2 is more promiscuous in that it also signals through $G\alpha_{q/11}$, and $G\alpha_{12/13}$. These couplings were initially revealed in deorphanisation studies with the use of chimeric $G\alpha$ in yeast cell lines (Brown et al., 2003), and coupling to $G\alpha_{i/o}$ and $G\alpha_{q/11}$ has been corroborated by multiple studies using functional assays measuring [³⁵S]-guanosine-5'-O-(3-thio)triphosphate ([³⁵S]GTP γ S) incorporation ($G\alpha_{i/o}$) or Ca²⁺ mobilisation ($G\alpha_{q/11}$) (Hudson et al., 2013, Hudson et al., 2012a). Signalling through $G\alpha_{12/13}$ has also been demonstrated in functional assays of transforming growth factor- α (TGF- α) shedding, where CRISPR/Cas9-edited cells lacking these subtypes displayed decreased responses (Sergeev et al., 2017). Recruitment of β -arrestin-2 has been demonstrated using BRET-based methods for FFA2 only, although the downstream effects from this remain unclear. Knock-down of β -arrestin-1/2 in FFA3-expressing Neuro2A cells showed no differences in cellular

response upon C3 treatment, further supporting the inability of FFA3 to signal through β -arrestins (Kimura et al., 2011). Finally, phosphorylation of extracellular signal-regulated kinase (ERK) has also been demonstrated in FFA2-expressing cells (Hudson et al., 2012a, Sergeev et al., 2016), however the specific signalling pathways contributing to this effect are incompletely understood.

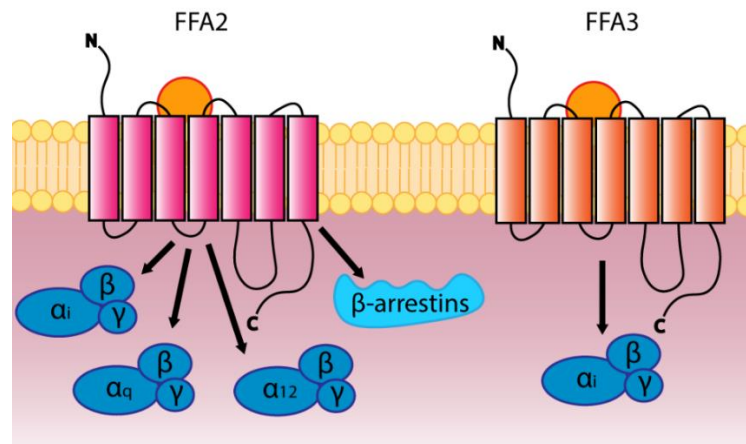


Figure 1.7. Signalling pathways through SCFA receptors. Activation by orthosteric agonists (orange circle) can induce downstream signalling through G protein-mediated or alternative pathways. FFA2 is able to signal through $G_{\alpha_{i/o}}$, $G_{\alpha_{q/11}}$, and $G_{\alpha_{12/13}}$, as well as through β -arrestins. FFA3 can induce signals exclusively through $G_{\alpha_{i/o}}$.

Despite the well-established rank order of SCFA potencies at the human orthologues of the receptors, these cannot be translated directly to animal orthologues. In the bovine orthologue of FFA2 (bFFA2), for example, C4, C5, C6 and C7 (heptanoic acid) all show higher potency than C2 and C3. Even longer chain FAs, octanoic (C8) and nonanoic (C9) acid are able to activate bFFA2 (Hudson et al., 2012a). Such variability between species orthologues is hardly surprising, considering the differences in the amount non-digestible dietary carbohydrates, and therefore in the amounts of various SCFAs. More important for pre-clinical studies is the difference in the pharmacology displayed by the mouse orthologues of FFA2 (mFFA2) and FFA3 (mFFA3). Initially, in the absence of selective synthetic ligands, C2 was used as an “FFA2-selective” ligand due to its 10-fold higher potency in comparison to FFA3 (Tolhurst et al., 2012). However, this selectivity of C2 does not exist in between mFFA2 and mFFA3. By contrast, C3 shows selectivity for mFFA3 over mFFA2, which does not exist for hFFA3 and hFFA2. Orthologue-specific residues in ECL2 are suggested as the contributors to these differences (Hudson et al., 2012b).

1.3.2 Physiological functions and therapeutic implications

The shared use of SCFAs as endogenous ligands is but one of the issues complicating SCFA receptor pharmacology. Importantly, FFA2 and FFA3 are co-expressed in several tissues where, in the absence of selective agonists, the contribution of each receptor to physiological functions cannot be confidently isolated. Due to the characteristics highlighted in the previous section, SCFAs on their own are not appropriate tools for the dissection of these contributions. Although KO animals of one SCFA receptor may display compensatory changes in expression of the other receptor (Zaibi et al., 2010), they can nevertheless inform our understanding about the physiological roles of the receptors. A more in-depth discussion of the use of KO and other transgenic models can be found in **Chapter 3**.

Before considering the various physiological effects that SCFA receptors mediate, it is important to take a detour to introduce one of the most important new tools for the investigation of SCFA receptor pharmacology. Designer Receptors Exclusively Activated by Designer Drugs (DREADD), as the name suggest, are mutant variants of a receptor which are unresponsive to endogenous ligands, while enabling otherwise inert synthetic ligands to activate the receptor. This approach has been particularly useful in the case of receptors which display large sequence homology and overlapping ligand profiles (Urban et al., 2009). An excellent example is the muscarinic acetylcholine receptor (mAChR) family whose 5 members are all activated by acetylcholine, and therefore show large homology in the ligand binding pocket. Through directed molecular evolution, Armbruster et al (2007) uncovered two point mutations which reduced acetylcholine activity at M_3 mAChR, while enabling activation by clozapine-N-oxide. The conservation of the two residues throughout the mAChR family has allowed the generation of DREADD versions of all members, thus potentiating the efforts to identify their individual roles (Bradley et al., 2018). In the case of hFFA2, the DREADD variant of the receptor was the result of rational chemogenetic engineering (*Figure 1.8*). On one hand, a Cys to glycine (Gly) mutation was introduced at residue position 141 to mimic the sequence of bFFA2, thus rendering the receptor more susceptible to activation by longer chain SCFAs (C5-C8) and small carboxylic acids (SCAs) (Hudson et al., 2012a). On

the other hand, responsiveness to endogenous SCFAs was ablated by the introduction of a second, histidine (His) to glutamine (Gln) mutation at position 242, thus changing a residue previously identified as playing a role in the binding of SCFAs (Stoddart et al., 2008). The resulting hFFA2-DREADD is activated by the SCA 2,4-hexadienoic acid (Sorbic acid; SA) and the recently identified synthetic agonist, 4-methoxy-3-methyl-benzoic acid (MOMBA) (Barki et al., 2022), while remaining amenable to inhibition by the available FFA2 antagonists (discussed in **Section 1.3.3**). Through the generation of knock-in mouse lines, hFFA2-DREADD can simultaneously inform on the roles of FFA2 and FFA3, upon activation by synthetic DREADD agonists and SCFAs, respectively (Bolognini et al., 2019, Barki et al., 2022).

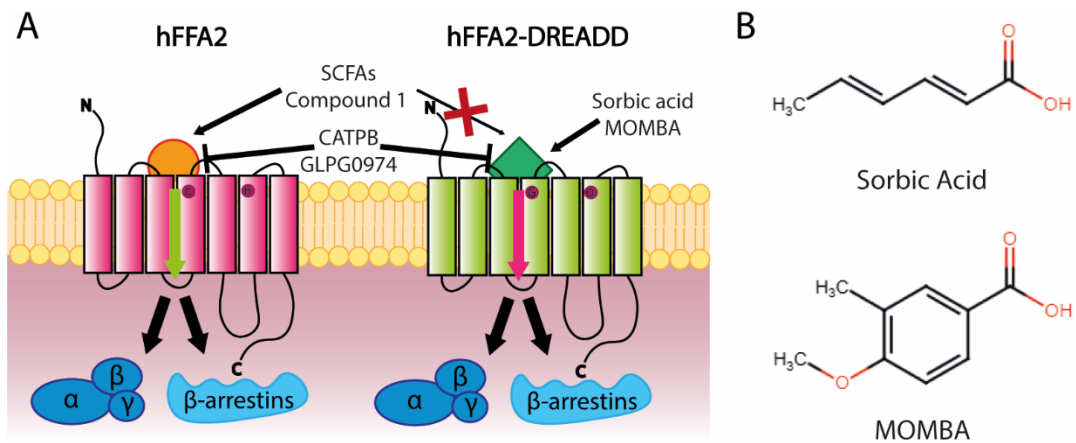


Figure 1.8. DREADD variant of human FFA2. A) Designer Receptor Exclusively Activated by Designer Drugs (DREADD) version of hFFA2, where two point mutations (Cys¹⁴¹Gly and His²⁴²Gln; purple circles) render the receptor non-responsive to endogenous orthosteric hFFA2 agonists, while simultaneously making it amenable to activation by either the natural but not endogenously produced ligand Sorbic Acid, or the synthetic ligand MOMBA. Antagonists retain their ability to inhibit receptor activation at the DREADD mutant. B) Structures of hFFA2-DREADD ligands Sorbic Acid (2,4-hexadienoic acid) and MOMBA (4-methoxy-3-methyl-benzoic acid).

1.3.2.1 Enteroendocrine functions

Considering that SCFAs originate from the microbiome, it is not surprising that both receptors are abundantly expressed in the gut, particularly in EECs (Karaki et al., 2008, Tazoe et al., 2009, Nohr et al., 2013). SCFA administration has been associated with the release of the anorexigenic hormone PYY and increased gut motility (Karaki et al., 2006). In other studies, both receptors were expressed in glucagon-like peptide-1 (GLP-1)-secreting L-cells, where GLP-1 release in response to SCFAs was mediated through increased Ca²⁺ (via Gα_{q/11}) and was reduced in colonic cultures from animals lacking FFA2, but not those lacking FFA3 (Tolhurst et al., 2012). These results were later confirmed *in vivo*,

whereby intracolonic infusion of C3 increased the secretion of PYY and GLP-1 in WT but not in FFA2-KO mice (Psichas et al., 2015). By contrast, a recent report suggested that GLP-1 release from mouse EECs and colonic crypts was mediated through endosomal FFA2 signalling via $G\alpha_i/p38$ (Caengprasath et al., 2020). As a result of feeding mice a diet supplemented with the fermentable carbohydrate inulin, there was an observable increase in PYY-secreting cell density and a reduction in food intake; effects which were absent in FFA2-KO mice (Brooks et al., 2017). Importantly, all animal studies hitherto mentioned rely on a loss of physiological responses as a result of receptor KO. More recently, the involvement of FFA2 in PYY and GLP-1 release was confirmed with the use of hFFA2-DREADD-expressing mice, *in vitro* and *in vivo* (Barki et al., 2022, Bolognini et al., 2019). Unlike previous studies, these involve direct activation of the receptor to produce a physiological response. The same mouse model was also used to demonstrate that FFA2 activation accelerates gut transit in mice (Bolognini et al., 2019). In addition to PYY and GLP-1, FFA2-KO mice have also been utilised to show the role of this receptor in the regulation of the orexigenic hormone ghrelin in the stomach, leading to $G\alpha_{i/o}$ -mediated reduction in ghrelin release upon SCFA treatment (Engelstoft et al., 2013). Considering that FFA2 activation appears to decrease appetite through at least 3 different hormones, it constitutes an attractive druggable target for the prevention or treatment of obesity. Indeed, in overweight human subjects, acute ingestion of inulin-propionate ester increased the levels of both PYY and GLP-1, while long-term supplementation was associated with reduced weight gain, although the involvement of FFA2 was not confirmed in this study (Chambers et al., 2015).

1.3.2.2 Roles in adipose tissue homeostasis

The expression of FFA2 in adipose tissue has been described in various studies (Kimura et al., 2013), while that of FFA3 has only been reported by one group (Xiong et al., 2004) and has been largely discredited (Zaibi et al., 2010). Perhaps the most well-established role of FFA2 in adipose tissue is the inhibition of lipolysis. Inhibition of isoproterenol-induced lipolysis has been demonstrated with adipocytes isolated from WT and FFA2-KO mice (Ge et al., 2008), and more recently using hFFA2-DREADD-expressing adipocytes (Bolognini et al., 2019). In each case, the process was shown to be sensitive to PTX, and thus mediated by $G\alpha_{i/o}$. While FFA2 is suggested to have a role in adipogenesis, the evidence for

this is contradictory. On one hand, adipocyte cell line differentiation was associated with increased FFA2 expression, and knock-down of FFA2 blocked differentiation (Hong et al., 2005). In addition, FFA2-KO mice displayed a lean phenotype, even on a HFD, with lower plasma cholesterol and liver triglyceride levels than WT (Bjursell et al., 2011). By contrast, Kimura et al (2013) found that FFA2-KO mice were obese on a normal diet, while those specifically overexpressing FFA2 in adipose remained lean on a HFD, suggesting that FFA2 inhibits fat accumulation. These results were corroborated by a subsequent study, whereby the probiotic *Bifidobacterium* subspecies GCL2505 was introduced, leading to increased plasma C2 levels and decreased fat accumulation in WT but not FFA2-KO mice (Horiuchi et al., 2020). There is also evidence of the ketone body acetoacetate acting as an additional ligand for FFA2, as ketogenic diet feeding resulted in weight loss and accelerated lipolysis in WT but not FFA2-KO mice (Miyamoto et al., 2019). Interestingly, in adipocytes isolated from human subjects, FFA2 activation was found not to affect adipocyte differentiation (Dewulf et al., 2013). When applied to overweight/obese subjects, rectal administration of SCFAs led to increased fasting fat oxidation and resting energy expenditure, in tandem with increased plasma C2 (Canfora et al., 2017). These findings were supported by Chambers et al (2018) with oral C3 administration to healthy subjects, however the specific involvement of FFA2 could not be demonstrated in these studies. SCFA receptors have also been implicated in insulin-stimulated glucose uptake. While immortalised adipocyte studies demonstrated increased glucose uptake via FFA3 activation (Han et al., 2014), FFA2 was shown to suppress insulin signalling *in vivo*, using FFA2-KO mice (Kimura et al., 2013). While not settling this controversy, human trials of overweight/obese adults revealed increased insulin sensitivity upon supplementation with inulin-propionate ester (Chambers et al., 2019). Finally, SCFAs have been suggested as mediators for leptin secretion, both through FFA2 (Zaibi et al., 2010) and through FFA3 (Xiong et al., 2004). However, the expression of FFA3 in adipose tissue is now largely discredited. Although FFA2 is clearly involved in a number of adipose tissue functions, due to the contradictory data it is currently unclear whether agonists or antagonists would be desired to elicit beneficial effects.

1.3.2.3 Roles in the pancreas and glucose homeostasis

With their roles in the regulation of appetite and energy expenditure, SCFA receptors are already highly implicated in obesity. In turn, obesity is closely linked to diabetes, therefore it could be expected that FFA2 and FFA3 would affect glucose homeostasis in some manner. Indeed, both receptors are expressed in pancreatic β -cells (Kebede et al., 2009), however their functions are not clearly defined. Various groups have reported that SCFAs inhibit (Tang et al., 2015), potentiate (Pingitore et al., 2019), or simply do not affect (Orgaard et al., 2019) glucose-stimulated insulin secretion (GSIS) in isolated pancreatic islets. While this diversity in responses could be the result of differences in experimental strategies, the signalling pathways elicited by each of the SCFA receptors are also a contributing factor. In fact, a combination of FFA2 agonists and FFA2-KO mouse-derived islets have been used to demonstrate that FFA2 activation inhibits GSIS through $G\alpha_{i/o}$ (Priyadarshini et al., 2015) but potentiates it via $G\alpha_{q/11}$ (Mcnelis et al., 2015, Pingitore et al., 2019). Activation of FFA3 has also been shown to inhibit GSIS, in a $G\alpha_{i/o}$ -dependent manner (Priyadarshini and Layden, 2015). Whereas FFA3-KO increased, FFA3-overexpression decreased GSIS *in vitro* (Veprik et al., 2016). *In vivo*, FFA3-KO on HFD have been shown to exhibit attenuated glucose intolerance in comparison to WT (Priyadarshini et al., 2020). While FFA2 and FFA3 appear to be an attractive target in the pancreas, their opposing physiological effects may complicate drug development efforts. Indeed, in human trials, neither oral administration of C3 to fasted subjects (Chambers et al., 2018), nor rectal administration of various SCFAs to overweight/obese patients had an effect on glucose and insulin concentrations (Canfora et al., 2017). In order to potentiate only the beneficial effects, FFA2 ligands which display a $G\alpha_{q/11}$ bias would make ideal candidates, potentially in combination with potent FFA3 inhibitors, however such ligands described to date have modest potency and bias (Bolognini et al., 2021, Villa et al., 2017).

1.3.2.4 Roles in the peripheral nervous system

The expression of FFA3 on neurones of the peripheral nervous system (PNS) has been shown both at the messenger RNA (mRNA) (Kimura et al., 2011, Nohr et al., 2015) and protein levels (Nohr et al., 2013, Colina et al., 2018). Initial studies indicated the excitatory role of FFA3 in superior cervical ganglia on heart rate and oxygen consumption. This group, based on pharmacological and knock-

down experiments, suggested that these functions were mediated via the G β γ -PLC β -mitogen-activated protein kinase (MAPK) (Kimura et al., 2011) or G β γ -PLC β -ERK1/2-synapsin 2 pathways (Inoue et al., 2012), rather than G $\alpha_{i/o}$. FFA3 is expressed in sympathetic ganglia even during embryonic development, where its KO was found to lead to decreased heart innervation, heart rate and oxygen consumption (Kimura et al., 2020). These findings all point to FFA3 having a role in energy metabolism. FFA3 has also been shown to inhibit N-type Ca²⁺ channels, thus having a potential negative effect on neurotransmitter release, at least in sympathetic neurones (Won et al., 2013) and neurones with a vasoconstrictor phenotype (Colina et al., 2018). In addition, FFA3 expression has been demonstrated in the enteric nervous system: the mucosal, submucosal and myenteric plexus of the small intestine (Nohr et al., 2013) and the colon (Kaji et al., 2016, Kaji et al., 2018). In the latter case, FFA3-expressing neurones were found to be cholinergic and activation of FFA3 by a (potentially) selective agonist resulted in G $\alpha_{i/o}$ -dependent inhibition of anion secretion and motility effects *in vitro*. These effects were also demonstrated in human colonic specimens (Tough et al., 2018). By contrast, by using the hFFA2-DREADD-HA mouse model, no contribution of FFA3 to gut motility was found (Bolognini et al., 2019). Most recently, using the same mouse model in combination with novel selective ligands for hFFA2-DREADD and FFA3, Barki et al (2022) demonstrated that FFA3 selectively enhanced neuronal firing by gut afferent neurones. In addition, neuronal and non-neuronal cells of dorsal root (DRG) and nodose ganglia were found to express both FFA2 and FFA3, whose activation led to increases in intracellular Ca²⁺ via G $\alpha_{q/11}$ and G $\alpha_{i/o}$, respectively. Based on these discoveries, the existence of a SCFA-gut-brain axis has been suggested, which may open up novel avenues for the treatment of central nervous system (CNS) disorders (Barki et al., 2022). *Figure 1.9* provides a visual summary of physiological effects of FFA2 and FFA3.

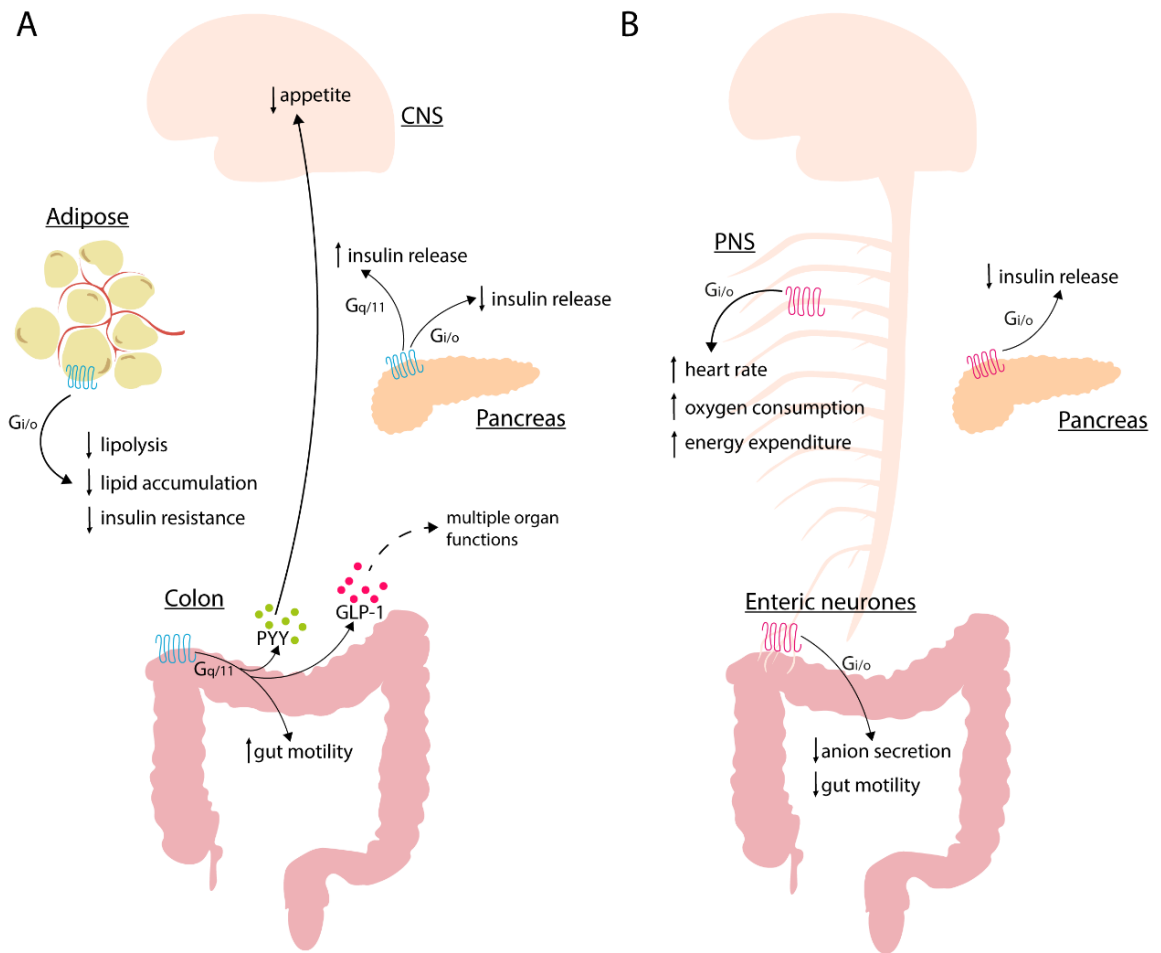


Figure 1.9. Physiological functions of SCFA receptors. A) In the colon, FFA2 activation induces gut motility, as well as the release of the anorectic hormones GLP-1 and PYY, in a $G\alpha_{q/11}$ -dependent manner. These in turn affect multiple organs, including the CNS, resulting in decreased appetite. In pancreatic β -cells, FFA2 signalling through $G\alpha_{q/11}$ and $G\alpha_{i/o}$ increases or decreases insulin release, respectively. Activation of FFA2 in adipocytes leads to the $G\alpha_{i/o}$ -mediated decrease in lipolysis, lipid accumulation and insulin resistance. B) In pancreatic β -cells, FFA3 activation inhibits insulin release. Activation of FFA3 in enteric neurones leads to decreased gut motility and anion secretion. Evidence supports the role of FFA3 expressed in PNS in increasing heart rate, oxygen consumption and energy expenditure. CNS - central nervous system; PNS - peripheral nervous system; PYY - peptide YY; GLP-1 - glucagon-like peptide. Adapted from Bolognini et al (2021).

1.3.2.5 Immune functions

Even at the point of discovery, SCFA receptors were shown to be expressed on immune cell populations (Brown et al., 2003, Le Poul et al., 2003). In particular, the various roles of FFA2 in immune homeostasis have been demonstrated in cells of the innate immune system (Nilsson et al., 2003). FFA2 has been widely described as a chemotactic receptor on neutrophils, inducing recruitment of these cells to the site of infection or inflammation. This effect has been demonstrated in isolated neutrophils, from FFA2-KO mice (Maslowski et al., 2009, Vinolo et al., 2011, Sina et al., 2009) or from humans, induced with a selective allosteric ligand (Bolognini et al., 2016, Lind et al., 2021). There is some evidence that FFA2 might promote neutrophil apoptosis at the site of

infection, thus combatting pathogens such as *Klebsiella pneumoniae* (Galvao et al., 2018). In line with the antibacterial effects, FFA2 has been found to promote reduced nicotinamide adenine dinucleotide phosphate (NADPH) oxidase assembly, and thus superoxide production in response to SCFAs in the presence of various phenylacetamide compounds (Lind et al., 2020, Martensson et al., 2018). Similar effects are produced by crosstalk between FFA2 and the adenosine triphosphate (ATP) receptor P2Y₂ (Lind et al., 2019). The recently discovered expression of FFA2 on type 3 innate lymphoid cells (ILC3s) in mouse intestines has revealed not only new immunological functions (Chun et al., 2019), but also novel interactions between neutrophils and these ILC3s. Such interactions, mediated by IL-1 β , result in the release of IL-22 from ILC3s, which in turn was shown to maintain tissue integrity and effectively protect against *Clostridium difficile* infection in a mouse model (Fachi et al., 2020). The contradictory pro- and anti-inflammatory effects of FFA2 as seen in neutrophils is further complicated when further FFA2-expressing immune cell types are considered. For one, adipose tissue M₂-type macrophages were reported to express FFA2. There they mediate the release of the pro-inflammatory cytokine tumour necrosis factor α (TNF α), which in turn may maintain adipose homeostasis (Nakajima et al., 2017). FFA2 activation on dendritic cells (DCs) by SCFAs was found to trigger plasma cell differentiation and subsequent immunoglobulin A (IgA) and G (IgG) production, by the release of B-cell activating factor and retinoic acid-regulating protein aldehyde dehydrogenase 1 (Wu et al., 2017, Yang et al., 2019). By contrast, a more recent report on the effect of C4 on IgA class switching argued that signalling occurred through the activation of FFA3 on DCs (Isobe et al., 2019). Regardless of which receptor is involved, SCFAs appear to have a role in the maintenance of gut immune homeostasis via Ig production. Furthermore, FFA2 has been shown to mediate B cell differentiation *in vivo* in a mouse model of rheumatoid arthritis (Yao et al., 2022). The interaction of FFA2 with viral pathogens has also been described recently. On one hand, FFA2 activation in pulmonary epithelial cells mediated antiviral effects against the respiratory syncytial virus through the release of interferon- β (Antunes et al., 2019). On the other hand, in the case of the influenza A virus (IAV), FFA2 appears to act as a coreceptor for virus internalisation on cultured mouse macrophages, thus contributing to the viral life cycle (Wang et al., 2020). However, activation of FFA2 by C2 positively

affects alveolar macrophages, at least in the context of IAV infections, thus protecting against secondary bacterial infections (Sencio et al., 2020). The immunological roles of FFA2 are summarised in *Figure 1.10*, and are further discussed in *Chapter 4*.

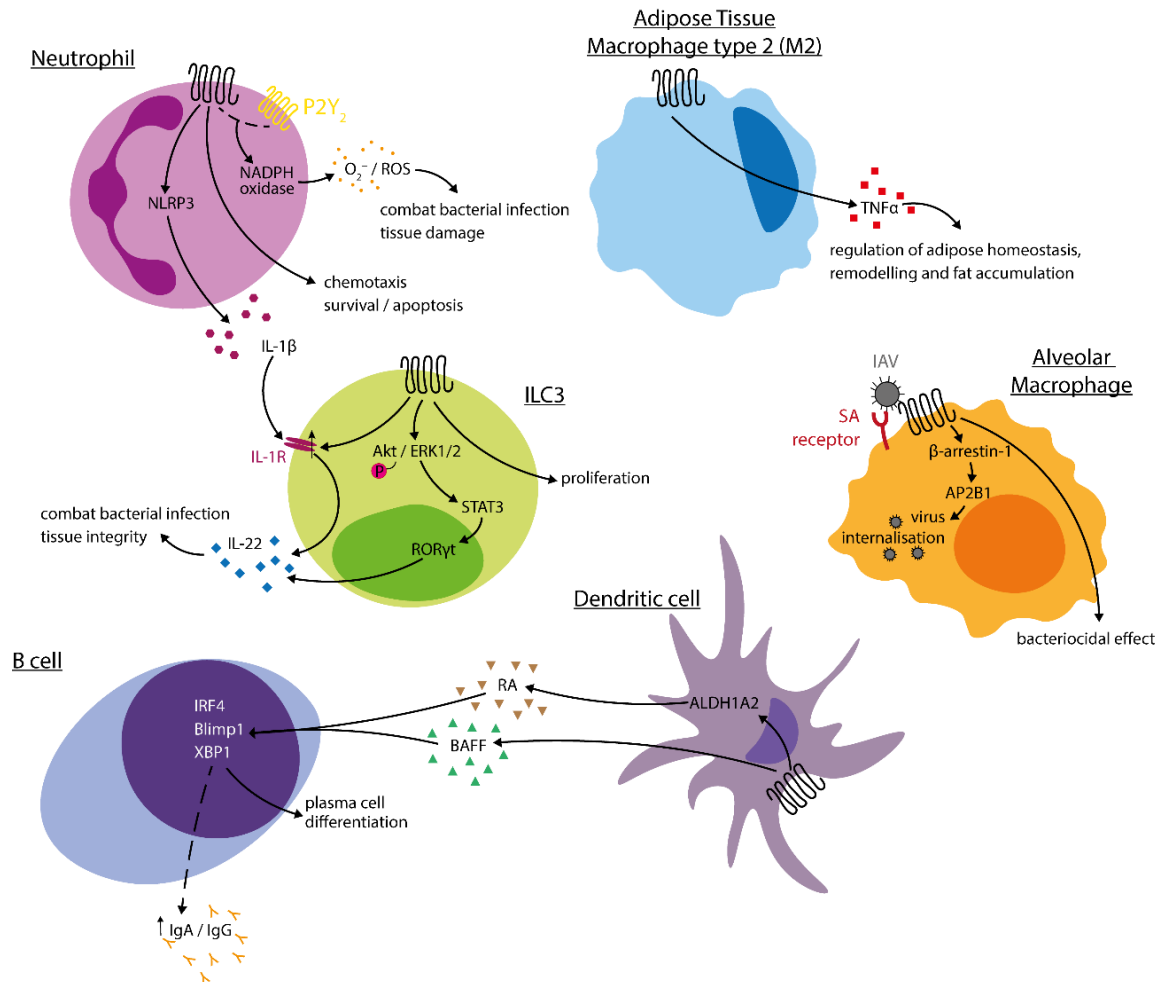


Figure 1.10. Immune functions of FFA2. In neutrophils, SCFA activation of FFA2 promotes chemotaxis, as well as potential survival or apoptosis. In crosstalk with P2Y₂ receptors, FFA2 activation promotes the assembly of NADPH oxidase, and thus superoxide production to combat bacterial infection. In addition, FFA2 activation on neutrophils leads to the release of IL-1 β . In ILC3 cells, FFA2 activation leads to a complementary upregulation of IL-1 receptors (IL-1R), which upon activation leads to the production of IL-22. FFA2 also mediates ILC3 proliferation, as well as the production of further IL-22 through the Akt/ERK1/2/STAT3/ROR γ t axis. FFA2 activation in dendritic cells leads to the production of both retinoic acid (RA) and B-cell activating factor (BAFF), which mediate B cell differentiation into plasma cells. Adipose tissue homeostasis may be regulated through tumour necrosis factor α (TNF α) released by type 2 adipose tissue macrophages upon FFA2 activation. FFA2 may also have a role in the β -arrestin-1-mediated internalisation of the influenza A virus (IAV), acting as a coreceptor. Akt - protein kinase B; ALDH1A2 - aldehyde dehydrogenase 1 family, member A2; AP2B1 - AP-2 complex subunit B; Blimp1 - B-lymphocyte-induced maturation protein-1; ERK - extracellular signal-regulated kinase; IgA - immunoglobulin A; IgG - immunoglobulin G; IL-1 β - interleukin 1 β ; IL-22 - interleukin-22; ILC3 - type 3 innate lymphoid cells; IRF4 - interferon regulatory factor 4; NADPH - reduced nicotinamide adenine dinucleotide phosphate; NLRP3 - NOD-, LRR- and pyrin domain-containing protein 3; P2Y₂ - P2Y purinoreceptor 2; ROS - reactive oxygen species; STAT3 - signal transducer and activator of transcription 3; ROR γ t - RAR-related orphan receptor γ t; SA - sialic acid; XBP1 - X-box binding protein 1. Adapted from Bolognini et al (2021).

1.3.3 Drug development efforts for SCFA receptors

Undoubtedly the pleiotropic physiological responses mediated through FFA2 and FFA3 truly warrant efforts into the development of therapeutic agents targeting these receptors. While SCFAs have been shown to mediate some beneficial effects in human trials (Chambers et al., 2015, Chambers et al., 2018), their characteristics make them inappropriate candidates for intervention in specific diseases. For one, the potency with which they activate their receptors is low, in the millimolar range. In addition, they do not display marked selectivity between FFA2 and FFA3, making them less than ideal tools in tissues where both receptors are expressed and mediate distinct effects. Selective compounds are important not only for therapeutic purposes but also as tool compounds in the effort to dissect the pharmacology of SCFA receptors. The structures of selected compounds for each receptor are shown in *Figure 1.11*.

Understanding the binding mechanism of SCFAs has greatly aided the design of novel compounds. Initially, the sequences of FFA2 and FFA3 were aligned with that of FFA1, which in conjunction with homology modelling and mutagenesis studies helped the identification of a number of conserved residues. Of these, arginine (Arg)¹⁸⁰ in TM5 and Arg²⁵⁵ in TM7, alongside His²⁴² in TM6 were found to be essential for coordinating the binding of the carboxylate group of SCFAs. In FFA3, an additional His in TM4 (His¹⁴⁰) was found to be important for SCFA-mediated responses in certain assays (Stoddart et al., 2008). Since SCFAs only differ in their aliphatic carbon tails, initial efforts aimed at finding more potent alternatives explored SCAs with various aliphatic tails. Although the SCAs identified did not prove to be more potent than SCFAs, they revealed the underlying basis of ligand selectivity between FFA2 and FFA3. That is, FFA3 was preferentially activated by SCAs with sp³-hybridised α -carbons, such as 1-methylcyclopropanecarboxylic acid (**1-MCPC**), while ligands containing sp²- and sp-hybridised α -carbons, such as *trans*-2-methylcrotonic acid (**tiglic acid**) and **2-butynoic acid**, preferred FFA2 (Schmidt et al., 2011). *In vitro*, **2-butynoic acid** and **propionic acid** (which also contains an sp-hybridised carbon), were shown to enhance GSIS in mouse islets, in what appeared to be a FFA2-dependent G $\alpha_{q/11}$ -biased response, albeit with low potency (Priyadarshini et al., 2015). By contrast, **1-MCPC** inhibited GSIS in rat insulinoma cells via G $\alpha_{i/o}$ (Lorza-Gil et al.,

2020). Importantly, **1-MCPC** and **tiglic acid** maintain their selectivity for FFA3 and FFA2, respectively, even in the mouse orthologues. This further corroborates the involvement of the conserved Arg and His residues in orthosteric ligand binding for each of the receptors (Hudson et al., 2012b).

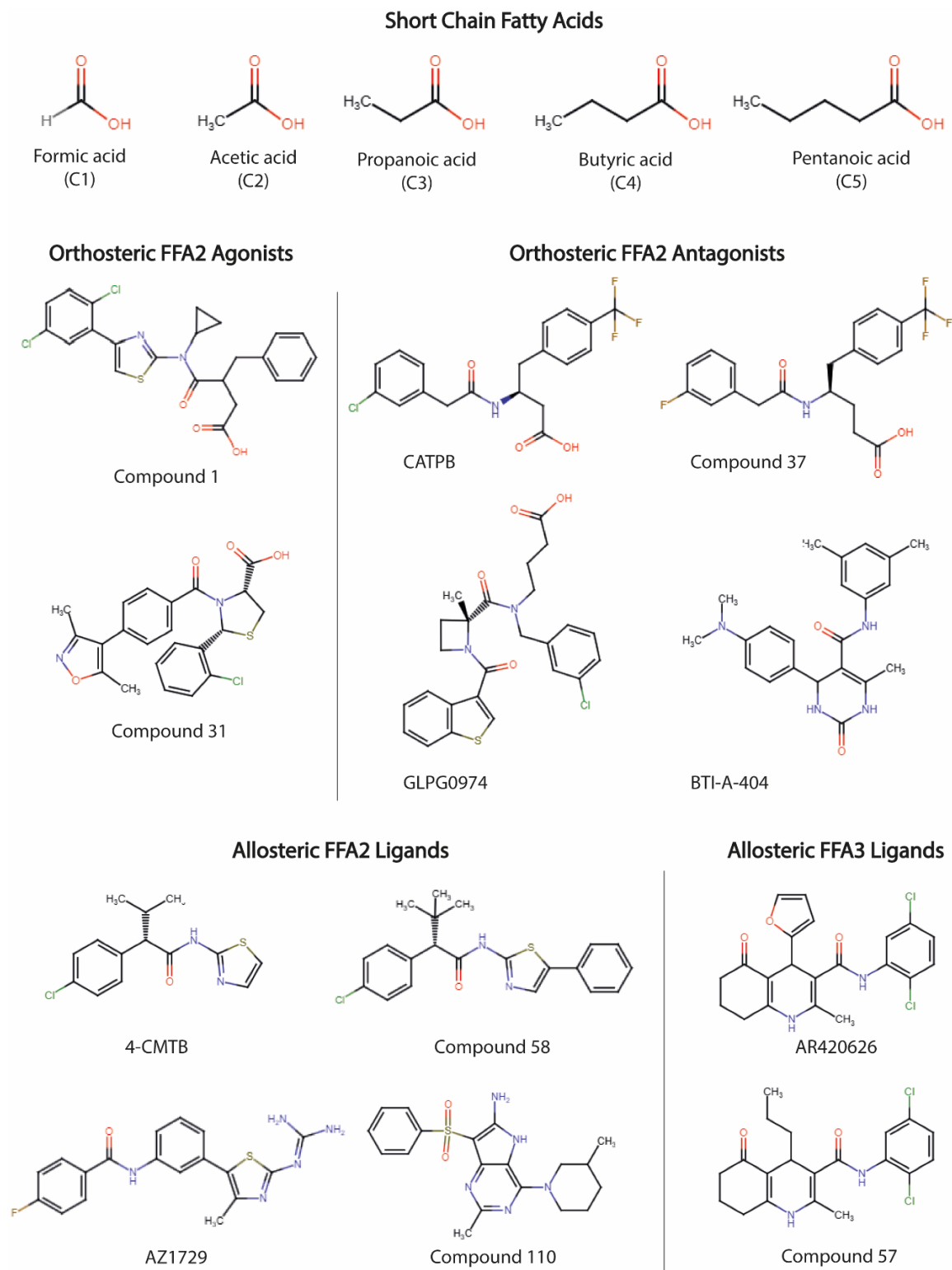


Figure 1.11. SCFA receptor ligands. Chemical structures of short chain fatty acids, which act as endogenous ligands for FFA2 and FFA3, alongside a selection of synthetic ligands for FFA2 and FFA3. Full chemical names are provided in the main text.

Perhaps due to the similarities in the orthosteric binding sites of FFA2 and FFA3, or perhaps due to hitherto undiscovered mechanisms exclusive to FFA3, **1-MCPC** remains to this day the only (somewhat) selective, orthosteric FFA3 ligand. On the other hand, a series of allosteric ligands have been synthesised based on a patent from Arena Pharmaceuticals; the only patent to date for compounds targeting FFA3 (Leonard et al., 2006). One member, **AR420626** (*N*-(2,5-dichlorophenyl)-4-(furan-2-yl)-2-methyl-5-oxo-1,4,5,6,7,8-hexahydro-quinoline-3-carboxamide) has been shown to reduce cAMP *in vitro* (Engelstoft et al., 2013), and to cause a modest increase in GLP-1 release from murine colonic crypts (Nohr et al., 2013). Employing a different member of the series, **FHQC** (4-(furan-2-yl)-2-methyl-5-oxo-*N*-(*o*-tolyl)-1,4,5,6,7,8-hexahydroquinoline-3-carboxamide), has revealed that mutating Arg¹⁸⁰ and Arg²⁵⁵ to alanine (Ala) had no effect on agonist effect, revealing the allosteric mode of binding (Hudson et al., 2014). This is perhaps not surprising, considering the absence of a carboxylate group which is necessary for SCFA binding. Nevertheless, **FHQC** was able to inhibit GSIS in rat insulinoma cells but not in human or mouse islets (Lorza-Gil et al., 2020). Further structure-activity relationship (SAR) exploration based on **FHQC** revealed that minor modifications could significantly change ligand pharmacology. Thus, while **FHQC** acts as an agonistic PAM, other compounds in the series were found to be PAMs, NAMs, or even completely lacking activity (Hudson et al., 2014). Much more recently, Ulven et al (2020) conducted further SAR exploration of **FHQC**, resulting in the synthesis of two compounds with identical potency (measured as cAMP inhibition) but improved solubility: **Compound 57** (*N*-(2,5-dichlorophenyl)-2-methyl-5-oxo-4-propyl-1,4,5,6,7,8-hexahydroquinoline-3-carboxamide) and **Compound 63** (4-cyclopentyl-*N*-(2,5-dichlorophenyl)-2-methyl-5-oxo-1,4,5,6,7,8-hexahydroquinoline-3-carboxamide). In addition, through mutagenesis and homology modelling, Gln¹³¹ was identified as an interacting partner in ligand binding, albeit probably not an exclusive one (Ulven et al., 2020). *Ex vivo*, **Compound 57** has been shown to elevate intracellular Ca²⁺ in DRGs, and also to activate vagal afferents in the proximal colon in an FFA3-dependent manner (Barki et al., 2022).

Interestingly, FFA2 has received significantly more attention in terms of drug development efforts. It is unclear, whether this is due to greater interest in

manipulating the physiological effects mediated by FFA2, or if it is the result of more serendipitous discoveries for this receptor. In fact, several patents have been filed for compounds targeting FFA2, most likely identified through high-throughput screening (HTS). The first of these, filed by the drug discovery company Euroscreen (Hoveyda et al., 2010), identified a compound backbone which yielded the first synthetic agonists for FFA2. Of these, **Compound 1** (3-benzyl-4-(cyclopropyl-(4-(2,5-dichlorophenyl)thiazol-2-yl)amino)-4-oxobutanoic acid) and **Compound 2** ((*R*)-3-(cyclopentyl-methyl)-4-(cyclopropyl-(4-(2,6-dichlorophenyl)thiazol-2-yl)amino)-4-oxobutanoic acid) have been explored in detail (Hudson et al., 2013). While both compounds appeared to be potent activators of both hFFA2 and mFFA2, they lacked this activity at FFA3. As in the case of SCFAs and SCAs, ligand binding was dependent on Arg¹⁸⁰, Arg²⁵⁵ and His²⁴², suggesting that the mode of binding is orthosteric. These compounds also share molecular features of SCFAs, namely the presence of a carboxylate moiety. In fact, replacement of the carboxylate with ester moieties on **Compound 2** resulted in loss of function, indicating the importance of this group in orthosteric agonist function (Hudson et al., 2013). Unlike **Compounds 1** and **2**, which act as full agonists across different assay formats, other compounds from this series display more complex signalling. **Compound 9** ((*S*)-4-(4-(2-chlorophenyl)thiazol-2-ylamino)-4-oxo-3-phenylbutanoic acid) and **Compound 101** (*cis*-2-((4-(2-chlorophenyl)thiazol-2-yl)(methyl)carbamoyl)-cyclohexanecarboxylic acid) thus both act as full agonists in [³⁵S]GTPγS incorporation, as partial agonists in cAMP inhibition and as inverse agonists in yeast-based gene reported assays (Brown et al., 2015). This is particularly surprising, considering that all of these assays investigate Gα_{i/o}-coupled responses. The function of **Compounds 1** and **2** has been demonstrated in physiological assays, leading to the inhibition of lipolysis and secretion of GLP-1 (Hudson et al., 2013). Furthermore, **Compound 14** ((*R*)-3-benzyl-4-((4-(2-chlorophenyl)thiazol-2-yl)(methyl)amino)-4-oxobutanoic acid) was found to activate FFA2 on human neutrophils and inhibit lipolysis in mouse but not in human adipocytes (Brown et al., 2015). Such results may indicate either species-specific receptor activation patterns or reflect differences in ligand selectivity for species orthologues. Indeed, **Compound 2** displayed a 420-fold lower potency at rodent orthologues than at hFFA2 in Ca²⁺-release assays (Hudson et al., 2013). Considering that this difference is only 14-fold for **Compound 1**, the latter is a

more promising tool compound for use *in vivo*. Further attempts at lead optimisation from this series has yielded compounds with improved lipophilicity, such as **Compound 10** ((*R*)-3-(cyclopentylmethyl)-4-(cyclopropyl(4-(2-(6-methoxypyridin-3-yl)phenyl)thiazol-2-yl)amino)-4-oxobutanoic acid). However, this compound was found to display off-target effects in oral glucose tolerance tests (Hoveyda et al., 2018).

In a separate patent by Euroscreen, another agonist series was identified (Hoveyda et al., 2011a). One compound, confusingly also called **Compound 1** ((*2S,5R*)-5-(2-chlorophenyl)-1-(2'-methoxy-[1,1'-biphenyl]-4-carbonyl)-pyrrolidine-2-carboxylic acid), has been explored in *ex vivo* and *in vivo* physiological assays. While this **Compound 1** exerted a beneficial effect on food intake and gut transit in mice fed a HFD, it also decreased glucose tolerance and plasma insulin. Although GLP-1 release was observed *in vivo*, the effects observed were found to be mediated through PYY (Forbes et al., 2015). More recently, this compound was used as a basis for SAR investigations, wherein the pyrrolidine scaffold was replaced by a thiazolidine (Hansen et al., 2018). Of the compound series thus generated, **Compound 31** ((*2R,4R*)-2-(2-chlorophenyl)-3-(4-(3,5-dimethylisoxazol-4-yl)-benzoyl)thiazolidine-4-carboxylic acid) displayed not only increased potency in cAMP inhibition assays, but also an improved pharmacokinetic profile in comparison to **Compound 1**. In physiological assays, this compound was also able to inhibit lipolysis in murine adipocytes, induce chemotaxis in human neutrophils (Hansen et al., 2018), and inhibit GSIS in human pseudo-islets (Lorza-Gil et al., 2020).

Two further patents were also filed by Euroscreen (Hoveyda et al., 2011b, Hoveyda et al., 2015), however these have received little attention to date. On the other hand, novel *in silico* approaches have been utilised to identify novel ligands for FFA2. For this, homology models of FFA2 were generated for virtual screening of large compound libraries. One study identified nearly 300 compounds, of which 28 displayed EC₅₀ below 10 μM in cAMP inhibition assay (Fells et al., 2020). In a separate study, 50 compounds were identified, of which at least one was able to induce GSIS, in an apparent G_{α_{q/11}}-biased manner, with a 100-fold increased potency compared to SCAs previously described as G_{α_{q/11}}-biased (Villa et al., 2017, Priyadarshini et al., 2015). This latter study, however,

did not confirm binding mode or selectivity for FFA2 *in vitro*, therefore the conclusions drawn should be treated with caution.

Although it is of great importance to find orthosteric agonists which mimic the function of SCFAs, allosteric ligands also have a potential both as therapeutic and as tool compounds. In fact, the first compound series produced by Amgen, which has yielded numerous allosteric ligands for FFA2, predates those describing orthosteric ligand backbones (Lee et al., 2008). The phenylacetamide compound series was first identified through HTS, measuring Ca²⁺ mobilisation and cAMP inhibition as indicators of Gα_{q/11} and Gα_{i/o} activation, respectively. One of the lead compounds from this discovery, named **4-CMTB** ((S)-2-(4-chlorophenyl)-3-methyl-N-(thiazol-2-yl)butanamide) has been widely used in research due to its commercial availability and its increased potency in comparison to SCFAs. Mutating the residues associated with the orthosteric binding site (Arg¹⁸⁰, Arg²⁵⁵ and His²⁴²) resulted in no change in **4-CMTB** potency and only insignificant decrease in its efficacy, suggesting an allosteric mode of binding (Smith et al., 2011). In addition to demonstrating significantly higher potency than SCFAs, 4-CMTB has been shown to act as a PAM of potency for SCFAs in [³⁵S]GTPγS incorporation, cAMP inhibition and Ca²⁺ mobilisation assays (Lee et al., 2008). This allosteric effect appeared to be dependent on hFFA2 ECL2, as replacement of this domain with the corresponding segment of hFFA3 ablated PAM effects, while only moderately decreasing **4-CMTB** agonist efficacy (Smith et al., 2011). However, this PAM effect is not clear, due to the lack of cooperativity with thiazolyl-based **Compounds 1** and **2**. In addition, the S-enantiomer of **4-CMTB** only displayed PAM effects at concentrations over 20 μM, while below 1 μM it acted as a NAM of C2 in Ca²⁺-release assays (Schofield et al., 2018). Nevertheless, this compound has been used as a selective FFA2 agonist to demonstrate various physiological responses, including human neutrophil chemotaxis (Vinolo et al., 2011) and GSIS in mouse islets. Interestingly, **4-CMTB** was found to inhibit GSIS at concentrations over 100 μM but promote it at lower concentrations; effects inconsistent with the potencies at which **4-CMTB** can induce each of these pathways *in vitro* (Lorza-Gil et al., 2020). SAR exploration of the initial phenylacetamide series has yielded a number of compounds, of which **Compound 58** ((S)-2-(4-chlorophenyl)-3,3-dimethyl-N-(5-phenylthiazol-2-yl)butanamide; also referred to as CPTB or CFMB) received attention (Wang et

al., 2010). This compound has been used to demonstrate FFA2-mediated physiological responses, including GSIS inhibition in mouse islets (Priyadarshini et al., 2015) GLP-1 release from mouse colonic crypts (Nohr et al., 2013), and inhibition of ghrelin release in mouse gastric mucosal cells (Engelstoft et al., 2013). Much more recently, **Compound 58** has been employed in a series of studies investigating neutrophil priming through FFA2. These studies revealed complex interactions between various orthosteric and allosteric ligands, alongside FFA2 crosstalk with P2Y₂ receptors (Martensson et al., 2018, Lind et al., 2019, Lind et al., 2020, Lind et al., 2021).

A separate compound series was identified by a patent filed by AstraZeneca (Berg and Kolmodin, 2007), resulting in one lead compound to date, **AZ1729** (*N*-[3-(2-carbamimidamido-4-methyl-1,3-thiazol-5-yl)phenyl]-4-fluorobenzamide) (Bolognini et al., 2016). Initial studies revealed that **AZ1729** bound to orthosteric binding site mutants of FFA2 and potently promoted [³⁵S]GTPγS incorporation and cAMP inhibition via both hFFA2 and mFFA2. Interestingly, **AZ1729** was unable induce Gα_{q/11} activation as measured by inositol monophosphate (IP1) accumulation, suggesting Gα_{i/o}-biased signalling. In addition, **AZ1729** was found to act as a PAM of potency for both SCFAs and thiazolyl-based **Compound 1** at hFFA2 in cAMP inhibition assays, while acting as a NAM of efficacy in IP1 accumulation assays, thus displaying Gα_{i/o}-bias in its allosteric effects as well. While maintaining the PAM effect on Gα_{i/o}-mediated responses in mFFA2, at this orthologue **AZ1729** acts as a PAM of potency and efficacy of the Gα_{q/11}-mediated IP1 response. Despite this discrepancy, **AZ1729** has been shown to inhibit lipolysis in primary mouse adipocytes while having no effect on GLP-1 release from mouse colonic crypts, Gα_{i/o}- and Gα_{q/11}-mediated effects, respectively (Bolognini et al., 2016). Investigating the pure agonist effects of **AZ1729** *ex vivo* and *in vivo* would be possible with the use of hFFA2-DREADD-HA mice, as **AZ1729** maintains its effects at this receptor mutant. Recently, Lind et al (2021) explored the interactions of **AZ1729**, **Compound 58**, some their related compounds and a new group of dihydroisoquinolines in neutrophil activation. Through functional studies of pre-sensitisation and subsequent treatment with various combinations of these ligands, it was found that while none of the allosteric ligands induced a response, certain pairings led to NADPH oxidase assembly and superoxide production. Based on these, this

group has proposed a novel model for allosteric FFA2 activation on human neutrophils, suggesting two distinct binding sites for “AZ1729-like” and “Compound 58-like” compounds. This was based on the observation that activation by a ligand could only occur after pre-sensitisation by a ligand from the other group (Lind et al., 2021).

The most recent patent, filed by Takeda Pharmaceutical (Barker et al., 2015), described a series of which two compounds were investigated. **Compound 110** (2-methyl-4-(3-methylpiperidin-1-yl)-7-(phenylsulfonyl)-5H-pyrrolo[3,2-d]pyrimidine-6-amine) and **Compound 187** (4-[(2R,6S)-2,6-dimethylmorpholin-4-yl]-7-(2-fluorobenzenesulfonyl)-2-methyl-5H-pyrrolo[3,2-d]pyrimidin-6-amine) displayed high potency in both cAMP inhibition and Ca²⁺ flux assays, with **Compound 187** showing 18,000-fold and 3,000-fold higher potency than C3 in these assays, respectively. Both compounds were also found to be PAMs of potency in Ca²⁺ flux assays, while acting as PAMs of potency and efficacy in β -arrestin-2 recruitment. *In vivo*, **Compound 110** was found to alleviate the symptoms of a mouse colitis model, while **Compound 187** did not (Park et al., 2022). Although authors suggested this to be the result of selectivity for the human orthologue, no corroborating data has been published.

While activation of FFA2 certainly seems to be important for mediating beneficial effects, the involvement of the receptor in inflammatory processes suggests that antagonists may also hold therapeutic potential in inflammatory diseases. The first antagonist for FFA2 to be reported was based on yet another patent by Euroscreen (Brantis et al., 2011). **CATPB** ((S)-3-(2-(3-chlorophenyl)-acetamido)-4-(4-(trifluoromethyl)phenyl)butanoic acid) has been shown to be a competitive orthosteric antagonist, since increasing concentrations caused a rightward shift in concentration-response curves of C3 and thiazolyl-based **Compounds 1** and **2** (Hudson et al., 2013). In addition, **CATPB** has also been shown to inhibit hFFA2 constitutive activity in [³⁵S]GTP γ S incorporation and cAMP inhibition assays, thus acting as an inverse agonist (Hudson et al., 2012b, Park et al., 2016). *In vitro*, **CATPB** also blocked FFA2-mediated lipolysis in human-derived cell lines. Importantly, **CATPB** was found to be selective for the human orthologue, having no antagonist effects on mFFA2 (Hudson et al., 2013). SAR exploration of **CATPB** has recently yielded a series of compounds with higher

potency. Of these, **Compound 37** ((*R*)-4-(2-(3-fluorophenyl)acetamido)-5-(4-(trifluoromethyl)phenyl)pentanoic acid) displayed a 6-fold increase in potency in [³⁵S]GTPγS incorporation, along with increased solubility and favourable pharmacokinetics (Hansen et al., 2021).

The second antagonist to be described was developed by the biotechnology company Galapagos and was the result of SAR exploration of azetidine scaffold compounds, identified through HTS (Pizzonero et al., 2014). Commonly referred to as **GLPG0974** (4-[[(*R*)-1-(benzo[*b*]thiophene-3-carbonyl)-2-methyl-azetidine-2-carbonyl]-(3-chloro-benzyl)-amino]-butyric acid), this compound was found to competitively inhibit Ca²⁺ flux, [³⁵S]GTPγS incorporation and β-arrestin-2 recruitment through hFFA2 but not through rodent orthologues (Sergeev et al., 2016). **GLPG0974** was also found to inhibit human neutrophil chemotaxis induced by C2, along with activation-dependent expression of cluster of differentiation (CD)11b (Pizzonero et al., 2014). Although the species orthologue selectivity prevented *in vivo* studies, **GLPG0974** was nevertheless entered into clinical trials for the treatment of ulcerative colitis. Despite safety and successful target engagement (measured as reduction in neutrophil activation and flux), the lack of improvement of clinical symptoms has led to these trials being abandoned (Namour et al., 2016, Vermeire et al., 2015). Even though this series has not been further explored to date, **GLPG0974** itself has served as the basis of two important tools for exploring FFA2 pharmacology. For one, by attaching a nitrobenzoxadiazole, a fluorescent tracer molecule, **TUG-1609** (1-(2-(benzo[*b*]thiophen-3-yl)acetyl)-2-methyl-*N*-(4-((3-((7-nitrobenzo[*c*][1,2,5]-oxadiazol-4-yl)amino)propyl)amino)-4-oxobutyl)-*N*-(4-(trifluoromethyl)benzyl)-azetidine-2-carboxamide), was created (Hansen et al., 2017). In conjunction with N-terminally Nanoluciferase (NLuc)-tagged hFFA2, **TUG-1609** can be utilised in BRET-based ligand binding assays. Working under the same principles as radioligand binding, this approach can be utilised to determine the affinity and binding kinetics of novel compounds (Hansen et al., 2017, Hansen et al., 2021). Prior to this, a tritiated radioligand form of **GLPG0974** had been developed, and used to determine hFFA2 ligand kinetics (Sergeev et al., 2016). Importantly, [³H]**GLPG0974** used in combination with mutagenesis and homology modelling has revealed that while Arg¹⁸⁰ and Arg²⁵⁵ are both obligate interactive partners with orthosteric agonists, carboxylate moieties on the antagonists

preferentially interact with one of the two residues. That is, the Arg¹⁸⁰Ala mutant of hFFA2 displayed reduced affinity for **GLPG0974** but not **CATPB**, while the Arg²⁵⁵Ala mutant demonstrated the opposite trend (Sergeev et al., 2016). The same homology model was later used to identify a single lysine (Lys) residue at position 65 which coordinated binding of amide-carbonyls on both **GLPG0974** and **CATPB**. Mutagenesis and [³H]**GLPG0974** radioligand binding were then employed again to confirm that the Lys⁶⁵Arg variation between hFFA2 and mFFA2 was responsible for antagonist species selectivity. The reciprocal Arg⁶⁵Lys mutant of mFFA2 was therefore able to bind [³H]**GLPG0974**, and was shown to gain antagonist function by both **GLPG0974** and **CATPB** (Sergeev et al., 2017).

One further group of moderately potent pyrimidinecarboxamide compounds have been described (Park et al., 2016). Both reported compounds, **BTI-A-404** (4-[4-(dimethylamino)phenyl]-*N*-(3,5-dimethylphenyl)-6-methyl-2-oxo-1,2,3,4-tetrahydro-5-pyrimidinecarboxamide) and **BTI-A-292** (4-[4-(dimethylamino)phenyl]-*N*-(4,5-dimethylphenyl)-6-methyl-2-oxo-1,2,3,4-tetrahydro-5-pyrimidinecarboxamide), were able to reverse SCFA-induced cAMP inhibition and Ca²⁺ mobilisation. In addition, both compounds inhibited constitutive responses, thus acting as inverse agonists. Both compounds significantly increased GLP-1 release *in vitro* in a human-derived cell line. Interestingly, both compounds from this series also display selectivity for hFFA2 (Park et al., 2016). Although neither compound has a carboxylate group, they do have an amide-carbonyl which may facilitate binding to Lys⁶⁵, thus regulating species specificity. Considering that other, more potent antagonists have been established, these compounds are unlikely to be of use without further SAR improvements of the series.

Although there are differences in the structures and potencies of existing antagonists, one important feature seems to be shared by all: selectivity for hFFA2. This is a serious limitation since animal studies constitute an integral part of pre-clinical testing of potential therapeutic agents. Considering that a decade of drug discovery programmes has failed to identify antagonists which act on mFFA2 with affinity close to observed at hFFA2, other approaches had to be applied to overcome this obstacle. For one, the role of Lys⁶⁵ in antagonist binding can be exploited by the use of the Arg⁶⁵Lys mutant of mFFA2. This has been demonstrated *in vitro* (Sergeev et al., 2017), and could conceptually be

the basis for transgenic mouse models. Since the binding of antagonists does not involve either of the residues mutated in hFFA2-DREADD (Sergeev et al., 2016, Hudson et al., 2012a), it would be expected that they retain their antagonist properties at this receptor variant. Indeed, with the use of the hFFA2-DREADD-HA mouse model, **GLPG0974** has been shown to reverse agonist-mediated inhibition of lipolysis (Bolognini et al., 2019) and blocked GLP-1 and PYY release (Barki et al., 2022) *ex vivo*. The desire to create a mouse model in which FFA2 responds to antagonists while maintaining its responsiveness to physiological levels of SCFAs has led to the generation of the hFFA2-HA expressing transgenic mice. **Chapter 3** of this work focuses on the characterisation of this mouse strain, while **Chapter 4** utilises the model for *ex vivo* studies centred around neutrophils.

1.4 Aims

While FFA2 is undoubtedly involved in a range of physiological responses, and by extension in a number of disease conditions, attempts to exploit the receptor therapeutically have been unsuccessful. This may in part be due to the lack of appropriate research tools for the investigation of receptor pharmacology. The work presented herein aims to establish novel tools which can aid understanding of FFA2 signalling and facilitate pre-clinical drug development efforts. Although a number of selective compounds are now available, the species-orthologue selectivity of antagonists limits their use in studies employing traditional rodent models. Thus the question arises: how could these issues be circumvented to improve translatability and clinical outcomes? Could a novel transgenic mouse line bridge the gap between pre-clinical testing and clinical trials? To this end, a novel transgenic mouse line was designed to express hFFA2 C-terminally epitope-tagged with haemagglutinin (HA). **Chapter 3** explores whether hFFA2-HA is expressed in the mouse line, and whether this reflects the expression profile of mFFA2 in WT animals. Once the expression profile of the hFFA2-HA line was established, the ability of the hFFA2-HA receptor to mediate functional responses was evaluated. **Chapter 4** thus investigates whether hFFA2-selective antagonists are able to block agonist-induced responses in bone marrow-derived neutrophils. While G protein-mediated signalling of FFA2 is well-established, its interactions with β -arrestins has received considerably less attention. Since β -arrestins mediate differential cellular responses through other GPCRs (Bradley et

al., 2020) could they do so through FFA2? If so, could biased targeting of such pathways constitute a feasible treatment option for conditions associated with FFA2? How such signalling manifests in hFFA2 and its mutants is explored in **Chapter 5**. The use of novel phosphosite-specific antisera allowed the investigation of FFA2 phosphorylation both *in vitro* and *ex vivo* in neutrophils. By providing a model for potential *in vivo* studies, and by allowing the investigation of tissue-specific phosphorylation, these novel tools will further inform our understanding of FFA2 pharmacology, thus aiding drug development efforts.

CHAPTER 2 - MATERIALS AND METHODS

2.1 Reagents

2.1.1 Pharmacological compounds

[³H]-GLPG0974 ([³H]-4-[[1-(benzo[*b*]thiophene-3-carbonyl)-2-methylazetidine-2-carbonyl]-(3-chlorobenzyl)amino]butyric acid)

[³⁵S]-GTPγS ([³⁵S]-guanosine-5'-O-(3-thio)triphosphate)

2-HTP (2-hexylthiopyrimidine-4,6-diol)

Anacardic acid (2-hydroxy-6-pentadecylbenzoic acid)

AZ1729 (*N*-[3-(2-carbamimidamido-4-methyl-1,3-thiazol-5-yl)phenyl]-4-fluorobenzamide)

CATPB ((*S*)-3-(2-(3-chlorophenyl)-acetamido)-4-(4-trifluoromethyl)phenyl)-butanoic acid)

GLPG0974 (4-[[1-(benzo[*b*]thiophene-3-carbonyl)-2-methylazetidine-2-carbonyl]-(3-chlorobenzyl)amino]butyric acid)

Sodium propionate (C3)

Sorbic Acid (SA) 2,4-hexadienoic acid

2.1.2 Primers

Sequencing:

mFfar2: GGTGGGCACTGAGAACCAAA (forward) and
CCACACGAAGCGCCAATAAC (reverse)

hFfar2: GTGTGGGTCAAGGAGAAGGGATG (forward) and
GCGTAATCTGGAACATCGTACGG (reverse)

B-actin: GACAGGATGCAGAAGGAGATTACTG (forward) and
CTCAGGAGGAGCAATGATCTTGAT (reverse)

Site-directed mutagenesis:

hFFA2-Ser²⁹⁶Ala-Ser²⁹⁷Ala

CTGCGGAATCAGGGCGCCGCCCTGTTGGGACGCAGAG (forward) and
CTCTGCGTCCCAACAGGGCGGCGCCCTGATTCCGCAG (reverse)

hFFA2-Thr³⁰⁶Ala

CGCAGAGGCAAAGACGCTGCAGAGGGGACAAATG (forward) and
CATTGTCCCCTCTGCAGCGTCTTTGCCTCTGCG (reverse)

hFFA2-Thr³¹⁰Ala

CAAAGACGCTGCAGAGGGGGCTAATGAGGACAGGGGTGTG (forward) and
CACACCCCTGTCCTCATTAGCCCCCTCTGCAGCGTCTTTG (reverse)

hFFA2-Ser³²⁴Ala-Ser³²⁵Ala

CAAGGAGAAGGGATGCCAGCAGCGGACTTCACTACAGAG (forward) and
CTCTGTAGTGAAGTCCGCTGCTGGCATCCCTTCTCCTTG (reverse)

2.1.3 Antibodies

Anti-CD11b primary (rabbit; ab184308), **Anti-CD11c primary** (rabbit; ab219799), **Anti-CD3 primary** (rabbit; ab5690), **Anti-CD45 primary** (rabbit; ab208022), **Anti-chromogranin A primary** (rabbit; ab15160), **Anti-GLP-1 primary** (rabbit; ab22625) and **Anti-PYY primary** (rabbit; ab22663) from abcam

Anti-HA high affinity primary (rat; 11867423001) from Sigma-Aldrich

Anti-rabbit IgG AlexaFluor488 secondary (goat; A-11034), **Anti-rabbit IgG AlexaFluor546 secondary** (goat; A-11010), **Anti-rat IgG AlexaFluor488**

secondary (goat; A-11006) and Anti-rat IgG AlexaFluor546 secondary (goat; A-11081) from Invitrogen

Anti-pSer²⁹⁶/pSer²⁹⁷-FFAR2 primary (rabbit; 7TM0226A), Anti-pThr³⁰⁶/pThr³¹⁰-FFAR2 primary (rabbit; 7TM0226B) and Anti-pSer³²⁴/pSer³²⁵-FFAR2 primary (rabbit; 7TM0226C) from 7TM Antibodies

Anti-GFP primary (goat) generated in-house

Anti-rabbit IgG IRDye 800CW secondary (donkey; 926-32213), Anti-goat IgG IRDye 800CW secondary (donkey; 926-32214) and Anti-rat IgG IRDye 800CW secondary (goat; 926-32219) from LICOR

2.1.4 Enzymes

DpnI (*Diplococcus pneumoniae* G41; R0176S) and λ -Protein phosphatase (Bacteriophage lambda, recombinant *E. coli*; P0753S) from New England Biolabs

Micrococcal nuclease (*Staphylococcus aureus*; N3755-50UN) from Sigma-Aldrich

PfuTurbo DNA Polymerase (*Pyrococcus furiosus*; 600250-52) from Agilent Technologies

2.1.5 Other reagents

ATPlite Luminescence Assay kit (6016941), MicroScint-20 (6013621), Ultima Gold XR (6013119) from PerkinElmer

EasySep Mouse Neutrophil Enrichment kit (19762) from Stemcell Technologies

Fast SYBR Green Master Mix (4385612), NuPAGE 4-12%, Bis-Tris Gel (1.0mm) (NP0321BOX), NuPAGE MOPS SDS Running buffer (20 \times) (NP0001) from Invitrogen

Red blood cell lysing buffer Hybri-Max (R7757-100mL), Monoclonal Anti-HA-Agarose antibody (mouse; A2095-1mL), TWEEN-20 (P1379-500mL), Ampicillin sodium salt (A0166-25g), Goat serum donor herd (G6767-100mL), Triton X-100

(T9284-500mL), Paraformaldehyde (P6148-500g), Poly-D-lysine hydrobromide (P6407-5mg), DMEM (high glucose, 4500mg/mL) (D5671-500mL), Trypsin-EDTA (0.25%) (T4049-100mL), Penicillin-Streptomycin solution (10,000U/mL-10mg/mL) (P0781-100mL), L-Glutamine solution (200mM) (G7513-100mL) from Sigma-Aldrich

Pierce BCA Protein Assay kit (23227), Quant-iT PicoGreen dsDNA assay kit (P7589), SYBR Safe DNA gel stain (S33102), Bovine Serum Albumin (standard grade) (BP9702-100) from ThermoFisher

Sodium Bicarbonate (7.5%) (25080-060), RPMI-1640 (no glutamine) (31870-025), RPMI-1640 (no glutamine, no phenol red) (32404-014), HBSS (Ca²⁺, Mg²⁺, no phenol red) (10×) (14065-049), DMEM (high glucose, no pyruvate) (41965-039) from ThermoFisher (Gibco)

QuantiTect Reverse Transcription kit (205311), RNase-free DNase set (79254), RNEasy Mini kit (74104), QIAprep Spin Miniprep kit (27106), QIAGEN Plasmid Maxi kit (12162) from Qiagen

Nano-Glo Dual-Luciferase Reporter Assay System (N113A) from Promega

dNTP Solution mix (N0447S), Gel loading dye (6×) (B7024S), from New England Biolabs

GFP-Trap Agarose kit (gtak-20) from Chromotek

Bovine serum albumin Fraction V (10735086001), cComplete and cComplete Mini EDTA-free protease inhibitor (4693132001, 4693159001), PhosSTOP phosphatase inhibitor (4906845001) from Roche

XL1-Blue Competent Cells (200249) from Agilent Technologies

VECTASHIELD Vibrance mounting medium with DAPI (H-1800-10), ImmEdge Hydrophobic PAP pen (H-4000) from Vector Laboratories

Chameleon Duo Pre-Stained Protein Ladder (928-60000) from LICOR

Tryptone (TRP02), Yeast extract powder (YEA02), Agar (AGA02) from Formedium

Bovine serum albumin (fatty acid-free) (P6156-100gr) from BioWest

Hygromycin B Gold (100mg/mL) (ant-hg-5), Blastcidin (10mg/mL) (ant-bl-1) from InvivoGen

Agarose (1613102) from Bio-Rad Laboratories

Polyethyleneimine (PEI) (P3143-100mL) from Supelco

Amersham Protran 0.45µm nitrocellulose membrane (10600002) from Cytiva Life Sciences

2.1.6 Media, buffers and solutions

Chemotaxis medium - phenol red-free Roswell Park Memorial Institute (RPMI)-1640 supplemented with 0.5% (w/v) FA-free bovine serum albumin (BSA)

Complete medium - RPMI-1640 supplemented with 2mM L-glutamine, 1% (v/v) penicillin/streptomycin (P/S) and 10% (v/v) FA-free BSA

Flp-In T-REx 293 medium - Dulbecco's Modified Eagle's Medium (DMEM) with high glucose and no sodium pyruvate, supplemented with 10% (v/v) foetal bovine serum (FBS), 1% (v/v) P/S, 5µg/mL blastcidin and 200µg/mL hygromycin B Gold

Flp-In T-REx 293 parental medium - DMEM with high glucose and no sodium pyruvate, supplemented with 10% (v/v) FBS, 1% (v/v) P/S and 5µg/mL blastcidin

HEK293T medium - DMEM with high glucose (4500mg/L), supplemented with 10% (v/v) FBS, 1% (v/v) P/S and 2mM L-glutamine

L-Broth medium - 1% (w/v) tryptone, 0.5% (w/v) yeast extract, 171mM NaCl

[³⁵S]GTPγS buffer - 20mM HEPES, 5mM MgCl₂, 100mM NaCl and 0.05% (w/v) FA-free BSA at pH7.5

Lysis buffer - 150mM NaCl, 50mM Tris-HCl, 5mM EDTA, 1% (v/v) Nonidet P-40, 0.5% (w/v) Na-deoxycholat, 0.1% (w/v) sodium dodecyl sulphate (SDS) at pH7.4

MACS buffer - sterile PBS supplemented with 1% (w/v) FA-free BSA and 2mM EDTA

Phosphate-buffered saline (PBS) buffer - 137mM NaCl, 2.7mM KCl, 10mM Na₂HPO₄, 1.8mM KH₂PO₄ at pH7.4

Radioligand binding buffer - 50mM Tris-HCl, 100mM NaCl, 10mM MgCl₂, 1mM EDTA at pH7.4

SDS-PAGE loading buffer - 62.5mM Tris (at pH7.6), 2% (w/v) SDS, 20% (v/v) glycerol, 100mM dithiothreitol, 0.005% (w/v) bromophenol blue

TAE buffer - 40mM Tris-base, 20mM glacial acetic acid, 1mM EDTA at pH8.3

Tris-buffered saline (TBS) buffer - 20mM Tris-HCl, 150mM NaCl at pH7.6

TE buffer - 10mM Tris, 0.1mM EDTA at pH7.4

Transfer buffer - 25mM Tris-Base, 192mM glycine, 20% (v/v) methanol

Antibody solution (WB) - TBS supplemented with 0.1% (v/v) TWEEN and 5% (w/v) BSA

Blocking solution (ICC - HEK) - TBS supplemented with 0.05% (w/v) saponin, 1% (w/v) FA-free BSA and 3% (v/v) goat serum

Blocking solution (ICC - Neutrophils) - PBS or TBS supplemented 4% (v/v) FA-free BSA, 4% (w/v) skimmed milk

Blocking solution (IHC) - PBS supplemented with 0.1% (v/v) TRITON X-100, 10% (v/v) goat serum and 5% (w/v) BSA

Blocking solution (WB) - TBS supplemented with 5% (w/v) BSA

2.2 Molecular biology

2.2.1 Site-directed mutagenesis - generation of hFFA2 PD mutants

In order to introduce specific point mutations into the pcDNA5/FRT/TO-hFFA2-eYFP (enhanced yellow fluorescent protein) construct, the Stratagene QuickChange method was employed. Mutagenesis primers containing the desired base substitution were identified using PrimerX software (<http://www.bioinformatics.org/primerx/>) and custom generated by ThermoFisher Custom DNA Oligos Synthesis Services. Primers thus designed had to be 20-40bp in length, with GC-content below 60% and melting temperature above 75 °C. All primers are listed in **Section 2.1.2**.

For the mutagenesis reaction, template plasmid DNA was diluted to 5ng/μL, and 4μL was added to sterile 500-μL PCR tubes. To each reaction tube, 1.25μL 10mM dNTPs, 1.25μL 10μM forward and 1.25μL 10μM reverse primers were added, alongside 1μL (2.5 units) PfuTurbo DNA Polymerase and 5μL PfuTurbo buffer (10×). Sterile nuclease free water was used to bring the final volume to 50μL.

Amplification was performed in a MasterCycler 5333 thermal cycler, with conditions determined by primer melting temperatures and template size. After initial preheating to 95 °C for 5min, 18 cycles of amplification were performed with 30s denaturation at 95 °C, 1min annealing at 55 °C and 16min extension at 72 °C. Following a final 10min extension at 72 °C, samples were held at 4 °C. Finally, methylated template DNA was digested by incubation with 10U DpnI for 16h at 37 °C.

In the case of the hFFA2-Thr³⁰⁶Ala-Thr³¹⁰Ala mutant, due to the distance between the residues, sequential mutagenesis was employed. As such, the above methods were employed first with the Thr³⁰⁶Ala primers, followed by the Thr³¹⁰Ala primers. Similarly, for “multiple-site” PD mutants, a series of mutagenesis experiments were performed, with confirmed mutant plasmids acting as templates.

2.2.2 Bacterial cloning strategy

In order to express and purify the newly generated plasmids, XL1-Blue Competent Cells (Agilent) were transformed with the mutant plasmid according to the manufacturer's instruction. For this, 100 μ L competent cells were aliquoted into pre-chilled 14-mL Falcon tubes, and 1.7 μ L of β -mercaptoethanol was added to each aliquot. Tubes were chilled on ice for 10min, with the samples swirled gently every 2min. 10 μ L of plasmid DNA was added to the reaction tubes, which were then incubated on ice for 30min. Tubes were subjected to a heat pulse at 42°C for 45s, followed by 2min incubation on ice. Preheated sterile L-Broth medium (LB) (1% (w/v) tryptone, 0.5% (w/v) yeast extract, 171mM NaCl; 42°C) was added at 900 μ L to each tube, and samples were incubated for 1h at 37°C with shaking at 225 revolutions per minute (rpm).

Transformed cells were plated on LB agar plates (LB with 1.5% (w/v) bacto-agar) supplemented with 50 μ g/mL ampicillin. After 16h at 37°C, 7-mL (for Miniprep) or 100-mL (for Maxiprep) LB cultures supplemented with 50 μ g/mL ampicillin were inoculated with single colonies and grown for further 16h at 37°C with shaking at 200rpm.

2.2.3 Plasmid DNA purification

In order to purify mutant plasmids from bacterial cultures, one of two kits was used. Although the same theoretical background underlies both methods, the DNA yield differs. Therefore, Minipreps were utilised to prepare plasmids in the μ g range for initial sequencing, while Maxipreps were used to generate larger quantities of DNA for downstream applications.

Plasmids intended for sequencing were prepared using QIAprep Spin Miniprep kit (Qiagen) according to the manufacturer's instructions. In short, 5mL of the overnight bacterial culture was centrifuged at 6800 \times g for 3 min at room temperature (RT). The bacterial pellet was resuspended in 250 μ L Buffer P1 (supplemented with RNase A; 1:100 dilution), followed by the addition of 250 μ L Buffer P2. After the solution became clear, 350 μ L Buffer N3 was mixed with the sample, and the tube was centrifuged for 10min at 17,900 \times g. Supernatant was added at 800 μ L to a QIAprep 2.0 spin column and centrifuged for 1min at

17,900×g. Flow-through was discarded, and the column was washed with 750µL Buffer PE. After two 1min centrifugations at 17,900×g, the spin column was transferred into a clean 1.5-mL microcentrifuge tube. DNA was eluted into a sterile microcentrifuge tube by adding 50µL nuclease-free water to the centre of the spin column, followed by 1min incubation at RT, and a subsequent 1min centrifugation at 17,900×g. If not used immediately, samples were stored at -20°C. The sequences of samples purified by this method were confirmed by sequencing as described in **Section 2.2.4**.

For downstream applications, plasmids were purified using QIAGEN Plasmid Maxi kit (Qiagen) according to the manufacturer's instructions. In short, 100-mL overnight cultures were harvested by two consecutive centrifugations in 50-mL Falcon tubes at 6000×g for 15min at 4°C. Bacterial pellets were resuspended in 10mL Buffer P1 (supplemented with RNase A; 1:100 dilution). Next, 10mL of Buffer P2 was added, followed by 5 vigorous inversions of the tube to mix the reaction components. After 5min incubation at RT, 10mL chilled Buffer P3 was added, mixed by 5 vigorous inversions, and the reaction was incubated on ice for 20min. Samples were centrifuged at maximum velocity for 15min at 4°C, after which the supernatant was transferred to a clean 50-mL Falcon tube, and centrifuged for a further 15min at 4°C. In the meantime, an appropriate number of QIAGEN-tip 500's were equilibrated with 10mL Buffer QBT, allowing emptying by gravity flow. Supernatant from the centrifuged samples was transferred to the QIAGEN-tip and allowed to move through the resin. QIAGEN-tips were subsequently washed twice with 30mL Buffer QC, again allowing emptying by gravity flow. DNA was eluted into clean 50-mL Falcon tubes using 15mL Buffer QF, followed by precipitation by the addition of 10.5mL isopropanol. Samples were centrifuged at maximum velocity for 30min at 4°C. The DNA pellet was washed with 5mL 70% ethanol (EtOH) and centrifuged for 10min at maximum velocity. The DNA pellet was air-dried for 10min, followed by resuspension in 1mL sterile water. Plasmids thus purified were utilised for the generation of stably transfected Flp-In T-REx 293 cells (**Section 2.3.2**) and the transient transfection of Human embryonic kidney cell line 293T (HEK293T) cells (**Section 2.3.3**).

2.2.4 Sequencing

In order to confirm the success of mutagenesis, plasmid DNA purified by Minipreps were sequenced. Sequencing was performed by the MRC PPU DNA Sequencing and Services (Medical Sciences Institute, School of Life Sciences, University of Dundee, Scotland; <https://dnaseq.co.uk/>) with the use of Applied Biosystems 3730 automated capillary DNA analyser. Primers targeting sequences flanking the sequence of interest were utilised: the CMV promoter for the forward and the bGH-poly(A) signal for the reverse primer. Resulting sequences were analysed using the SnapGene Software (Version 5.1.5; Dotmatics).

2.3 Cell culture

2.3.1 Mammalian cell line maintenance

All cell culture work was conducted under sterile conditions, in class II biosafety cabinets.

HEK293T cells were maintained in DMEM with high glucose (4500mg/L), supplemented with 10% (v/v) FBS, 1% (v/v) P/S and 2mM L-glutamine at 37°C and 5% CO₂.

Parental Flp-In T-REx 293 cells were maintained in DMEM with high glucose and no sodium pyruvate, supplemented with 10% (v/v) FBS, 1% (v/v) P/S and 5µg/mL blasticidin at 37°C and 5% CO₂. In the case of stably transfected Flp-In T-REx 293 cell lines, the above medium was also supplemented with 200µg/mL hygromycin B Gold.

In order to passage cells, the medium was first aspirated from the 75cm² flask. Cells were washed once with sterile PBS (137mM NaCl, 2.7mM KCl, 10mM Na₂HPO₄, 1.8mM KH₂PO₄ at pH7.4), followed by incubation with sterile-filtered trypsin-EDTA (0.25%) at RT for 2-5min. Fresh cell culture medium was added in order to terminate proteolytic cleavage, and detached cells were suspended. The cell suspension was centrifuged at 300×g for 5min at RT, and the resulting pellet was resuspended in fresh culture medium. Depending on the desired dilution of cells, varying volumes of the suspension were added to a new 75cm² flask or 10cm dish containing appropriate volume of fresh cell culture medium.

For medium- and long-term storage, cell lines were cryopreserved at -80°C or at -150°C , respectively. For this, cell culture medium was first removed from the flask. Cells were washed, then incubated with 0.25% sterile-filtered trypsin-EDTA at RT for 2-5min. Detached cells were suspended in fresh cell culture medium in order to terminate proteolytic cleavage. The suspension was centrifuged at $300\times g$ at RT for 5min. The resulting pellet was resuspended in 3mL FBS with 10% (v/v) dimethyl sulfoxide (DMSO). The suspension was transferred to cryogenic tubes to make 1-mL aliquots, which were then stored at -80°C and subsequently transferred to -150°C . In order to recover cells from long-term storage, aliquots were thawed in a water bath at 37°C , followed by transfer into a flask containing fresh cell culture medium. Medium was replaced with fresh cell culture medium after 4-5h in order to remove residual DMSO.

2.3.2 Generation of stably transfected Flp-In T-REx 293 cell lines

In Flp-In T-REx 293 cell lines, stable expression of the desired receptor construct is induced by the addition of doxycycline (DOX), as expression is under the control on the *tet* repressor cassette. Flp-In T-REx 293 parental cells were co-transfected with pcDNA5/FRT/TO expression vectors with the gene of interest and the pOG44 plasmid. Flp recombinase expressed from the pOG44 plasmid catalyses the recombination between FRT sites in the expression vector and the host parental cells.

In short, Flp-In T-REx 293 parental cells were cultured to 60% confluence in 10cm cell culture dishes. The pcDNA5/FRT/TO expression vector and pOG44 were diluted at a 1:9 ratio, as a total amount of $8\mu\text{g}$ DNA, along with $48\mu\text{L}$ PEI (1:6 dilution), in 150mM sterile NaCl to make a final volume of $500\mu\text{L}$. Negative controls without the pcDNA5/FRT/TO expression plasmid were also included. After vortexing, the reaction between PEI and the plasmid DNA was allowed to progress for 10min at RT. Fresh Flp-In T-REx 293 parental culture medium was added to the culture dishes, followed by dropwise addition of the $500\mu\text{L}$ reaction mixture. After 24h, medium in the cell culture dishes was replaced, in order to avoid the cytotoxic effects of PEI. Following 48h, cells were removed using sterile-filtered trypsin-EDTA (0.25%), and seeded into 75cm^2 flasks at 1:10, 1:15 and 1:20 ratios. After a further 24h, Flp-In T-REx 293 parental medium was

replaced with Flp-In T-REx 293 maintenance medium (containing hygromycin), allowing for selection of transfected cell, as these possess hygromycin resistance. Cell culture medium was replaced every 2-3 days, until colony formation could be observed without the use of a microscope (14-28 days). Cells were detached using 0.25% trypsin-EDTA, and colonies were combined, yielding polyclonal cell lines. Expression of the integrated mutant genes could be induced by incubation with 100ng/mL DOX for 16-24h. In order to confirm successful transfection, cells were visualised under the epifluorescent Nikon ECLIPSE Ti microscope equipped with a mercury light source and an eYFP filter set.

2.3.3 Generation of transiently transfected cell lines

For transient transfection, HEK293T cells were plated onto 10cm cell culture dishes and incubated for 24h at 37°C and 5% CO₂, until approximately 60% confluency was reached. Plasmid DNA was diluted at 5µg in 250µL of 150mM sterile NaCl, then added to 30µg PEI diluted in 250µL of 150mM sterile NaCl. The DNA mixture was vortexed and incubated for 10 min at RT, then added to the cell culture dishes in a dropwise fashion. Cells were incubated for further 24h at 37°C and 5% CO₂ before downstream application.

2.4 Animals

2.4.1 Source

Transgenic mice were previously generated in a C57BL/6N genetic background, using a knock-in approach as described by Bolognini et al (2019). In summary, a HA-tagged version of hFFA2 or hFFA2-DREADD was knocked into the mouse *Ffar2* locus under the control of the LoxP-flanked stop cassette, producing the minus-CRE mouse line. These mice were utilised as functional FFA2 KO mice. Mice which constitutively express hFFA2-HA or hFFA2-DREADD-HA were produced from the cross-breeding of the respective minus-CRE mice with Cre-recombinase-expressing mice. Mice were bred as homozygous.

WT mice had a C57BL/6N genetic background. FFA2-KO mice were obtained from AstraZeneca.

2.4.2 Mouse maintenance

Mice were maintained in individually ventilated cages, on a 12h dark-light cycle and were fed a normal chow diet *ad libitum*. Unless otherwise stated, male and female animals at 12-20 weeks old were used.

2.4.3 Ethics statement

Mice were maintained under the project licences 70/8473 and PP0894775 held by Professor Andrew B. Tobin at the University of Glasgow. Animals were culled humanely in accordance with Schedule 1 of the Animals (Scientific Procedures) Act 1986. Regulated procedures were performed by personal licence holders under the same project licence.

2.5 Gene expression analysis

2.5.1 RNA extraction

Male mice (15-20 weeks old) were sacrificed, and samples were taken from the epididymal adipose, proximal colon, liver, lungs, pancreas and spleen, and stored immediately on dry ice, then stored at -80°C until utilised. Neutrophils isolated using the EasySep method (described in **Section 2.6.1**) were centrifuged at $300\times g$ for 5min at 4°C and the pellet containing the neutrophils was resuspended in RLT buffer (Qiagen) with 1:100 dilution of β -mercaptoethanol, then stored at -80°C . After thawing on ice, other tissues were weighed and a sample of 30mg was placed in a clean 2-mL RNase-free microcentrifuge tube. RNA was extracted from the tissues using the RNEasy Mini kit (Qiagen) according to the manufacturer's instructions. In short, for every 30mg of tissue, 600 μL of RLT buffer (with 1:100 β -mercaptoethanol) was added to the tubes, along with two 5-mm stainless steel beads. Tissues were disrupted and homogenised using the TissueLyser LT (Qiagen) at 50Hz for 10min at RT. After allowing the samples to settle, supernatant was transferred to new 2-mL microcentrifuge tubes and centrifuged at full speed for 2min. In a clean tube, 600 μL of the supernatant was mixed with 600 μL of 70% EtOH. The mixture was transferred to a mini-column and centrifuged at $8,000\times g$ for 30s; this step was repeated after the disposal of the flow-through. RW1 buffer was added at 350 μL per column, and centrifuged at $8,000\times g$ for 30s, followed by the discard of the flow-through. For on-column

DNA digestion using the Qiagen RNase-free DNase set, 80 μ L of DNase I (Qiagen; 1:8 dilution in buffer RDD) was added to each column membrane, followed by 15min incubation at RT. Further 350 μ L RW1 buffer was added to each column, followed by centrifugation at 8,000 \times g for 30s. After discarding the flow-through, 500 μ L of RPE buffer (1:5 dilution in 98% EtOH) was added to each column, followed by centrifuging at 8,000 \times g for 30s. After the addition of a further 500 μ L of RPE buffer, the columns were centrifuged for 2min at 8,000 \times g. The columns were subsequently replaced into new collection tubes and centrifuged at 8,000 \times g for 1min. Columns were then replaced into a clean 1.5-mL collection tube and the column membranes were hydrated for 5min with 30-50 μ L RNase-free water. RNA was eluted by centrifuging at 8,000 \times g for 2min and samples were placed on ice until further use. RNA was quantified using the NanoDrop 2000 spectrophotometer (ThermoFisher).

2.5.2 Agarose gel electrophoresis

In order to assess RNA quality, 1% (w/v) agarose solution was prepared in TAE buffer (40mM Tris-base, 20mM glacial acetic acid, 1mM EDTA at pH8.3) and heated in a microwave oven for 2min. SYBR Safe DNA gel stain (ThermoFisher) was added to the solution at a 1:10,000 dilution. The mixture was poured into the Horizon58 gel casting system (Life Technologies) and allowed to solidify for 30min. RNA samples were prepared as a 100ng/ μ L dilution in RNase-free water, with 1:6 dilution of purple gel loading dye (New England BioLabs) added. The gel casting system was filled with TAE buffer, covering the solidified agarose gel. RNA samples were loaded onto the gel at 6 μ L/well and run at 100V for 15min. The gel was imaged using the Gel Doc 2000 (BioRad) system.

2.5.3 Reverse transcription

In order to produce complementary DNA (cDNA) from the isolated RNA samples, QuantiTect Reverse Transcription kit (Qiagen) was employed according to the manufacturer's instructions. In short, 1 μ g of RNA was added to 2 μ L of gDNA Wipeout Buffer and RNase-free water to make up a total reaction volume of 14 μ L. Using the MasterCycler 5333 thermal cycler, the reaction was heated to 42 $^{\circ}$ C for 2 min, followed by immediate cooling to 4 $^{\circ}$ C. The reverse transcription master mix was prepared as a 1:4:1 mixture of Quantiscript reverse transcriptase

(RTase), Quantiscript RTase buffer and RTase primer mix, and was added at 6 μ L per tube to the DNA Wipeout reactions. The reaction tubes were subsequently heated to 42 $^{\circ}$ C for 15min, followed by 3min at 95 $^{\circ}$ C. Samples were cooled to 4 $^{\circ}$ C and used immediately for qRT-PCR or stored at -20 $^{\circ}$ C.

2.5.4 Quantitative reverse transcription polymerase chain reaction

In order to quantify cDNA, a quantitative reverse transcription polymerase chain reaction (qRT-PCR) approach was taken. Sequencing primers were identified using SnapGene Software (Version 5.1.5; Dotmatics) and sequence information from hFFA2-HA and mFFA2. Primers thus target ECL2 (forward) and TM5 (reverse) on mFFA2, and the C-terminus (forward) and the HA-tag (reverse) on hFFA2-HA. As a housekeeping gene, mouse β -actin was targeted with primers designed in the same manner. All sequencing primers were synthesised by ThermoFisher Custom DNA Oligos Synthesis Services and are listed in full in *Section 2.1.2*.

Fast SYBR Green mix (Invitrogen) was prepared according to the manufacturer's instructions, as 5 μ L SYBR Green Master Mix, 0.2 μ L forward primer (10 μ M), 0.2 μ L reverse primer (10 μ M) and 2.6 μ L RNase-free water for each sample. Diluted cDNA samples were loaded at 2 μ L/well to a MicroAmp 384-well plate (ThermoFisher), followed by the addition of 8 μ L of SYBR Green mix to each well. Plates were sealed using MicroAmp optical adhesive film, and centrifuged briefly at 1,200rpm.

The qRT-PCR measurements were conducted using the QuantStudio 7 Flex RT-PCR system (ThermoFisher). After initial preheating to 95 $^{\circ}$ C for 20s, 40 cycles of PCR were performed with 1s denaturation at 95 $^{\circ}$ C and 20s annealing at 60 $^{\circ}$ C. This was followed by 15s heating at 95 $^{\circ}$ C, 60s annealing at 60 $^{\circ}$ C and finally a slow increase to 95 $^{\circ}$ C, during which time data for melting curves was collected. After 15s at 95 $^{\circ}$ C, plates were cooled to RT.

In order to generate standard curves for each of the primers, 1 in 4 serial dilutions of colon cDNA samples were prepared using nuclease-free water. In order to quantify gene expression, cDNA samples from each tissue were diluted 1 in 3 using nuclease-free water. Comparative cycle threshold (C_T) values were

obtained using the QuantStudio Real-Time PCR Software (Version 1.3; ThermoFisher). Data analysis was performed as described in **Section 2.10.1**.

2.6 Ex vivo pharmacological assays

2.6.1 Neutrophil isolation

Following culling by cervical dislocation, the hind legs of mice were collected and stored on ice in Complete medium (RPMI-1640 supplemented with 2mM L-glutamine, 1% (v/v) P/S and 10% (w/v) FA-free BSA). The muscles and connective tissue were removed from the femur and tibia, and the clean bones were stored in ice cold RPMI-1640 medium (10% (w/v) FA-free BSA, 1% (v/v) P/S).

All subsequent steps were performed under sterile conditions in a class II biosafety cabinet.

Following the removal of the epiphyses of the bones, a syringe with a 25G needle was used to flush the bones with Complete medium. Bone marrow cells were resuspended and passed through a 70- μ m cell strainer. The cell suspension was centrifuged at 300 \times g for 5 min at 4°C, followed by resuspension in Hybri-Max red blood cell lysis buffer (Sigma-Aldrich) for 1min. The lysis step was terminated by washing with 10mL Complete medium and centrifuging at 300 \times g for 5 min at 4°C twice. Cells were resuspended and counted with the use of a haemocytometer, followed by final centrifugation at 300 \times g for 5 min at 4°C.

In order to isolate neutrophils from the full complement of bone marrow cells, a negative selection approach was used. Specifically, the EasySep™ Mouse Neutrophil Enrichment Kit (Stemcell Technologies) was utilised in accordance with the manufacturer's instructions. In short, bone marrow cells were diluted to 100,000,000 cells/mL in MACS buffer (1% (w/v) FA-free BSA and 2mM EDTA in sterile PBS). Mouse Neutrophil Enrichment Cocktail was added at 50 μ L/mL of cells and incubated for 15min at 4°C. Samples were washed by adding MACS buffer to reach 15mL volume, and centrifugation at 300 \times g for 10min at RT. Cells were resuspended in MACS buffer at 100,000,000 cells/mL. Biotin Selection Cocktail was added to the cell suspension at 50 μ L/mL, followed by 15min incubation at 4°C. Following thorough vortexing, EasySep D Magnetic Particles were added to the cell suspension, at 150 μ L/mL cells, followed by a further

10min incubation at 4°C. Depending on the volume of the sample, MACS buffer was added to bring the final volume to 5mL or 10mL. The 15-mL tube containing the cell suspension was placed in the “Big Easy” EasySep Magnet without a lid and incubated at RT for 5min. When turning upside down, the magnet retains the magnetically tagged cells, and the untagged neutrophils can be collected in a new 15-mL tube. Isolated neutrophils were counted in MACS buffer using a haemocytometer. Neutrophils were centrifuged at 300×g for 5min at RT and resuspended according to downstream application.

2.6.2 Neutrophil chemotaxis (ATPlite assay)

Drug preparation, treatment and chemotaxis were performed under sterile conditions in a class II biosafety cabinet.

Assay method (including time-points) was adapted from Bolognini et al. (2016) and optimised for a 96-well format. Agonist were prepared at 2× concentration in Chemotaxis medium (phenol red-free RPMI-1640 supplemented with 0.5% (w/v) FA-free BSA) and were added to the bottom wells of a Corning HTS Transwell 96-well plate at 118µL in the presence of the same volume of Chemotaxis medium or 2µM AZ1729 (1µM final concentration). 1µM 2-HTP (final concentration), a GPR84 agonist and a moderate chemotactic agent, was used as positive control in these experiments. The covered plate was allowed to equilibrate with compounds for 5min at 37°C. Isolated neutrophils were resuspended in Chemotaxis medium and, in the case of antagonist experiments, were preincubated with vehicle or 1µM CATPB for 15min at 37°C (with 5% CO₂). Neutrophils were then added to the middle well of the Transwell 96-well plate insert at 220,000 cells/well, in a volume of 75µL. The plate was covered and incubated for 90min at 37°C (with 5% CO₂) in order to allow the chemotaxis of neutrophils.

The extent of neutrophil migration was quantified using the ATPlite luminescence ATP detection kit (PerkinElmer) according to the manufacturer’s instructions. In short, 100µL of the suspension was moved from the bottom wells of the Transwell 96-well plate to a white 96-well plate. Mammalian cell lysis solution was added to each well at 50µL, followed by 5min in an orbital shaker at 100rpm. Substrate solution was also added at 50µL/well. Plates were covered

in foil, in order to avoid exposure of the light-sensitive substrate, followed by a further 5min of shaking at 90rpm. The plates were transferred to a PHERAstar FS microplate reader (BMG Labtech), and after 10min of equilibration, total luminescence was measured.

2.6.3 Neutrophil extracellular trap quantification

Drug preparation, treatment and NET formation were performed under sterile conditions in a class II biosafety cabinet.

In order to measure neutrophil extracellular trap (NET) production in response to FFA2 ligands, double-stranded DNA (dsDNA), was quantified using methods (including time-points) described previously by Hollands et al (2016). In short, isolated neutrophils were resuspended in Hank's Balanced Salt Solution (HBSS; with $\text{Ca}^{2+}/\text{Mg}^{2+}$) and added to a 96-well cell culture plate at 200,000 cells/well. Compounds were prepared in HBSS at a 10 \times concentration and added to the wells, along with HBSS to make up a final volume of 200 μL . In the case of inhibition assays, neutrophils were pre-incubated with the antagonists for 15min at 37 $^{\circ}\text{C}$ (with 5% CO_2), before the addition of the agonist. After the addition of the agonist, the plate was incubated for 2h at 37 $^{\circ}\text{C}$ (with 5% CO_2).

In order to cleave the produced dsDNA, 50 μL of 1mU/ μL *Staphylococcus aureus* micrococcal nuclease was added to each well, followed by incubation at 37 $^{\circ}\text{C}$ (with 5% CO_2) for a further 10min. To halt the cleavage, 50 μL EDTA was added to each well at a final concentration of 5mM. The plate was centrifuged for 8min at 200 $\times g$ at RT. From the supernatant in each well, 100 μL was transferred to a black-bottom 96-well plate. For the quantification of dsDNA, 100 μL of the Quant-iT reagent (diluted 1:200 in TE buffer (10mM Tris, 0.1mM EDTA at pH7.4)) was added to each well. After a 5min incubation in the dark at RT, fluorescence intensity was measured at 490nm excitation and 525nm emission using the PHERAStar FS microplate reader.

2.7 *In vitro* functional assays

2.7.1 Membrane preparation

Stably transfected Flp-In T-REx 293 cells were cultured in 10-cm dishes to confluency. In order to induce the expression of the receptor of interest, cultures were treated with 100ng/mL DOX for 16-24h under sterile conditions. Following a wash with ice cold PBS, cells were detached by scraping in the presence of 2mL non-sterile PBS. Cell suspensions were centrifuged at 450×g for 5min at 4°C and incubated at -80°C for a minimum of 30 min. Pellets were resuspended in ice cold TE buffer containing cOmplete Protease Inhibitor Cocktail (EDTA-free; Roche). The cell suspension was passed through a 5-mL handheld homogeniser 50×, followed by passing through a 25G needle 5×. Cell debris was pelleted by centrifugation at 450×g for 5 min at 4°C and the resulting supernatant was subsequently transferred to ultracentrifuge tubes and centrifuged at 90,000×g for 45 min at 4°C. The pellet containing the membranes was resuspended in TE buffer (with protease inhibitor) and passed through a 25G needle 5×. Membrane protein concentration was determined using a Bicinchoninic acid (BCA) assay, as described in **Section 2.7.2**. Membranes were either used immediately or aliquoted and stored at -80°C.

Neutrophil membranes were prepared following the methods described by Varani et al (1998). The isolated neutrophil pellet was resuspended in 1mL 50mM Tris-HCl (pH7.4) supplemented with 10mM MgCl₂, transferred to a sterile microcentrifuge tube, and centrifuged at 11,000×g for 15 min at 4°C. The cells were resuspended in 1mL 50mM Tris-HCl, centrifuged at 11,000×g, and finally resuspended in 500µL 50mM Tris-HCl. Cells were finally passed through a 25G needle 5×. Membrane protein concentration was determined using a BCA assay (**Section 2.7.2**). Membranes were aliquoted and stored at -80°C.

2.7.2 Determination of protein concentration (BCA Assay)

Protein concentration of prepared membranes was quantified using the Pierce BCA Protein Assay kit (ThermoFisher) according to the manufacturer's instructions. For this, a standard curve of 0.2-2.0µg/µL BSA was added to a clear 96-well plate at 10µL/well. Membrane samples were diluted (1:2 to 1:5) and added at 10µL/well to the same 96-well plate. BCA Reagent B was diluted in BCA

Reagent A at a 1:50 ratio and was added to each of the BSA standards and membrane samples at 200 μ L/well. The plate was incubated at 37°C for 20 min, followed by measurement of absorbance at 562nm using a POLARStar Omega microplate reader (BMG Labtech). Sample concentrations were interpolated from the BSA standard curve and multiplied by the dilution factor in order to calculate protein concentrations. Protein concentrations thus determined were used to calculate the amount of membranes to be used in *in vitro* assays.

2.7.3 [³⁵S]-GTP γ S incorporation assay

The [³⁵S]-GTP γ S incorporation assay was employed in order to measure G α_i -mediated signalling. As the terminal S substitution renders this analogue of GTP non-hydrolysable, GTP γ S remains bound to G α_i upon G protein activation. By quantifying the accumulation of the [³⁵S]-radiolabelled form, the extent of G α_i activation by GPCRs can be quantified. Methods (including incubation times) were adapted from Sergeev et al. (2017). Buffer conditions were optimised for improved signal.

In a 96-deep well plate, membranes prepared from Flp-In T-REx 293 cells or from mouse-derived neutrophils were added at 5 μ g/well to assay buffer (20mM HEPES, 5mM MgCl₂, 100mM NaCl, 0.05% (w/v) FA-free BSA at pH7.5) containing a range of agonist concentrations (prepared at 10 \times concentrations). In order to assess antagonists, membranes were preincubated with a range of antagonist concentrations (prepared at 10 \times) for 15 min at RT, followed by the addition of EC₈₀ concentration of the agonist. The reaction was initiated by the addition of 50nCi/well of [³⁵S]GTP γ S in assay buffer supplemented with 1 μ M GDP and 30 μ g/ μ L saponin. The plate was incubated for 1h at 30°C, after which the reaction was terminated by rapid filtration through UniFilter-96 GF/C glassfibre filter-bottom plates (PerkinElmer) pre-soaked in ice-cold PBS using a FilterMate 96-well Harvester (PerkinElmer). Filter plates were washed 3 \times with ice-cold PBS in order to remove unbound [³⁵S]GTP γ S. After drying for a minimum of 2 h at RT, MicroScintTM-20 scintillation cocktail (PerkinElmer) was added at 50 μ L/well. [³⁵S]GTP γ S incorporation was quantified as counts per minute (CPM) over 5 min, using a TopCount NXT scintillation counter (Packard). CPM was normalised and plotted against log ligand concentrations using GraphPad Prism Software (Version

8.4.3; Dotmatics). Agonist and antagonist curves were fitted as described in **Section 2.10.4**. Cooperativity was explored by the use of an allosteric operational model, as described in **Section 2.10.5**.

2.7.4 Heterologous [³H] radioligand binding assay

Radioligand binding methods (including incubation times) were adapted from Sergeev et al. (2017). Buffer conditions were optimised for improved signal. Assays were conducted using glass tubes, and a final assay volume of 200 μ L for saturation binding and 1mL for single concentration binding. In each case, after 2h incubation with the radioactively labelled antagonist [³H]GLPG0974 at 25 $^{\circ}$ C, reactions were terminated by rapid filtration with a 24-well semi-automated harvester (Brandel). Filters were washed with ice-cold PBS in order to remove unbound radioligand and were left to dry overnight. Filters were deposited into 6-mL scintillation vials, along with 3mL Ultima Gold XR scintillation cocktail. Standards containing equivalent amount of [³H]GLPG0974 were also set up in 6-mL scintillation vials. Total and non-specific binding of [³H]GLPG0974 was quantified as disintegrations per minute (DPM) using the Tri-Carb 2910TR liquid scintillation counter (PerkinElmer). DPM data was transformed based on standard measurements and the known activity of [³H]GLPG0974:

$$\frac{\text{Standard (DPM)}}{\text{Specific activity } (50.16 \frac{\text{DPM}}{\text{fmol}})} \times \frac{1}{\text{Assay volume (200}\mu\text{L)}} = \frac{\text{fmol}}{\mu\text{L}} = \frac{\text{nmol}}{\text{L}} = \text{nM}$$

Specific binding was then calculated by subtracting non-specific binding from total binding.

Saturation binding

In saturation binding assays, 5 μ g of membranes prepared from Flp-In T-REx 293 cells induced to express hFFA2-eYFP were added in 40 μ L binding buffer (50mM Tris-HCl, 100mM NaCl, 10mM MgCl₂, 1mM EDTA at pH7.4). Vehicle or 10 μ M CATPB was added in 20 μ L in order to measure total and non-specific binding, respectively. Finally, varying concentrations of [³H]GLPG0974 were added to the assay in 100 μ L binding buffer.

Saturation binding curve was fitted as described in *Section 2.10.3*.

Single concentration binding

In order to determine binding to neutrophils, 50µg of mouse neutrophil membranes were utilised at a concentration of 0.25µg/µL in binding buffer. Vehicle or 10µM CATPB was added to the assay in 100µL, and 20nM [³H]GLPG0974 was added in 500µL binding buffer to make up a final assay volume of 1mL.

2.7.5 BRET-based β-arrestin-2 recruitment assay

HEK293T cells were transiently transfected (as described in *Section 2.3.3*) at a 1:100 ratio with pcDNA5/FRT/TO plasmids containing eYFP-tagged receptor constructs and with pcDNA5 plasmid containing NLuc-tagged β-arrestin-2. As a control, one 10cm dish was co-transfected with NLuc-β-arrestin-2 and an empty pcDNA5 vector. After 24h of incubation, cells were detached from the dishes and resuspended in 20-40mL HEK293T cell culture medium. White 96-well plates were covered with 40µL of 50µg/mL Poly-D-lysine hydrobromide (PDL; diluted from 1mg/mL stock using HEK293T cell culture medium) and left to incubate for 15min at RT. Following the removal of PDL, 100µL of the cell suspension was added to each well.

After further 24h incubation at 37°C and 5% CO₂, the medium was aspirated, and the wells were washed with 100µL HBSS. In order to reach a final assay volume of 100µL, 80µL HBSS was added to each well and incubated for 30min at 37°C. Nano-Glo Luciferase assay substrate (Promega) was diluted 1:80 in HBSS, added at 10µL/well and incubated for 10min at 37°C. Finally, agonists prepared in HBSS at 10× concentration were added at 10µL/well, followed by further 5min incubation at 37°C (based on previous studies by Hudson et al. (2013)). BRET luminescence of eYFP and NLuc was measured at 535nm and 475nm, respectively, using a PHERAstar FS plate reader. Data was normalised as mBRET using the following formula:

$$mBRET = \left(\frac{\text{sample @535nm}}{\text{sample @475nm}} - \text{mean} \left(\frac{NLuc \text{ control @535nm}}{NLuc \text{ control @475nm}} \right) \right) \times 1,000$$

Calculated mBRET was plotted against log agonist concentrations using GraphPad Prism Software (Version 8.4.3; Dotmatics). Agonist curves were fitted as described in *Section 2.10.4*.

2.8 Histology

2.8.1 Immunocytochemistry (ICC)

For all ICC experiments, slides were stored at 4°C, protected from light until further use, and allowed to warm to RT before imaging. Imaging was performed using the 63× Plan-Apochromat objective of the Zeiss 880 Axio Observer Z1 Laser Scanning Confocal Microscope (Zeiss). Samples were excited by lasers (at 0.1-0.2% power) at 561nm, 488nm and 405nm, inducing emission at 623nm, 532nm and 459nm, respectively. Track 1 detected emission between 566nm and 679nm, Track 3 detected between 410nm and 492nm, while the central GaAsP detector was tuned to detect weak fluorescence at wavelength between 493nm and 583nm. Detector gain, offset and digital gain were optimised for each antibody or fluorophore, and used at the same settings in consecutive experiments. Each field-of-view was scanned unidirectionally, as a composite average of 4 scans. Pseudocoloured images were generated, where emission at 623nm, 532nm and 459nm corresponded to magenta, green and blue, respectively. In these images, co-localisation of magenta and green appeared as white. Fluorescence intensity was quantified as described in *Section 2.10.2*.

Flp-In T-REx 293 cells

Flp-In T-REx 293 cells harbouring HA- or eYFP-tagged receptors were cultured on 16-mm round coverslips in 12-well cell culture plates, previously coated for 15min with 50µg/mL DPL (diluted in cell culture medium). In order to induce expression of the harboured receptors, cells were treated with 100ng/mL DOX for 16h. In experiments using phosphosite-specific antisera, cells were serum starved for 4h (using Flp-In T-REx 293 cell culture medium without FBS) prior to agonist treatment. In the case of antagonist-treated samples, cells were pre-incubated with 100µM CATPB prepared in Flp-In T-REx 293 cell culture medium for 1h at 37°C, followed by agonist treatment for 2min at RT. This time-point was selected as a result of optimisation based on predicted timeframes for receptor phosphorylation (Luttrell et al., 2001). Cells were fixed for 5min using

4% (w/v) paraformaldehyde supplemented with PhosSTOP phosphatase inhibitor (Roche). After fixation, cells were permeabilised with TBS (20mM Tris-HCl, 150mM NaCl at pH7.6) supplemented with 0.05% (w/v) saponin for 5min on an orbital rotator. Cells were then washed 2× for 5min with TBS. Following the washes, cells were blocked for 30-60min at RT with using TBS supplemented with 0.05% (w/v) saponin, 1% (w/v) FA-free BSA and 3% (v/v) goat serum. The blocking solution was aspirated, and cell were incubated with primary antibodies (prepared 1:250 in blocking solution) overnight at 4°C. Cells were washed 3× for 10min with TBS in order to remove residual primary antibodies. AlexaFluor secondary antibodies were prepared in blocking solution (1:400), and incubated with the cells at RT for 2h, protected from light. Cells were again washed 3×, while being protected from light, with TBS for 15min. Coverslips were mounted onto a microscopy slide with a droplet of Vectashield Vibrance mounting medium with DAPI (4',6-diamidino-2-phenylindole) (Vector Laboratories) and sealed with nail polish around the edges.

Mouse-derived neutrophils

In the case of neutrophils, following isolation and final centrifugation (*Section 2.6.1*), cells were resuspended in 1mL 4% (w/v) paraformaldehyde and transferred to a sterile microcentrifuge tube for overnight fixing at 4°C. Cells were centrifuged at 300×g for 5min and resuspended in 500µL PBS with 0.05% (w/v) saponin for 15min for permeabilisation. The suspension was centrifuged and washed in PBS, followed by resuspension in 500µL blocking solution (PBS supplemented with 4% (w/v) FA-free BSA and 4% (w/v) skimmed milk) for 2h. After centrifugation, neutrophil pellets were resuspended in primary antibodies for HA and other relevant cellular markers (prepared 1:100 in blocking solution) and incubated overnight at 4°C. Samples were centrifuged and washed with PBS 2×, followed by 2h incubation at RT with AlexaFluor secondary antibodies prepared in blocking solution (1:400). After 3 washes with PBS, pellets were resuspended in 15µL PBS. On a slide, 10µL Vectashield Vibrance mounting medium with DAPI was added to 10µL of the neutrophil suspension. Coverslips (22×40mm) were applied and, after 30min drying at RT, nail polish was used to seal the edges.

In experiments using phosphosite-specific antisera in neutrophils, cells were preincubated 100 μ M CATPB or vehicle for 1h at 37 $^{\circ}$ C, followed by 2min incubation with agonists. In these experiments, PBS was replaced with TBS in all solutions, and 4% (w/v) paraformaldehyde was supplemented with PhosSTOP. Primary antibodies for these experiments were prepared at 1:250 dilution in blocking solution, while secondary antibodies were prepared at 1:400 as before.

2.8.2 Immunohistochemistry (IHC)

Male mice (13-20 weeks old) were anaesthetised using 3% isoflurane, followed by transcardial perfusion with 20mL ice cold PBS, then 20mL ice cold 4% (w/v) paraformaldehyde solution. Samples were immediately taken from epididymal adipose, liver, lungs, pancreas, spleen, and intestines (duodenum, jejunum, ileum, caecum, and colon), and further fixed in 4% (w/v) paraformaldehyde solution overnight at RT. Samples were subsequently washed with and stored in 70% EtOH until being processed.

Tissue samples were embedded in paraffin wax by the Histology Research Service (Veterinary Diagnostic Services, School of Veterinary Medicine, College of Medical, Veterinary and Life Sciences, University of Glasgow, Scotland), following dehydration in increasing concentrations of EtOH and clearing in xylene. For antigen retrieval, 3 μ m sections were cut with a Thermo Shando HM340 rotary microtome and mounted on microscope slides. Paraffin was removed from slides by passaging through Histo-Clear histological clearing agent (National Diagnostics) multiple times. Sections were then rehydrated with decreasing concentrations of EtOH (to 70%) and rinsed in water. Heat-induced epitope retrieval was performed with Menarini Access retrieval unit in sodium citrate buffer (pH6.0) for 1min 40s at 125 $^{\circ}$ C at full pressure. Samples were transferred to water until further processing.

For IHC, slides were first washed 3 \times in PBS supplemented with 0.1% (v/v) TRITON X-100 (Sigma), on a rotator at 60rpm, for 15-30min each time. After permeabilization, slides were gently dried and ImmEdge Hydrophobic Barrier PAP pen (Vector Laboratories) was used to frame the tissue samples. Samples were incubated for 2h at RT with 150 μ L blocking solution (PBS supplemented with 0.1% (v/v) TRITON X-100, 10% (v/v) goat serum and 5% (w/v) BSA). After

blocking, slides were gently dried and primary antibodies for HA and other relevant cellular markers (prepared 1:100 in blocking solution) were added at 150 μ L to each slide. Slides were incubated overnight at 4°C in a closed container. Following incubation with primary antibodies, slides were washed 3 \times in PBS (with 0.1% (v/v) TRITON X-100) for 30-45min each time. Protected from light, AlexaFluor secondary antibodies (prepared 1:400 in blocking solution) were added to the slides. Slides were then incubated in the dark for 2h at RT, followed by 3 45-min washes in PBS (with 0.1% (v/v) TRITON X-100) in a covered container. Using a sterile pastette, 2 droplets of Vectashield Vibrance mounting medium with DAPI was added to each slide, followed by covering with a coverslip (22 \times 40mm). After 30min drying at RT, nail polish was applied to seal the edges of the coverslip.

Slides were stored at 4°C, protected from light until further use and allowed to warm to RT before imaging. Imaging was performed using the 40 \times and 63 \times Plan-Apochromat objectives of the Zeiss 880 Axio Observer Z1 Laser Scanning Confocal Microscope (Zeiss). Samples were excited by lasers (at 0.2-2.2% power) at 561nm, 488nm and 405nm, inducing emission at 623nm, 532nm and 459nm, respectively. Track 1 detected emission between 566nm and 679nm, Track 3 detected between 410nm and 492nm, while the central GaAsP detector was tuned to detect weak fluorescence at wavelength between 493nm and 583nm. Detector gain, offset and digital gain were optimised for each antibody and fluorophore, and used at the same settings in consecutive experiments. Each field-of-view was scanned unidirectionally, as a composite average of 2 scans. Pseudocoloured images were generated, where emission at 623nm, 532nm and 459nm corresponded to magenta, green and blue, respectively. In these images, co-localisation of magenta and green appeared as white. In samples with apparent high background autofluorescence, only cells which showed fluorescence intensity 50% above the average background intensity were considered to be positively stained. For analysis, the total number of cells, as well as the number of magenta, green and white coloured cells within each field-of-view was counted manually. Calculations of relative expression were based on these numbers.

For low magnification images of the spleen, the 4x objective of the Evos FL Auto 2 cell imaging system (ThermoFisher) was used under the same excitation

conditions. Pseudocoloured images were generated, where emission at 623nm, 532nm and 459nm corresponded to red, green and blue, respectively. In these images, co-localisation of red and green appeared as yellow.

2.9 Immunoblotting

2.9.1 Lysate preparation

Flp-In T-Rex 293 cells harbouring eYFP- or HA-tagged versions of FFA2 were cultured in 10cm dishes for 24h and treated with DOX in order to induce expression of the receptor of interest. After 24h, the cell culture media was replaced with serum-free Flp-In T-REx 293 cell culture media. Following 4h of serum-starvation, the cells were either pre-incubated with 3 μ M CATPB or vehicle for 15min, or treated immediately with agonists for 5min. This treatment time was selected as a result of optimisation based on predicted timeframes for receptor phosphorylation using similar antisera (Butcher et al., 2014). Drug treatment was followed by a rapid but gentle wash with TBS. Detached cells were centrifuged for 5min at 1750 \times g, and the resulting pellet was stored at -80 $^{\circ}$ C.

Pellets were resuspended in 200-500 μ L lysis buffer (150mM NaCl, 50mM Tris-HCl, 5mM EDTA, 1% (v/v) Nonidet P-40, 0.5% (w/v) Na-deoxycholat, 0.1% (w/v) SDS at pH7.4) supplemented with phosSTOP phosphatase inhibitor and cComplete EDTA-free protease inhibitor. The suspension was moved to a sterile microcentrifuge tube and rotated for 30min at 4 $^{\circ}$ C to ensure lysis of the cells. Samples were then centrifuged at 21,000 \times g for 15min at 4 $^{\circ}$ C. The supernatant was moved to a clean microcentrifuge tube, and the amount of protein was quantified using Pierce BCA Assay (see *Section 2.7.2*).

2.9.2 Immunoprecipitation

In order to immunoprecipitate eYFP-tagged receptors, green fluorescent protein (GFP)-trap agarose kit (Chromotek) was used according to the manufacturer's instructions. In short, 15-25 μ L anti-GFP agarose resin was washed 3 \times in 500 μ L dilution buffer (Chromotek), with 2-min centrifugations at 2,500 \times g at 4 $^{\circ}$ C between washes. Lysate concentrations were equalised, then 200 μ g/gel well was transferred into a sterile microcentrifuge tube, and the volume was topped up

to 500 μ L with dilution buffer. After the final wash, the agarose resin pellet was resuspended with the diluted lysates and left on a rotating wheel overnight at 4°C.

For the immunoprecipitation of HA-tagged receptors, Monoclonal Anti-HA-Agarose antibody (Sigma-Aldrich) was employed according to the manufacturer's instructions. In short, 20-30 μ L of suspension was washed 5 \times with 500 μ L lysis buffer, with 2-min centrifugations at 2,500 \times g and 4°C between washes. Lysates were diluted and added to the resin as in the case of the GFP traps, and rotated overnight at 4°C.

In order to remove unbound proteins following immunoprecipitation, eYFP-tagged samples were washed 3 \times with 500 μ L wash buffer (Chromotek) and HA-tagged samples were washed with 4 \times with 500 μ L lysis buffer, with 2-min centrifugations at 2,500 \times g at 4°C between washes.

In experiments involving λ -protein phosphatase (λ PP), lysates were incubated with 10unit/ μ L λ PP in 40 μ L dilution buffer (without PhosSTOP) and 5 μ L MgCl₂ for 90min at 30°C. Samples were then centrifuged for 4 minutes at 2,500 \times g at RT, and the supernatant discarded.

Samples were resuspended in SDS-PAGE (polyacrylamide gel electrophoresis) sample buffer (62.5mM Tris (at pH7.6), 2% (w/v) SDS, 20% (v/v) glycerol, 100mM dithiothreitol, 0.005% (w/v) bromophenol blue), then eluted at 60°C for 10min. Eluted samples were centrifuged at 2,500 \times g at RT. The supernatant was subsequently used for SDS-PAGE in Western blotting.

2.9.3 Western blotting

Samples eluted in 2 \times SDS-PAGE sample buffer were loaded at 20 μ L/well onto 12-well NuPAGE 4-12% Bis-Tris 1.0mm gels (Invitrogen), alongside the Chameleon Duo Pre-Stained Protein Ladder (LICOR). Immunoprecipitated proteins were separated on the gels in NuPAGE MOPS SDS Running buffer (Invitrogen) at 180V over 70min. Gels were subsequently layered into a transfer cassette in the order: sponge, pre-soaked 3mm filter paper, gel facing down, pre-soaked 0.45 μ m nitrocellulose membrane, filter paper, sponge. Electrophoretic transfer

of separated proteins to the nitrocellulose membrane was performed in transfer buffer (25mM Tris-Base, 192mM glycine, 20% (v/v) methanol) at 30V over 90min.

Following the transfer, nitrocellulose membranes were blocked individually in 20mL blocking solution (TBS supplemented with 5% (w/v) BSA) for 1h, shaken at 45rpm at RT. Primary antibodies were prepared in antibody solution (TBS supplemented with 0.1% (v/v) TWEEN and 5% (w/v) BSA) at 1:500-1:10,000 dilution, and added at 10mL/membrane. Membranes were incubated with the primary antibodies overnight at 4°C, rotated at 70rpm on an orbital shaker. Following the overnight incubation, membranes were washed 3× with TBS (with 0.1% (v/v) TWEEN) for 10min at 75rpm at RT. IRDye secondary antibodies were prepared in antibody solution at 1:10,000 dilution, added to the membranes at 10mL/membrane, and incubated in the dark for 2h at 45rpm at RT. Membranes were subsequently washed 3× with TBS (with 0.1% (v/v) TWEEN) for 10min at 75rpm at RT. Finally, membranes were gently dried, then imaged using LICOR Odyssey 9260 fluorescent imaging system and the ImageStudio Software (Version 5.2; LICOR).

2.10 Data analysis and curve fitting

Unless otherwise stated, data represents mean±SEM from 3 replicate experiments, analysed with GraphPad Prism Software (Version 8.4.3; Dotmatics). Curve fitting and analysis methods for various experimental procedures are outlined below.

2.10.1 Tissue expression analysis

Relative expression of gene products was determined as $\Delta\Delta C_T$. To this end, C_T values obtained through qRT-PCR (**Section 2.5.4**) were first compared to housekeeping gene (in this case β -actin) which acted as an internal control:

$$\Delta C_T = C_T(\text{test gene}) - C_T(\beta - \text{actin})$$

ΔC_T of the test tissues were subsequently compared to the ΔC_T of the reference tissue (adipose) of the same mouse strain, in order to determine $\Delta\Delta C_T$:

$$\Delta\Delta C_T = \Delta C_T(\text{test tissue}) - \text{mean}\Delta C_T(\text{adipose})$$

Results were then reported as fold difference in expression relative to expression in adipose tissue, calculated as:

$$\text{Fold difference} = 2^{-\Delta\Delta C_T}$$

2.10.2 Fluorescence intensity analysis

Immunocytochemistry experiments in mouse neutrophils (**Section 2.8.1**) were analysed with the ZEN Blue software (Version 3.4; Zeiss). Fluorescence intensities from each channel were determined using the software, by selecting three cells and three background areas, from three individual images. Fluorescence intensity was then corrected for area and background fluorescence using the following formula:

$$\text{Fluorescence} = \left(\frac{\text{cell fluorescence}}{\text{cell area (nm}^2\text{)}} \times 10^6 \right) - \left(\frac{\text{background fluorescence}}{\text{background area (nm}^2\text{)}} \times 10^6 \right)$$

Subsequently, the mean of individual fluorescence values was calculated for further statistical analysis.

2.10.3 Binding parameter analysis

The use of radioligand binding studies allows the direct measurement of ligand affinity for the receptor. In saturation binding experiments (**Section 2.7.4**), specific binding of a radioligand at increasing concentrations is anticipated to display a hyperbolic curve with the following formula:

$$\text{Specific binding (Y)} = \frac{B_{\max} \times [\text{radioligand}](X)}{K_d + [\text{radioligand}](X)}$$

Based on this formula, the maximum concentration of ligand binding sites can be determined in terms of B_{\max} , presented routinely as fmol/mg protein.

Importantly, the affinity of the radioligand for the receptor can also be calculated in terms of the equilibrium binding constant (K_d) which represents the ligand concentration which occupies 50% of the available receptor sites.

2.10.4 Functional agonist and antagonist assay analysis

Both agonist and antagonist response curves were analysed using non-linear regression analysis on a three-parameter sigmoidal function. In each case, the Hill slope of the curve was constrained to unity, in order to allow better fit in cases where data quality was variable. This allowed the calculation of pharmacological parameters for these ligands. For agonists:

$$Response (Y) = Bottom + \frac{Top - Bottom}{1 + 10^{\log EC_{50} - [Ligand](X)}}$$

The formula was used to determine the bottom and top asymptotes, the latter of which represents the maximal response (E_{max}), and therefore agonist efficacy. Agonist potency can be derived from $\log EC_{50}$, where EC_{50} is the concentration of agonist which is required to generate a half-maximal response. For statistical analysis, agonist potency was analysed as pEC_{50} ($-\log EC_{50}$).

By contrast, for antagonists:

$$Response (Y) = Bottom + \frac{Top - Bottom}{1 + 10^{[Ligand](X) - \log IC_{50}}}$$

The formula was used to determine IC_{50} , which is the antagonist concentration required to reduce agonist-induced response by 50%. For statistical analysis, pIC_{50} ($-\log IC_{50}$) values were utilised.

2.10.5 Allosteric operational model

In [^{35}S]-GTP γ S incorporation experiments where the interaction of C3 and AZ1729 was investigated, the following operational model of allosteric modulation was utilised (Keov et al., 2011):

$$E = \frac{E_{max}(\tau_A[A](K_B + \alpha\beta[B]) + \tau_B[B]K_A)^n}{([A]K_B + K_AK_B + [B]K_A + \alpha[A][B])^n + (\tau_A[A](K_B + \alpha\beta[B]) + \tau_B[B]K_A)^n}$$

This formula allows the calculation of α and β , which are the measures of the allosteric effect on binding affinity and efficacy, respectively. τ_A and τ_B , by contrast, represent the ability of the orthosteric and allosteric ligands, respectively, to directly activate the receptor. Finally, K_B represents the binding

affinity of the allosteric ligand. In order to estimate these values, the system maximum response (E_{\max}), slope factor (n) and orthosteric binding affinity (K_A) functions were constrained in all cases.

2.10.6 Statistical analysis

Statistical analyses were performed using GraphPad Prism Software (Version 8.4.3; Dotmatics). In all cases, data were assumed to be normally distributed and involved the comparison of three or more groups, allowing analysis by one of the following parametric tests: one-way Analysis of Variance (ANOVA) in cases of experiments with one independent variable, and two-way ANOVA in cases with two. In addition, in cases where the number of data-points differed between groups, a mixed-effects analysis was employed. These were followed by multiple-comparisons post-hoc analyses in order to detect differences between the analysed groups. Tukey's post-hoc analysis was employed to compare all means to each other. On the other hand, Sidak's post-hoc analysis was employed to compare selected sets of means. In each case, a P value of <0.05 was considered statistically significant.

CHAPTER 3 - CHARACTERISATION OF hFFA2-HA-EXPRESSING MICE

3.1 Introduction

As discussed in *Chapter 1*, experiments in animal tissues, both *ex vivo* and *in vivo*, constitute a crucial step in the drug development process. Due to the species-selectivity of the available FFA2 antagonists for the human orthologue, animal studies of these compounds have not been feasible, considerably hindering drug development efforts. Transgenic animals have widely been used in order to bridge the gap between *in vitro* experiments and clinical trials. As FFA2 antagonists only block activation of hFFA2, a mouse model expressing this orthologue of the receptor would allow the examination of the effect of these compounds in a physiological context.

To generate a model that expresses hFFA2 but not mouse mFFA2, a knock-in approach was used. Specifically, the gene coding for the C-terminally HA epitope-tagged version of hFFA2 (hFFA2-HA) was knocked into the locus coding for *mFfar2* on chromosome 7. Since the transgene is under the control of the original promoter of *mFfar2*, the pattern and level of expression of hFFA2-HA should reflect that of mFFA2 in C57BL/6N (WT) mice, while the expression of mFFA2 should be eliminated. There is, however, an additional layer of control inserted in the form of loxP-flanked “stop cassette”. In effect, the expression of hFFA2-HA is suppressed in these mice. Upon crossing with mice expressing CRE-recombinase, in the resulting offspring the CRE-recombinase enzyme leads to the excision of the “stop cassette”, thus allowing the constitutive expression of hFFA2-HA (Orban et al., 1992, Lakso et al., 1992). Since in the absence of CRE-recombinase neither hFFA2-HA nor mFFA2 are expected to be expressed, this “minus-CRE” mouse strain can be considered a functional KO of FFA2 (Bolognini et al., 2019). This is especially useful, as previously reported KO of FFA2 and FFA3 have shown compensatory changes in the expression of the other receptor (Bjursell et al., 2011, Zaibi et al., 2010).

Before functional studies could be conducted on this novel transgenic mouse line, the expression of hFFA2-HA had to be demonstrated. qRT-PCR is a widely used technique based on the traditional polymerase chain reaction which allows quantification of a target sequence in a sample (Heid et al., 1996). Besides

primers flanking the sequence-of-interest, this experiment also involves a dsDNA dye, SYBR Green I, which emits increased fluorescence upon binding the amplification products. As the sequence-of-interest is being amplified, the fluorescence from the dye increases proportionally (Wittwer et al., 1997). The point where fluorescence surpasses the threshold value designates the threshold cycle (C_T) which can then be utilised as a basis for calculations to establish relative expression amount of the sequence-of-interest in each of the tissue samples (Livak and Schmittgen, 2001). β -actin, a house-keeping gene which is expressed throughout all of the investigated tissues, serves as an endogenous reference and as a basis for the normalisation of sample load. As adipose is one of the tissues where FFA2 is canonically expressed, this tissue was used as the “calibrator” relative to which the expression in other tissues is expressed (Winer et al., 1999). The primers used in qRT-PCR target regions of FFA2 which are unique for hFFA2 and mFFA2. For the former, this is a 73bp segment of the C-terminal tail including the HA epitope tag introduced into the construct design and for the latter a 148bp segment spanning the majority of ECL2 and TM5 regions of the receptor.

While qRT-PCR is extremely useful in demonstrating the presence and quantifying the amount of mRNA present in each tissue, this does not directly demonstrate the presence of translated proteins. In IHC and ICC studies, a primary antibody targeting a macromolecule of interest can in turn be targeted by a secondary antibody conjugated to a fluorophore (such as AlexaFluor dyes). Samples labelled this way can be subsequently imaged through laser scanning confocal microscopy. In this technique, light from multiple lasers is focused onto a specimen through a pinhole aperture, acousto-optic filters, a dichromatic mirror, and an objective. Light returning from the excited fluorophores passes through the same objective and mirror, followed by a barrier filter and a separate pinhole, to finally reach a number of photomultipliers. Signals from the photomultiplier are translated into an image through the imaging software of the connected computer (Paddock and Eliceiri, 2014). Confocal microscopy can be utilised with both fixed cells and tissues in order to visualise the localisation of molecules of interest, therefore it is a useful technique for demonstrating the tissue-distribution of hFFA2-HA.

The current lack of useful structural antibodies for FFA2 led to the inclusion of the C-terminal HA epitope tag on the hFFA2-HA construct. This enables the use of antibodies targeting the HA-tag, rather than the FFA2 receptor itself. Beside HA, markers characteristic of certain cell types were also targeted by primary antibodies in order to identify cell populations where hFFA2-HA is expressed.

Chromogranin A (ChgA) is a glycoprotein found in EECs throughout the length of the digestive tract. They are released in small amounts from peptide hormone endocrine cells but in large amounts from cells which release the monoamines serotonin and histamine (Engelstoft et al., 2015). Although several groups have found that ChgA is not indiscriminately expressed by all EECs, this target is still widely used as a broad-range marker for this cell type (Engelstoft et al., 2015, Portela-Gomes et al., 1997). FFA2 in both humans and mice is expressed in L-cells, a subset of EECs which release the anorexigenic hormones PYY and GLP-1. Indeed, antibodies targeting these hormones have been used to demonstrate various degrees of colocalization with FFA2 in the ileum (Nohr et al., 2013, Li et al., 2013) and the colon (Karaki et al., 2008, Kaji et al., 2011).

In addition to EECs, the expression of FFA2 has been observed in the leukocytes of the lamina propria in the small intestine (Nohr et al., 2013). Since FFA2 is known to be expressed in a wide range of immune cell types (Brown et al., 2003, Le Poul et al., 2003, Nilsson et al., 2003), and since the lamina propria is populated by a heterogenous population of leukocytes (Hamada et al., 2002), identification of FFA2-expressing sub-populations of the lamina propria is an attractive next step. To this end, markers for various immune cell subtypes were utilised. CD45 is a receptor-like protein tyrosine phosphatase which has essential roles in immune cells. Due to its abundant expression on the surface of all nucleated haematopoietic cells (Hermiston et al., 2003), CD45 can be used as broad-range immune cell marker in IHC studies. In order to identify T-lymphocytes, CD3 was targeted due to its involvement in the activation and signal transduction of these cells (Smith-Garvin et al., 2009). CD11b is an integrin expressed in myeloid cells, mainly neutrophils, but also in natural killer cells, mast cells and some subpopulations of T-lymphocytes, while the integrin CD11c is found primarily in DCs and macrophages (Arnaout, 2016). Employing a

panel of antibodies, FFA2-expressing immune cell populations would be identifiable.

Since FFA2 is expressed in a wide range of immune cells, it is not surprising that it is also expressed in the spleen (Nilsson et al., 2003). The structure of the spleen is divided into two distinct zones: the white pulp and the red pulp. The white pulp itself is subdivided into the periarteriolar lymphoid sheath (PALS), the splenic follicle and the marginal zone. The PALS contains T-lymphocytes exclusively, while the majority of the cells in the follicle are B-lymphocytes. The marginal zone, which is a transitional zone to the red pulp, is made up of a mixture of B-lymphocytes, macrophages and DCs. The red pulp itself contains monocytes, macrophages and large quantities of erythrocytes, alongside loose fibrous tissue (Abbott et al., 2004, Zhao et al., 2015). Identification of the cell populations in each of these zones with the use of antibodies against immune cell markers has been demonstrated (Feng et al., 2016), therefore CD45, CD11b and CD11c would also be useful in this tissue.

Among immune cells, neutrophils show the highest expression of FFA2 (Brown et al., 2003, Le Poul et al., 2003), therefore this cell type is an ideal target for demonstrating the expression of hFFA2-HA. Neutrophils can be purified from a mixed suspension of bone marrow-derived cells with the use of a negative-selection method. For this, cells other than neutrophils are labelled with biotinylated antibodies and magnetic particles, resulting in labelled cells being retained by a magnet (Flø et al., 1991). As CD11b is the most abundantly expressed integrin on neutrophils (Arnaout, 2016), it could serve as a marker in ICC staining. CD11c, which is not expected to be highly expressed on neutrophils was used in parallel, in order to validate the negative selection method.

The aim of this chapter is to demonstrate the expression of hFFA2-HA in the transgenic hFFA2-HA mouse line, both at the mRNA and the protein level. Epididymal adipose tissue, colon, bone marrow-derived neutrophils, spleen and liver cDNA was used in qRT-PCR, while segments of the small intestine, colon, spleen and bone marrow-derived neutrophils were used in IHC and ICC studies. The expression of FFA2 has been observed in many of these tissues, both in human and mouse, providing a framework for the expected range of expression

in the constitutive hFFA2-HA mouse. Verification of this novel transgenic mouse strain will enable future functional studies, both *ex vivo* and *in vivo*.

3.2 Results

3.2.1 Quantitative reverse transcription PCR of mouse tissues

Before the hFFA2-HA primers were utilised in a range of mouse tissues, their efficiency and specificity was evaluated. Using a 1:4 serial dilution of hFFA2-HA and WT mouse colon, cDNA was amplified in a qRT-PCR reaction with primers targeting hFFA2-HA, mFFA2 and β -actin.

In amplification plots of these serial dilutions (*Figure 3.1*), a rightward shift at regular intervals can be observed in the sigmoid amplification curves. In other words, the cycle number required to generate a specific quantity of PCR product is inversely proportional to the quantity of cDNA added. There was no amplification observed in the no-template control, suggesting that no contaminants or unintended amplification products were present in the reactions.

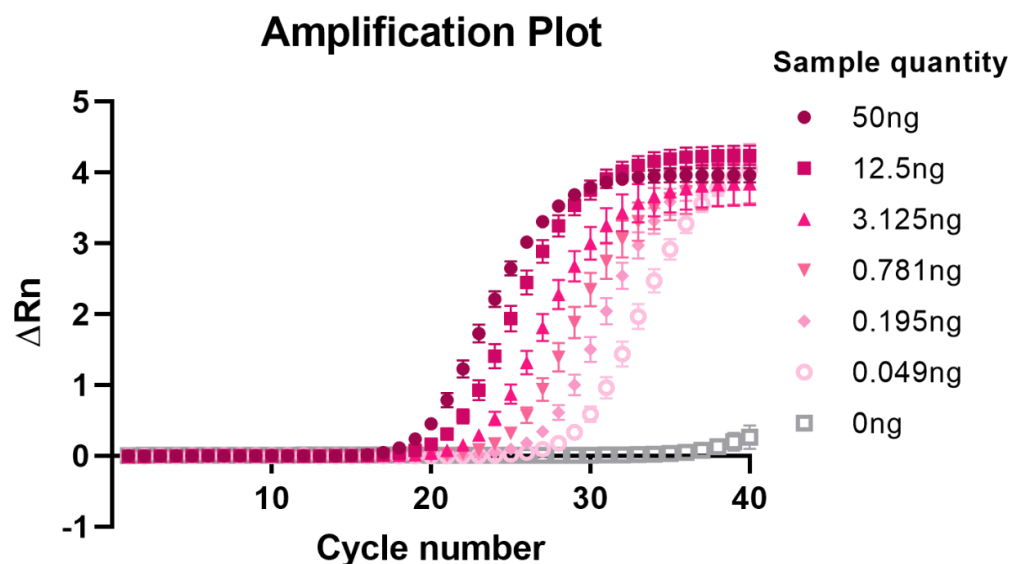


Figure 3.1. qRT-PCR amplification plot of hFFA2-HA colon dilutions. Change in fluorescence signal (as ΔR_n , change in the normalised reporter value) over 40 cycles of amplification of a 1:4 serial dilution of hFFA2-HA mouse colon cDNA with hFFA2-HA primers, using SYBR Green I DNA dye. Data shown as mean \pm SEM (n=4).

By plotting calculated C_T values against the initial cDNA concentrations, standard curves were constructed (Figure 3.2) Based on the slope of the standard curve, efficiency was calculated using the following formula (Rogers-Broadway and Karteris, 2015):

$$Efficiency(\%) = (10^{\frac{-1}{slope}} - 1) \times 100$$

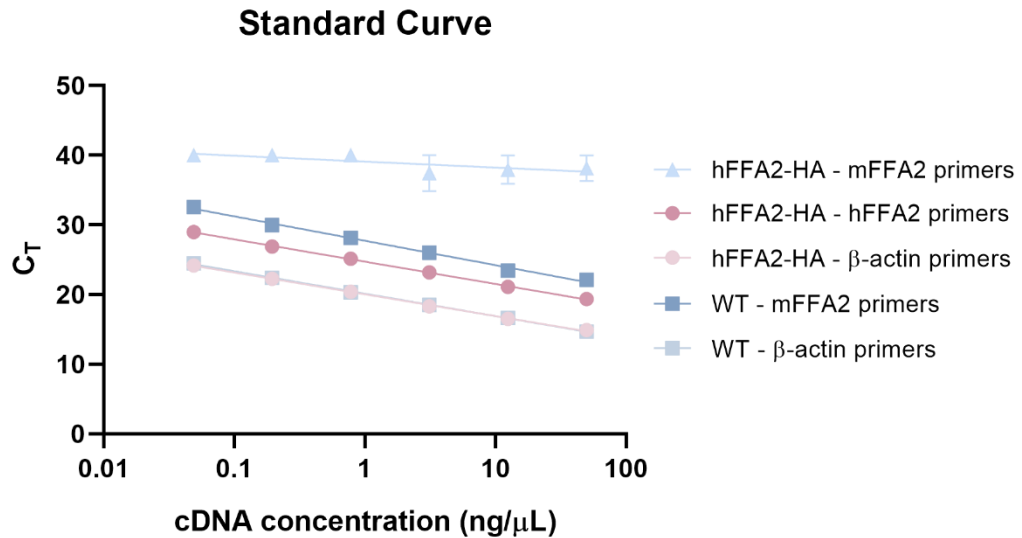


Figure 3.2. Standard curves for qRT-PCR primers in mouse colon. Serial dilutions (1:4) of hFFA2-HA and C57BL/6N (WT) mouse colon cDNA were amplified over 40 cycles with primers targeting hFFA2-HA, mFFA2 and β-actin, using SYBR Green I DNA dye. Threshold cycle (C_T) was plotted against initial cDNA concentrations as mean±SEM (n=4 for hFFA2; n=2 for WT).

The standard curve for hFFA2-HA using hFFA2-HA colon produced a slope of $-3.206 (\pm 0.182)$ ($r^2=0.947$), which corresponds to 105.1% primer efficiency. This contrasts to mFFA2 primers in these tissues which yielded a curve with a slope of $-0.853 (\pm 1.176)$ ($r^2=0.129$), rendering efficiency calculations impossible. In WT colon, on the other hand, mFFA2 primers produced a slope of $-3.503 (\pm 0.328)$ ($r^2=0.934$), corresponding to 93% primer efficiency. The control primers, targeting the housekeeping gene β-actin yielded slopes of $-3.127 (\pm 0.200)$ ($r^2=0.934$) and $-3.220 (\pm 0.206)$ ($r^2=0.968$), corresponding to 108.8% and 104.4% primer efficiency in hFFA2-HA and WT colon, respectively.

In order to quantify the expression of FFA2, cDNA of various tissues (epididymal adipose, colon, neutrophils, spleen and liver) from hFFA2-HA, minus-CRE and WT mice was amplified in a qRT-PCR reaction using hFFA2-HA and β-actin primers, alongside WT tissues amplified using mFFA2 primers. Relative expression ($\Delta\Delta C_T$) was calculated against β-actin C_T and adipose ΔC_T using the methods described in **Section 2.10.1**.

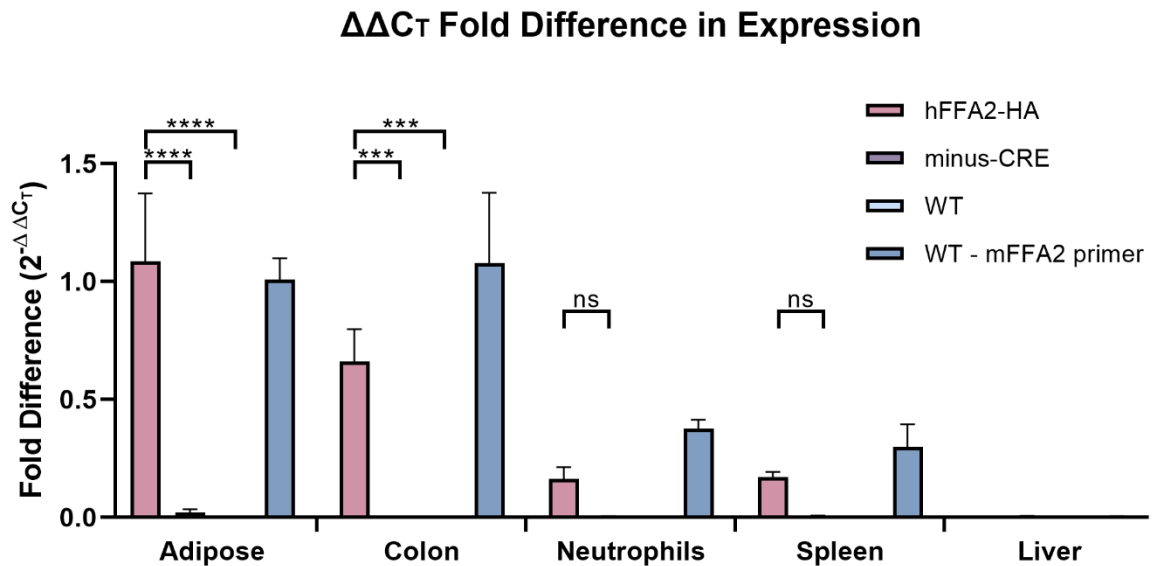


Figure 3.3. qRT-PCR quantification of hFFA2 and mFFA2 in mouse tissues. cDNA reverse-transcribed from mRNA isolated from hFFA2-HA, minus-CRE and C57BL/6N (WT) mouse tissues was amplified over 40 cycles with primers targeting hFFA2-HA, mFFA2 and β -actin, using SYBR Green I DNA dye. $\Delta\Delta C_T$ was calculated using the average C_T of housekeeping gene β -actin and ΔC_T of the calibrator adipose tissue. Data presented as mean \pm SEM (n=3) **** p<0.0001, *** p<0.001, * p<0.05 by two-way ANOVA with Tukey's post-hoc multiple comparisons test.

Expression of hFFA2-HA in hFFA2-HA adipose tissue, which served as the control tissue, was found to be 1.085 (\pm 0.289) (Figure 3.3). This value parallels mFFA2 expression in WT adipose (1.008 \pm 0.092). There was, however, a significant difference (p<0.0001; determined by two-way ANOVA with Tukey's post-hoc analysis) in the expression of hFFA2-HA in hFFA2-HA adipose compared to minus-CRE (0.021 \pm 0.013) and WT (0 \pm 0.000) adipose.

Similar trends were observed in colon samples. Although the expression of hFFA2-HA in hFFA2-HA colon appeared lower (0.660 \pm 0.138; ns) than in hFFA2-HA adipose, no such difference was observed in the expression of mFFA2 in WT colon (1.079 \pm 0.298). The expression of hFFA2-HA was significantly different (p<0.001) from its expression in minus-CRE (0.003 \pm 0.000) and in WT (0 \pm 0.000).

While hFFA2-HA and mFFA2 were found to be expressed in hFFA2-HA and WT neutrophils, respectively, their expression levels were significantly lower than that of adipose in each of these mouse strains (hFFA2-HA: 0.163 \pm 0.050, p<0.0001; mFFA2: 0.375 \pm 0.039, p<0.01). Unlike in the previous tissues, the expressions of hFFA2-HA was not significantly different in minus-CRE (0.004 \pm 0.001) and WT (0 \pm 0.000) neutrophils.

Spleen expression of hFFA2-HA and mFFA2 displayed a similar trend to that in neutrophils. The low expression of hFFA2-HA in hFFA2-HA (0.170 ± 0.023) and of mFFA2 in WT (0.298 ± 0.097) was significantly different from their expression in adipose ($p < 0.0001$ and $p < 0.001$, respectively). Expression of hFFA2-HA was negligible in both minus-CRE (0.007 ± 0.001) and WT (0 ± 0.000), however this difference in expression in comparison to hFFA2-HA was not found to be significant. Expression in the liver was negligible in tissues derived from each of the mouse strains (hFFA2: 0.002 ± 0.001 ; minus-CRE: 0.005 ± 0.002 ; WT: 0 ± 0.000 ; mFFA2 in WT: 0.004 ± 0.001), and no significant difference was observed between any of these values.

3.2.2 Immunohistochemical investigation of transgenic mouse intestine

In order to investigate the expression of the hFFA2-HA protein in mouse tissues, an IHC approach was used. In the absence of a useful structural antibody for hFFA2, primary antibodies targeting the HA-tag on the C-terminal tail of the receptor were used.

Initially, Flp-In T-REx 293 cells induced to express hFFA2-HA were stained with rat anti-HA primary antibody and visualised with goat anti-rat IgG AlexaFluor-546 secondary antibody (*Figure 3.4*). Strong cell surface staining and additional intracellular staining was observed with the anti-HA antibody in the cells expressing hFFA2-HA. On the other hand, no staining was observed in the Flp-In T-REx 293 parental cells, which were used as a negative control.

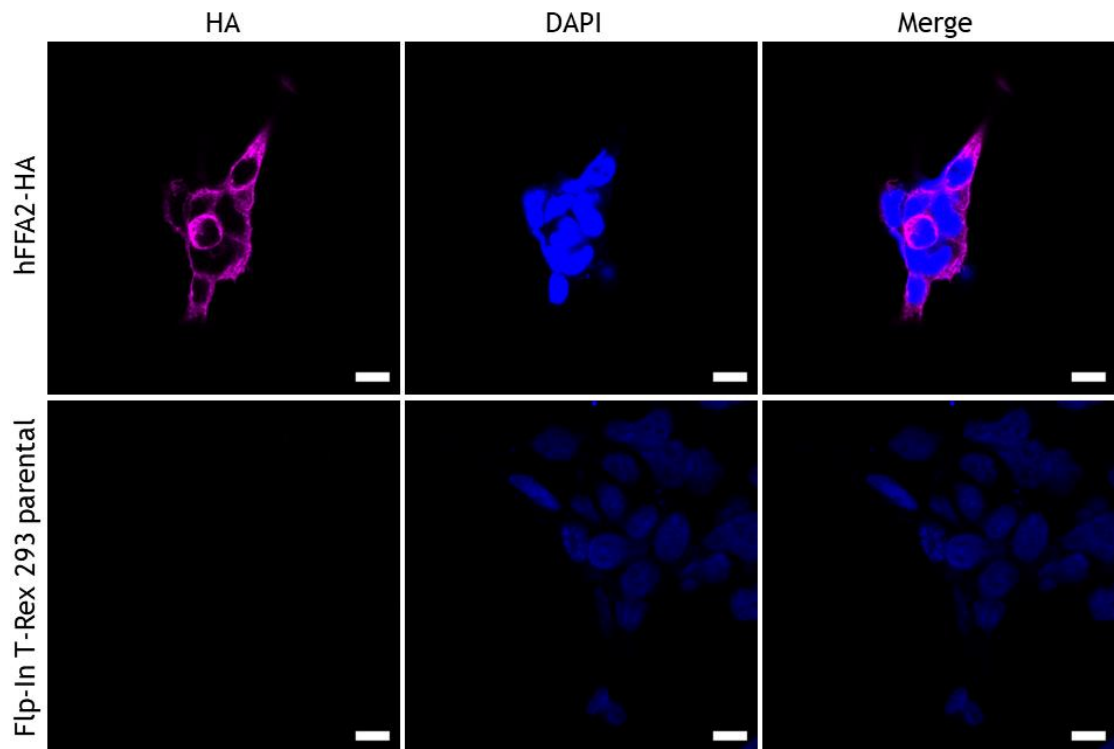


Figure 3.4. Immunocytochemical detection of hFFA2-HA in overexpressing cells. Flp-In T-REx 293 cells induced to express hFFA2-HA and Flp-In T-REx 293 parental cells were fixed with 4% paraformaldehyde and permeabilised with saponin. Cells were incubated with rat anti-HA primary antibody (1:250) overnight, and with goat anti-rat IgG AlexaFluor-546 secondary antibody (1:400; magenta) for 2h. Nuclear DNA was labelled with DAPI (blue). Images were taken with 63× objective of Zeiss 880 Laser Scanning Confocal Microscope. Scale bar represents 10µm. Representative of 3 fields of view each from 2 separate experiments (n=2). HA - haemagglutinin.

With the specificity of the anti-HA antibody established in the Flp-In T-REx 293 cell lines, histological samples of various mouse tissues were examined next. Initially, based on literature describing the presence of FFA2 in the EECs of the small intestine and colon, these tissues were stained with antibodies targeting the markers of populations of endocrine cells. No staining was observed in either of the channels in negative control stains of hFFA2-HA ileum and colon, which used secondary antibodies in the absence of primary antibodies (*Figure 3.5*).

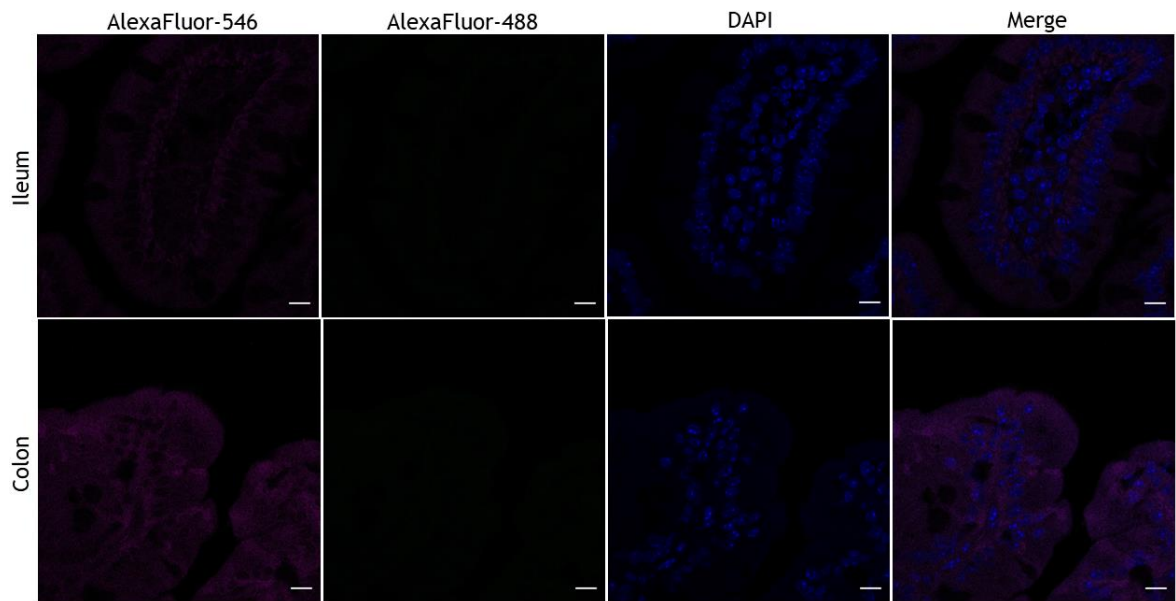


Figure 3.5. Immunohistochemical detection of hFFA2-HA in mouse ileum and colon. Sections of ileum and colon isolated from hFFA2-HA mice were fixed with 4% paraformaldehyde and permeabilised with TRITON-X. Cells were incubated in the absence of primary antibodies overnight, and with goat anti-rat IgG AlexaFluor-546 (1:400; magenta) and goat anti-rabbit IgG AlexaFluor-488 (1:400; green) secondary antibodies for 2h. Nuclear DNA was labelled with DAPI (blue). Images were taken with 63× objective of Zeiss 880 Laser Scanning Confocal Microscope. Scale bar represents 10µm. Representative of 3 fields of view each from 3 animals (n=3).

ChgA, a generic endocrine cell marker was used both in mouse ileum and in mouse colon. In the ileum, while only a small proportion of cells were found to express ChgA (*Figure 3.6*), those cells were found to co-express HA in the hFFA2-HA tissue. In addition to the cells expressing ChgA, some cells were observed to express HA without the expression of ChgA. A small proportion of cells was found to express ChgA in the minus-CRE mouse ileum as well. However, in the case of this mouse strain, no expression of HA was observed (co-expressed with ChgA or otherwise).

A similar trend was observed in the colon when stained with ChgA (*Figure 3.7*). A limited number of cells was found to be stained with ChgA in both hFFA2-HA and minus-CRE colon. While HA appeared to be co-expressed with ChgA in the hFFA2-HA colon, no expression of HA was observed in the minus-CRE mouse colon. Unlike the ileum, no expression of HA was observed in cells not stained with ChgA in the hFFA2-HA colon.

The findings from these images are summarised in *Figure 3.12*.

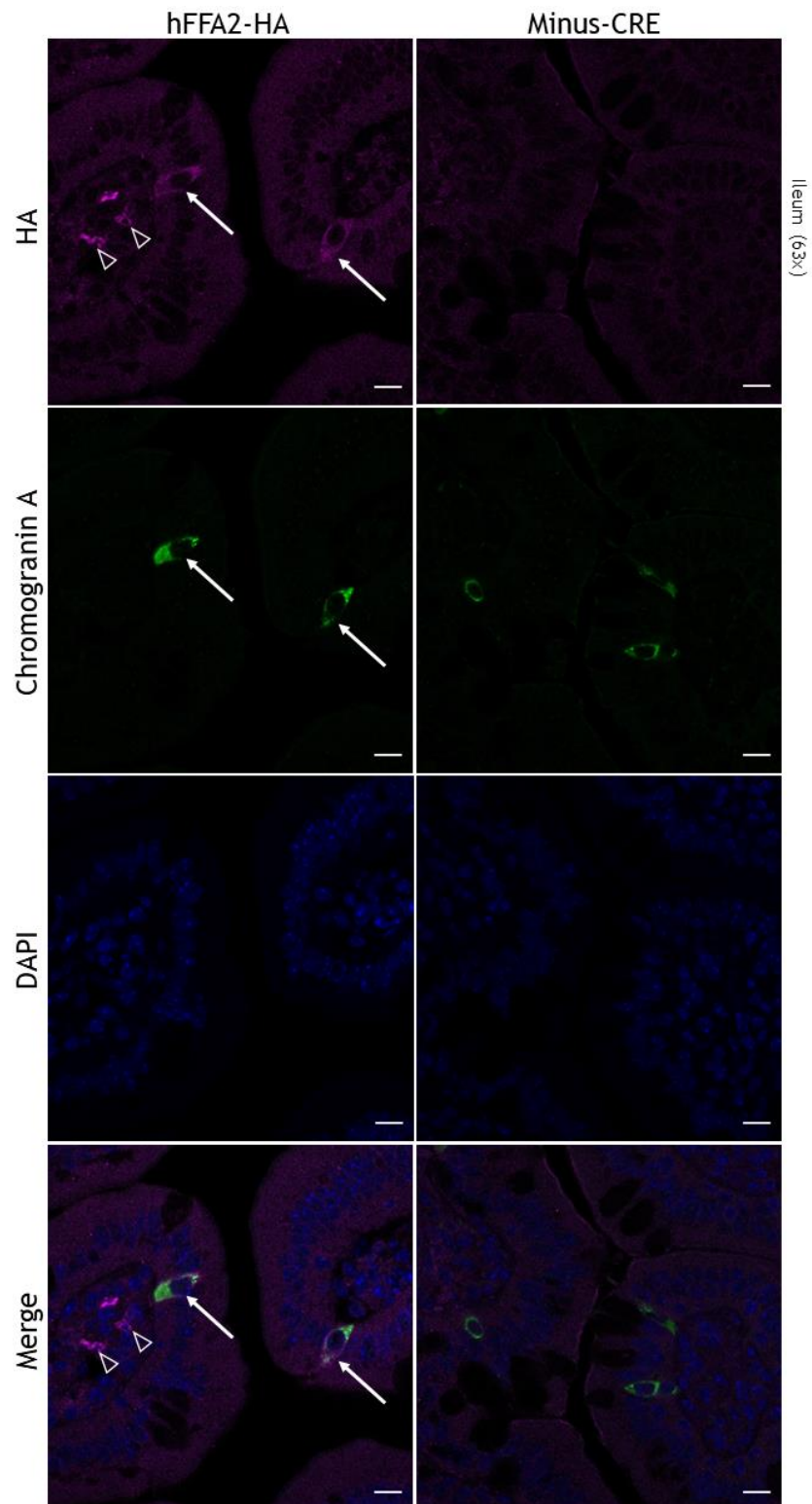


Figure 3.6. Immunohistochemical detection of hFFA2-HA in mouse ileum. Sections of ileum isolated from hFFA2-HA and minus-CRE mice were fixed with 4% paraformaldehyde and permeabilised with TRITON-X. Cells were incubated with rat anti-HA and rabbit anti-chromogranin A (ChgA) primary antibodies (1:100) overnight, and with goat anti-rat IgG AlexaFluor-546 (1:400; magenta) and goat anti-rabbit IgG AlexaFluor-488 (1:400; green) secondary antibodies for 2h. Nuclear DNA was labelled with DAPI (blue). Images were taken with 63 \times objective of Zeiss 880 Laser Scanning Confocal Microscope. Scale bar represents 10 μ m. Arrows represent examples of co-localisation of anti-ChgA and anti-HA antibodies; empty arrowheads represent examples of localisation anti-HA, but not anti-ChgA antibodies. Representative of 3 fields of view each from 3 animals (n=3). HA - haemagglutinin.

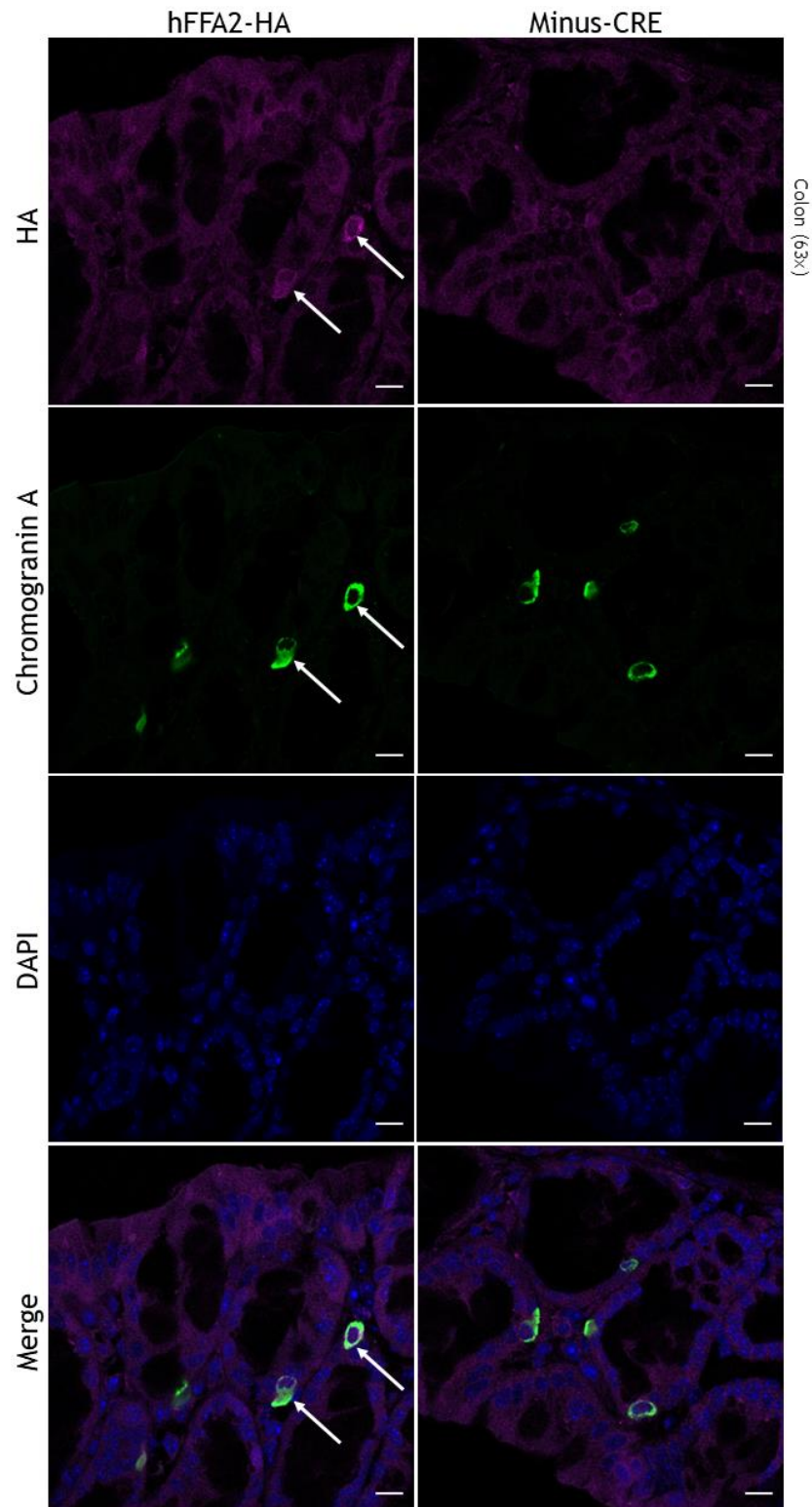


Figure 3.7. Immunohistochemical detection of hFFA2-HA in mouse colon. Sections of colon isolated from hFFA2-HA and minus-CRE mice were fixed with 4% paraformaldehyde and permeabilised with TRITON-X. Cells were incubated with rat anti-HA and rabbit anti-chromogranin A (ChgA) primary antibodies (1:100) overnight, and with goat anti-rat IgG AlexaFluor-546 (1:400; magenta) and goat anti-rabbit IgG AlexaFluor-488 (1:400; green) secondary antibodies for 2h. Nuclear DNA was labelled with DAPI (blue). Images were taken with 63× objective of Zeiss 880 Laser Scanning Confocal Microscope. Scale bar represents 10µm. Arrows represent examples of co-localisation of anti-ChgA and anti-HA antibodies. Representative of 3 fields of view each from 3 animals (n=3). HA - haemagglutinin.

Following ChgA, the enteroendocrine L-cell marker GLP-1 was targeted with antibodies for staining. The pattern of expression of GLP-1 differs from that of ChgA in the ileum (*Figure 3.8*). While there were a small number of cells on the villus endothelial layer expressing GLP-1, there was a larger population of cells stained for GLP-1 in submucosal layers. This trend was observed in both the hFFA2-HA and minus-CRE mouse ileum. In accordance with the ileum stain in *Figure 3.6*, HA was not expressed in minus-CRE ileum, while it was expressed in a small number of mucosal, and a larger number of submucosal cells in the hFFA2-HA ileum. In contrast to ChgA, no cells were found to co-express GLP-1 and HA.

As for the colon, GLP-1 was found to be strongly expressed in a small number of cells, similar to the distribution of ChgA in colon (*Figure 3.9*), in both hFFA2-HA and minus-CRE tissues. The expression of HA was also limited to a small number of cells in the hFFA2-HA colon, with no expression found in the minus-CRE colon. Consistently with the staining in the ileum, GLP-1 was not found to be co-expressed with HA.

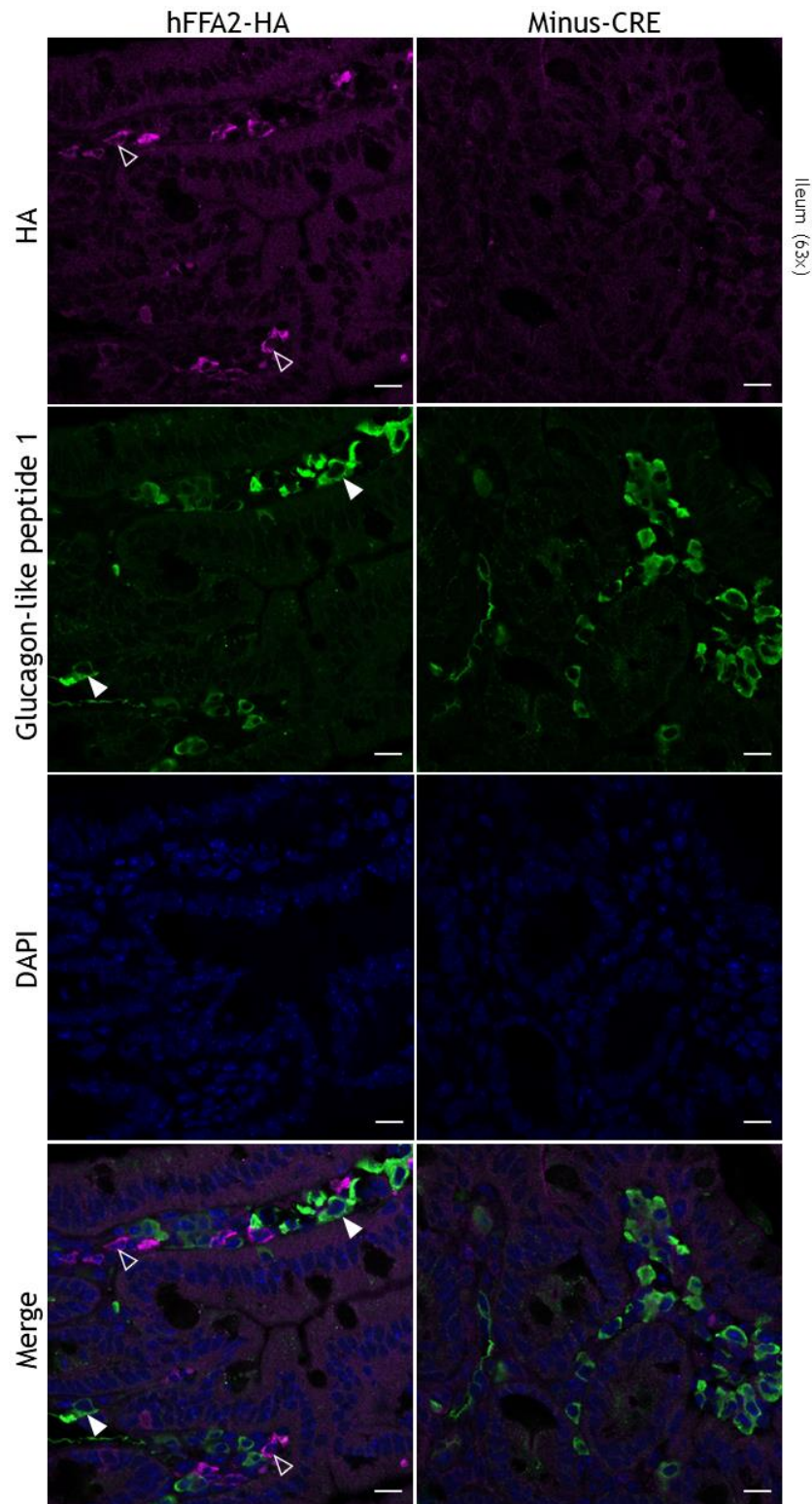


Figure 3.8. Immunohistochemical detection of hFFA2-HA in mouse ileum. Sections of ileum isolated from hFFA2-HA and minus-CRE mice were fixed with 4% paraformaldehyde and permeabilised with TRITON-X. Cells were incubated with rat anti-HA and rabbit anti-glucagon-like peptide 1 (GLP-1) primary antibodies (1:100) overnight, and with goat anti-rat IgG AlexaFluor-546 (1:400; magenta) and goat anti-rabbit IgG AlexaFluor-488 (1:400; green) secondary antibodies for 2h. Nuclear DNA was labelled with DAPI (blue). Images were taken with 63 \times objective of Zeiss 880 Laser Scanning Confocal Microscope. Scale bar represents 10 μ m. Solid arrowheads represent examples of localisation of anti-GLP-1, but not anti-HA antibodies; empty arrowheads represent examples of localisation anti-HA, but not anti-GLP-1 antibodies. Representative of 3 fields of view each from 3 animals (n=3). HA - haemagglutinin.

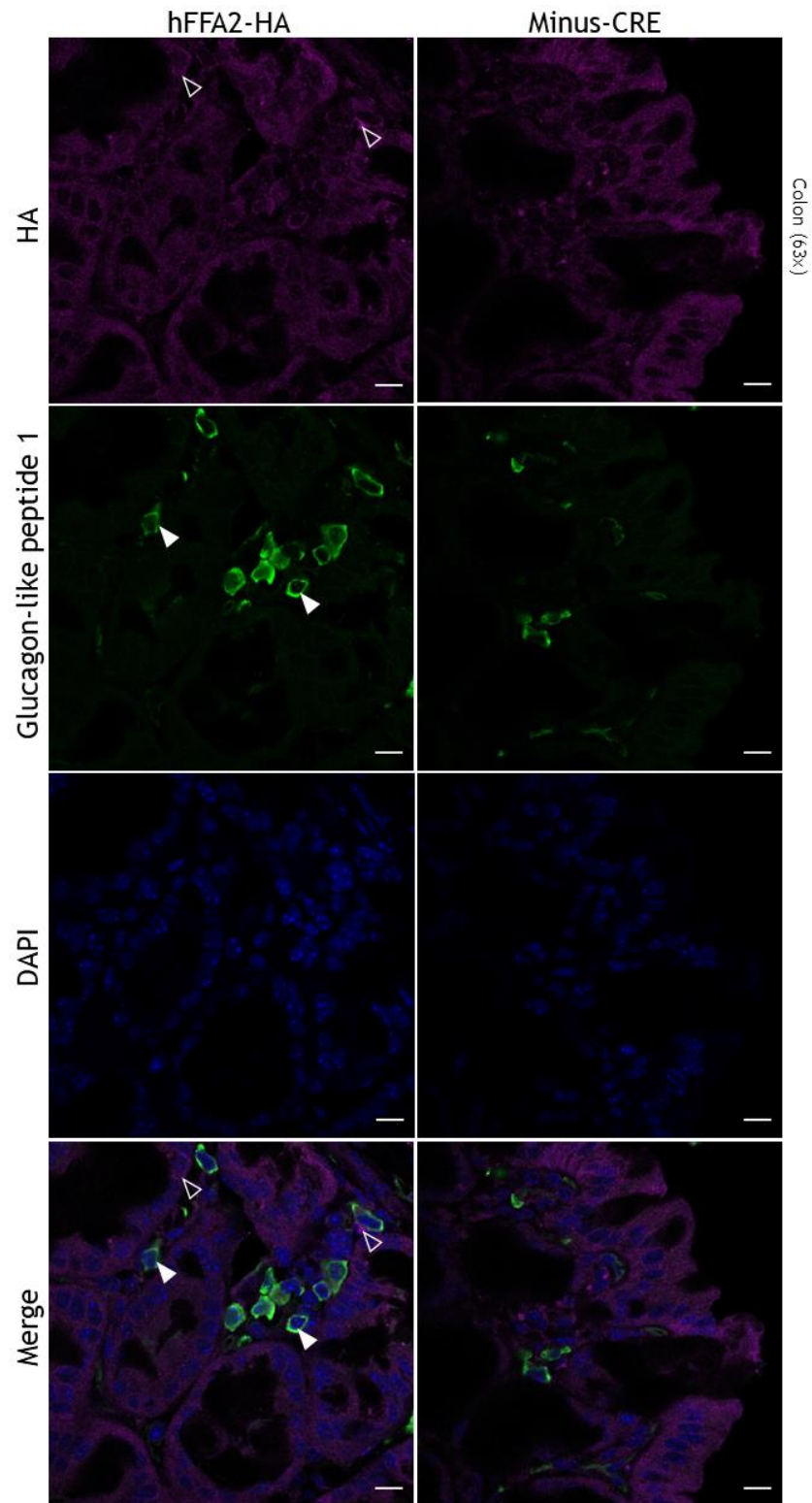


Figure 3.9. Immunohistochemical detection of hFFA2-HA in mouse colon. Sections of colon isolated from hFFA2-HA and minus-CRE mice were fixed with 4% paraformaldehyde and permeabilised with TRITON-X. Cells were incubated with rat anti-HA and rabbit anti-glucagon-like peptide 1 (GLP-1) primary antibodies (1:100) overnight, and with goat anti-rat IgG AlexaFluor-546 (1:400; magenta) and goat anti-rabbit IgG AlexaFluor-488 (1:400; green) secondary antibodies for 2h. Nuclear DNA was labelled with DAPI (blue). Images were taken with 63 \times objective of Zeiss 880 Laser Scanning Confocal Microscope. Scale bar represents 10 μ m. Solid arrowheads represent examples of localisation of anti-GLP-1, but not anti-HA antibodies; empty arrowheads represent examples of localisation anti-HA, but not anti-GLP-1 antibodies. Representative of 3 fields of view each from 3 animals (n=3). HA - haemagglutinin.

Finally, an antibody targeting another L-cell marker, PYY, was utilised (*Figure 3.10*). PYY expression was observed in both hFFA2-HA and minus-CRE ileum. In addition to sporadic expression in the endothelial layer, a more diffuse expression was observed at the tip of villi, in morphologically different cells. The expression of HA paralleled previous experiments; it was found in a handful of cells in hFFA2-HA ileum and not present at all in the minus-CRE ileum. As in the case of GLP-1, there was no apparent co-expression of PYY and HA.

Upon staining with PYY (*Figure 3.11*), colon samples displayed sporadic expression, with minus-CRE colon showing fewer positively stained cells. Expression of HA was observed only in the hFFA2-HA colon. Endothelial cells expressing HA were all found to be co-expressed with PYY.

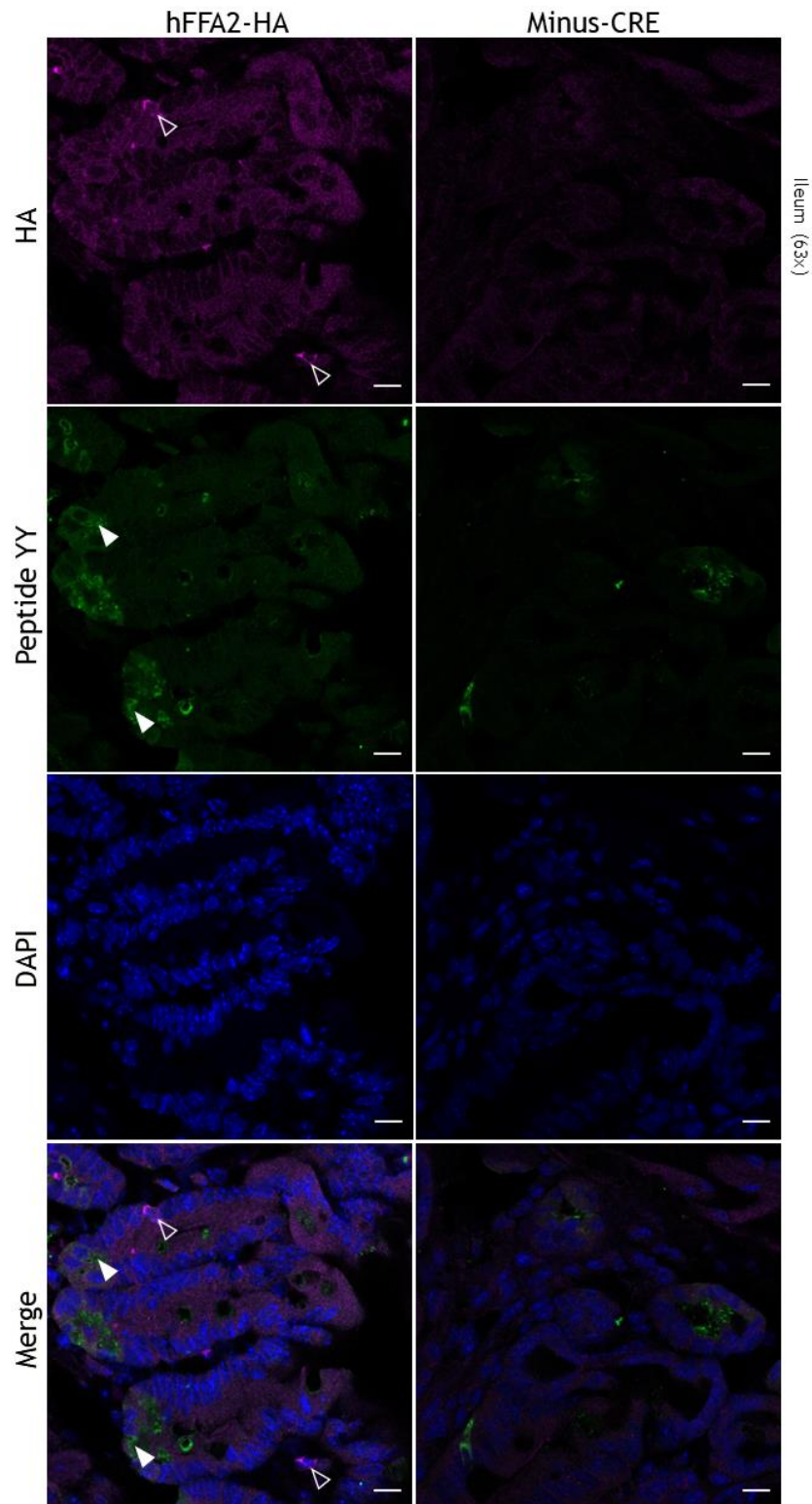


Figure 3.10. Immunohistochemical detection of hFFA2-HA in mouse ileum. Sections of ileum isolated from hFFA2-HA and minus-CRE mice were fixed with 4% paraformaldehyde and permeabilised with TRITON-X. Cells were incubated with rat anti-HA and rabbit anti-peptide YY (PYY) primary antibodies (1:100) overnight, and with goat anti-rat IgG AlexaFluor-546 (1:400; magenta) and goat anti-rabbit IgG AlexaFluor-488 (1:400; green) secondary antibodies for 2h. Nuclear DNA was labelled with DAPI (blue). Images were taken with 63× objective of Zeiss 880 Laser Scanning Confocal Microscope. Scale bar represents 10µm. Solid arrowheads represent examples of localisation of anti-PYY, but not anti-HA antibodies; empty arrowheads represent examples of localisation anti-HA, but not anti-PYY antibodies. Representative of 3 fields of view each from 3 animals (n=3). HA - haemagglutinin.

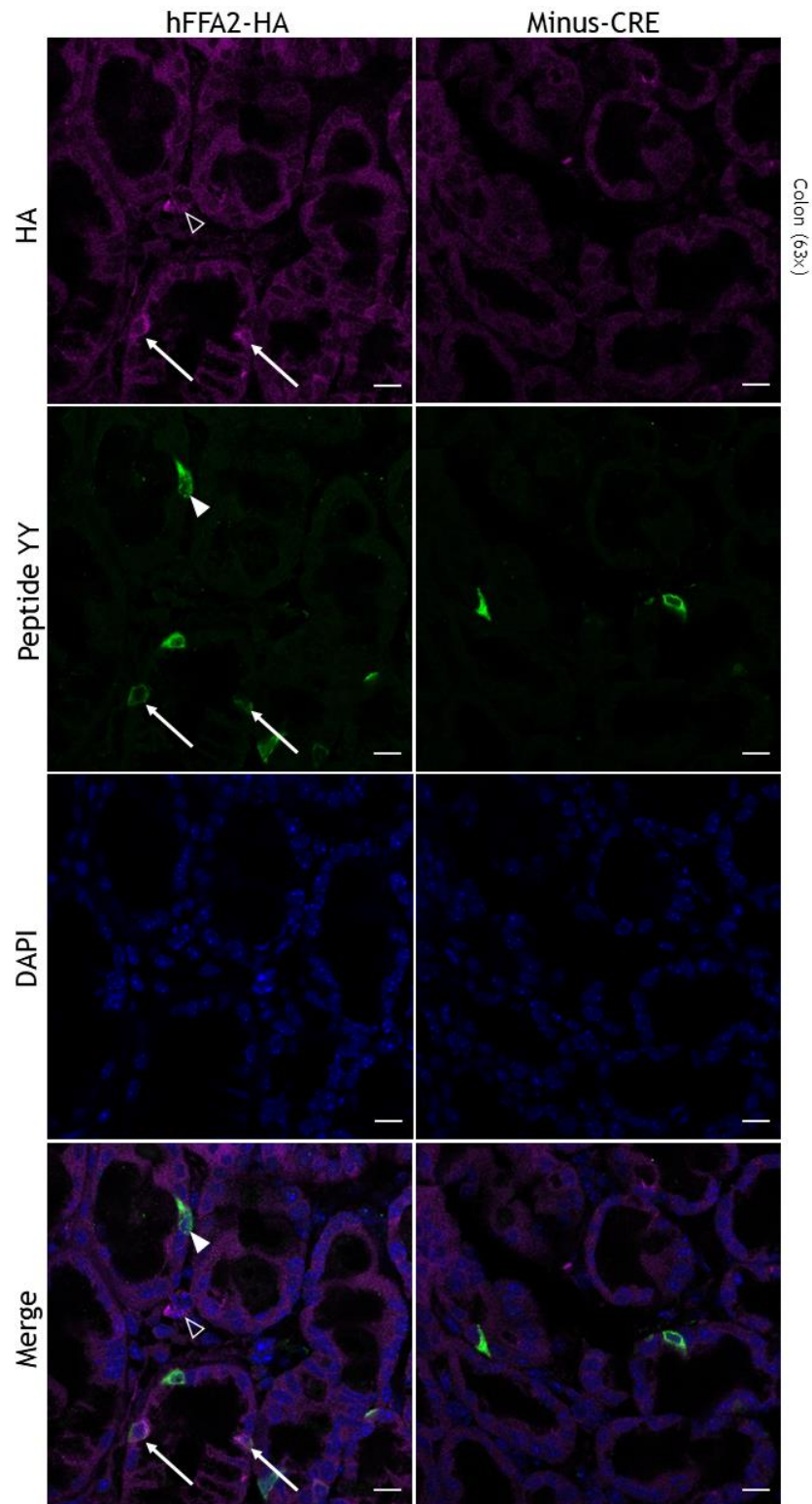


Figure 3.11. Immunohistochemical detection of hFFA2-HA in mouse colon. Sections of colon isolated from hFFA2-HA and minus-CRE mice were fixed with 4% paraformaldehyde and permeabilised with TRITON-X. Cells were incubated with rat anti-HA and rabbit anti-peptide YY (PYY) primary antibodies (1:100) overnight, and with goat anti-rat IgG AlexaFluor-546 (1:400; magenta) and goat anti-rabbit IgG AlexaFluor-488 (1:400; green) secondary antibodies for 2h. Nuclear DNA was labelled with DAPI (blue). Images were taken with 63× objective of Zeiss 880 Laser Scanning Confocal Microscope. Scale bar represents 10µm. Arrows represent examples of co-localisation of anti-PYY and anti-HA antibodies; solid arrowheads represent examples of localisation of anti-PYY, but not anti-HA antibodies; empty arrowheads represent examples of localisation anti-HA, but not anti-PYY antibodies. Representative of 3 fields of view each from 3 animals (n=3). HA - haemagglutinin.

To summarise these results, the overall expression of HA was not significantly different (determined by one-way ANOVA) between EECs of the ileum ($4.1\pm 0.8\%$) and the colon ($3.4\pm 0.4\%$), (*Figure 3.12A*). Neither of the tissues showed colocalisation of GLP-1 and HA. While colocalisation of HA with ChgA and PYY was observed in both sections of the intestine, a larger proportion of cells displayed this in the colon (*Figure 3.12B, C*).

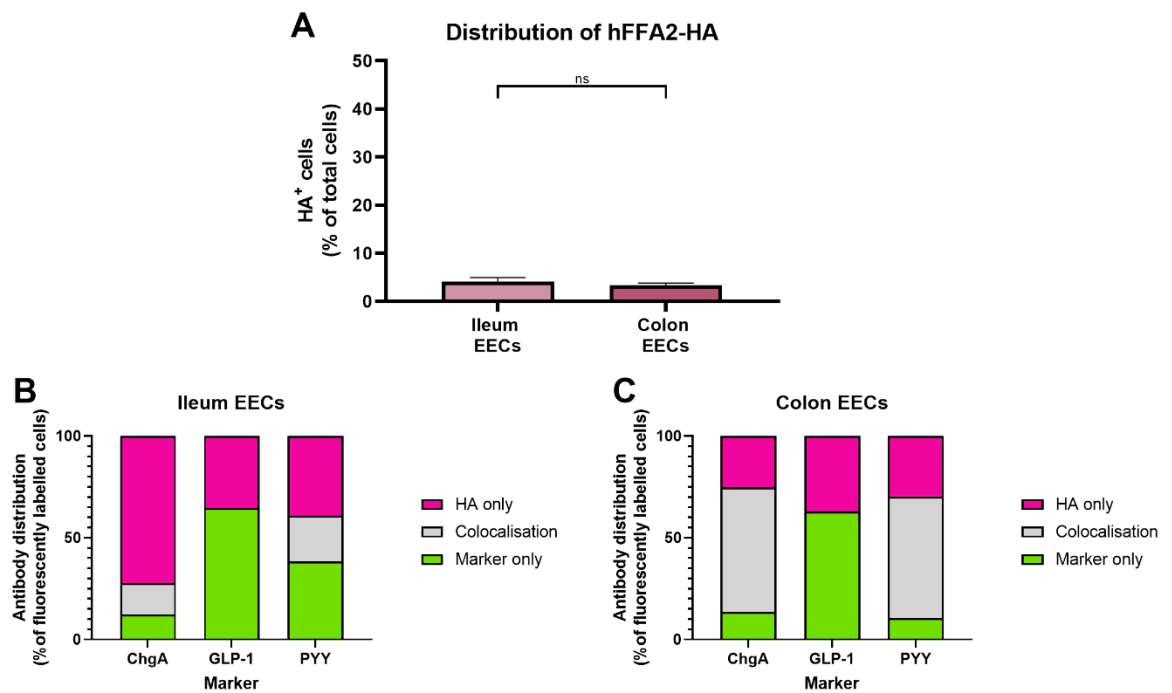


Figure 3.12. Distribution of hFFA2 and cellular markers in hFFA2-HA mouse enteroendocrine cells (EECs). Sections of ileum and colon isolated from hFFA2-HA mice were stained with rat anti-HA and rabbit anti-ChgA, anti-GLP-1 or anti-PYY antibodies. Images were taken with 63× objective of Zeiss 880 Laser Scanning Confocal Microscope. Fluorescent cells in each channel were quantified manually and analysed. A) HA-expressing cells were calculated as a percentage of the total number of cells in each field-of-view in each tissue. Cells showing fluorescence for HA only, cellular markers only or both (colocalisation) were calculated as a percentage of the total number of fluorescently labelled cells in each field-of-view for B) the ileum and C) the colon. Representative of 3 fields of view each from 3 animals (n=3). Data shown as mean±SEM (A) or mean (B, C). ns p>0.05 by one-way ANOVA with Tukey's post-hoc multiple comparisons test. HA - haemagglutinin; ChgA - chromogranin A; GLP-1 - glucagon-like peptide 1; PYY - peptide YY.

In addition to EECs, FFA2 has been observed to be expressed in submucosal lymphatic tissue. Based on this knowledge, antibodies targeting a range of immune markers were utilised in IHC stains of the small intestine. The findings from these images are summarised in *Figure 3.21*.

Firstly, the broad-range haematopoietic cell marker, CD45 was utilised to demonstrate the lineage of the cells in the subendothelial regions of the small intestine. In both the hFFA2-HA and minus-CRE duodenum (*Figure 3.13*), CD45 was found to be expressed all fluorescent cells. While no expression of HA was

observed in the minus-CRE duodenum, 35% of the fluorescently labelled cells in the hFFA2-HA duodenum expressed HA. All HA-expressing cells were found to co-express CD45.

In the ileum (*Figure 3.14*), the expression of CD45 was similar to that of the duodenum, with every fluorescent cell expressing in both hFFA2-HA and minus-CRE. All HA-expressing cells also expressed CD45, while only about 18% of CD45⁺ cells expressed HA. No HA expression was observed in the minus-CRE ileum.

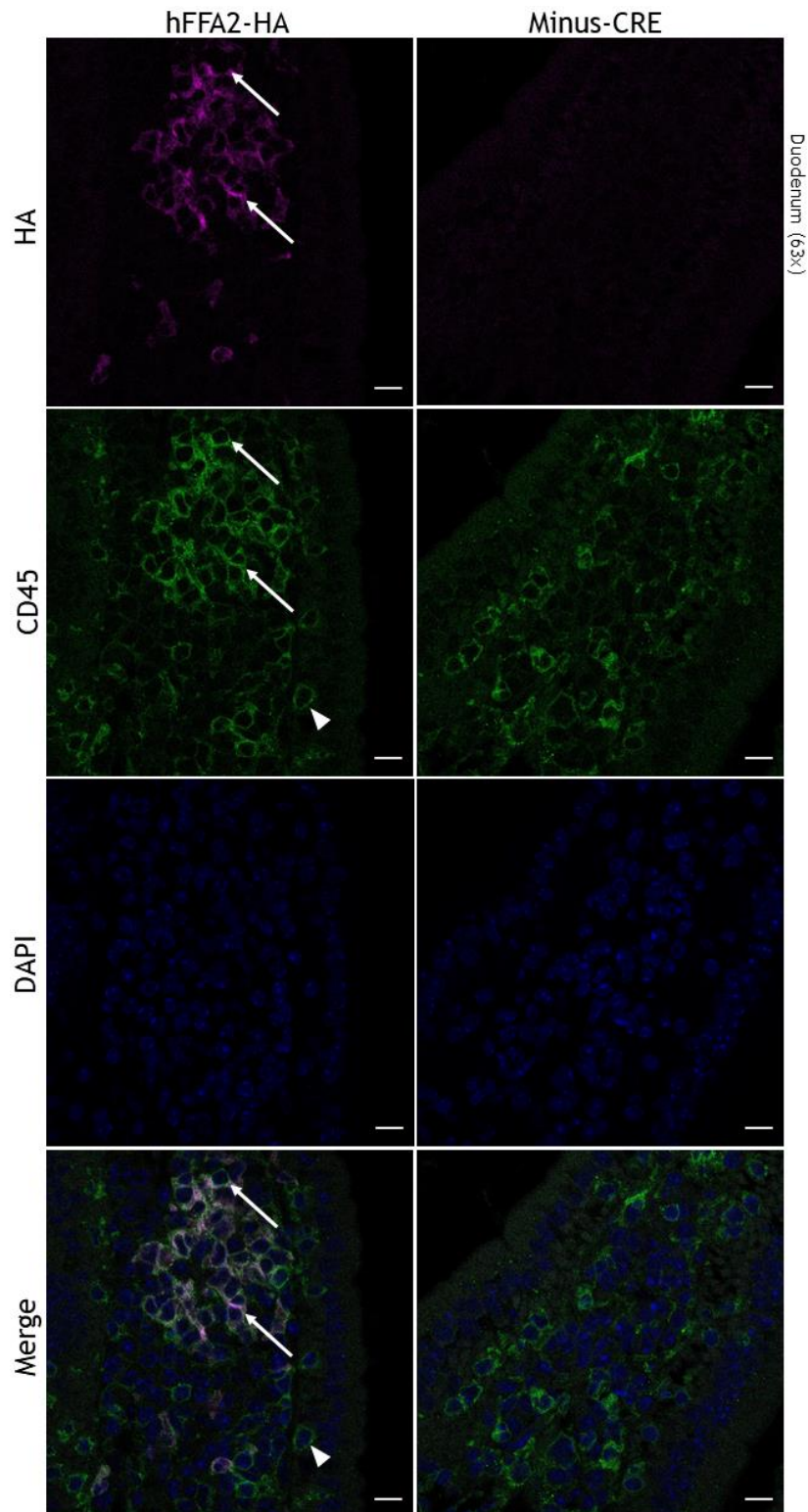


Figure 3.13. Immunohistochemical detection of hFFA2-HA in mouse duodenum. Sections of duodenum isolated from hFFA2-HA and minus-CRE mice were fixed with 4% paraformaldehyde and permeabilised with TRITON-X. Cells were incubated with rat anti-HA and rabbit anti-CD45 primary antibodies (1:100) overnight, and with goat anti-rat IgG AlexaFluor-546 (1:400; magenta) and goat anti-rabbit IgG AlexaFluor-488 (1:400; green) secondary antibodies for 2h. Nuclear DNA was labelled with DAPI (blue). Images were taken with 63 \times objective of Zeiss 880 Laser Scanning Confocal Microscope. Scale bar represents 10 μ m. Arrows represent examples of co-localisation of anti-CD45 and anti-HA antibodies; solid arrowheads represent examples of localisation of anti-CD45, but not anti-HA antibodies. Representative of 3 fields of view each from 3 animals (n=3). HA - haemagglutinin; CD45 - cluster of differentiation 45.

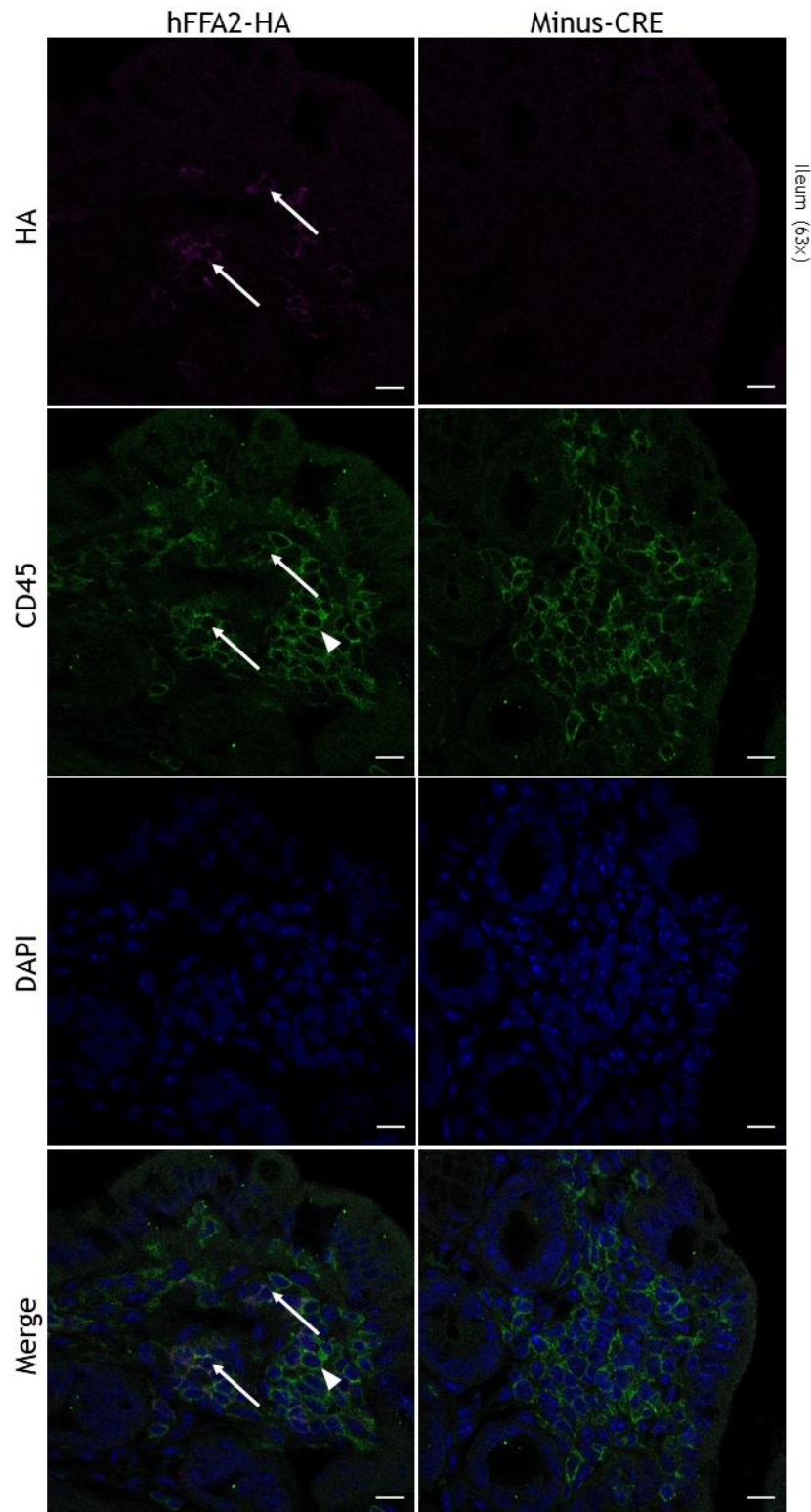


Figure 3.14. Immunohistochemical detection of hFFA2-HA in mouse ileum. Sections of ileum isolated from hFFA2-HA and minus-CRE mice were fixed with 4% paraformaldehyde and permeabilised with TRITON-X. Cells were incubated with rat anti-HA and rabbit anti-CD45 primary antibodies (1:100) overnight, and with goat anti-rat IgG AlexaFluor-546 (1:400; magenta) and goat anti-rabbit IgG AlexaFluor-488 (1:400; green) secondary antibodies for 2h. Nuclear DNA was labelled with DAPI (blue). Images were taken with 63× objective of Zeiss 880 Laser Scanning Confocal Microscope. Scale bar represents 10µm. Arrows represent examples of co-localisation of anti-CD45 and anti-HA antibodies; solid arrowheads represent examples of localisation of anti-CD45, but not anti-HA antibodies. Representative of 3 fields of view each from 3 animals (n=3). HA - haemagglutinin; CD45 - cluster of differentiation 45.

Next, CD3, a T-lymphocyte marker was utilised in the small intestine submucosal lymphatic tissue. In the duodenum (*Figure 3.15*), approximately 50% of the fluorescently labelled cells of the cluster was found to express HA in hFFA2-HA with no observable expression in minus-CRE. As no co-expression of CD3 and HA was observed, the remaining fluorescent cells all expressed CD3 only.

In contrast to the duodenum, the ileum was found to have a larger population of CD3-expressing cells (*Figure 3.16*), with nearly 70% of fluorescent cells showing positive staining in hFFA2-HA. In addition, only about 30% of the cells in hFFA2-HA exhibited HA expression, with a single cell showing co-expression of the two targets. No expression of HA was observed in the minus-CRE ileum.

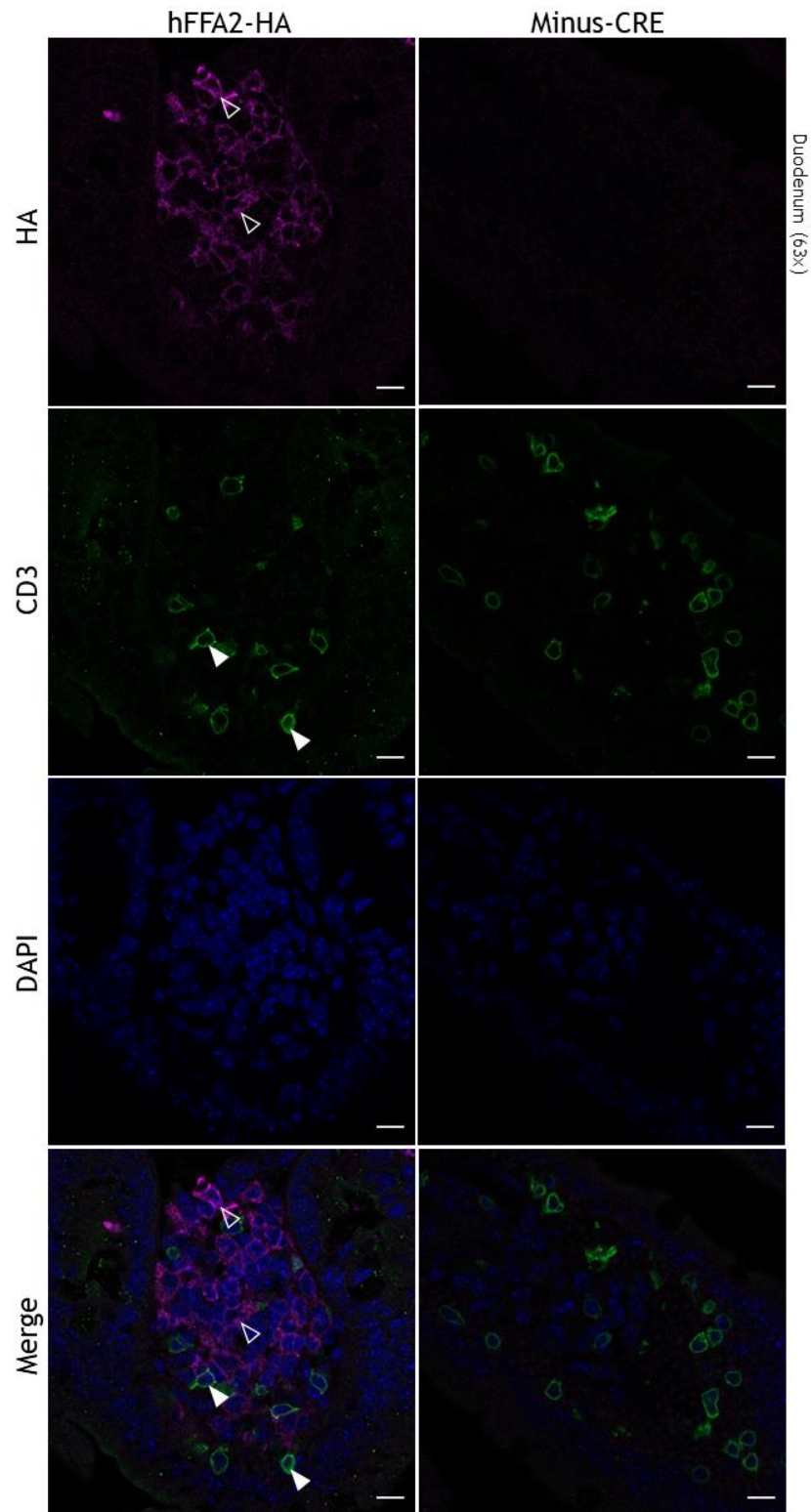


Figure 3.15. Immunohistochemical detection of hFFA2-HA in mouse duodenum. Sections of duodenum isolated from hFFA2-HA and minus-CRE mice were fixed with 4% paraformaldehyde and permeabilised with TRITON-X. Cells were incubated with rat anti-HA and rabbit anti-CD3 primary antibodies (1:100) overnight, and with goat anti-rat IgG AlexaFluor-546 (1:400; magenta) and goat anti-rabbit IgG AlexaFluor-488 (1:400; green) secondary antibodies for 2h. Nuclear DNA was labelled with DAPI (blue). Images were taken with 63× objective of Zeiss 880 Laser Scanning Confocal Microscope. Scale bar represents 10µm. Solid arrowheads represent examples of localisation of anti-CD3, but not anti-HA antibodies; empty arrowheads represent examples of localisation anti-HA, but not anti-CD3 antibodies. Representative of 3 fields of view each from 3 animals (n=3). HA - haemagglutinin; CD3 - cluster of differentiation 3.

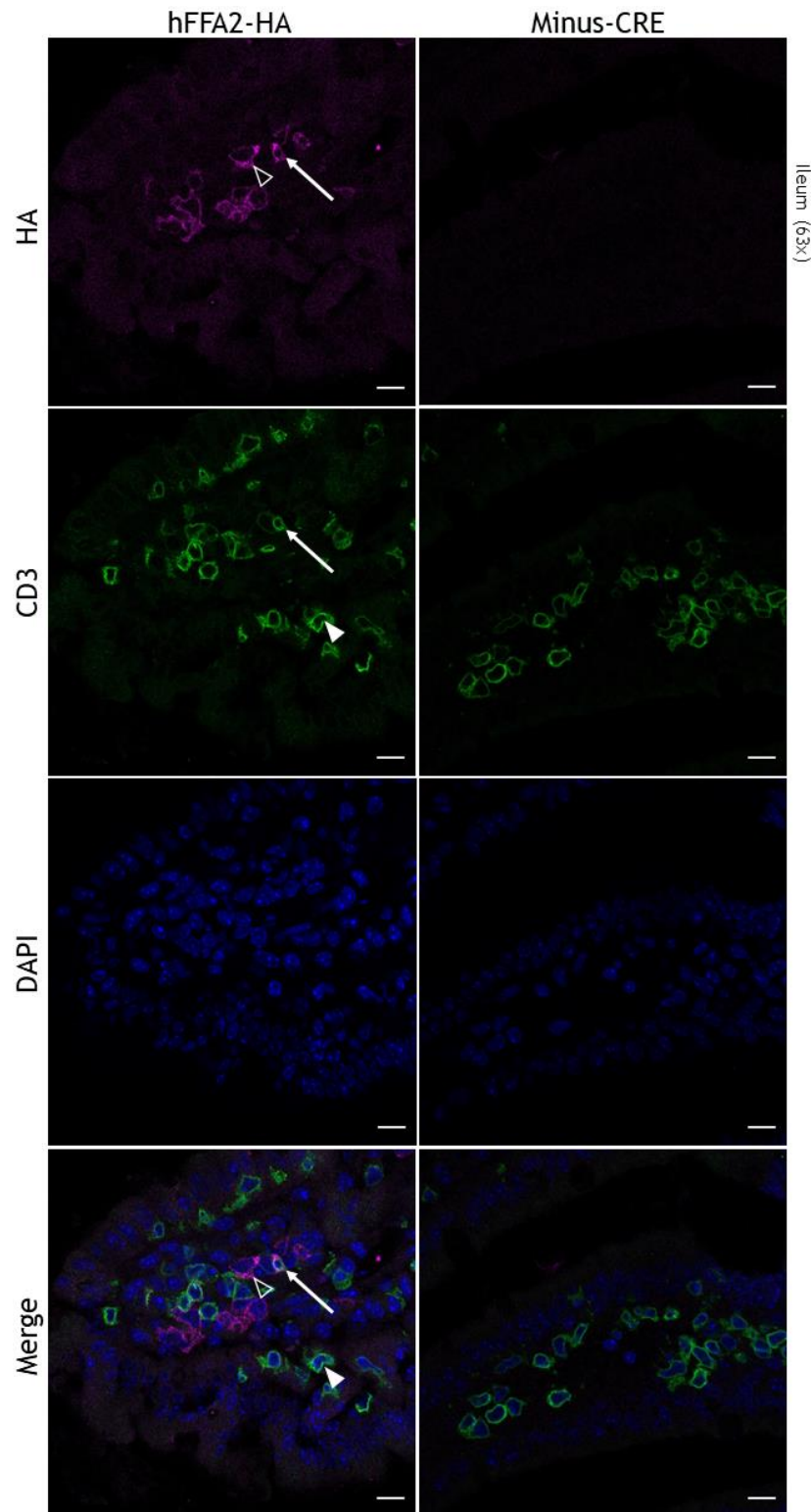


Figure 3.16. Immunohistochemical detection of hFFA2-HA in mouse ileum. Sections of ileum isolated from hFFA2-HA and minus-CRE mice were fixed with 4% paraformaldehyde and permeabilised with TRITON-X. Cells were incubated with rat anti-HA and rabbit anti-CD3 primary antibodies (1:100) overnight, and with goat anti-rat IgG AlexaFluor-546 (1:400; magenta) and goat anti-rabbit IgG AlexaFluor-488 (1:400; green) secondary antibodies for 2h. Nuclear DNA was labelled with DAPI (blue). Images were taken with 63 \times objective of Zeiss 880 Laser Scanning Confocal Microscope. Scale bar represents 10 μ m. Arrows represent examples of co-localisation of anti-CD3 and anti-HA antibodies; solid arrowheads represent examples of localisation of anti-CD3, but not anti-HA antibodies; empty arrowheads represent examples of localisation anti-HA, but not anti-CD3 antibodies. Representative of 3 fields of view each from 3 animals (n=3). HA - haemagglutinin; CD3 - cluster of differentiation 3.

CD11b is a marker for a range of leukocytes (including macrophages and natural killer cells) and was used to stain these cells in the small intestine. In the duodenum (*Figure 3.17*), nearly 60% of fluorescently labelled cells were found to express CD11b in hFFA2-HA. Expression of HA was only observed in the hFFA2-HA duodenum, in approximately 40% of fluorescent cells. There was no co-expression of CD11b and HA found in this tissue.

In the ileum of hFFA2-HA mice, cells expressing CD11b account for approximately 75% of the fluorescent cells (*Figure 3.18*). On the other hand, only 25% of the labelled cells in the hFFA2-HA ileum and no cells in the minus-CRE ileum were found to express HA. As in the duodenum, no co-expression of the two targets was observed in the hFFA2-HA ileum.

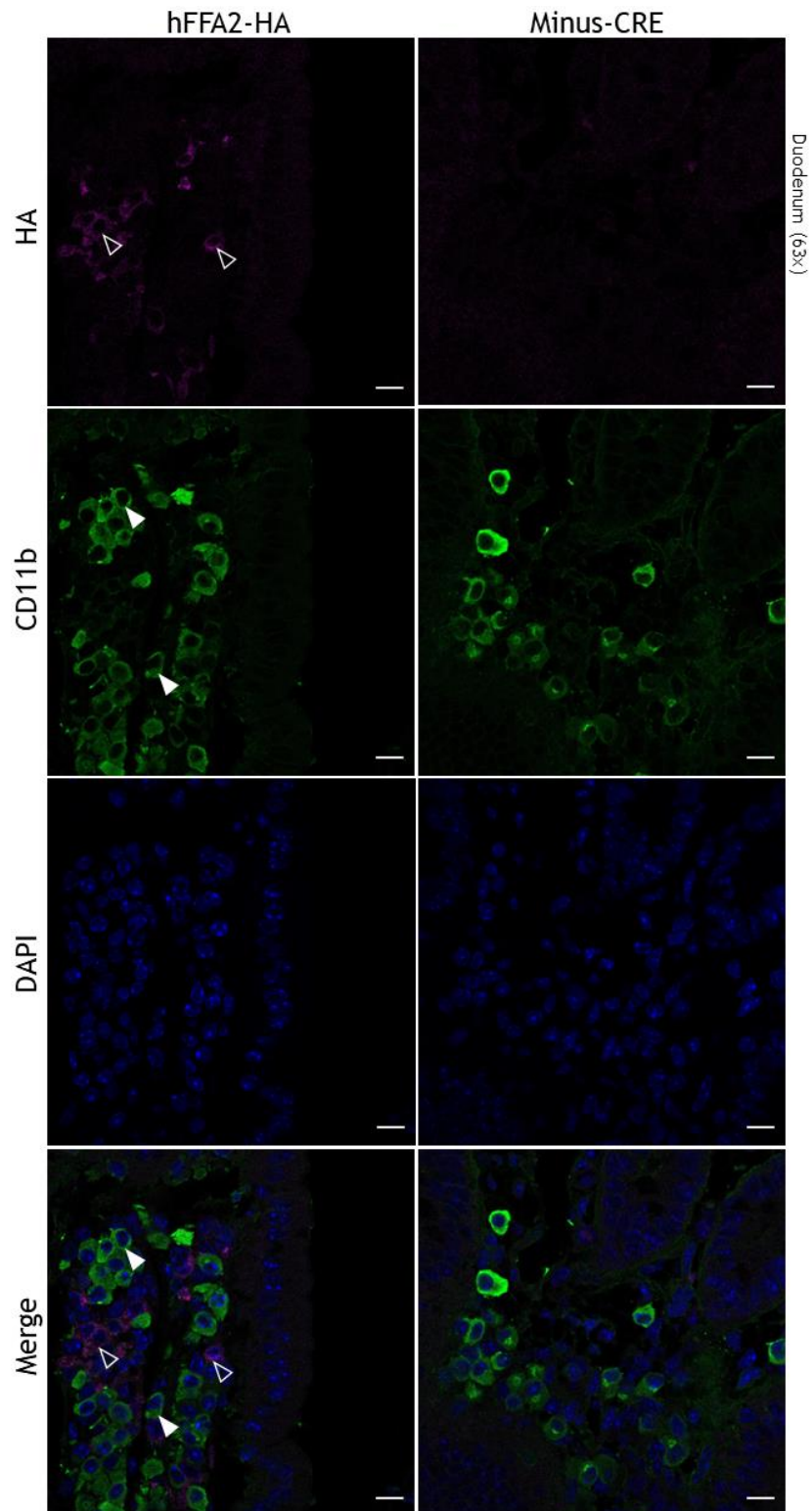


Figure 3.17. Immunohistochemical detection of hFFA2-HA in mouse duodenum. Sections of duodenum isolated from hFFA2-HA and minus-CRE mice were fixed with 4% paraformaldehyde and permeabilised with TRITON-X. Cells were incubated with rat anti-HA and rabbit anti-CD11b primary antibodies (1:100) overnight, and with goat anti-rat IgG AlexaFluor-546 (1:400; magenta) and goat anti-rabbit IgG AlexaFluor-488 (1:400; green) secondary antibodies for 2h. Nuclear DNA was labelled with DAPI (blue). Images were taken with 63 \times objective of Zeiss 880 Laser Scanning Confocal Microscope. Scale bar represents 10 μ m. Solid arrowheads represent examples of localisation of anti-CD11b, but not anti-HA antibodies; empty arrowheads represent examples of localisation anti-HA, but not anti-CD11b antibodies. Representative of 3 fields of view each from 3 animals (n=3). HA - haemagglutinin; CD11b - cluster of differentiation 11b.

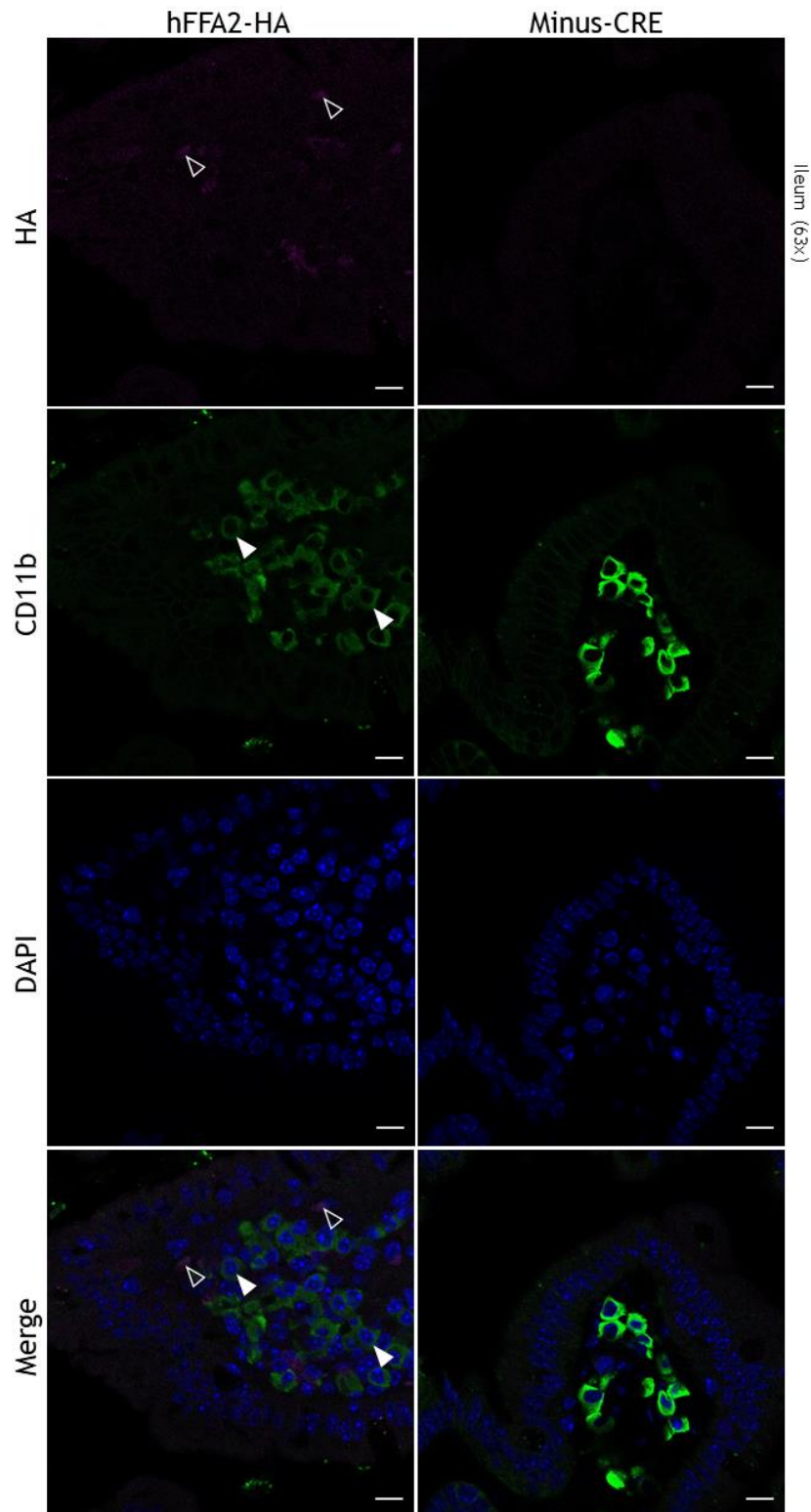


Figure 3.18. Immunohistochemical detection of hFFA2-HA in mouse ileum. Sections of ileum isolated from hFFA2-HA and minus-CRE mice were fixed with 4% paraformaldehyde and permeabilised with TRITON-X. Cells were incubated with rat anti-HA and rabbit anti-CD11b primary antibodies (1:100) overnight, and with goat anti-rat IgG AlexaFluor-546 (1:400; magenta) and goat anti-rabbit IgG AlexaFluor-488 (1:400; green) secondary antibodies for 2h. Nuclear DNA was labelled with DAPI (blue). Images were taken with 63× objective of Zeiss 880 Laser Scanning Confocal Microscope. Scale bar represents 10µm. Solid arrowheads represent examples of localisation of anti-CD11b, but not anti-HA antibodies; empty arrowheads represent examples of localisation anti-HA, but not anti-CD11b antibodies. Representative of 3 fields of view each from 3 animals (n=3). HA - haemagglutinin; CD11b - cluster of differentiation 11b.

CD11c, a marker primarily for DCs, was used next to stain the small intestine. In the duodenum (*Figure 3.19*), CD11c was found to be expressed in nearly all of the fluorescently labelled cells in hFFA2-HA. HA was not expressed in the minus-CRE duodenum but it was in circa 75% of the fluorescent cells in hFFA2-HA. Every cell positive for HA in the hFFA2-HA was also positive for CD11c.

In the hFFA2-HA ileum (*Figure 3.20*), 95% of labelled cells displayed staining with CD11c. Of the fluorescent cells in hFFA2-HA, merely 42% was found positive for HA, with only 5% not colocalised with CD11c. No HA expression was observed in the minus-CRE ileum.

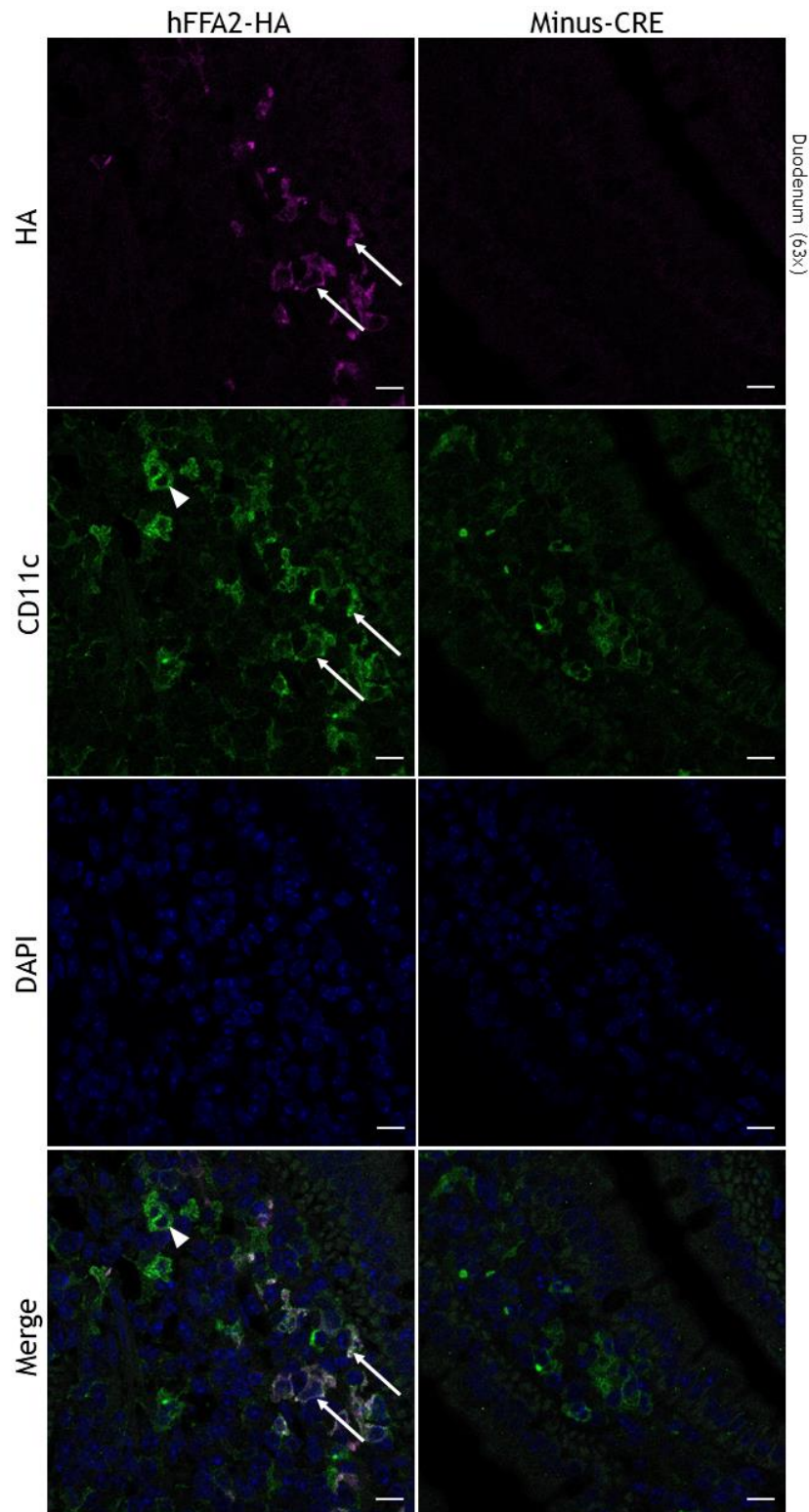


Figure 3.19. Immunohistochemical detection of hFFA2-HA in mouse duodenum. Sections of duodenum isolated from hFFA2-HA and minus-CRE mice were fixed with 4% paraformaldehyde and permeabilised with TRITON-X. Cells were incubated with rat anti-HA and rabbit anti-CD11c primary antibodies (1:100) overnight, and with goat anti-rat IgG AlexaFluor-546 (1:400; magenta) and goat anti-rabbit IgG AlexaFluor-488 (1:400; green) secondary antibodies for 2h. Nuclear DNA was labelled with DAPI (blue). Images were taken with 63× objective of Zeiss 880 Laser Scanning Confocal Microscope. Scale bar represents 10µm. Arrows represent examples of co-localisation of anti-CD11c and anti-HA antibodies; solid arrowheads represent examples of localisation of anti-CD11c, but not anti-HA antibodies. Representative of 3 fields of view each from 3 animals (n=3). HA - haemagglutinin; CD11c - cluster of differentiation 11c.

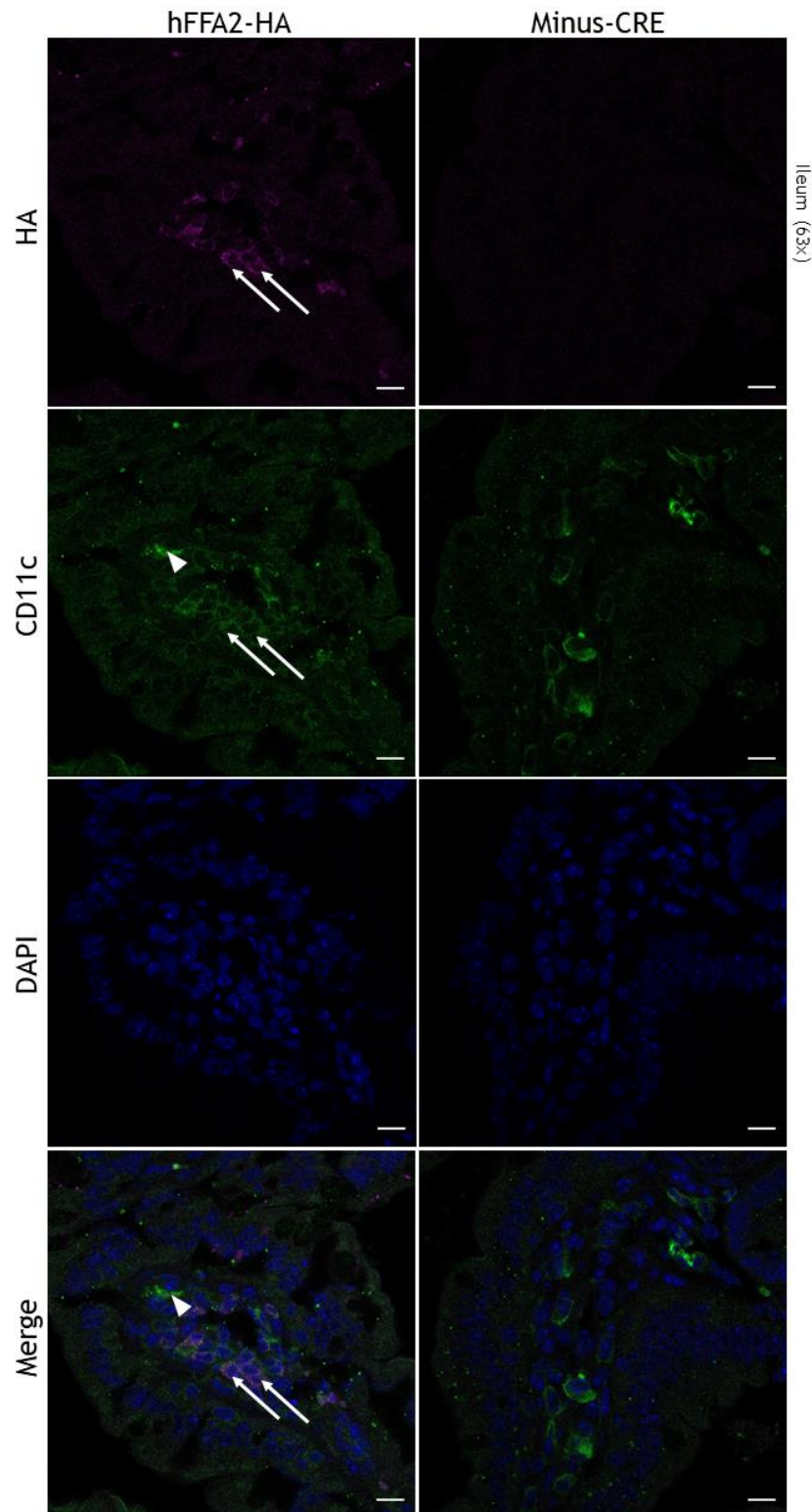


Figure 3.20. Immunohistochemical detection of hFFA2-HA in mouse ileum. Sections of ileum isolated from hFFA2-HA and minus-CRE mice were fixed with 4% paraformaldehyde and permeabilised with TRITON-X. Cells were incubated with rat anti-HA and rabbit anti-CD11c primary antibodies (1:100) overnight, and with goat anti-rat IgG AlexaFluor-546 (1:400; magenta) and goat anti-rabbit IgG AlexaFluor-488 (1:400; green) secondary antibodies for 2h. Nuclear DNA was labelled with DAPI (blue). Images were taken with 63× objective of Zeiss 880 Laser Scanning Confocal Microscope. Scale bar represents 10µm. Arrows represent examples of co-localisation of anti-CD11c and anti-HA antibodies; solid arrowheads represent examples of localisation of anti-CD11c, but not anti-HA antibodies. Representative of 3 fields of view each from 3 animals (n=3). HA - haemagglutinin; CD11c - cluster of differentiation 11c.

In summary, the overall expression of HA was significantly higher ($p > 0.05$, determined by one-way ANOVA) in immune cells of the duodenum ($11.7\% \pm 0.5\%$) than in the ileum ($5.0\% \pm 0.7\%$) (Figure 3.21A). This difference is also apparent in the percentage of fluorescent cells positive for HA. CD3 and CD11b did not colocalise with HA in either of the tissues. All HA⁺ cells also expressed CD45 in each tissue. In the duodenum, all HA⁺ cells co-expressed CD11c, while in the ileum around 12% of HA⁺ cell did not (Figure 3.21B, C).

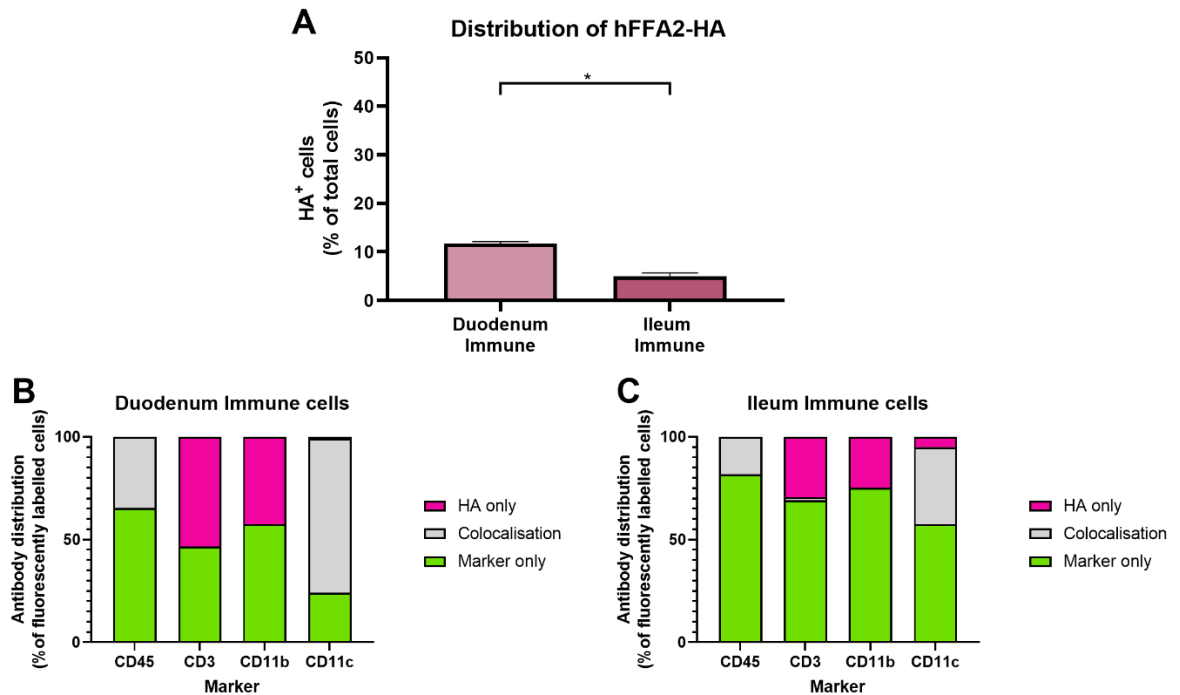


Figure 3.21. Distribution of hFFA2 and cellular markers in hFFA2-HA mouse intestinal immune cells. Sections of duodenum and ileum isolated from hFFA2-HA mice were stained with rat anti-HA and rabbit anti-CD45, anti-CD3, anti-CD11b or anti-CD11c antibodies. Images were taken with 63× objective of Zeiss 880 Laser Scanning Confocal Microscope. Fluorescent cells in each channel were quantified manually and analysed. A) HA-expressing cells were calculated as a percentage of the total number of cells in each field-of-view in each tissue. Cells showing fluorescence for HA only, cellular markers only or both (colocalisation) were calculated as a percentage of the total number of fluorescently labelled cells in each field-of-view for B) the duodenum and C) the ileum. Representative of 3 fields of view each from 3 animals ($n=3$). Data shown as mean \pm SEM (A) or mean (B, C). * $p < 0.05$ by one-way ANOVA with Tukey's post-hoc multiple comparisons test. HA - haemagglutinin; CD - cluster of differentiation.

3.2.3 Immunohistochemical investigation of transgenic mouse spleen

In order to further explore the expression of hFFA2-HA in immune cells, antibodies targeting a range of immune cell markers were used in mouse spleen immunostaining. The spleen has various distinguishable regions, each with distinct populations of immune cells, therefore these were investigated separately (white pulp (WP) and marginal zone (MZ) together, and red pulp (RP) separately). Despite transfusion with PFA during tissue preparation, the spleen

being a highly vascularised organ, the removal of erythrocytes was not efficient. In control stains even in the absence of primary antibodies, erythrocytes were highly fluorescent, particularly in the red and blue channels (*Figure 3.22*). Since these cells can be recognised from their characteristic shape and the overlapping fluorescence from the red and blue channels, they did not interfere with the interpretation of the spleen stains.

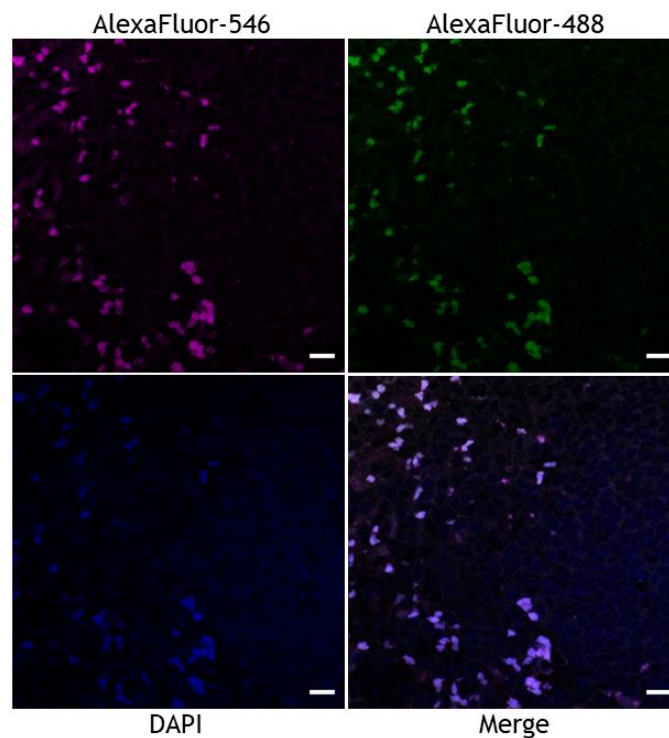


Figure 3.22. Immunohistochemical detection of erythrocytes in mouse spleen. Sections of spleen isolated from hFFA2-HA mice were fixed with 4% paraformaldehyde and permeabilised with TRITON-X. Cells were incubated in the absence of primary antibodies overnight, and with goat anti-rat IgG AlexaFluor-546 (1:400; magenta) and goat anti-rabbit IgG AlexaFluor-488 (1:400; green) secondary antibodies for 2h. Nuclear DNA was labelled with DAPI (blue). Images were taken with 63× objective of Zeiss 880 Laser Scanning Confocal Microscope. Scale bar represents 10µm. Representative of 3 fields of view each from 3 animals (n=3).

Initially, the broad-range haematopoietic cell marker CD45 was targeted with antibodies. In hFFA2-HA, of the fluorescently labelled cells 88% in WP/MZ and 95% in RP were positive for CD45. In the hFFA2-HA WP/MZ, approximately 14% of the cells were positively stained for HA, with no staining in the corresponding minus-CRE tissue (*Figure 3.23*). In the hFFA2-HA RP, the expression of HA was more widespread, with 40% of labelled cells being positive (*Figure 3.24*). Again, no HA⁺ cells were observed in the minus-CRE sample. While only 2% of labelled cells co-expressed HA and CD45 in the WP/MZ, in the RP co-expression was observed in 36% of fluorescent cells.

The findings from these images are summarised in *Figure 3.29*.

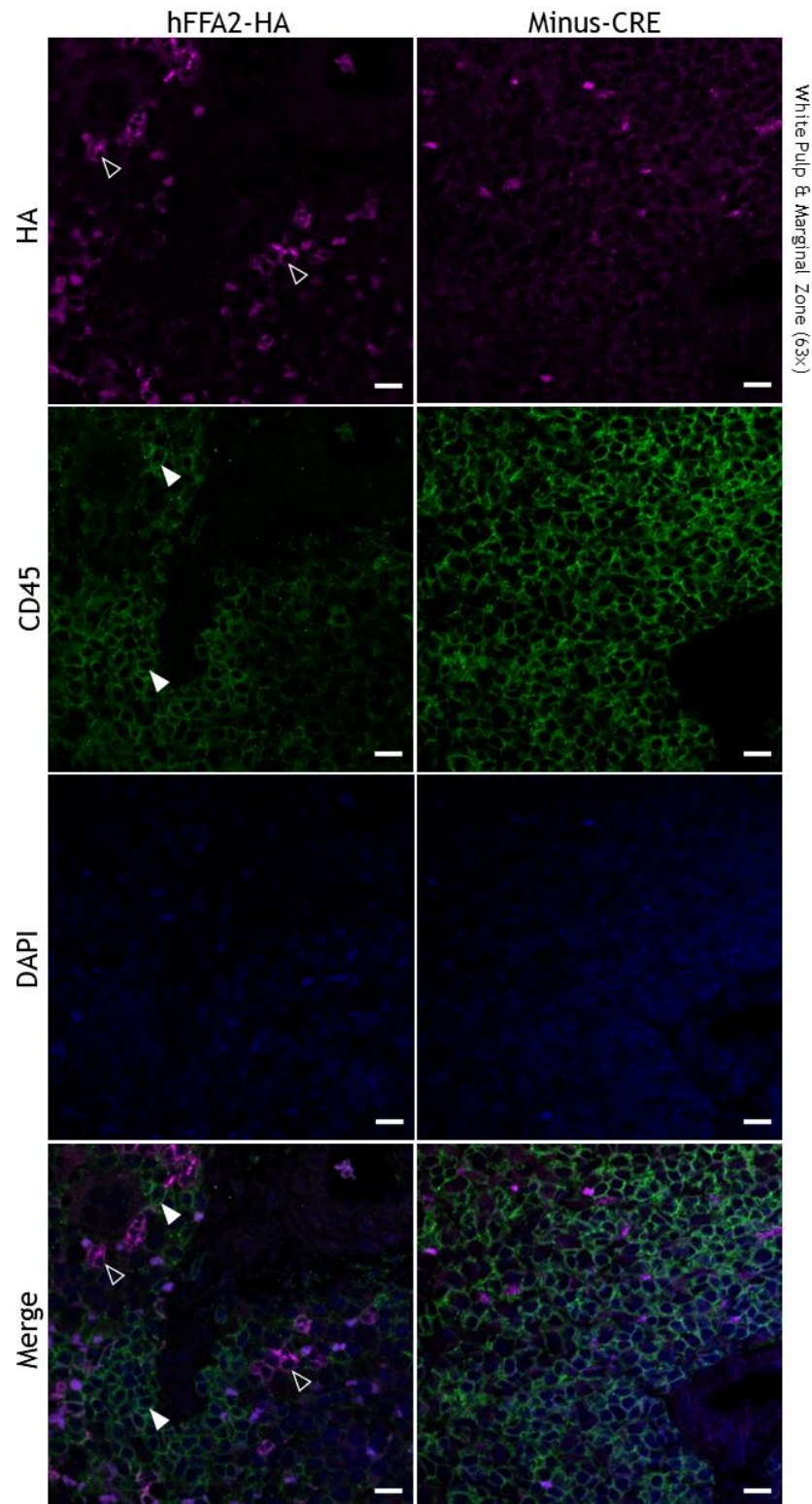


Figure 3.23. Immunohistochemical detection of hFFA2-HA in mouse spleen white pulp and marginal zone. Sections of spleen isolated from hFFA2-HA and minus-CRE mice were fixed with 4% paraformaldehyde and permeabilised with TRITON-X. Cells were incubated with rat anti-HA and rabbit anti-CD45 primary antibodies (1:100) overnight, and with goat anti-rat IgG AlexaFluor-546 (1:400; magenta) and goat anti-rabbit IgG AlexaFluor-488 (1:400; green) secondary antibodies for 2h. Nuclear DNA was labelled with DAPI (blue). Images were taken with 63× objective of Zeiss 880 Laser Scanning Confocal Microscope. Scale bar represents 10µm. Solid arrowheads represent examples of localisation of anti-CD45, but not anti-HA antibodies; empty arrowheads represent examples of localisation anti-HA, but not anti-CD45 antibodies. Representative of 3 fields of view each from 3 animals (n=3). HA - haemagglutinin; CD45 - cluster of differentiation 45.

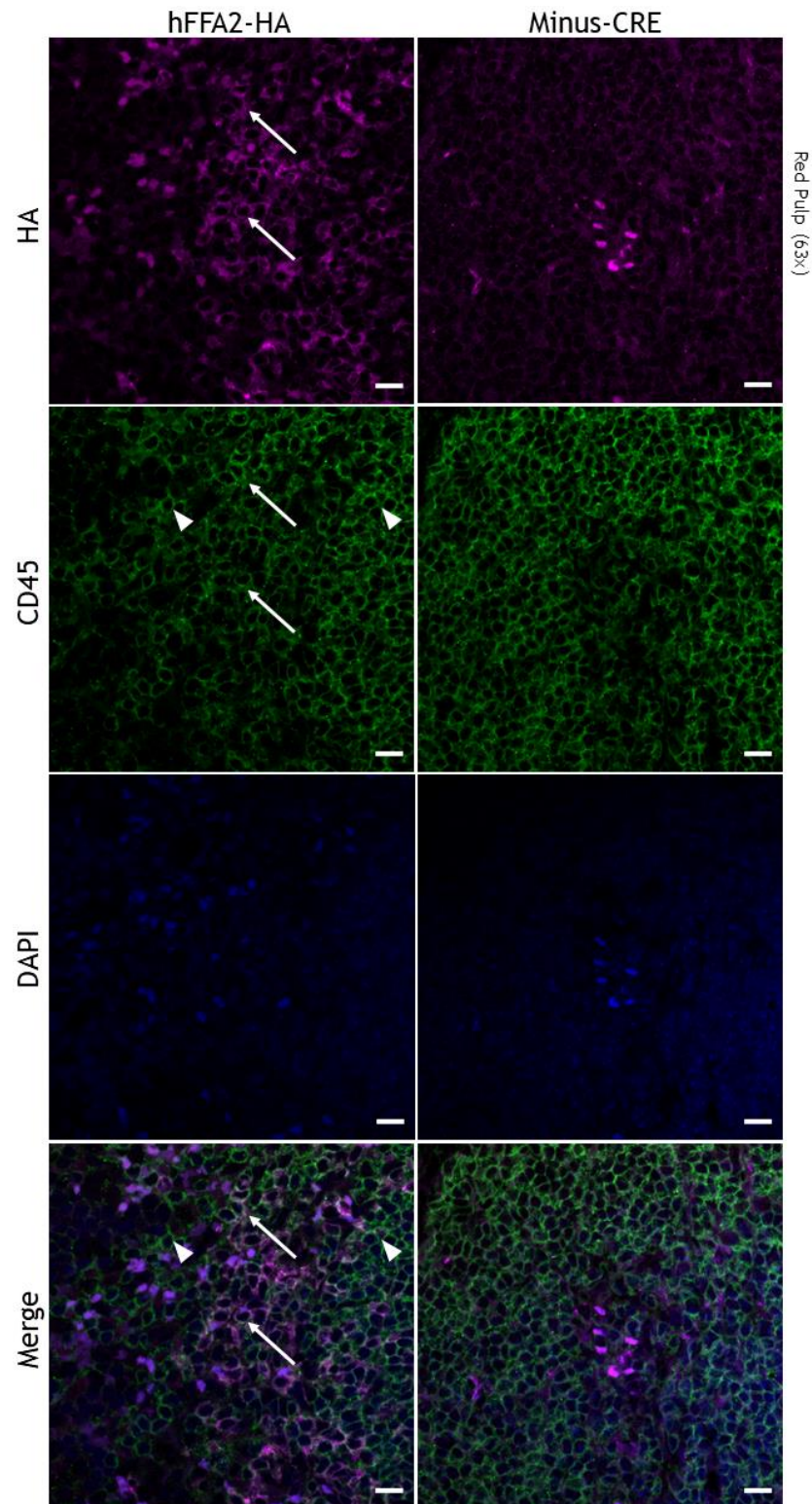


Figure 3.24. Immunohistochemical detection of hFFA2-HA in mouse spleen red pulp. Sections of spleen isolated from hFFA2-HA and minus-CRE mice were fixed with 4% paraformaldehyde and permeabilised with TRITON-X. Cells were incubated with rat anti-HA and rabbit anti-CD45 primary antibodies (1:100) overnight, and with goat anti-rat IgG AlexaFluor-546 (1:400; magenta) and goat anti-rabbit IgG AlexaFluor-488 (1:400; green) secondary antibodies for 2h. Nuclear DNA was labelled with DAPI (blue). Images were taken with 63 \times objective of Zeiss 880 Laser Scanning Confocal Microscope. Scale bar represents 10 μ m. Arrows represent examples of co-localisation of anti-CD45 and anti-HA antibodies; solid arrowheads represent examples of localisation of anti-CD45, but not anti-HA antibodies. Representative of 3 fields of view each from 3 animals (n=3). HA - haemagglutinin; CD45 - cluster of differentiation 45.

Following CD45, antibodies targeting the leukocyte marker CD11b were utilised. In comparison to CD45, the distribution of CD11b was more limited. While in the WP/MZ of hFFA2-HA approximately 37% of labelled cells express CD11b (*Figure 3.25*), only about 25% of fluorescent cells in hFFA2-HA RP (*Figure 3.26*). Minus-CRE spleen does not display expression of HA in either area. By contrast, in hFFA2-HA WP/MZ over 60%, and in the RP 75% of fluorescently labelled cells expressed HA. Co-expression of HA and CD11b was not observed in either of the areas.

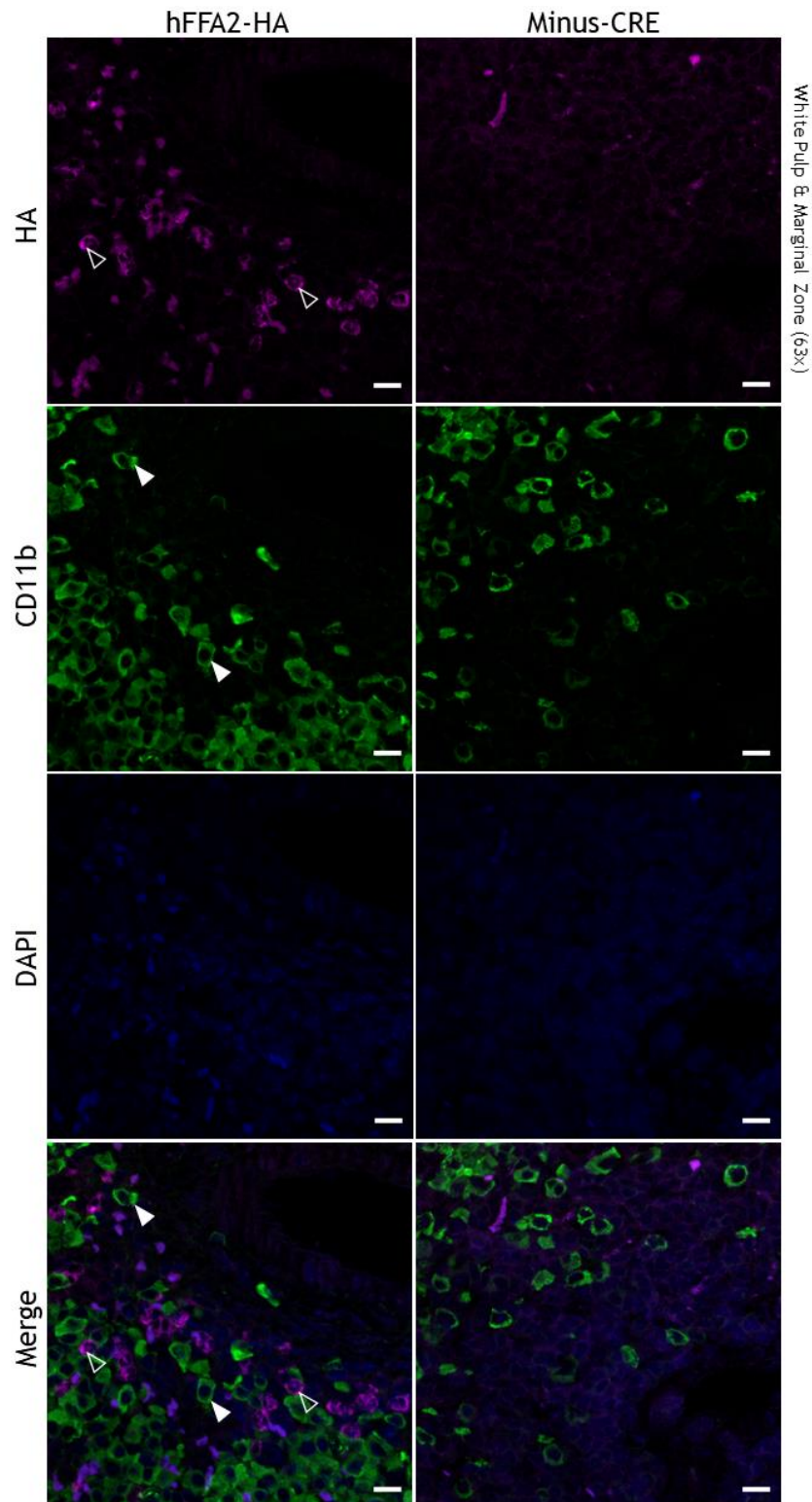


Figure 3.25. Immunohistochemical detection of hFFA2-HA in mouse spleen white pulp and marginal zone. Sections of spleen isolated from hFFA2-HA and minus-CRE mice were fixed with 4% paraformaldehyde and permeabilised with TRITON-X. Cells were incubated with rat anti-HA and rabbit anti-CD11b primary antibodies (1:100) overnight, and with goat anti-rat IgG AlexaFluor-546 (1:400; magenta) and goat anti-rabbit IgG AlexaFluor-488 (1:400; green) secondary antibodies for 2h. Nuclear DNA was labelled with DAPI (blue). Images were taken with 63× objective of Zeiss 880 Laser Scanning Confocal Microscope. Scale bar represents 10µm. Solid arrowheads represent examples of localisation of anti-CD11b, but not anti-HA antibodies; empty arrowheads represent examples of localisation anti-HA, but not anti-CD11b antibodies. Representative of 3 fields of view each from 3 animals (n=3). HA - haemagglutinin; CD11b - cluster of differentiation 11b.

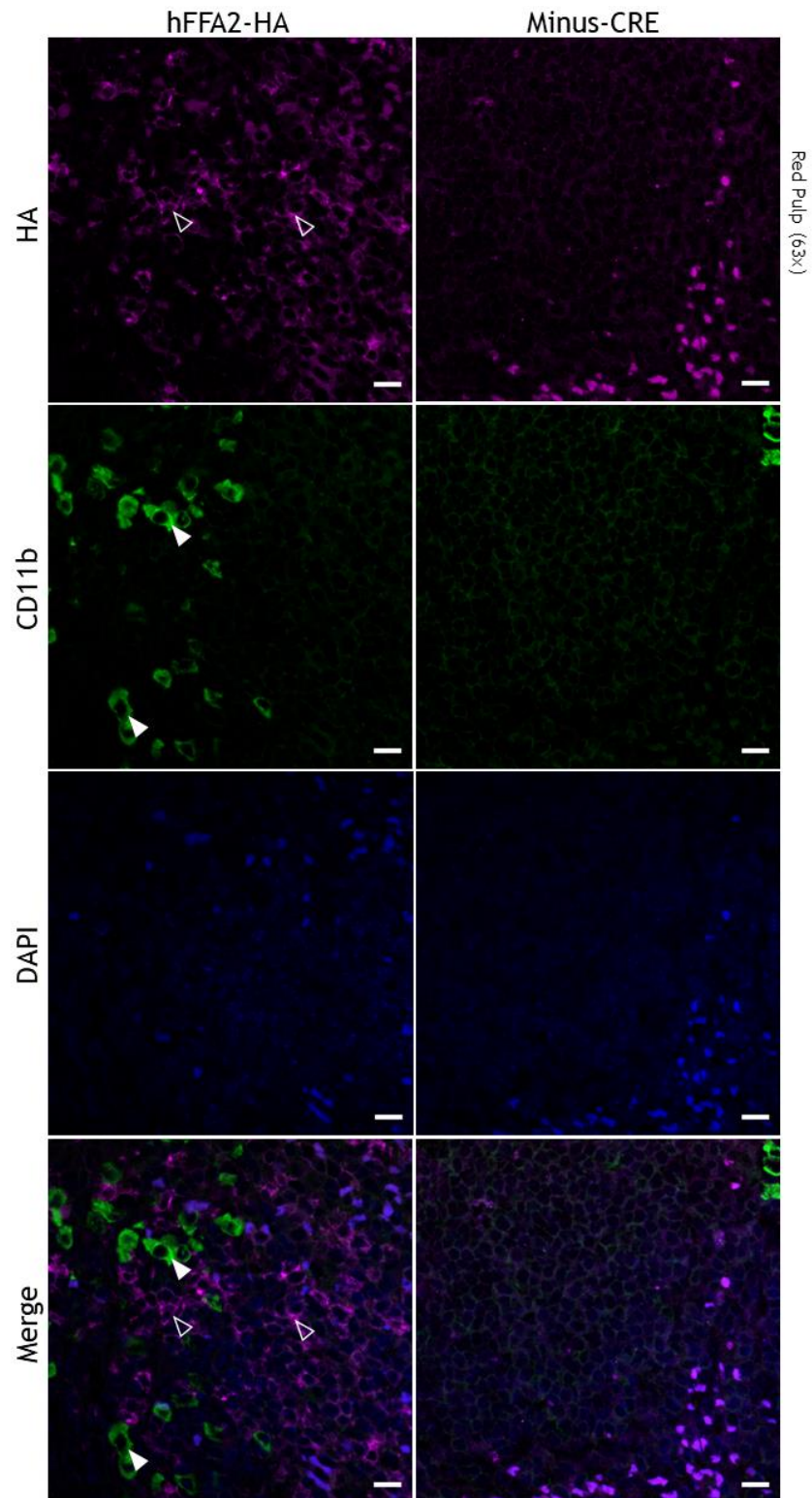


Figure 3.26. Immunohistochemical detection of hFFA2-HA in mouse spleen red pulp. Sections of spleen isolated from hFFA2-HA and minus-CRE mice were fixed with 4% paraformaldehyde and permeabilised with TRITON-X. Cells were incubated with rat anti-HA and rabbit anti-CD11b primary antibodies (1:100) overnight, and with goat anti-rat IgG AlexaFluor-546 (1:400; magenta) and goat anti-rabbit IgG AlexaFluor-488 (1:400; green) secondary antibodies for 2h. Nuclear DNA was labelled with DAPI (blue). Images were taken with 63× objective of Zeiss 880 Laser Scanning Confocal Microscope. Scale bar represents 10µm. Solid arrowheads represent examples of localisation of anti-CD11b, but not anti-HA antibodies; empty arrowheads represent examples of localisation anti-HA, but not anti-CD11b antibodies. Representative of 3 fields of view each from 3 animals (n=3). HA - haemagglutinin; CD11b - cluster of differentiation 11b.

The expression of CD11c, unlike that of previous markers, appeared to display more variation between the WP/MZ and the RP. Specifically, 89% of fluorescently labelled cells in the WP/MZ expressed CD11c, while only 40% in the RP did so. In the hFFA2-HA WP/MZ (*Figure 3.27*), about 42% of labelled cells were found to express HA while in the RP this was higher with 79% of labelled cells expressing HA (*Figure 3.28*). HA expression was not observed in the minus-CRE spleen. In the WP/MZ, 31% of the fluorescent cells co-expressed HA and CD11c, while in the RP only 19% of labelled cells did so.

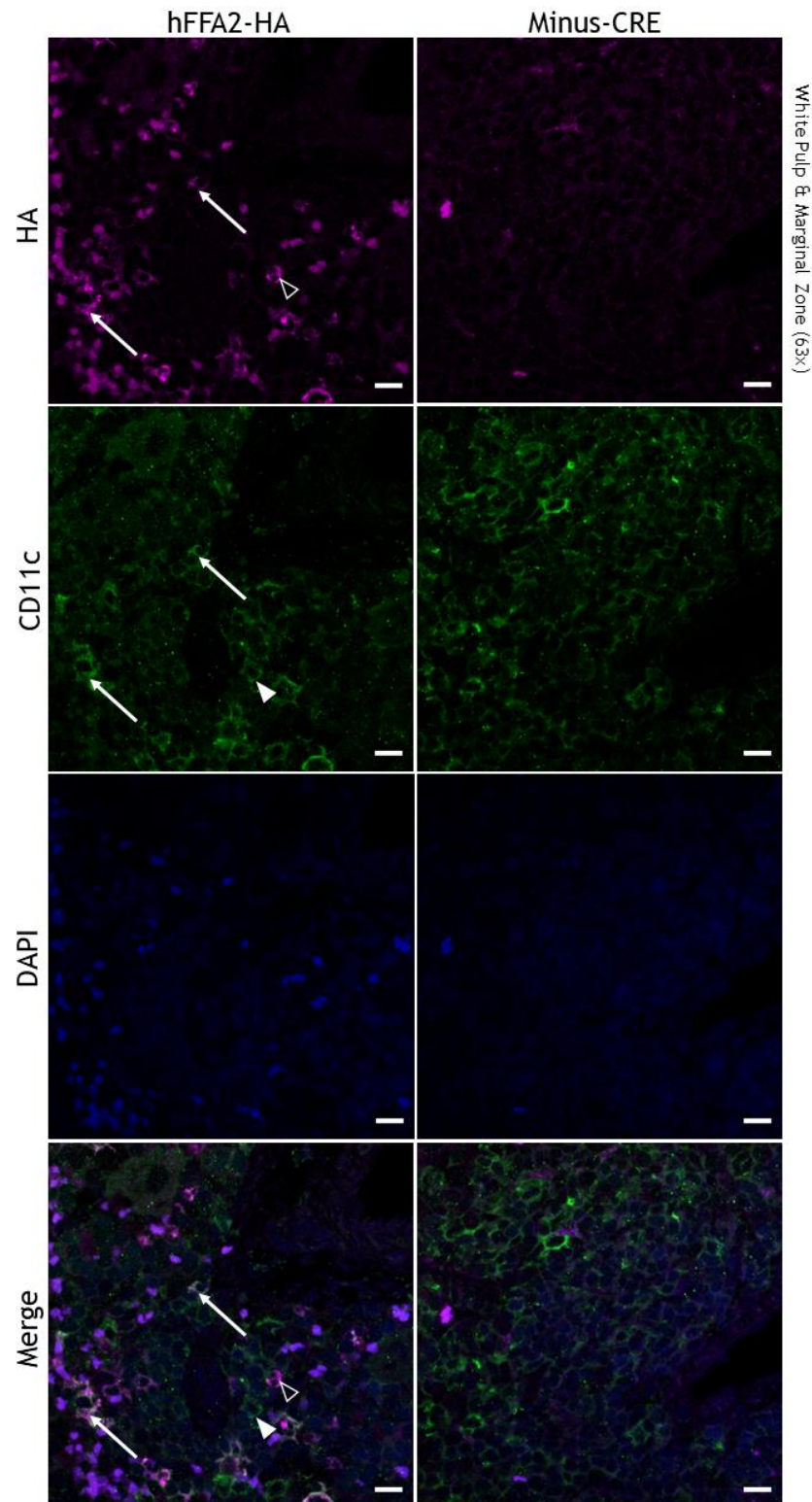


Figure 3.27. Immunohistochemical detection of hFFA2-HA in mouse spleen white pulp and marginal zone. Sections of spleen isolated from hFFA2-HA and minus-CRE mice were fixed with 4% paraformaldehyde and permeabilised with TRITON-X. Cells were incubated with rat anti-HA and rabbit anti-CD11c primary antibodies (1:100) overnight, and with goat anti-rat IgG AlexaFluor-546 (1:400; magenta) and goat anti-rabbit IgG AlexaFluor-488 (1:400; green) secondary antibodies for 2h. Nuclear DNA was labelled with DAPI (blue). Images were taken with 63 \times objective of Zeiss 880 Laser Scanning Confocal Microscope. Scale bar represents 10 μ m. Arrows represent examples of co-localisation of anti-CD11c and anti-HA antibodies; solid arrowheads represent examples of localisation of anti-CD11c, but not anti-HA antibodies; empty arrowheads represent examples of localisation anti-HA, but not anti-CD11c antibodies. Representative of 3 fields of view each from 3 animals (n=3). HA - haemagglutinin; CD11c - cluster of differentiation 11c.

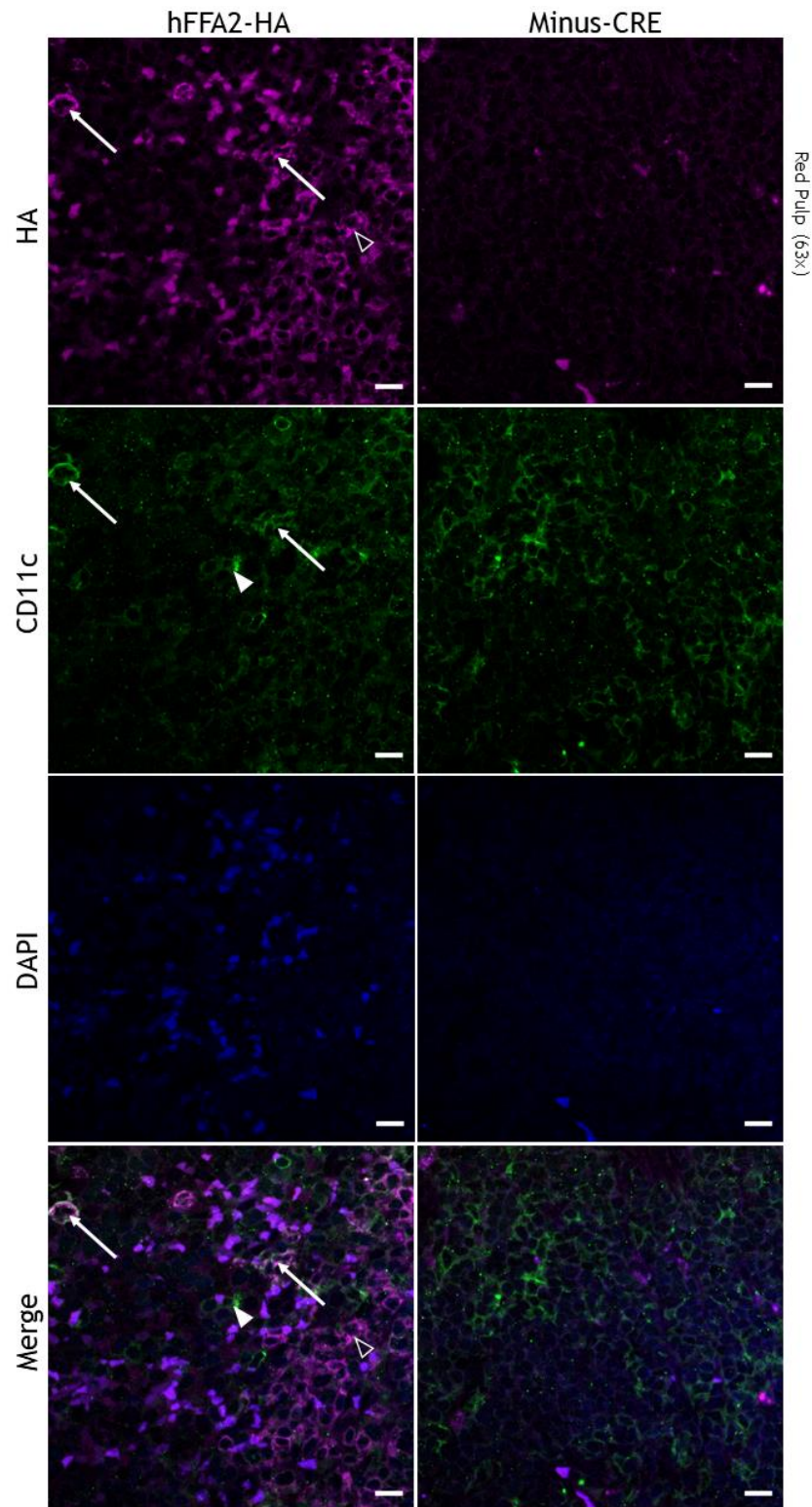


Figure 3.28. Immunohistochemical detection of hFFA2-HA in mouse spleen red pulp. Sections of spleen isolated from hFFA2-HA and minus-CRE mice were fixed with 4% paraformaldehyde and permeabilised with TRITON-X. Cells were incubated with rat anti-HA and rabbit anti-CD11c primary antibodies (1:100) overnight, and with goat anti-rat IgG AlexaFluor-546 (1:400; magenta) and goat anti-rabbit IgG AlexaFluor-488 (1:400; green) secondary antibodies for 2h. Nuclear DNA was labelled with DAPI (blue). Images were taken with 63× objective of Zeiss 880 Laser Scanning Confocal Microscope. Scale bar represents 10µm. Arrows represent examples of co-localisation of anti-CD11c and anti-HA antibodies; solid arrowheads represent examples of localisation of anti-CD11c, but not anti-HA antibodies; empty arrowheads represent examples of localisation anti-HA, but not anti-CD11c antibodies. Representative of 3 fields of view each from 3 animals (n=3). HA - haemagglutinin; CD11c - cluster of differentiation 11c.

To summarise, the overall expression of HA was significantly higher ($p > 0.001$, determined by one-way ANOVA) in the RP ($29.0\% \pm 3.2\%$) than in the WP/MZ ($13.6\% \pm 2.5\%$) (*Figure 3.29A*). CD11b did not colocalise with HA in either of the tissue areas. A larger proportion of HA⁺ cells colocalised with CD45 in the RP than in the WP/MZ. On the other hand, the trend was the opposite for co-expression with CD11b (*Figure 3.29B, C*).

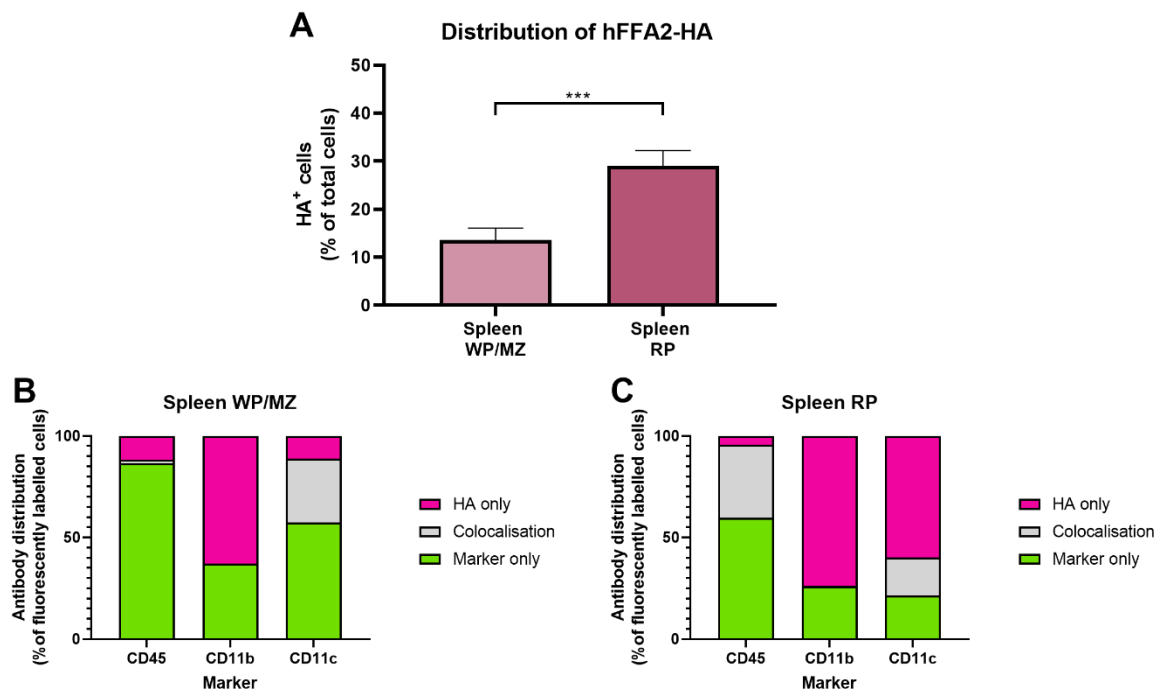


Figure 3.29. Distribution of hFFA2 and cellular markers in hFFA2-HA mouse spleen. Sections of spleen isolated from hFFA2-HA mice were stained with rat anti-HA and rabbit anti-CD45, anti-CD11b or anti-CD11c antibodies. Images were taken with 63× objective of Zeiss 880 Laser Scanning Confocal Microscope. Fluorescent cells in each channel were quantified manually and analysed. A) HA-expressing cells were calculated as a percentage of the total number of cells in each field-of-view in each tissue. Cells showing fluorescence for HA only, cellular markers only or both (colocalisation) were calculated as a percentage of the total number of fluorescently labelled cells in each field-of-view for B) the white pulp/marginal zone (WP/MZ) and C) the red pulp (RP). Representative of 3 fields of view each from 3 animals ($n=3$). Data shown as mean \pm SEM (A) or mean (B, C). *** $p < 0.001$ by one-way ANOVA with Tukey's post-hoc multiple comparisons test. HA - haemagglutinin; CD - cluster of differentiation.

In images of hFFA2-HA under low magnification (4× objective) (*Figure 3.30*), the WP/MZ and RP were clearly distinguishable in the presence antibodies for the various immune cell markers. By choosing characteristic landmarks in the structure, the same areas could be imaged in each of the individual experiments.

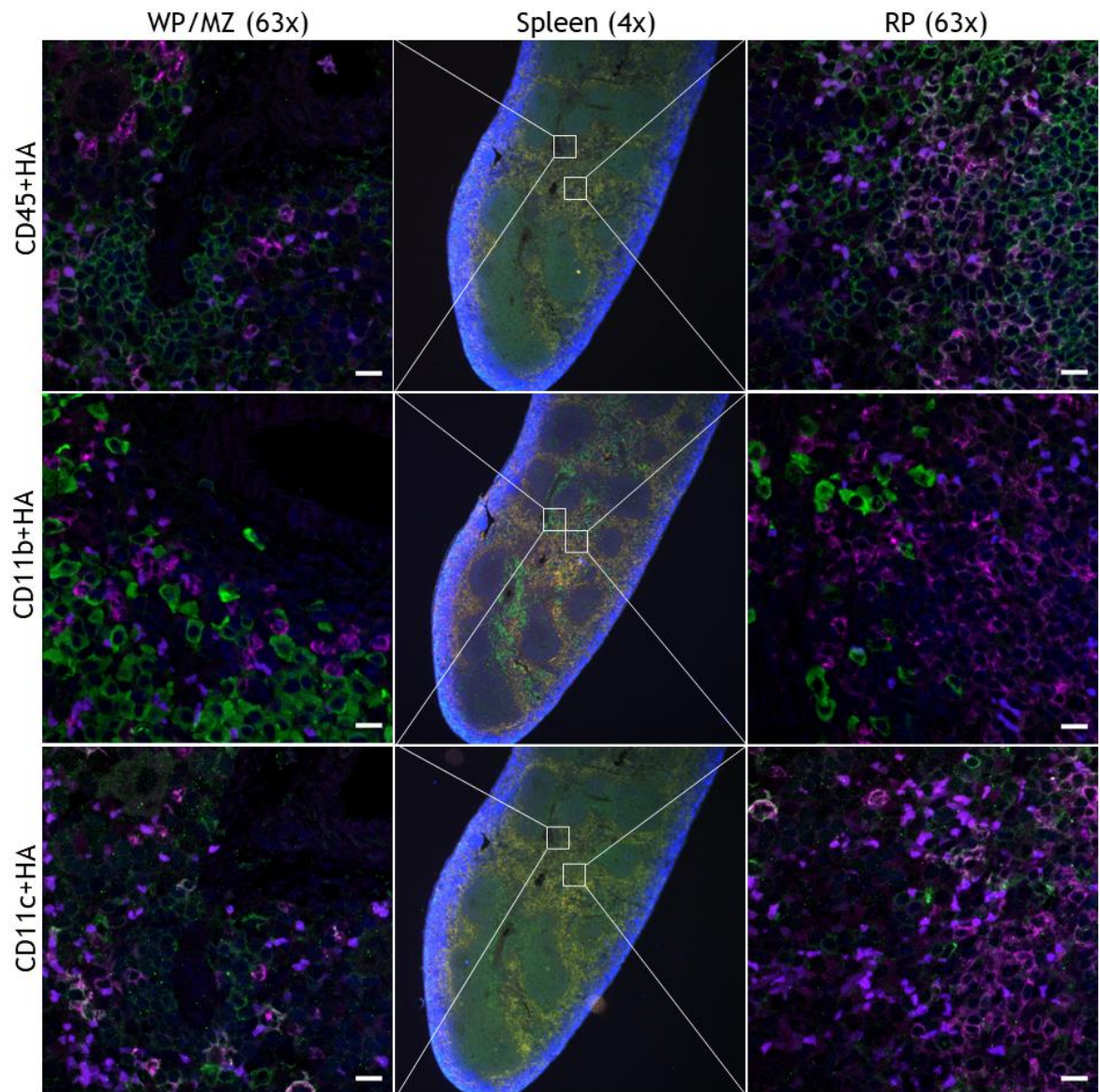


Figure 3.30. Immunohistochemical detection of hFFA2-HA in mouse spleen. Sections of spleen isolated from hFFA2-HA mice were fixed with 4% paraformaldehyde and permeabilised with TRITON-X. Cells were incubated with rat anti-HA and rabbit anti-CD11b, anti-CD11c or anti-CD45 primary antibodies (1:100) overnight, and with goat anti-rat IgG AlexaFluor-546 (1:400; magenta) and goat anti-rabbit IgG AlexaFluor-488 (1:400; green) secondary antibodies for 2h. Nuclear DNA was labelled with DAPI (blue). Images of white pulp/marginal zone (WP/MZ) and red pulp (RP) were taken with 63 \times objective of Zeiss 880 Laser Scanning Confocal Microscope. Scale bar represents 10 μ m. Images showing the gross structure of the spleen (middle panel) were taken with 4 \times objective of Evos FL Auto 2 Cell Imaging System. White squares represent areas imaged at 63 \times . Representative of 3 animals (n=3). HA - haemagglutinin; CD - cluster of differentiation.

At 40 \times magnification (*Figure 3.31*), focusing on an area where WP/MZ and RP meet, the differences in the expression between the two zones was clearly visible with each immune cell marker. In general, HA was more widely expressed in the RP than in the WP/MZ, which only showed scarce expression. CD11b, CD11c and CD45 were all widely expressed in the WP/MZ, while only CD11c and CD45 had a considerable expression in the RP. Co-expression of HA was observed

with CD11c and CD45, albeit not in every cell expressing either marker, but not with CD11b.

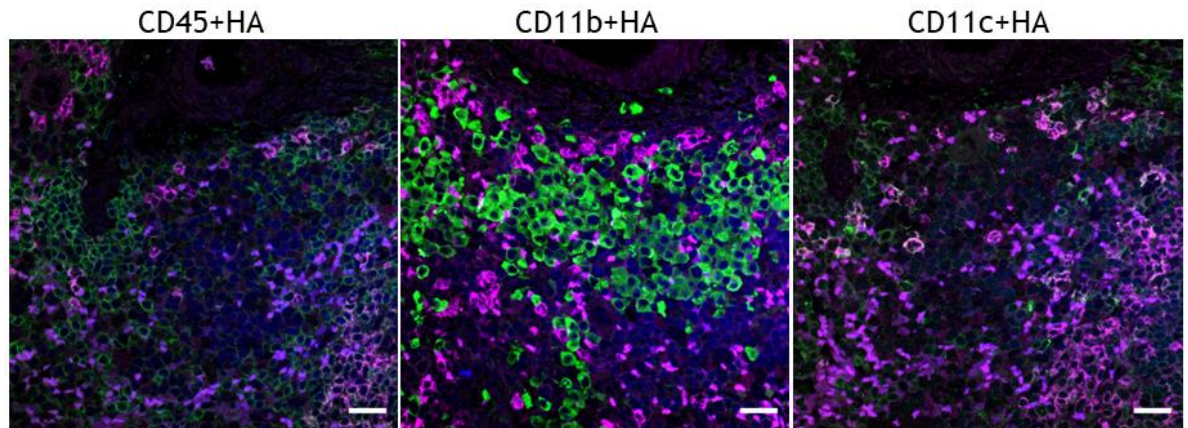


Figure 3.31. Immunohistochemical detection of hFFA2-HA in mouse spleen. Sections of spleen isolated from hFFA2-HA mice were fixed with 4% paraformaldehyde and permeabilised with TRITON-X. Cells were incubated with rat anti-HA and rabbit anti-CD11b, anti-CD11c or anti-CD45 primary antibodies (1:100) overnight, and with goat anti-rat IgG AlexaFluor-546 (1:400; magenta) and goat anti-rabbit IgG AlexaFluor-488 (1:400; green) secondary antibodies for 2h. Nuclear DNA was labelled with DAPI (blue). Images were taken with 40× objective of Zeiss 880 Laser Scanning Confocal Microscope. Scale bar represents 20µm. Representative of 3 fields of view each from 3 animals (n=3). HA - haemagglutinin; CD - cluster of differentiation.

3.2.4 Immunocytochemical investigation of transgenic mouse neutrophils

In order to explore the expression of hFFA2-HA in a specific population of immune cells, ICC staining was performed in mouse bone marrow-derived neutrophils. Due to the uniform size and shape of these cells, fluorescence intensity of secondary antibodies could be quantified. Thus, fluorescence intensity was measured in three cells and three zones in the background. Intensities were corrected first for area and then for background. Data was then collated from 2-3 individual images (see *Section 2.10.2*).

First, antibodies for the leukocyte marker CD11b were used alongside antibodies targeting HA (*Figure 3.32*). Expression of CD11b was observed in hFFA2-HA, minus-CRE and WT neutrophils, with intensities of 6.01 ± 0.58 , 5.79 ± 0.56 and 9.39 ± 2.14 , respectively. Fluorescence intensity of CD11b was significantly higher in WT than in hFFA2-HA and minus-CRE neutrophils ($p < 0.05$; determined by two-way ANOVA with Tukey's post-hoc analysis). The expression of HA showed a different trend. Expression in hFFA2-HA neutrophils (6.41 ± 0.35) was significantly higher than in minus-CRE (0.98 ± 0.13 ; $p < 0.001$) and WT (1.68 ± 0.18 ; $p < 0.01$). In hFFA2-HA, the expression of HA overlaps with that of CD11b. The intensity of

DAPI appeared significantly higher ($p < 0.05$) in minus-CRE neutrophils (10.96 ± 1.63) than hFFA2-HA (7.32 ± 0.44). Intensity in WT (7.75 ± 0.69) was not significantly different from either of the other strains (*Figure 3.34A*).

Following CD11b, the DC and natural killer cell marker CD11c was targeted (*Figure 3.33*). The intensity of CD11c staining was negligible in neutrophils from all three mouse strains (hFFA2-HA: 0.536 ± 0.055 ; minus-CRE: 0.427 ± 0.156 ; WT: 0.385 ± 0.088), with no significant difference between these. The expression of HA displayed the same trend as in experiments with CD11b, with expression in hFFA2-HA (4.400 ± 0.827) being significantly higher ($p < 0.005$) than in minus-CRE (0.722 ± 0.166) and WT (0.391 ± 0.044). Fluorescence intensity of DAPI was again found to be higher in minus-CRE (12.445 ± 1.666) than in hFFA2-HA (6.818 ± 0.512 ; $p < 0.0001$) and WT (8.958 ± 1.202 ; $p < 0.005$) (*Figure 3.34B*).

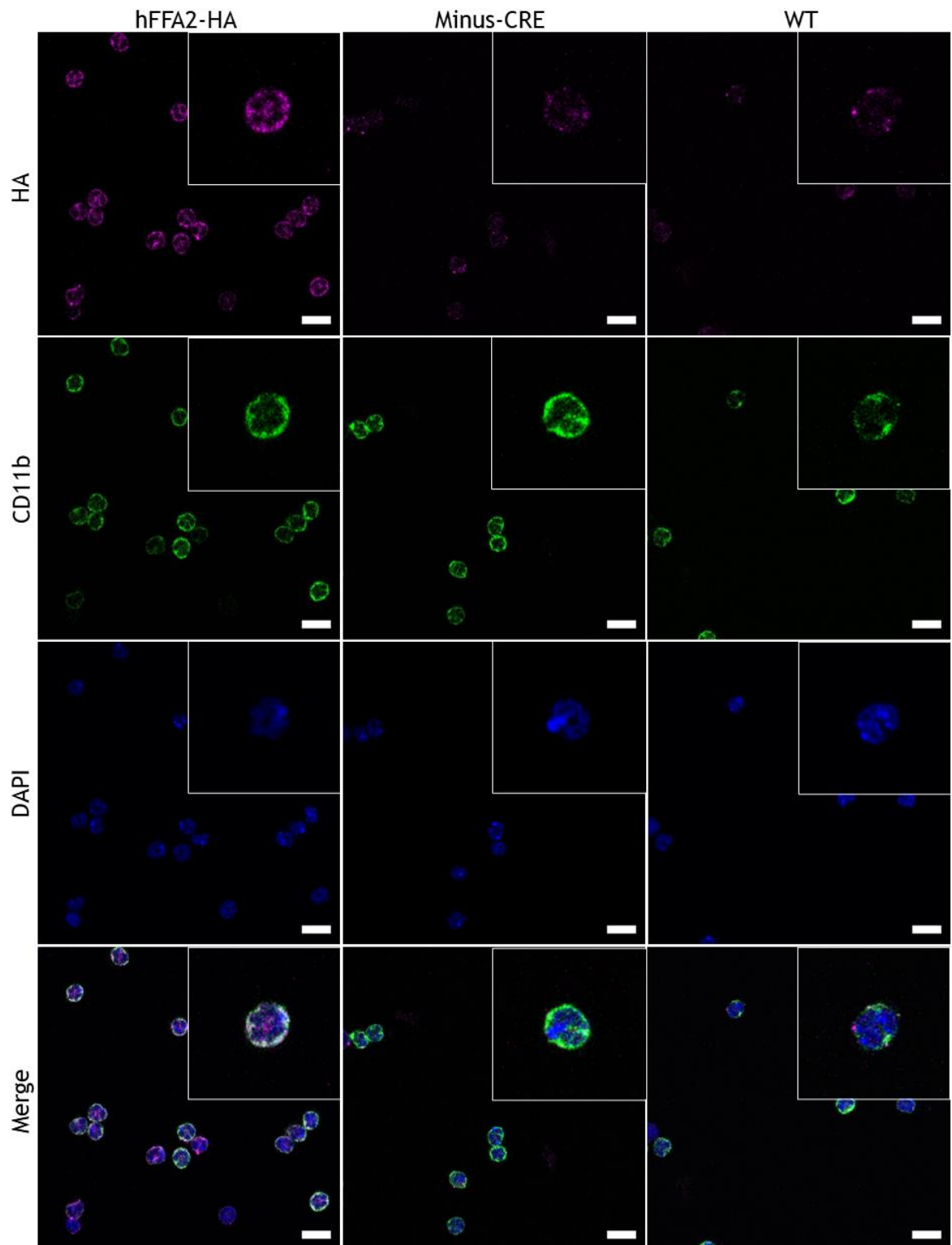


Figure 3.32. Immunocytochemical detection of hFFA2-HA in mouse neutrophils. Bone marrow-derived neutrophils isolated from hFFA2-HA, minus-CRE and C57BL/6N (WT) mice were fixed with 4% paraformaldehyde and permeabilised with saponin. Cells were incubated with rat anti-HA and rabbit anti-CD11b primary antibodies (1:100) overnight, and with goat anti-rat IgG AlexaFluor-546 (1:400; magenta) and goat anti-rabbit IgG AlexaFluor-488 (1:400; green) secondary antibodies for 2h. Nuclear DNA was labelled with DAPI (blue). Images were taken with 63× objective of Zeiss 880 Laser Scanning Confocal Microscope. Scale bar represents 10µm. Inset shows an enlarged image of a representative neutrophil from the corresponding main image. Representative of 3 fields of view each from 3 experiments (n=3, where each n represents neutrophils pooled from 2-4 mice). HA - haemagglutinin; CD11b - cluster of differentiation 11b.

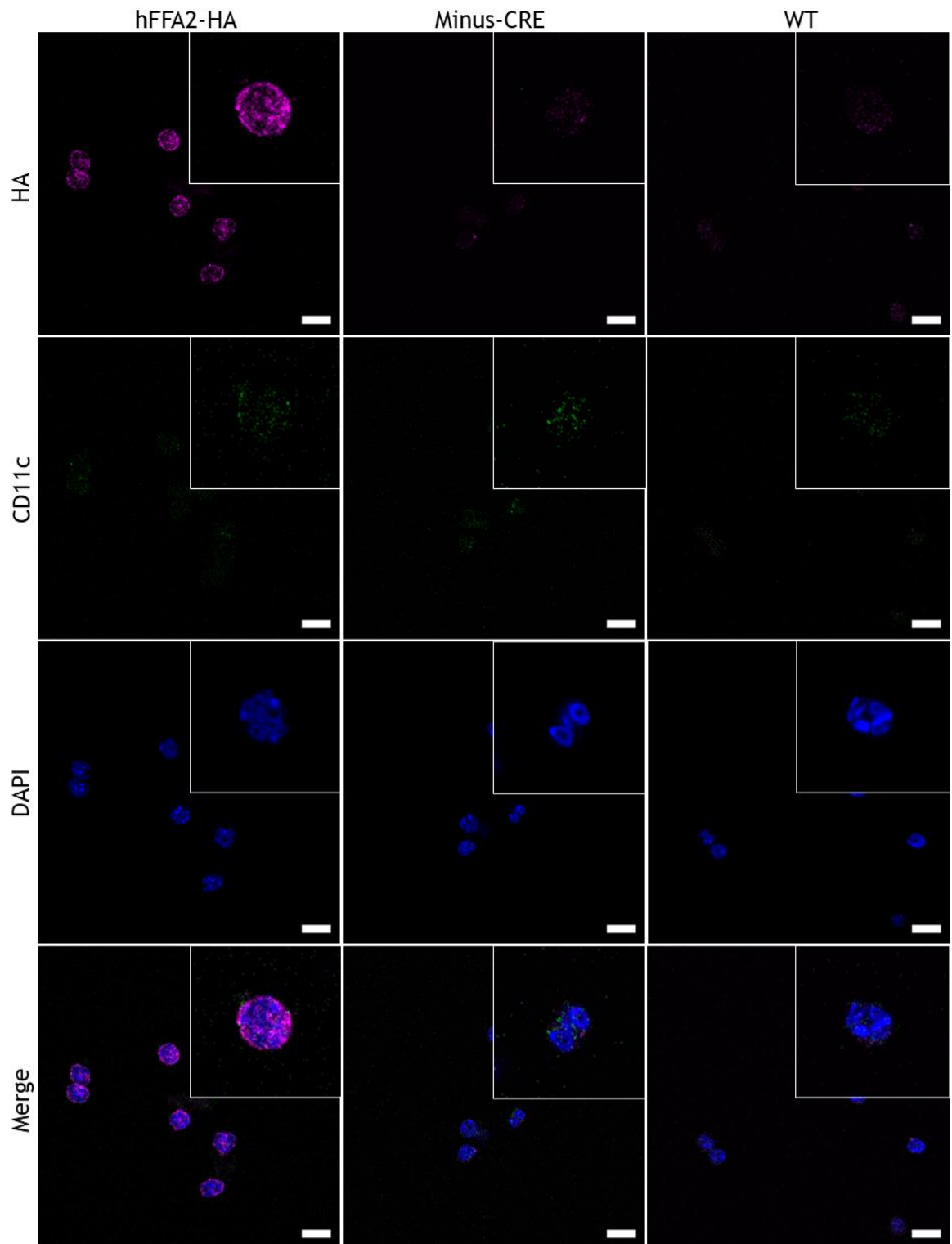


Figure 3.33. Immunocytochemical detection of hFFA2-HA in mouse neutrophils. Bone marrow-derived neutrophils isolated from hFFA2-HA, minus-CRE and C57BL/6N (WT) mice were fixed with 4% paraformaldehyde and permeabilised with saponin. Cells were incubated with rat anti-HA and rabbit anti-CD11c primary antibodies (1:100) overnight, and with goat anti-rat IgG AlexaFluor-546 (1:400; magenta) and goat anti-rabbit IgG AlexaFluor-488 (1:400; green) secondary antibodies for 2h. Nuclear DNA was labelled with DAPI (blue). Images were taken with 63× objective of Zeiss 880 Laser Scanning Confocal Microscope. Scale bar represents 10µm. Inset shows an enlarged image of a representative neutrophil from the corresponding main image. Representative of 3 fields of view each from 3 experiments (n=3, where each n represents neutrophils pooled from 2-4 mice). HA - haemagglutinin; CD11c - cluster of differentiation 11c.

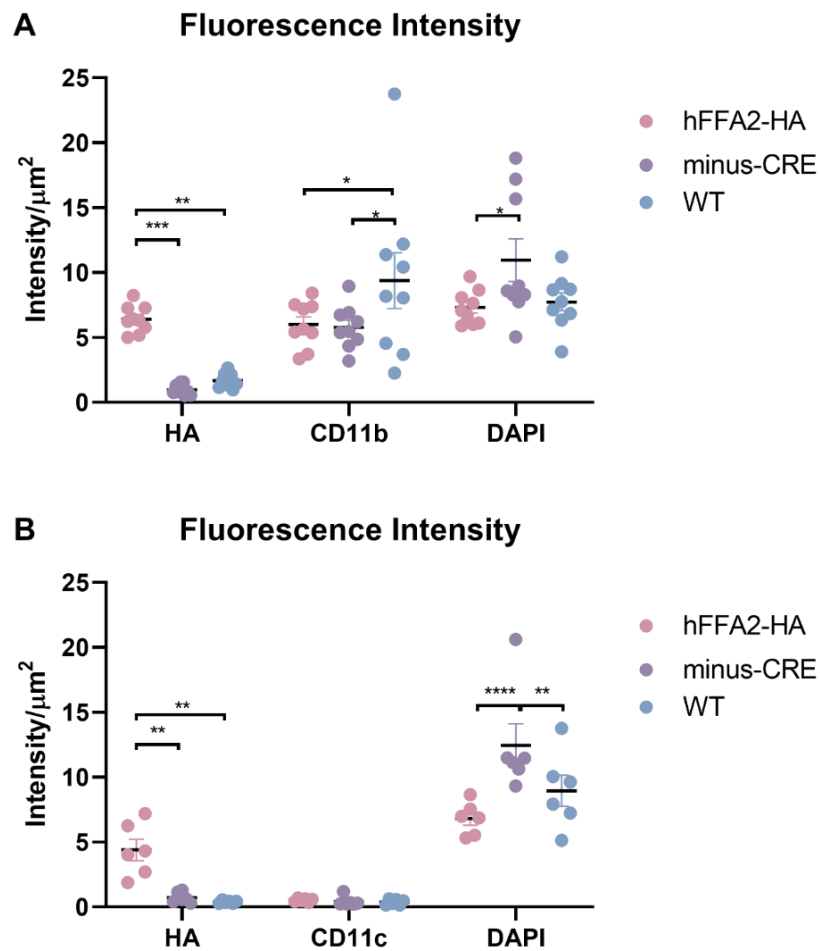


Figure 3.34. Immunocytochemical detection of hFFA2-HA in mouse neutrophils. Bone marrow-derived neutrophils isolated from hFFA2-HA, minus-CRE and C57BL/6N (WT) were stained with rat anti-HA and A) rabbit anti-CD11b or B) rabbit anti-CD11c antibodies. Nuclear DNA was labelled with DAPI. Images were taken with 63× objective of Zeiss 880 Laser Scanning Confocal Microscope. Fluorescence intensity of individual neutrophils was measured using ZENBlue software and corrected for area and background fluorescence. Data shown as mean±SEM (n=2-3, where each n represents neutrophils pooled from 2-4 mice) **** p<0.0001, *** p<0.001, ** p<0.01, * p<0.05 by two-way ANOVA with Tukey's post-hoc multiple comparisons test. HA - haemagglutinin; CD - cluster of differentiation.

3.3 Discussion

3.3.1 The transgenic hFFA2-HA mouse expresses hFFA2 mRNA in a number of tissues

The development of reliable animal models has greatly contributed to drug development efforts. In particular, transgenic strains in which the expression of the transgene depends on crossbreeding with strains expressing a specific enzyme (Cre- or Flp-recombinase) allow a greater control of tissue- and site-specific transgene modulation (Lakso et al., 1992, Orban et al., 1992). The Cre-lox system, upon which this new hFFA2-HA expressing mouse is based, allows for the generation of mice which constitutively express hFFA2-HA, from a parent

strain which is essentially a functional KO of FFA2. In qRT-PCR experiments, tissues where expression of FFA2 had been demonstrated (adipose, colon, bone marrow-derived neutrophils and spleen) were investigated alongside tissue where it is known not to be expressed (liver). In accordance with MIQE guidelines (Bustin et al., 2009), the efficiency of the sets of primers used was first evaluated by the generation of standard curves. As the efficiencies of all three primers were within the recommended 90-110% range (Rogers-Broadway and Karteris, 2015) for their respective mouse strains, their use to quantify gene expression was justified.

As no expression of hFFA2-HA was observed in any tissues from minus-CRE mice, this strain was confirmed to be a functional KO of FFA2, and therefore an appropriate negative control for future experiments where the hFFA2-HA mouse might be used. This is in line with expectations based on the conceptual background of this mouse line (Lakso et al., 1992) and previously described transgenic strains (Bolognini et al., 2019). In addition, hFFA2 primers were confirmed to be specific for hFFA2-HA, as expression of FFA2 was not detected in WT tissues with this set of primers. Importantly, the expression of hFFA2-HA in hFFA2-HA tissues was equivalent to the level of expression of mFFA2 observed in WT, with the notable exception of the colon. The expression of hFFA2-HA in the hFFA2-HA colon was found to be lower than that of mFFA2 in WT colon. This seems confusing, especially since the primer efficiency for mFFA2 was lower than for hFFA2. While an effort was made to use the same segment of colon from hFFA2-HA and WT mice, the discrepancy might be explained by the increasing expression of FFA2 along the length of the colon from proximal to distal end, as observed in rats (Kaji et al., 2011). Alternatively, were WT mice in a state of inflammation, FFA2-expressing neutrophils would have infiltrated colonic tissue to a greater extent (Kim et al., 2013), thus skewing the expression profile of FFA2 in the colon.

Expression of FFA2 in the adipose has been shown in both human and mouse (Le Poul et al., 2003, Ge et al., 2008, Nakajima et al., 2017), and here equivalent expression of hFFA2-HA and mFFA2 was observed in hFFA2-HA and WT mice, respectively. While the expression in the spleen and neutrophils was equivalent between the strains, these were not statistically different from expression in

minus-CRE. Early studies exploring the tissue distribution of FFA2 have highlighted that there was a 50-fold greater FFA2 expression in purified neutrophils in comparison to the whole spleen (Brown et al., 2003), however this difference was not observed in these experiments. As expected, based on previous studies, FFA2 mRNA was not detected in the liver of any of the mouse strains.

The rationale for establishing the transgenic hFFA2-HA mouse line was two-fold. Firstly, by generating a mouse line in which responses to endogenous or synthetic agonists would be expected to be blocked by antagonists selective for the human orthologue, these (and potentially future) compounds can be tested in a physiological context. In addition, in tissues where FFA2 is co-expressed with the closely related FFA3, the use of antagonists would allow the deconvolution of the contribution of each of these receptors to physiological responses. Specifically, in co-expressing tissues SCFAs will activate both receptors, however any response remaining after treatment with an antagonist can potentially be identified as FFA3-mediated.

While a single Arg to Lys mutation at position 65 of mFFA2 makes the receptor amenable to inhibition by various human selective antagonists, the somewhat lower binding affinity of such ligands at this mutant receptor makes this a less attractive construct for a transgenic mouse model (Sergeev et al., 2017). Moreover, the generation of the mouse line detailed here had been in progress before the information on the effect of the point mutation was available. In a mouse model designed along the same concept as the hFFA2-HA mouse, Bolognini et al (2019) generated a mouse line expressing a DREADD version of hFFA2. As discussed in **Section 1.3.2**, due to two point mutations (Cys¹⁴¹Gly and His²⁴²Gln) hFFA2-DREADD is not activated by SCFAs or other orthosteric FFA2 ligands but is activated by SA (Hudson et al., 2012a), and also by the recently identified ligand MOMBA (Barki et al., 2022), which are inert at hFFA2. As a result, any physiological response elicited by SCFAs is potentially mediated by FFA3, and FFA2 responses can only be elicited by the hFFA2-DREADD-selective ligands (Bolognini et al., 2019, Barki et al., 2022). As antagonists are able to block hFFA2-DREADD, specificity of the FFA2 response can be confirmed. This mouse model has been used to establish the contributions of FFA2 and FFA3 to

the release of enteroendocrine hormones, the regulation of gut transit (Bolognini et al., 2019), and the activation of DRGs (Barki et al., 2022).

In order to have a reliable physiological response, it is of great importance to be able to generate a mouse model in which the expression profile of the transgene corresponds to that of the mouse orthologue in WT animals. KO models described in early literature have been observed to display compensatory mechanisms in the expression FFA2 and FFA3, potentially due to the proximity of the corresponding genes at chromosomal location 7A3. In FFA2-KO mice described by Bjursell et al (2011), the expression of FFA3 in white adipose tissue was significantly higher than in WT mice when fed a chow diet. Conversely, Zaibi et al (2010) describe a FFA3-KO mouse in which the expression of FFA2 was significantly reduced in a range of tissues. More recently, an FFA2-FFA3 double KO mouse has been utilised by Tang et al (2015) to investigate the role of both receptors in insulin secretion. This latter mouse model, however, cannot be used on its own to establish the roles of each individual receptor. Theoretically, this would be possible only in conjunction with single KO animals but due to the compensatory changes in expression, conclusions drawn from these studies would be less reliable. By contrast, knocking the construct-of-interest into the locus of the WT receptor under the control of the original promoter, rather than using a classical KO or knock-down approach, should theoretically circumvent this issue. While the expression of FFA3 was not quantified in this work, the conceptually equivalent hFFA2-DREADD-HA mice showed no difference in FFA3 expression in comparison to WT and minus-CRE mice (Bolognini et al., 2019). Thus, the minus-CRE strain, which is parental to the hFFA2-HA strain, can indeed act as a functional KO of FFA2.

3.3.2 The hFFA2-HA protein is expressed in enteroendocrine and immune cells of hFFA2-HA mice

While qRT-PCR is a useful technique in demonstrating the expression of hFFA2-HA mRNA in various tissues, the results generated do not necessarily translate to protein expression in these tissues (Sriram et al., 2019). Tissue localisation of endogenous proteins can be visualised with IHC methods, using primary antibodies specific for the molecule-of-interest. FFA2, like many other GPCRs,

lacks well-validated structural antibodies. This has led to the inclusion of the HA epitope tag on the C-terminal of the transgene. The HA-tag can be targeted by antibodies in both mammalian cell culture (Bhatt et al., 2016) and in tissues (Lobbestael et al., 2010) in order to determine protein expression. As the epitope tag is derived from the influenza virus, untagged mammalian proteins should not be stained when using highly specific antibodies. The anti-HA antibody was first evaluated in an overexpressing mammalian cell line, where it was able to bind to cells induced to express the hFFA2-HA but not to parental cells lacking the hFFA2-HA construct. Importantly, none of the minus-CRE tissues displayed any staining with the anti-HA antibody, providing further support for the usefulness of this mouse strain as a negative control alongside hFFA2-HA mice. In neutrophils, where WT cells were used as a further control, no HA-staining was observed either.

It is important to note the variable background autofluorescence between tissues. These are most likely to be artefacts resulting from the image acquisition methods employed (Sun et al., 2017). Specifically, some images of intestinal samples have higher background autofluorescence in the magenta channel than other samples. Due to the thickness of the tissues, combined with the sparsity of positively stained cells, a higher laser power was generally employed for these samples. As a result, photobleaching occurred at a faster rate, necessitating a further increase in power. Also due to the relative thickness of the samples, differences in the extent of antibody permeation may have occurred. Even though all effort was made to ensure that the same Z-position was imaged for each sample, the inherent drift of the microscope may have introduced errors in the otherwise consistent methods. Although images can be corrected for background using the software Image J, however this replaces the magenta pseudocolour with red, thus making the images less accessible. In order to account for these differences, in samples with apparent high background autofluorescence, only cells which showed fluorescence intensity 50% above the average background intensity were considered to be positively stained.

The role of FFA2 in various functions of the intestine has been the subject of extensive research. This is not surprising, considering that the SCFAs which serve

as endogenous ligands for the receptor are produced by the commensal bacteria of the gut. FFA2 has been described in colonic L-cells in human (Karaki et al., 2008), mouse (Tolhurst et al., 2012) and rat (Karaki et al., 2006). L-cells are a subset of EECs which release anorexigenic hormones PYY and GLP-1 in response to stimuli from the gut environment, hence markers for these were used along with the more generic EEC marker, ChgA. Although not a universal marker (Engelstoft et al., 2015), a subset of ChgA⁺ cells was expected to correspond with the entire hFFA2-HA expressing EEC population. This trend was observed in both hFFA2-HA colon and ileum. In the case of GLP-1, no co-localisation was observed, however this was very likely to be the result of non-specific binding by the anti-GLP-1 antibody. Indeed, all staining was observed in the cells of the submucosal layer, which is uncharacteristic of the expression of GLP-1 which would be expected to stain triangular L-cells in the mucosal layer (Kaji et al., 2011). The L-cell marker PYY, on the other hand, identified a small population of mucosal cells, all of which co-expressed hFFA2-HA (Gene Skyline, Immunological Genome Project <http://rstats.immgen.org/Skyline/skyline.html>).

The presence of FFA2 has been demonstrated in various immune cell types in the intestinal submucosa (Nohr et al., 2013), bone marrow (Le Poul et al., 2003), peripheral blood, and the spleen (Nilsson et al., 2003). In accordance with this, IHC imaging has revealed the expression of hFFA2-HA in the submucosa of various parts of the small intestine. In order to identify hFFA2-HA expressing cell populations in these regions, a range of immune cell markers were employed. As FFA2 expression is limited to certain leukocyte populations, it was not surprising that only some of the CD45⁺ cells were found to co-express hFFA2-HA in both the duodenum and the ileum. Co-expression of CD3 and hFFA2-HA was not observed in either segment of the small intestine. Considering that CD3 is a T-lymphocyte marker, and hFFA2-HA is not canonically expressed on these cells, this is another unsurprising outcome. The outcomes of co-staining with the myeloid cell marker CD11b were, however, somewhat unexpected. While the expression of CD11b appears to be widespread, no co-expression of hFFA2-HA and CD11b was observed even though hFFA2-HA was expected to be expressed in several populations. The expression of CD11c was observed as similarly widespread, with a subset of cells also expressing hFFA2-HA. While CD11c is a marker for DCs and

macrophages, in the small intestine they are expressed in trace amounts on ILC3s which also express FFA2 (Gene Skyline, Immunological Genome Project).

Immune cell clusters along the small intestine and colon have been of interest, especially in relation to their interactions with the gut commensal bacteria. Based on their composition and location, these clusters can be categorised into Peyer's Patches (PPs), isolated lymphoid follicles (ILFs) and cryptopatches (CPs). PPs are macroscopic structures, organised under a layer of epithelium. DCs within the PP have been shown to display one of three distinct phenotypes. CD11b⁺ DCs are located in the subepithelial dome while CD8 α ⁺ DCs are present in the interfollicular regions. "Double negative" cells lacking both markers are dispersed through both of these regions (Iwasaki and Kelsall, 2000, Iwasaki and Kelsall, 2001). Luminal antigens transported through M-cells in the epithelial layer are captured by DCs which leads to the release of IL-10 and the priming of naïve T-lymphocytes, and the subsequent activation of follicular B-lymphocytes (Shreedhar et al., 2003). More recently, the presence of ILCs has also been shown in PP with a potential role in regulating the composition and expansion of commensal bacteria (Hashiguchi et al., 2015). As hFFA2 is expressed on ILC3s (Chun et al., 2019), these structures constitute a potentially essential location for FFA2-mediated immune effects in the gut. Based on the imaging experiments in this chapter, it would be tempting to conclude that there are a higher number of hFFA2-expressing cells in the duodenum than in the colon (also observed by Bolognini et al., 2019). However, it is important to note that PPs, which are expected to contain FFA2-expressing leukocyte populations, are more sparsely distributed along the length of the colon. Thus, these structures require targeted manual dissection before they can be visualised. This approach is required in order to gain a clearer understanding of receptor distribution along the length of the gut.

ILFs of the small intestine are smaller clusters, present in short, barrel-shaped villi (Hamada et al., 2002). These structures are rich in CD45⁺ B-lymphocytes which not only go through IgA class switching independent of T-lymphocyte interactions (Tsuji et al., 2008) but also are, potentially due to their proximity to the stimuli, more activated than B-lymphocytes in PPs or the spleen (Wang et al., 2006a). While B-lymphocytes constitute the majority of these sites, CD45⁺

CD11c⁺ DCs (McDonald et al., 2010) and a small population of T-lymphocytes are also present (Lorenz and Newberry, 2004). CPs are the smallest of these structures, composed mostly of lineage negative cells (Pabst et al., 2006).

Due to the use of single cell markers, the stains presented in this chapter cannot inform about the specific identity of each hFFA2-HA-expressing cell type, however some inferences can be made. Based on the moderate size and composition of the cell clusters investigated, they represent examples of ILFs. Since FFA2 expressing cells all appear to express CD45 and CD11c in separate stains, they potentially represent the population of CD45⁺ CD11c⁺ DCs as described above (Lorenz and Newberry, 2004). While CD3⁺ T-lymphocytes and CD11b⁺ myeloid cells are present in these clusters, none of these appeared to co-express hFFA2-HA. Since ILC markers such as CD90.2 were not targeted in this study, hFFA2-HA expressing ILCs could not be identified (Chun et al., 2019). In order to gain a complete understanding of the expression of FFA2 in these gut-associated immune cell clusters, simultaneous staining with a wider panel of antibodies would be required (Rochereau et al., 2011, Hamada et al., 2002).

While early research does suggest FFA2 expression in the spleen, the identity of FFA2-expressing cells in this tissue has not been revealed (Le Poul et al., 2003). Here, although in a limited way, an attempt was made to delineate some hFFA2-HA expressing cell populations in the spleen. Generally, hFFA2-HA was found to be widely expressed in the RP with only sporadic expression observed in the WP/MZ. Not surprisingly, CD45 was widely expressed throughout the entirety of the organ. While in the red pulp all hFFA2-HA expressing cells co-expressed CD45, this was not the case in the white pulp. Although hFFA2-HA was not found to be co-expressed with CD11b in either of the areas, a subset of hFFA2-HA-expressing cells was found to be colocalised with CD11c in both. This expression profile could suggest that, similar to ILFs, CD45⁺ CD11c⁺ DCs are present, however a large number of CD11c⁻ RP cells express hFFA2-HA. Monocytes and macrophages are the main components of the RP, and of these monocytes are known to express FFA2 (Brown et al., 2003). However, monocytes are expected to express CD11b, therefore this population of cells may be excluded (Swirski et al., 2009). Considering that a relatively large population of hFFA2-HA-expressing cells do not co-express CD11b or CD11c, a question arises considering the

identity of these cells. In spleen-derived stromal fraction cultures, a heterogeneous set of CD11b⁻ CD11c⁻ cells have been identified as progenitor cells (Lim and O'Neill, 2019) but based on the available data it cannot be determined whether the hFFA2-HA-expressing cells correspond to these. It is also unclear what the function of the receptor would be in such cells. Similarly to the staining in the ILFs, the simultaneous use of multiple cell markers would aid the identification efforts (Feng et al., 2016).

From the earliest studies, FFA2 has been shown to be highly expressed in bone marrow and neutrophils (Le Poul et al., 2003, Brown et al., 2003), therefore the expression of hFFA2-HA in neutrophils purified from bone marrow was evaluated. Since neutrophils were expected to express CD11b but not CD11c, these two markers were utilised in staining experiments. Not only was hFFA2-HA expressed in CD11b⁺ cells, but the DAPI staining revealed the multi-lobular morphology characteristic of neutrophil nuclei. While additional neutrophil-specific markers could be used to distinguish isolated cells from other CD11b⁺ cells that could have escaped the negative selection, the combination of the cell marker display and nucleus morphology provide evidence that the examined cells represent a pure neutrophil population, which express hFFA2-HA to a similar degree.

In conclusion, the transgenic hFFA2-HA mouse strain is not only able to express hFFA2-HA, but the pattern of expression corresponds to that described in literature. Due to this expression profile spanning the gut and immune cells, FFA2 is implicated in inflammatory diseases of the gut, such as ulcerative colitis and colonic cancer (Carretta et al., 2021). Although the functionality of the expressed hFFA2-HA construct remains to be demonstrated (**Chapter 4**), the mouse model could potentially prove a valuable asset in drug development efforts for FFA2.

CHAPTER 4 - FUNCTIONAL CHARACTERISATION OF hFFA2-HA NEUTROPHILS

4.1 Introduction

As it was demonstrated in *Chapter 3*, the hFFA2-HA receptor is expressed at the protein level in a range of tissues of hFFA2-HA mice, corresponding to cell populations described in published literature (Brown et al., 2003, Le Poul et al., 2003, Tolhurst et al., 2012). The hFFA2-DREADD-HA mouse model, which is based on the same conceptual background as the hFFA2-HA model, has been used to determine the contribution of FFA2 to lipolysis and GLP-1 secretion (Bolognini et al., 2019), as well as to the activation of components of the gut-brain axis (Barki et al., 2022). Despite the expression of FFA2 on a range of immune cell types, the mouse model has not yet been used to examine functions mediated by them. Considering that neutrophils appear to be key components of SCFA-mediated immune responses (Vinolo et al., 2011, Chun et al., 2019), and that neutrophils from hFFA2-HA mice expressed the receptor both at the mRNA and the protein level, these cells were selected for further functional characterisation.

Although animal experiments are a necessary stage in drug development preceding clinical trials, there are important preliminary steps which are required to be completed before proceeding to *in vivo* experiments. *In vitro* characterisation generally requires an immortalised cell line, which can be cultured under controlled conditions. One such cell line is the stably expressing HEK293-based Flp-In T-REx 293 cell system, in which Flp-recombinase induces recombination between a previously inserted genomic Flp Recombination Target (FRT) site and the pcDNA5/FRT/TO plasmid containing the construct of interest. As the expression of the construct is under the control of a tetOp element (normally deactivated by tetR), the addition of DOX is required to induce the expression of the construct of interest. As a result, the level of expression can be controlled by varying the amount of DOX added (Ward et al., 2011). Beyond *in vitro* experiments, *ex vivo* studies focusing on specific tissues or cell populations can be utilised to examine physiological functions in isolation. This not only eliminates systematic effects but also allows for the examination of compounds with poor pharmacokinetic characteristics.

The first step in any receptor-mediated response is the binding of a ligand. The extent of ligand binding is largely determined by ligand affinity (and the law of mass action). As detailed in *Section 1.1.3*, radioligand binding studies have been routinely used to determine radioligand affinity (specifically as its dissociation constant, K_d). They also provide information on the number or concentration of specific ligand binding sites (B_{max}) (Flanagan, 2016). Additionally, competition binding assays can be utilised to determine the binding affinity (K_i) of an unlabelled ligand that binds to the same site as the radioligand (Hulme and Trevethick, 2010, Flanagan, 2016). In each case, disintegration of [3H] is measured as scintillation, which is proportional to radioligand concentrations.

In the case of FFA2, the radioactively labelled antagonist, [3H]GLPG0974 has been utilised in Flp-In T-REx 293 cells for all of the above applications, as well as for determining the kinetics of the radioligand (Sergeev et al., 2016, Sergeev et al., 2017). Since the radioligand is based on the human orthologue-specific antagonist GLPG0974, its use is limited to hFFA2 (Pizzonero et al., 2014) and is not suitable to assess numbers of mFFA2 receptor sites. Although any orthosteric ligand could be utilised, by using CATPB as the unlabelled ligand, the ability of both hFFA2-specific antagonist to bind hFFA2-HA neutrophil membranes would be determined simultaneously.

Following ligand binding, receptor activation leads to the exchange of GDP for GTP in the heterotrimeric G protein complex. Subsequently, the heterotrimer dissociates from the receptor and its α - and $\beta\gamma$ -subunits separate, inducing downstream signalling cascades depending on their identities. The process of G protein activation can be examined by numerous methods, including BRET-based assays (Inoue et al., 2019). As FFA2 couples to $G\alpha_{i/o}$ (in addition to $G\alpha_{q/11}$), [^{35}S]GTP γ S incorporation assays provide a simple, convenient method to examine receptor activation and determine ligand potency and efficacy. For this, an analogue of GTP is used, in which the terminal phosphate group is replaced by a sulphate group, rendering the bond to the adjacent phosphate resistant to the GTPase activity of the G protein α -subunit. With the incorporation of the [^{35}S] radiolabel, the incorporation and accumulation of [^{35}S]GTP γ S can be quantified through scintillation chromatography as a proportional measure of receptor activation (Milligan, 2003, Strange, 2010). In these experiments, of particular

interest was the use of the $G\alpha_{i/o}$ -biased ago-allosteric modulator, AZ1729. This compound has been shown to positively modulate the effect of C3 in cAMP inhibition assays in Flp-In T-REx 293 cells, in GLP-1 release assays in colonic crypts and in chemotaxis assays in human neutrophils (Bolognini et al., 2016). Since the PAM effects of AZ1729 have been demonstrated both in overexpressing cell lines and in neutrophils, findings from [³⁵S]GTP γ S incorporation assays in both cell types were anticipated to be supportive of these effects.

Downstream of receptor activation, second messenger signalling cascades mediate both localised and cell-wide effects. In a physiological context, activation of neutrophils leads to their recruitment to the site of infection or inflammation, followed by further pro-and anti-inflammatory responses. In fact, the role of FFA2 in chemotaxis has been studied in human (Pizzonero et al., 2014), as well as mouse (Kamp et al., 2016, Vinolo et al., 2011) neutrophils. These experiments often rely on two chambers separated by a permeable membrane, containing the cells and the chemotactic agents, respectively. Following incubation, cells from the second chamber are quantified by flow cytometry or by quantification of total ATP (Stanley, 1989, Zhang et al., 2013). The chemotactic effect of SCFAs through FFA2, although moderate, is mediated through $G\alpha_{i/o}$. This allows the use of the $G\alpha_{i/o}$ -biased PAM AZ1729, as it has been done previously using human neutrophils (Bolognini et al., 2016), with an expectation of increased chemotaxis upon co-addition. The ability of GLPG0974 to block chemotaxis has been demonstrated in human neutrophils (Pizzonero et al., 2014), however the novel hFFA2-HA mouse model here allows the use of antagonists in these “first-in-mouse” chemotaxis experiments.

While the involvement of FFA2 in migration has been researched widely, its involvement in another neutrophil function, namely the formation of NETs has not been explored. Upon encountering pathogens or other activating factors, neutrophils release NETs which are composed primarily of chromatin fibres interspersed with histones, granular enzymes and other peptides (Urban et al., 2009). As the name suggests, these chromatin fibres form tangles which ensnare encountered pathogens, which are then neutralised by the bactericidal and fungicidal activity of the protein components of the NETs (Brinkmann et al., 2004). As NETs are composed of nuclear DNA, their formation leads to cell death

(termed NETosis) distinct from apoptosis and necrosis (Fuchs et al., 2007). While the enzymes found in NETs (such as leukocyte elastase or myeloperoxidase) can be visualised and quantified by immunostaining (Fuchs et al., 2007, Urban et al., 2009), the primary chromatin component can be quantified in a higher-throughput 96-well plate format. To this end, the PicoGreen fluorescent dsDNA dye can be utilised, which allows for the measurement of fluorescence proportional to the amount of dsDNA released (Dragan et al., 2010).

While signals mediated via GPCRs have not traditionally been described to be activators of NET production, there is some evidence that activation of sphingosine-1-phosphate receptor 4 (S1PR₄) by anacardic acid (AA; 2-hydroxy-6-pentadecylbenzoic acid) is able to induce NETs (Hollands et al., 2016). In addition, the activation of NADPH oxidase is understood to be a requirement for NET formation under most conditions (Parker et al., 2012). In human neutrophils, stimulation of FFA2 by a combination of agonists and PAMs leads to the activation of the NADPH oxidase complex (Martensson et al., 2018, Lind et al., 2021). Furthermore, the SCFA C4 induces G α_q -dependent NET release in bovine neutrophils, although the direct involvement of FFA2 in this process has not been demonstrated (Carretta et al., 2016). Based on these observations, it was proposed that activation of FFA2 could potentially lead to the formation of NETs in mouse neutrophils.

The aims of this chapter are two-fold. On the one hand, it aims to corroborate the conclusions of **Chapter 3** about the utility of the hFFA2-HA mouse model by the use of specific functional assays. Specifically, it intends to characterise three important stages of hFFA2-HA receptor activation in neutrophils: ligand binding, engagement of G-proteins and whole-cell responses. On the other hand, it attempts to establish the use of a number of *in vitro* and *ex vivo* assays which have not been used in mouse neutrophils, and which would have the potential to be used in further studies preceding *in vivo* animal studies.

4.2 Results

4.2.1 *In vitro* evaluation of ligand binding and efficacy in transgenic mouse-derived neutrophils

In order to evaluate the ability of the hFFA2-HA protein expressed in mouse bone marrow-derived neutrophils to bind various ligands, radioligand binding assays using [³H]GLPG0974 were employed. The methods were based on kinetic studies around [³H]GLPG0974 (Sergeev et al., 2017), with buffer conditions optimised for improved signal.

Initially, saturation binding curves were constructed *in vitro* using membranes of Flp-In T-REx 293 cells induced to express hFFA2-eYFP. These allowed definition of the concentration of [³H]GLPG0974 to be used in experiments with neutrophils from transgenic hFFA2-HA expressing mouse lines. To this end, increasing concentrations of [³H]GLPG0974 were incubated with a single concentration (10 μ M) of the unlabelled antagonist CATPB (*Figure 4.1A*). Fitting a one-site binding model to the specific binding curve (see *Section 2.10.3*), which was calculated as the difference between total and non-specific binding (*Figure 4.1A inset*), yielded a K_d of 12.5 ± 2.3 nM for [³H]GLPG0974. The B_{max} for this preparation was calculated as 16.03 ± 0.12 pmol/mg.

Based on preliminary data (not shown), neutrophil membranes were required at a 10-fold higher amount than Flp-In T-REx 293 membranes in order to generate detectable and robust signals. As a result, in the case of neutrophils, single concentration binding studies were employed. For this, a K_d concentration of [³H]GLPG0974 (assessed from the studies above) was incubated with neutrophil membranes, in the absence and presence of unlabelled CATPB (10 μ M) (*Figure 4.1B*). Total binding in the absence of CATPB was found to be 615.7 ± 52.2 fmol/mg for hFFA2-HA which was significantly higher than the non-specific binding remaining in the presence of CATPB (388.2 ± 26.2 fmol/mg; $p<0.01$ determined by one-way ANOVA). Total binding in neutrophils isolated from hFFA2-HA expressing mice was also significantly higher than the total binding in minus-CRE (445.0 ± 42.5 fmol/mg; $p<0.05$) and in FFA2-KO neutrophils (418.6 ± 43.5 fmol/mg; $p<0.01$). Non-specific binding in minus-CRE (372.1 ± 18.9 fmol/mg) and FFA2-KO (379.2 ± 8.7 fmol/mg) was not significantly

different from total binding in the same membranes and from non-specific binding in hFFA2-HA membranes.

Specific binding was calculated as a difference between total and non-specific binding (*Figure 4.1B inset*). Conceptually, neutrophils from both minus-CRE and FFA2-KO mice should lack specific [³H]GLPG0974 binding, if this ligand is indeed specific for the hFFA2 receptor. Indeed, observed specific binding in both minus-CRE (72.9±61.2fmol/mg) and FFA2-KO (39.4±35.0fmol/mg) was found to be not significantly different from 0. Specific binding in hFFA2-HA neutrophil membranes, however, was found to be significant (227.5±51.3fmol/mg; p<0.05).

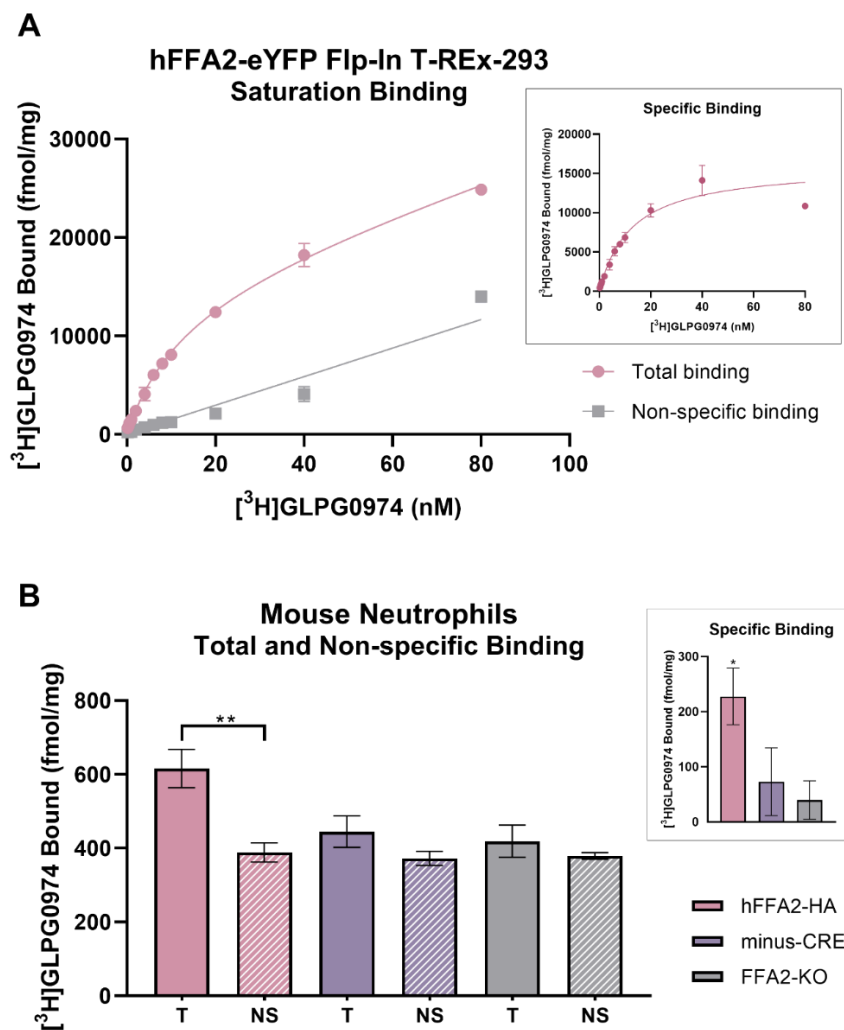


Figure 4.1. Heterologous radioligand binding in mouse neutrophils. (A) Membranes prepared from Flp-In T-REx 293 cells stably expressing hFFA2-eYFP were incubated with a range of concentrations of [³H]GLPG0974 for 2h at 25 °C, in the absence or presence of 10µM CATPB, and (B) membranes prepared from bone marrow-derived neutrophils isolated from hFFA2-HA, minus-CRE and FFA2-KO mice were incubated with a K_d concentration of [³H]GLPG0974 for 2h at 25 °C, in the absence or presence of 10µM CATPB in order to obtain total (T) and non-specific (NS) binding, respectively. Insets show specific binding of [³H]GLPG0974 calculated as the difference between total and non-specific binding. Data presented as mean±SEM (n=2 for A; n=3 for B, where each n represents neutrophil membranes pooled from 2-4 mice). ** p<0.01, * p<0.05 by one-way ANOVA with Sidak's post-hoc multiple comparisons test.

Once the ability of hFFA2-HA neutrophil membranes to bind hFFA2-specific antagonists was established, the ability of these ligands to block agonist-induced activation was explored. To this end, a [³⁵S]GTPγS incorporation assay was utilised (adapted from Sergeev et al., 2017). Upon agonist activation, this analogue of GTP is incorporated into the G protein complex, however the terminal S-substitution prevents effective hydrolysis of the molecule, leading to a build-up that reflects and is proportional to the extent of receptor activation.

Initially, the overexpressing Flp-In T-REx 293 cell lines stably expressing eYFP-tagged versions of hFFA2 and mFFA2 were used to establish the potency of C3 at these receptor orthologues (*Figure 4.2A*). Non-linear regression curves were fitted to this data as described in **Section 2.10.4**. C3 displayed pEC₅₀ 3.57±0.21 and 3.43±0.13 at hFFA2-eYFP and mFFA2-eYFP, respectively. In neutrophil membranes (*Figure 4.2B*), pEC₅₀ for C3 was 4.36±0.21 and 3.82±0.28 in hFFA2-HA and WT neutrophils, respectively. Although the difference between hFFA2-HA and WT appeared to be somewhat greater than that between hFFA2-eYFP and mFFA2-eYFP expressed in Flp-In T-REx 293 cells, this was not statistically significant (determined by one-way ANOVA). There was also no significant difference between hFFA2-eYFP in Flp-In T-REx 293 cells and hFFA2-HA neutrophil membranes, or between mFFA2-eYFP in Flp-In T-REx 293 cells and WT neutrophil membranes. In minus-CRE and FFA2-KO neutrophil membranes (*Figure 4.2C*), C3 did not produce a concentration-dependent effect.

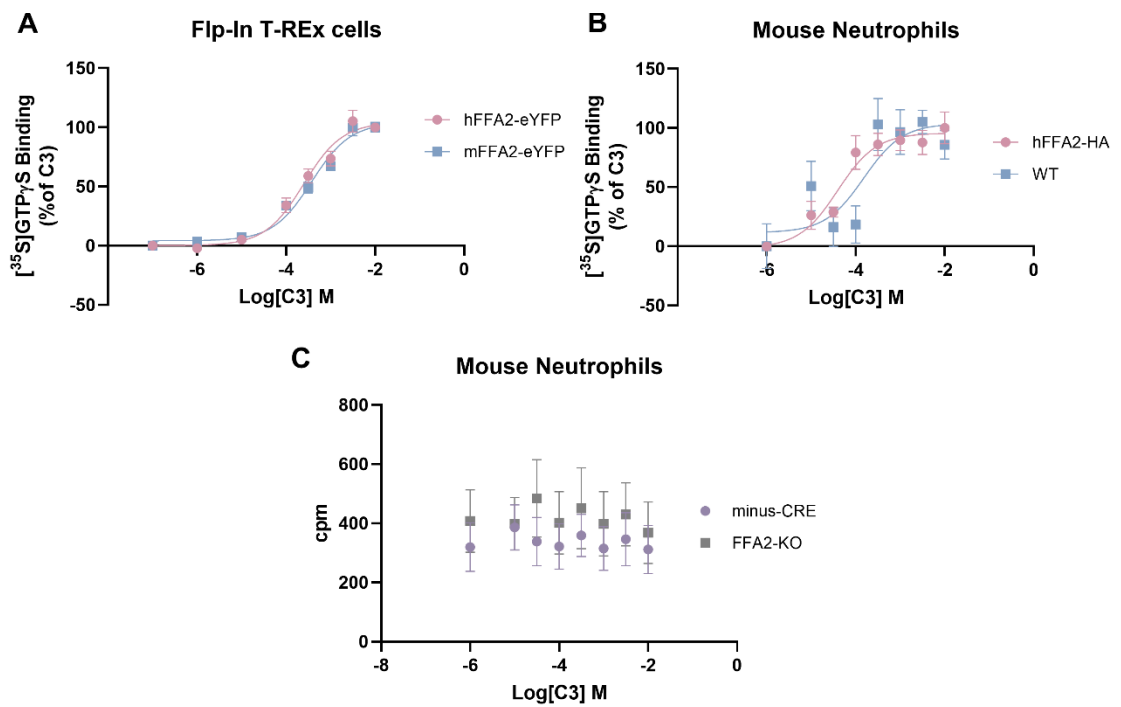


Figure 4.2. Agonist-induced $[^{35}\text{S}]\text{GTP}\gamma\text{S}$ incorporation. Membranes prepared from (A) Flp-In T-REx 293 cells induced to express hFFA2-eYFP or mFFA2-eYFP, (B) Bone marrow-derived neutrophils isolated from hFFA2-HA or C57BL/6N (WT) mice and (C) minus-CRE or FFA2-KO mice were incubated with various concentrations of propionate (C3) for 1h at 30°C, and the incorporation of $[^{35}\text{S}]\text{GTP}\gamma\text{S}$ was measured as counts per minute (cpm). Response was normalised separately for each cell line and mouse strain. Data presented as mean \pm SEM ($n=3$; for B and C each n represents neutrophil membranes pooled from 2-4 mice).

Next, the possible allosteric effects of AZ1729 in neutrophils was examined. To determine a suitable concentration of AZ1729 to be used in neutrophils, C3 concentration-response curves were constructed in membranes from Flp-In T-REx 293 cells in the presence of increasing concentrations of AZ1729 (*Figure 4.3A and C*). Even at 10nM, the lowest concentration assessed, AZ1729 increased the maximal response (E_{max}) produced by C3. The E_{max} of C3 in the presence of 100nM AZ1729 was $148\% \pm 5\%$ in hFFA2-eYFP and $144\% \pm 17\%$ in mFFA2-eYFP expressing membranes when normalised to the response produced by C3 only. Although there appeared to be an increase of potency of C3 in the presence of AZ1729 across the datasets, which would be consistent with the function of a PAM, there was no significant difference (determined by one-way ANOVA) found between the pEC_{50} values in the absence and presence of 100nM AZ1729, with the latter producing pEC_{50} of 3.72 ± 0.48 and 4.27 ± 0.21 for hFFA2-eYFP and mFFA2-eYFP, respectively. However, an ago-allosteric effect of AZ1729 was evident with this ligand promoting binding of $[^{35}\text{S}]\text{GTP}\gamma\text{S}$ even in the absence of C3. The allosteric effect on C3 was estimated with the use of an allosteric operational model (see *Section 2.10.5*), by which $\alpha\beta$ was determined to be as

60.98 and 50.33 at hFFA2-eYFP and mFFA2-eYFP, respectively. Interestingly, the model predicted AZ1729 acting primarily as a PAM of potency at hFFA2-eYFP ($\alpha=31.55$; $\beta=1.93$), while at mFFA2-eYFP it was equally a PAM of potency and efficacy ($\alpha=6.75$; $\beta=7.45$). In addition, higher direct agonist effect was observed at mFFA2-eYFP ($\tau=6.16$) than at hFFA2-eYFP ($\tau=2.92$).

Because the addition of 100nM AZ1729 to the lowest concentration (100nM) of C3 generated a response close to the maximal response produced by C3 on its own, this concentration of the PAM was selected for use in neutrophils (*Figure 4.3B and D*). Similar to the effect seen in Flp-In T-REx 293 cells, in hFFA2-HA neutrophil membranes AZ1729 increased the effect of the lowest concentration of C3 (1 μ M) to a level equivalent to the effect produced by the highest concentration of C3 alone. In the presence of AZ1729, the E_{max} produced by C3 increased to 145% \pm 34%, however this was not found to be significant (determined by one-way ANOVA). Interestingly, the synergistic effect of AZ1729 appeared to be stronger in WT neutrophil membranes with the lowest and E_{max} responses measured as 143% and 289% of C3 alone, respectively. The pEC_{50} values in the presence of 100nM AZ1729 were found to be 4.66 \pm 0.82 and 4.09 \pm 0.60 for hFFA2-HA and WT, respectively. Neither of these pEC_{50} values were significantly different from the pEC_{50} values in the absence of AZ1729. The use of a single concentration of AZ1729 limited the ability of the allosteric model to accurately calculate the PAM effects of AZ1729 in neutrophils. Nevertheless, $\alpha\beta$ values of 161.81 and 61.09 were estimated in hFFA2-HA and WT neutrophil membranes, respectively. Unlike in Flp-In T-REx 293 cells, here AZ1729 showed PAM effects exclusively on efficacy.

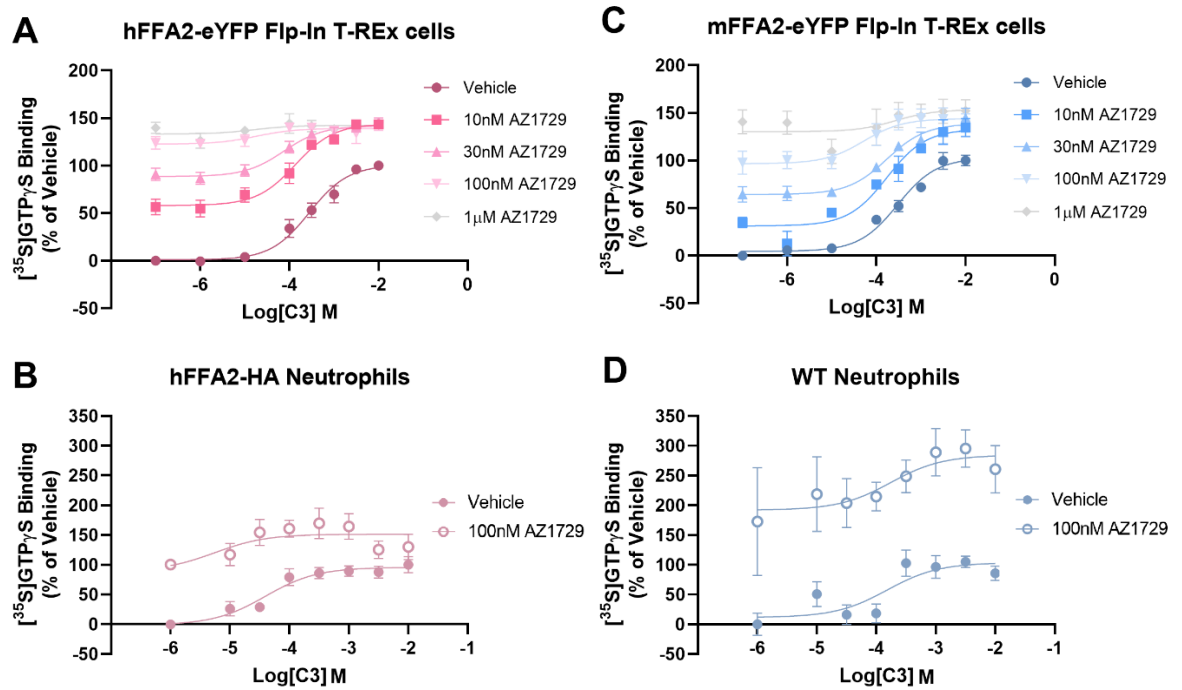


Figure 4.3. PAM effect on agonist-induced $[^{35}\text{S}]\text{GTP}\gamma\text{S}$ incorporation. Membranes prepared from Flp-In T-REx 293 cells induced to express (A) hFFA2-eYFP (C) mFFA2-eYFP were incubated with propionate (C3) at various concentrations for 1h at 30°C , in the absence or presence of various concentrations of AZ1729. Membranes prepared from bone marrow-derived neutrophils isolated from (B) hFFA2-HA or (D) C57BL/6N (WT) mice were incubated with C3 at various concentrations in the absence or presence of 100nM AZ1729. The incorporation of $[^{35}\text{S}]\text{GTP}\gamma\text{S}$ was measured as counts per minute, and the response was normalised to C3 in the absence of AZ1729. Data presented as mean \pm SEM (n=2-3; for B and D each n represents neutrophil membranes pooled from 2-4 mice).

Finally, the ability of the antagonist GLPG0974 to inhibit C3-induced activation was explored in mouse neutrophil membranes. To this end, an EC_{80} concentration of C3 was used in the presence of increasing concentrations of GLPG0974, and non-linear regression curves were fitted (see *Section 2.10.4*). In the case of hFFA2-HA (*Figure 4.4A*), GLPG0974 was able to fully inhibit the response produced by C3, with pIC_{50} of 6.01 ± 0.49 . In WT neutrophil membranes (*Figure 4.4B*), on the other hand, although GLPG0974 displayed some inhibitory effect, it was only down to 65% of the E_{max} produced by C3. Although pIC_{50} of 6.27 ± 1.48 could be calculated for GLPG0974 in WT, the high error range make this value less reliable.

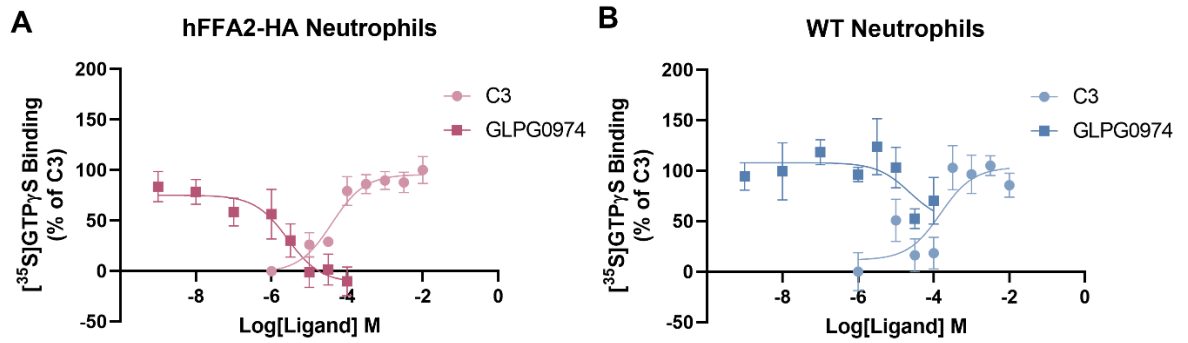


Figure 4.4. Antagonist effect on agonist-induced $[^{35}\text{S}]\text{GTP}\gamma\text{S}$ incorporation. Membranes prepared from bone marrow-derived neutrophils isolated from (A) hFFA2-HA or (B) C57BL/6N (WT) mice were preincubated with various concentrations of GLPG0974 for 15min, followed by incubation with EC_{80} concentration of propionate (C3) for 1h at 30°C . The incorporation of $[^{35}\text{S}]\text{GTP}\gamma\text{S}$ was measured as counts per minute, and the response was normalised to the C3 concentration-response curves. Data presented as mean \pm SEM (n=3, where each n represents neutrophil membranes pooled from 2-4 mice).

4.2.2 Evaluation of transgenic mouse-derived neutrophil function *ex vivo*

Once the molecular characteristics of hFFA2-HA had been established in neutrophil-derived membranes, the ability of the receptor to induce a physiological response in live cells was examined. As literature suggests a role for FFA2 in neutrophil chemotaxis (Vinolo et al., 2011), this response was selected for further examination.

For measuring chemotaxis, methods described by Bolognini et al. (2016) were adapted and optimised for a 96-well format. For this, 96-well Transwell plates with inserts containing permeable membranes were utilised. Neutrophils were added to the insert (top chamber) and incubated with the appropriate compounds in the bottom well. Following the incubation, the contents of the bottom well were collected, lysed, and the amount of total ATP quantified using a bioluminescence-based reaction. As no cells were added to the bottom well, all ATP is derived from neutrophils, and the amount is therefore proportional to the extent of chemotaxis. Chemotaxis was calculated as the percentage increase in fluorescence in relation to vehicle.

Initially, the GPR84 agonist 2-HTP (2-hexylthiopyrimidine-4,6-diol) was utilised as a positive control, as this receptor has been shown to mediate chemotaxis in human neutrophils (Sundqvist et al., 2018). Incubation with $1\mu\text{M}$ 2-HTP induced a significant increase in chemotaxis in comparison to vehicle in hFFA2-HA

($58.9 \pm 20.6\%$; $p < 0.05$ by one-way ANOVA), WT ($85.2 \pm 11.0\%$; $p < 0.01$) and minus-CRE ($97.5 \pm 19.3\%$; $p < 0.001$) neutrophils (*Figure 4.5*). In hFFA2-HA neutrophils (*Figure 4.5A*), C3 induced an apparent concentration-dependent response, yielding $26.2 \pm 13.9\%$, $38.4 \pm 10.6\%$ and $57.6 \pm 19.7\%$ increase in chemotaxis at 0.1mM, 1mM and 10mM concentration, respectively. Despite this clear trend, none of these increases were found to be statistically significant. In WT neutrophils (*Figure 4.5B*), on the other hand, the highest response ($37.7 \pm 16.1\%$) was elicited by 1mM C3, while 0.1mM and 10mM produced $9.2 \pm 3.9\%$ and $27.5 \pm 15.1\%$ increase, respectively. Again, none of these results were found to be statistically significant.

As the synergistic effect of AZ1729 with C3 had already been demonstrated in [^{35}S]GTP γ S incorporation assays in neutrophils, its ability to exert a similar effect on chemotaxis was examined (*Figure 4.5C and D*). Incubation with 1mM C3 or 1 μ M AZ1729 individually yielded non-significant increases in both hFFA2-HA ($38.4 \pm 10.6\%$ and $15.0 \pm 5.4\%$, respectively) and WT neutrophils ($21.0 \pm 10.0\%$ and $11.1 \pm 13.4\%$, respectively). Coaddition of the same concentrations of C3 and AZ1729, however, yielded a significant ($p < 0.01$) increase in chemotaxis, corresponding to $78.2 \pm 11.9\%$ in hFFA2, and $65.2 \pm 15.4\%$ in WT neutrophils. In both strains, there was also a significant difference in the increases caused by 1 μ M AZ1729 added on its own and in conjunction with C3 ($p < 0.05$). In minus-CRE neutrophils, used as a negative control, individual treatment by, and co-addition of C3 and AZ1729 all yielded results close to zero (*Figure 4.5E*).

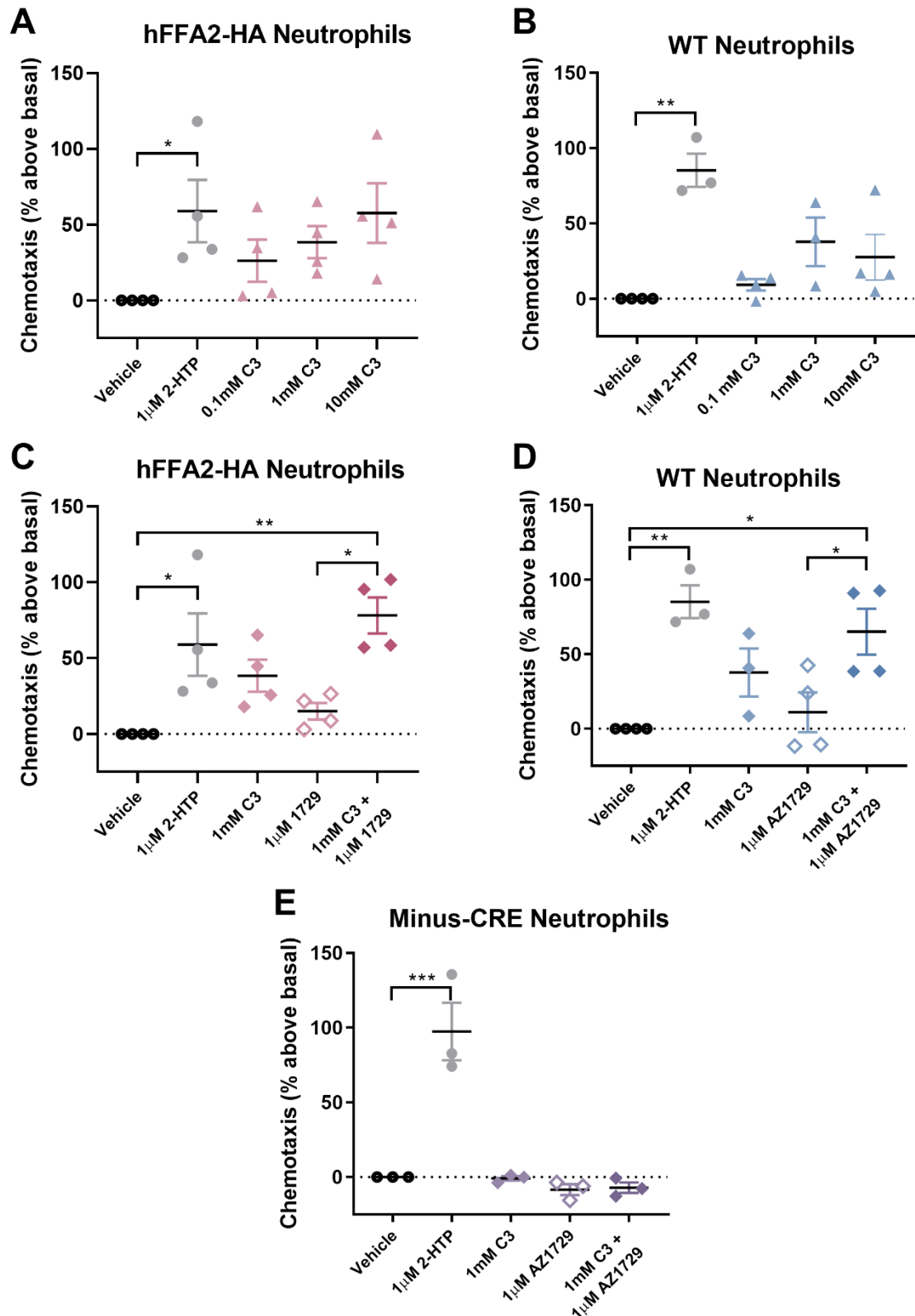


Figure 4.5. Agonist effects on mouse neutrophil chemotaxis. Neutrophils isolated from (A, C) hFFA2-HA, (B, D) C57BL/6N (WT) and (E) minus-CRE mice were incubated for 90min at 37°C with (A, B) 3 concentrations of propionate (C3) or (C, D, E) 1mM C3 and 1 μ M AZ1729 individually or simultaneously. Chemotaxis through a trans-well membrane was quantified as the total amount of ATP in the bottom well, itself measured as total luminescence from the ATPlite ATP detection kit. Vehicle, 2-HTP and 1mM C3 data shown in A and B represent the same measurements as those in C and D, respectively. Results were normalised to vehicle and are presented as mean \pm SEM (n=3-4, where each n represent neutrophils pooled from 2-4 mice). *** p<0.001, ** p<0.01, * p<0.05 by one-way ANOVA with Tukey's post-hoc multiple comparisons test. Data produced in conjunction with Dr Daniele Bolognini.

In a separate set of experiments, the ability of the inverse agonist CATPB to inhibit agonist-induced chemotaxis was evaluated (*Figure 4.6*). As before, in the absence of CATPB, C3 failed to produce a significant increase in chemotaxis in hFFA2-HA ($30.9 \pm 9.3\%$), while the combination of C3 and AZ1729 did so ($56.8 \pm 12.1\%$; $p < 0.001$ by two-way ANOVA). Similarly, in WT neutrophils C3 induced a non-significant increase on its own ($3.5 \pm 6.9\%$) but a significant increase in conjunction with AZ1729 ($97.1 \pm 16.1\%$; $p < 0.0001$ by mixed-effects analysis).

When hFFA2-HA neutrophils were pre-treated with $1 \mu\text{M}$ CATPB (*Figure 4.6A*), the response to C3 was abolished (down to $1.6 \pm 8.8\%$; $p < 0.05$ by two-way ANOVA). While CAPTB treatment led to a moderate decrease in the response produced by the co-addition of C3 and AZ1729 ($39.4 \pm 13.5\%$), this was not found to be significant. CAPTB treatment in WT neutrophils produced markedly different results (*Figure 4.6B*). The response produced by C3 was moderately, but non-significantly increased ($14.2 \pm 9.0\%$), while that produced by the co-addition of C3 and AZ1729 was unaffected ($97.4 \pm 18.3\%$).

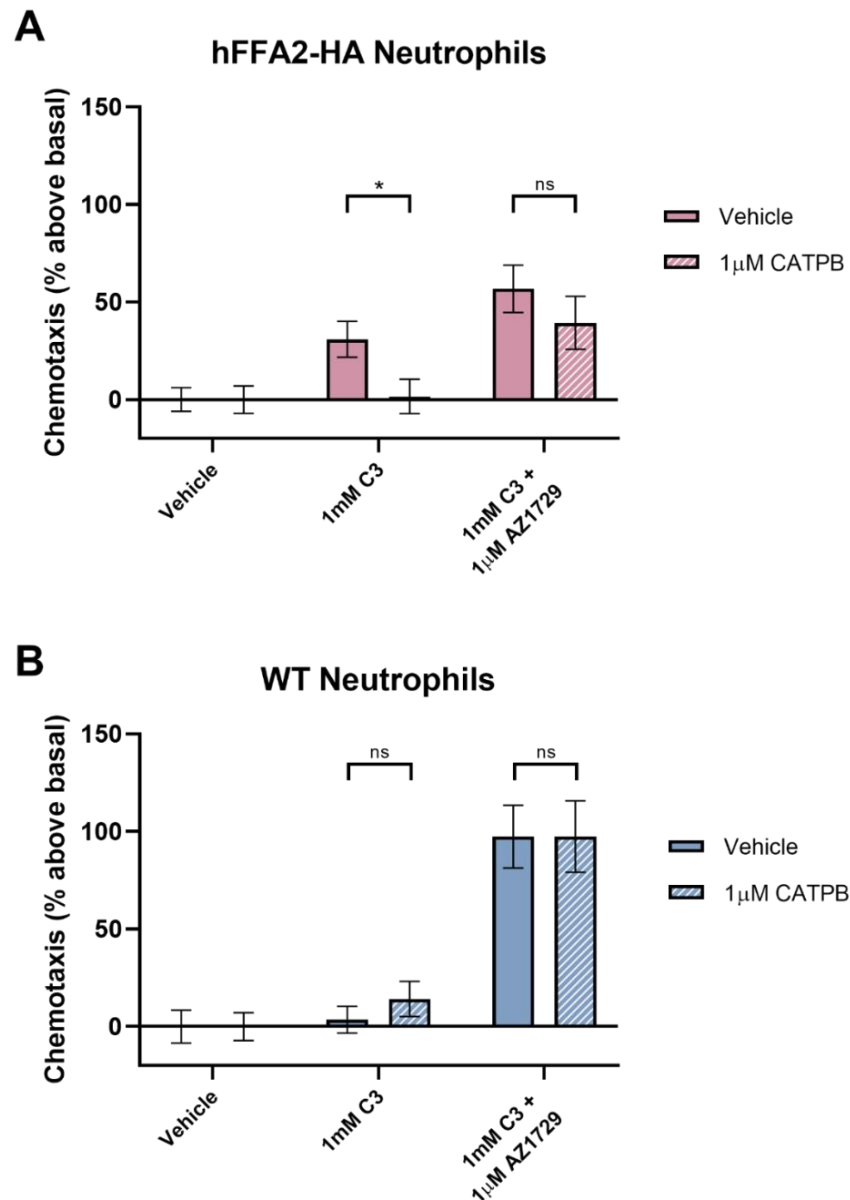


Figure 4.6. Antagonist effects on mouse neutrophil chemotaxis. Neutrophils isolated from (A) hFFA2-HA and (B) C57BL/6N (WT) mice were pre-incubated with 1µM CATPB for 15min, followed by incubation with 1mM propionate (C3) for 90min at 37°C, in the presence or absence of 1µM AZ1729. Chemotaxis through a trans-well membrane was quantified as the total amount of ATP in the bottom well, itself measured as total luminescence from the ATPlite ATP detection kit. Results were normalised to vehicle and are presented as mean±SEM (n=3, where each n represent neutrophils pooled from 2-4 mice). * p<0.05 by two-way ANOVA with Sidak's post-hoc multiple comparisons test.

In addition to chemotaxis, another neutrophil physiological function in which FFA2 is implicated is the release of NETs (Carretta et al., 2016). As NETs are primarily composed of dsDNA, the fluorescent dsDNA dye PicoGreen was used for their quantification (adapted from Hollands et al., 2016). NET formation was calculated as the percentage increase in fluorescence in relation to vehicle. As a positive control, 10µM AA was utilised, as this compound has been shown to induce the release of NETs (Figure 4.7A inset). Indeed, AA was able to induce a

significant increase in NET production in hFFA2-HA ($363.4 \pm 113.9\%$; $p < 0.05$ by one-way ANOVA), WT ($394.4 \pm 64.0\%$; $p < 0.05$) and minus-CRE ($642.4 \pm 123.7\%$; $p < 0.0001$).

To test activation of NET production, C3 was used at 10mM (*Figure 4.7A*). Although the effect produced by C3 was not as dramatic as that of AA, it was found to be significant in both hFFA2-HA ($42.3 \pm 12.1\%$; $p < 0.001$ by mixed-effects analysis) and WT neutrophils ($34.6 \pm 10.3\%$; $p < 0.05$). In minus-CRE neutrophils, however, no significant effect of C3 was observed ($16.2 \pm 5.6\%$).

Although there was a noticeable variation in the extent of NET formation between individual experiments, the assay was nevertheless employed to examine the effect of pre-incubation with antagonists CATPB and GLPG0974 in hFFA2-HA neutrophils (*Figure 4.7B*). CATPB at 1 μ M moderately inhibited (to $25.8 \pm 13.1\%$), and at 10 μ M all but ablated the response (down to $2.9 \pm 2.1\%$ above basal) produced by 10mM C3. The inhibition by GLPG0974 was even more moderate, with NET production by 1 μ M and 10 μ M C3 reduced to $32.1 \pm 7.1\%$ and $16.4 \pm 9.4\%$ above basal, respectively. Despite the apparent concentration-dependent inhibition, none of these data were found to be significant (determined by one-way ANOVA).

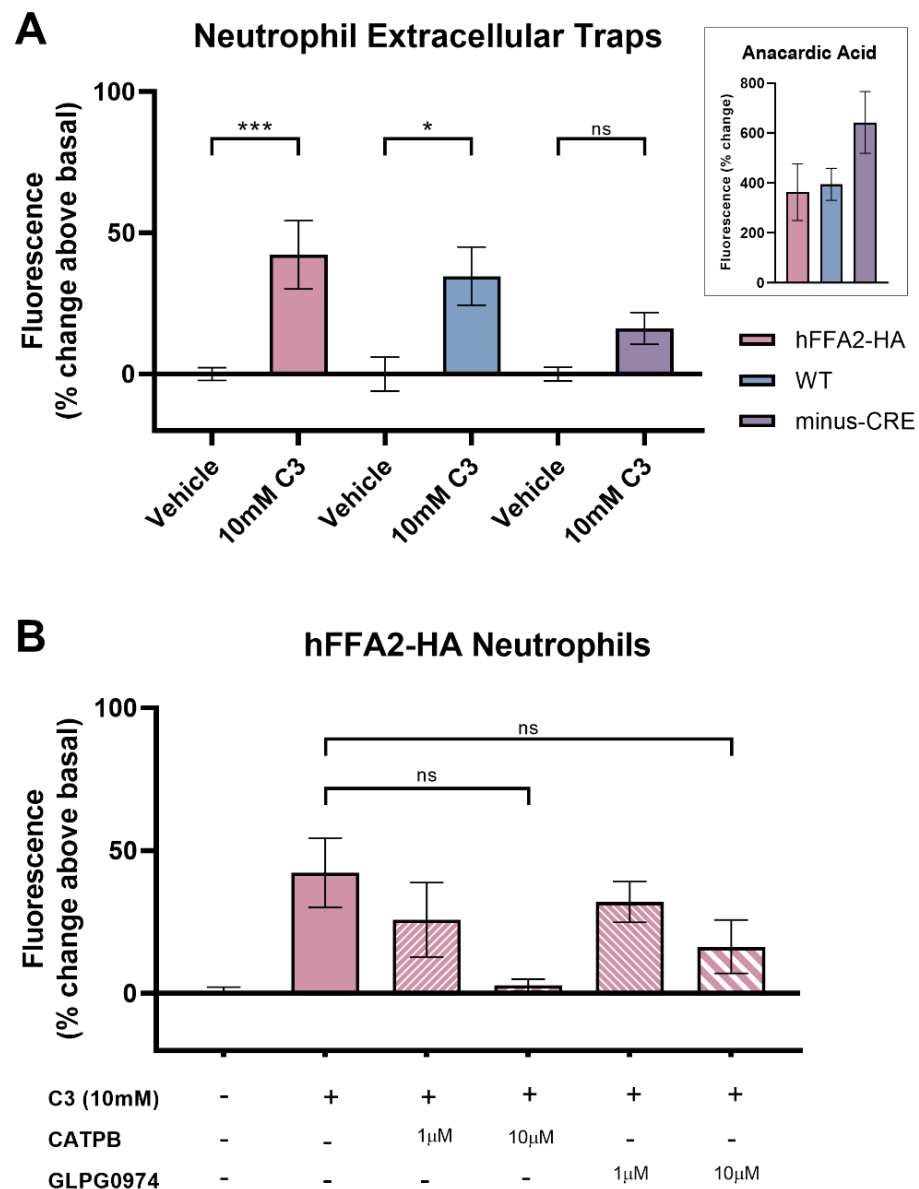


Figure 4.7. Neutrophil extracellular trap formation. (A) Neutrophils isolated from hFFA2-HA, C57BL/6N (WT) and minus-CRE mice were incubated for 2h at 37 °C with vehicle, 10mM propionate (C3) or anacardic acid (inset). (B) Neutrophils isolated from hFFA2-HA mice were pre-incubated for 15min with 1µM or 10µM CATPB or GLPG0974 before incubation with 10mM C3 for 2h at 37 °C. Double-stranded DNA was stained with Quant-iT PicoGreen dsDNA reagent, and fluorescence was measured. Results were normalised to vehicle and are presented as mean±SEM (n=3, where each n represent neutrophils pooled from 2-4 mice). *** p<0.001, ** p<0.01 by Mixed-effects analysis with Sidak's post-hoc multiple comparisons test.

4.3 Discussion

4.3.1 Human orthologue-specific FFA2 ligands bind to and affect activation of hFFA2-HA in mouse-derived neutrophils

While the hFFA2-HA protein has been shown to be expressed in endocrine and immune tissues (*Chapter 3*), its functionality has not yet been demonstrated. *In vitro* assays which are well-established in transfected cell lines can aid the

effort of functional characterisation of primary cells derived from this mouse strain. Although the expression of hFFA2-HA was found to be lower in neutrophils than in either the colon or in white adipose tissue, the uniformity of isolated neutrophils circumvent the necessity of dissecting the contribution of different cell types to a tissue-wide response. In addition, the involvement of FFA2 in neutrophil functions has been researched widely but primarily in human neutrophils. As a result, mouse neutrophils became the tissue of choice to conduct *ex vivo* experiments.

Radioligand binding assays are generally used to determine the kinetics and affinity of ligand binding. In addition, the B_{\max} of samples can also be estimated, which is particularly important as an overexpressing cell line is being compared to primary cells. Initial saturation binding in hFFA2-eYFP-expressing Flp-In T-REx 293 cells have revealed the K_d of [^3H]GLPG0974 as $12.5 \pm 2.3 \text{ nM}$. Although this suggests a lower affinity for hFFA2-eYFP than published work (Sergeev et al., 2016), this concentration was nevertheless used in further experiments with neutrophils. While some groups have successfully used neutrophil-derived membranes to generate complete saturation binding curves of other receptors (Varani et al., 1998), this was not possible in the case for hFFA2-HA mouse neutrophils. This is perhaps best explained by the fact that, as primary cells, the specific binding was found to be under 250 fmol/mg in comparison to the B_{\max} of $16,000 \text{ fmol/mg}$ in the overexpressing cell line. The specific binding calculated for neutrophils is not equivalent to B_{\max} , however it suggests that the predicted B_{\max} in neutrophils is likely to be considerably lower than in Flp-In T-REx 293 cells.

While in the absence of saturation and competition binding curves it is impossible to draw conclusions about ligand binding affinities in neutrophils, the single concentration binding studies were able to provide valuable information. On one hand, the fact that [^3H]GLPG0974 was found to bind specifically in hFFA2-HA neutrophil membranes but not in minus-CRE and traditional FFA2-KO neutrophils suggests that the hFFA2-HA is indeed expressed on neutrophils, and that the ability of the receptor to bind its specific ligand was not affected. In addition, the other human orthologue-specific antagonist CATPB was able to displace [^3H]GLPG0974, further confirming the ability of hFFA2-HA on

neutrophils to bind the ligands. While agonists could have been used in the same set of displacement experiments, the use of the antagonists provides evidence to the presence and functionality of hFFA2-HA in these neutrophil membranes. In the future, in order to further explore ligand kinetics in neutrophil membranes, a dual-point competition binding assay could be employed, whereby radioactivity in the presence of a competitor is measured at two distinct time points, thus providing a relative indication of dissociation rate (Guo et al., 2013). Although the assay is useful in its current form, there is clear incentive to optimise for a high-throughput format. This would allow the construction of full saturation curves, as well as the conduction of a full-scale kinetic analysis to determine ligand interactions with hFFA2-HA on neutrophil membranes. Additionally, this would provide a platform for the characterisation of the affinity of new compounds in a primary cell line.

One of the crucial steps in GPCR activation is the engagement and dissociation of their eponymous G proteins. It is the replacement of GDP with GTP in the $G\alpha$ subunit which the [³⁵S]GTP γ S incorporation assay exploits. Due to the fact that the terminal sulphate substitution prevents hydrolysis, the build-up of the radioactive GTP analogue is a proportional measure of receptor activation. For initial experiments, the endogenous ligand C3 was chosen, as it has similar potencies at hFFA2 and mFFA2 and its water solubility allows to circumvent potential DMSO effects which would be seen with synthetic agonists. Results from Flp-In T-REx 293 membranes show not only lower potency of C3 at both orthologues (3.57 instead of 4.25 at hFFA2-eYFP and 3.43 instead of 3.73 at mFFA2-eYFP) but also a diminished difference between the pEC₅₀ values (1.4-fold difference instead of 3-fold difference) (Hudson et al., 2012b). Interestingly, however, pEC₅₀ values acquired from neutrophil membranes resembled expected values much more closely, with 4.36 and 3.82 for hFFA2-HA and WT, respectively. This reflects both the expected order and magnitude of difference of potencies between the two orthologues. In minus-CRE and FFA2-KO neutrophil membranes, C3 failed to produce a concentration-dependent response, thus further supporting results from radioligand binding experiments.

As the PAM AZ1729 was intended to be used in functional assays in live neutrophils, its effects were first explored *in vitro*. Although the modulatory

effects of this PAM had not previously been explored in [³⁵S]GTPγS incorporation assays, the effects in Gα_{i/o}-mediated cAMP inhibition assays can give an indication of the expected effects (Bolognini et al., 2016). Indeed, in Flp-In T-REx 293 cells expressing either orthologue of FFA2, the co-addition of increasing concentrations of AZ1729 with C3 yielded an enhanced efficacy (including an increase in E_{max}) without a significant increase in pEC₅₀ values. This PAM effect on efficacy was surprising, considering that AZ1729 has been described as a PAM of potency in cAMP inhibition assays. It is important to note, however, that although both of these assay systems measure signalling through Gα_{i/o}, cAMP inhibition occurs downstream of the Gα_{i/o} activation measured by [³⁵S]GTPγS incorporation assays. Thus, the PAM effects exerted by AZ1729 may be subject to probe-dependency. Although AZ1729 appeared to enhance the efficacy of C3 to a greater extent in WT than in hFFA2-HA neutrophils, the estimated cooperativity factors suggest that AZ1729 was a stronger PAM of efficacy at the latter. Application of the allosteric model in neutrophils was certainly limited by the single concentration of AZ1729 used. As such the direct agonist effect (τ) could not be calculated. Considering that higher τ was observed in mFFA2-eYFP than in hFFA2-eYFP, such a difference could account for an apparently higher efficacy in WT neutrophils. In earlier studies, AZ1729 displayed not only species-specific effects but also probe-dependence in combination with different agonists (Bolognini et al., 2016). Therefore, in order to fully understand the allosteric effects of AZ1729 on both hFFA2-HA and WT neutrophils, a wider range of AZ1729 concentrations must be used, in conjunction with a range of available agonist ligands.

While it is unclear how the differential results reflect on the ability of AZ1729 to positively modulate C3-induced FFA2 activation in neutrophil membranes, they pinpoint the potential shortcomings of the assay system used. While Flp-In T-REx 293 membranes have been used in these experiments for a long time, no available literature has utilised neutrophil membranes for this purpose. While much of the intracellular machinery can be lost during the membrane preparation process, this has not caused any obvious drawbacks in overexpressing cell lines. On the other hand, neutrophil membranes tended to aggregate throughout the preparation process, potentially leading to unpredictable responses as a result of uneven distribution of membrane

proteins. Another potential cause for the difference in responses between the two strains is the relatively low raw CPM count gained from WT neutrophil membranes in comparison to hFFA2-HA. This could either be the result of either the above-mentioned uneven membrane preparations or even of differential inflammatory states between mice from which the neutrophils were isolated. While the latter problem could be limited to some extent by individual housing of animals, in order to solve the former, a different approach to sample preparation could be used. In fact, whole cultured rat cerebellar granule cells permeabilised with saponin have been utilised to examine [³⁵S]GTPγS incorporation in response cannabinoid agonists (Breivogel et al., 2004). Were a similar approach be optimised for mouse neutrophils, it would eliminate the issues encountered with membrane preparations, and would allow more accurate comparisons with other whole cell functional assays (Strange, 2010).

Of course, the main rationale for establishing the hFFA2-HA mouse strain was the expected ability of human orthologue-specific antagonists to block agonist effects in mouse tissues. It is evident from the [³⁵S]GTPγS incorporation assays that GLPG0974 is in fact able to inhibit C3-induced activation in hFFA2-HA neutrophil membranes, albeit with a lower potency than previously reported in Flp-In T-REx 293 cells (pEC₅₀ of 6.0 instead of 6.7 (Sergeev et al., 2016)). This was the first step in truly demonstrating the functional utility of the hFFA2-HA mouse model. The ability of GLPG0974 to moderately inhibit C3 in WT neutrophil membranes was surprising, however the same issues with membrane preparations detailed above are applicable to this set of experiments as well.

While [³⁵S]GTPγS incorporation measures the initial step of receptor activation, it does so reliably only for Gα_{i/o}. FFA2, however, is promiscuous in that it couples not only to Gα_{i/o} but also to Gα_{q/11}. In recombinant cell lines, activation of G proteins of each class can be tracked using BRET-based methods (Inoue et al., 2019). Of course, this approach would not be possible in primary cells, therefore Gα_{q/11} activation would have to be measured indirectly by examining the downstream second messenger systems. While Ca²⁺ flux assays have been used in human neutrophils (Lind et al., 2019), they do not necessarily account for non-GPCR-mediated release of Ca²⁺. IP1 is a metabolite of IP3 which in turn is a product generated by PLC as a result of Gα_{q/11} activation (Trinquet et al.,

2011). Homogeneous time-resolved fluorescence (HTRF)-based methods exist for the detection of this second messenger (as well as for cAMP to measure $G\alpha_{i/o}$ -mediated responses) which would eliminate the potential non-specific Ca^{2+} responses. Similarly, the phosphorylation of ERK1/2 could also be measured by similar methods as a measure of receptor activation (Osmond et al., 2005). Unfortunately, neither Ca^{2+} flux, nor HTRF-based second messenger assays were successfully optimised during this project but their use in published literature means that they nevertheless present useful approaches. Ideally, these second messenger responses would have been explored further in order to relate G protein activation to whole-cell functional responses presented below.

4.3.2 Whole cell responses are mediated by hFFA2-HA in the transgenic hFFA2-HA mouse-derived neutrophils

The role of FFA2 in inflammation has been controversial, mainly due to the cell- and ligand-dependent pro- and anti-inflammatory responses mediated by the receptor. For example, on one hand, C2 inhibits LPS-induced release of the pro-inflammatory cytokine TNF α in human and mouse mononuclear cells through FFA2 (Masui et al., 2013). By contrast, C2 induces increased expression of TNF α mRNA via FFA2 in M2-type macrophages in adipose tissue (Nakajima et al., 2017). With such contradictory effects, it is not surprising that there is no consensus as to whether agonists or antagonists of FFA2 would be desirable in the treatment of inflammatory conditions (Li et al., 2018).

Under conditions of inflammation or infection, recruitment of neutrophil to the site constitutes a crucial early event (Maslowski et al., 2009). FFA2 has been well-established as a chemoattractant receptor for SCFAs (Le Poul et al., 2003), and this function has been widely researched in human and mouse neutrophils. In the past, experiments with mouse neutrophils involved the use of traditional FFA2-KO strains (Vinolo et al., 2011, Maslowski et al., 2009), investigating the effects on chemotaxis in the absence of the receptor. As discussed in detail in **Chapter 3**, the use of traditional KOs has several drawbacks in relation to compensatory mechanisms. In the case of hFFA2-HA mice, no such mechanisms are at play, and receptor functions are, as demonstrated in *in vitro* experiments, amenable to inhibition by hFFA2 antagonists.

In initial experiments, while the chemotactic effect of C3 was not significant, it did show what appeared to be a concentration-dependent response. In fact, despite the limited range of C3 concentrations used, the response in WT neutrophils appeared to diminish at the highest concentration. This would be in line with bell-shaped concentration-response curves previously observed in neutrophils stimulated with formyl methionyl-leucyl-phenylalanine (fMLP) (Hii et al., 2004, Bolognini et al., 2016). Importantly, co-addition of C3 and the PAM AZ1729 led to a significant increase in chemotaxis in both hFFA2-HA and WT, but not in minus-CRE neutrophils. Not only does this demonstrate that the response is mediated by FFA2 but, due to the $G\alpha_{i/o}$ -bias of AZ1729, the second messengers involved in the response can also be inferred. Indeed, neutrophil chemotaxis has been shown to be independent of intracellular Ca^{2+} levels (Zigmond et al., 1988), and is rather mediated through PTX-sensitive $G\alpha_{i/o}$, via phosphatidylinositol 3-kinase γ (PI3K γ), Rac2 and MAPK. In addition, pre-incubation with the antagonist CATPB ablated C3-induced effects in hFFA2-HA neutrophils but not in WT neutrophils, further corroborating the *in vitro* results demonstrating the value of the hFFA2-HA mouse model. Interestingly, while CATPB caused a small (albeit insignificant) decrease in the response produced by the co-addition of C3 and AZ1729 in hFFA2-HA neutrophils, much of the response was unaffected. This would perhaps not be surprising, considering that AZ1729 binds to a distinct site from CATPB, however AZ1729 was shown to have no chemotactic effect on its own. Recently, AZ1729 and other allosteric modulators were shown to display a complex system of inter-dependent signalling profiles in human neutrophils, regulating neutrophil chemotaxis (Dahlgren et al., 2020). In fact, the antagonist GLPG0974 was found to display PAM properties in response to allosteric activation of hFFA2 (Lind et al., 2022). While these signalling pathways have only been explored in relation to Ca^{2+} flux and superoxide production, similar interactions could potentially exist in $G\alpha_{i/o}$ -mediated processes and involving CATPB or other compounds.

Following recruitment to the site of inflammation, primed neutrophils can display a range of functions in order to maintain or resolve inflammation. In response to pathogens, NETs containing dsDNA and granular enzymes are released. The release of NETs can also be stimulated *in vitro* through the activation of GPCRs (Hollands et al., 2016), and as such, the potential role of

FFA2 in this process was of interest. A single high concentration of C3 was able to induce NET release in hFFA2-HA and WT, but not in minus-CRE neutrophils. While the results obtained were not significant, both GLPG0974 and CATPB appeared to have a concentration-dependent inhibitory response on C3-induced NET formation in hFFA2-HA neutrophils. Despite using methods adapted from Hollands et al (2016), the assay employed somewhat lacked consistency across repeated measures. This of course could have arisen from issues discussed earlier in the chapter, relating to the inflammatory state of the individual animals being used, which in turn could affect the priming state of neutrophils, and thus the response (Martensson et al., 2018).

The signalling pathways involved in NET formation depend on the stimuli inducing the response. While bacterial stimulation generates a response dependent on NADPH oxidase activation, stimulation by ionomycin does not require the same signalling (Parker et al., 2012). Upstream of NADPH oxidase, activity through the Raf-MEK-ERK axis is involved in NET formation (Hakim et al., 2011). In human neutrophils, allosteric activation of FFA2 can lead to the activation of NADPH oxidase, displaying an intricate network of downstream signalling interactions. Neither agonists, nor PAMs AZ1729 or Compound 58 are able to induce NADPH oxidase activation individually, however pre-treatment with PAMs leads to superoxide production via NADPH oxidase (Lind et al., 2019). Stimulation by both PAMs in the absence of an orthosteric agonist also leads to potent NADPH oxidase activation without the agonist-induced Ca^{2+} flux, while agonist treatment following pre-treatment by both PAMs leads to a diminished NADPH-oxidase response (Lind et al., 2020). The extent to which these interactions are preserved in mouse neutrophils is unclear, however the hFFA2-HA strain would allow further investigation. As C3 appeared to induce the release of NETs even in the absence of PAMs, it is unlikely that the response is mediated by the NADPH oxidase-dependent pathway and could, in fact, be mediated by a $G_{\alpha_{i/o}}$ -dependent Ca^{2+} response (Martensson et al., 2018, Gupta et al., 2014).

In addition to chemotaxis, NET formation and superoxide release, stimulation through FFA2 on neutrophils can induce the release of pro-inflammatory cytokines, including IL-1 β . IL-1 β , in turn, binds IL-1 receptors (IL-1R) on ILC3

cells, leading to the production of IL-22. Activation of FFA2 on ILC3 cells leads to IL-22 production via a pathway involving ERK1/2, signal transducer and activator of transcription 3 (STAT3) and RAR-related orphan receptor γ t (ROR γ t), as well as to an increase in the surface expression of IL-1R, thus further augmenting IL-22 release (Chun et al., 2019, Fachi et al., 2020). The interplay of FFA2-mediated responses between neutrophils and ILC3s could result in more effective resolution of bacterial infection. In addition, IL-22 released from ILC3s promotes tissue integrity, thus counteracting the tissue damage caused by reactive oxygen species released by neutrophils (Martensson et al., 2018, Chun et al., 2019). The expression profile of FFA2, alongside its role in such a range in immune functions explains its appeal as a target for chronic inflammatory diseases (Namour et al., 2016, Soehnlein et al., 2017).

The signalling of FFA2 is incredibly complex both at the level of downstream effectors and at that of the intercellular communication. The discovery of additional layers of complexity is encouraging for drug development efforts, as it could eventually allow selective targeting to enhance beneficial responses while inhibiting detrimental ones. As demonstrated in this chapter, the receptor expressed by hFFA2-HA mice is functional and is blocked by selective antagonists in neutrophils *ex vivo*. Therefore, this mouse strain provides a model for the investigation of hFFA2 function in immune tissues implicated in disease both *ex vivo* and *in vivo*.

CHAPTER 5 - NON-G PROTEIN-MEDIATED SIGNALLING IN FFA2

5.1 Introduction

Besides signalling through their eponymous G proteins, GPCRs have been shown to couple to additional, alternative signalling pathways. Following receptor activation and G protein dissociation, various GRKs are recruited to intracellular segments of the receptor where they phosphorylate specific serine (Ser) and threonine (Thr) residues. Receptor phosphorylation can, in turn, lead to the recruitment of arrestins to the receptor. This interaction between GPCRs and arrestins has been known to act as a regulator of receptor signalling. On one hand, binding of the arrestin creates a physical barrier to G protein binding, thus preventing G protein-mediated signalling (Gurevich and Gurevich, 2019). On the other hand, β -arrestins (also known as non-visual arrestins) both have affinity for clathrin and its adaptor complex, AP2, thus facilitating GPCR internalisation into clathrin-coated pits (Goodman et al., 1996, Laporte et al., 1999, Gurevich and Gurevich, 2003). In recent decades, however, it has become increasingly clear that arrestins are able to generate downstream signals in their own right. Both β -arrestins have been shown to promote ERK1/2 activation both through c-Src activation and via the C-Raf1-MEK1-ERK1/2 axis (Luttrell et al., 2001). In fact, proteomics analysis using the angiotensin II type 1A receptor as a model identified over a hundred interacting partners for both β -arrestins (Xiao et al., 2007), and activation by a β -arrestin-biased ligand has led to differential phosphorylation of more than 200 proteins identified through phosphoproteomics (Xiao et al., 2010). These downstream effectors range in function from protein kinases, through DNA-binding proteins to cytoskeleton constituent proteins. Due to such a diverse range of responses, biased activators of β -arrestin-mediated signalling might be of interest both as tool compounds and as potential therapeutic options.

The fact that merely two β -arrestins are able to interact with hundreds of GPCRs, as well as with hundreds of downstream partners to generate distinct signalling has led to the conception of the “barcode” theory. According to this, the different patterns of GPCR phosphorylation by various GRKs would lead to various distinct signalling effects. Upon interaction with these phosphorylated residues, β -arrestins would undergo conformational changes depending on the

“barcode”, thus mediating individual downstream signals. Conceptually, the “barcode” on a GPCR could depend on both the activating ligand and the GRK and β -arrestin expression profile of the cells investigated (Tobin, 2008, Matthees et al., 2021). Variations of this theory exist, termed the Flute Model (Yang et al., 2017) and the QR Code Model (Chen et al., 2022) which mainly differ in the emphasis each component of the interaction receives.

In recent years, the development of phosphorylation-site specific antisera for a number of GPCRs has greatly aided our understanding of non-traditional signalling pathways. This is due to the fact that they detect crucial first steps in non-G protein-mediated responses. In particular, opioid and somatostatin receptors have been extensively studied (Mann et al., 2020, Lehmann et al., 2014). As for metabolite-sensing receptors, such antisera have been utilised for the study of FFA4 (Butcher et al., 2014), and more recently, GPR84 (Marsango et al., 2022b). In order to generate these antisera, peptides encompassing regions of interest within the intracellular segments of the receptor were synthesised, with Ser and Thr replaced by their phosphorylated counterparts. Rabbits were then immunised with these peptides in order to mount an immune response. Finally, the antisera thus generated were affinity purified before further analysis (Mann et al., 2021).

While the generation of these antisera has generally been informed by mass spectrometry data (Butcher et al., 2016, Mann et al., 2019), the set of antisera for FFA2 were developed using insights of the scientist at 7TM Antibodies, based on their experience with other GPCRs. Although the ICLs of FFA2 (*Figure 5.1*) contain residues which are potential phosphate acceptors, it was pairs of residues within the C-terminal tail that were targeted on this receptor. Antisera for FFA2 used herein target phosphorylated Ser residues at positions 296 and 297 (pSer²⁹⁶/pSer²⁹⁷), phosphorylated Thr residues at positions 306 and 310 (pThr³⁰⁶/pThr³¹⁰) and another pair of phosphorylated Ser residues at positions 324 and 325 (pSer³²⁴/pSer³²⁵). These choices, although appearing arbitrary, are in fact all identified by PhosCoFinder (<http://tools.vai.org/phoscofinder/>) as “partial phosphorylation codes” as defined by Zhou et al (2017). According to this definition, when phosphorylated, these residues could contribute to β -

arrestin recruitment through electrostatic interactions with positively charged pockets on β -arrestin.

Intracellular Ser and Thr residues are highly conserved between the human and the mouse orthologues of FFA2 (*Figure 5.1*). In fact, the pairs of residues targeted by the putative phosphosite-specific antisera are identical between the two orthologues, despite the surrounding sequences differing greatly. Even though the antisera were raised against the peptide sequence of hFFA2, they were nevertheless tested against mFFA2 as well, in order to explore their species selectivity.

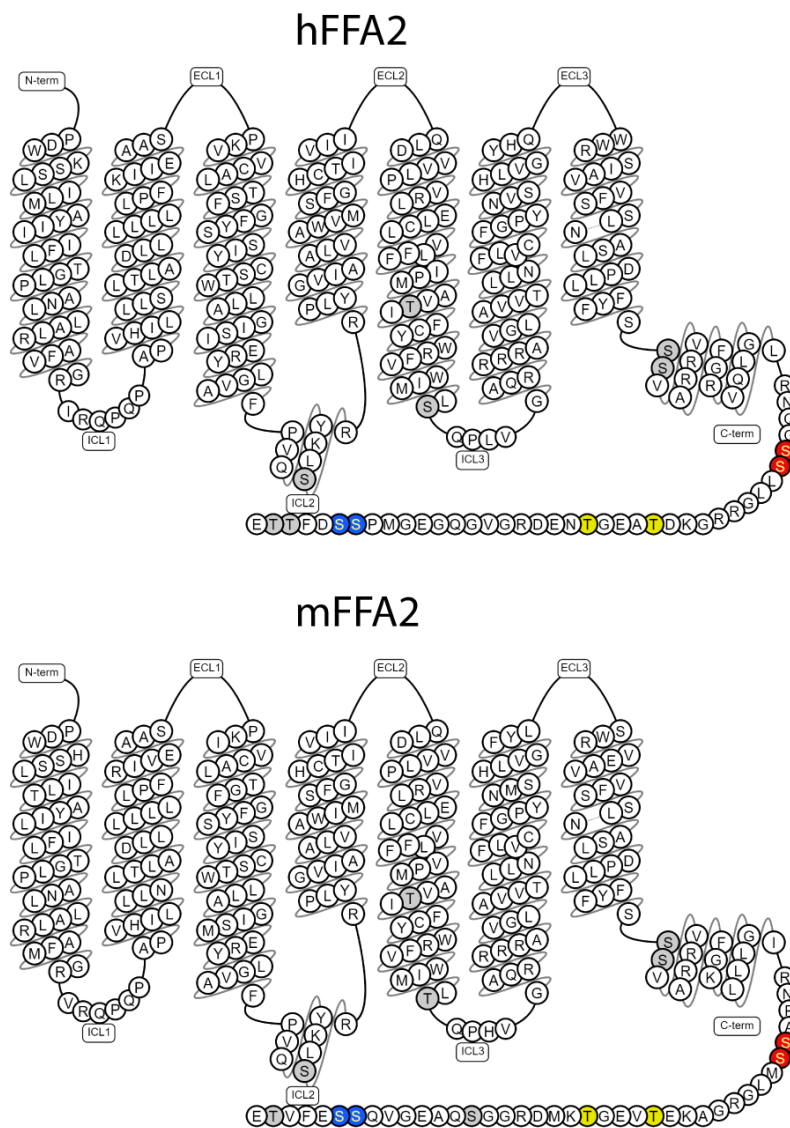


Figure 5.1. Putative phosphorylation sites on human and mouse FFA2. Amino acid sequence of human (hFFA2) and mouse FFA2 (mFFA2), with potential phosphate-acceptors highlighted. Residues targeted by phosphosite-specific antisera are highlighted in colour: pSer²⁹⁶/pSer²⁹⁷ (red), pThr³⁰⁶/pThr³¹⁰ (yellow) and pSer³²⁴/pSer³²⁵ (blue). Other potential phosphate acceptor residues are highlighted in grey. Snake plot generated with GPCRdb based on information from 7TM.

Western blotting (WB) is a quintessential part of the experimental toolkit exploring protein expression and phosphorylation. The basic concept relies on a primary antibody targeting a specific peptide (or phosphopeptide) and a secondary antibody conjugated to either an enzyme or a fluorescent dye. After initial SDS-PAGE of the protein samples, the separated polypeptides are transferred to nitrocellulose or other support surface, on which the subsequent incubations with the antisera occur. Traditionally, secondary antibodies conjugated to horseradish peroxidase were used, which upon the addition of a suitable substrate generates chemiluminescence. Such signals would subsequently be visualised on X-ray film (Taylor et al., 2013). Although the chemiluminescence method, in combination with digital imaging, constitutes a semi-quantitative method, it relies on the measurement of an indirect signal. Further limitations include dependence on substrate availability and exposure time. Fluorescent antibodies are unaffected by such factors, generating a stable signal and a linear signal to sample ratio (Eaton et al., 2014, Pillai-Kastoori et al., 2020). As such, the fluorescent antibody IRDye 800CW was selected for WB analyses, as it possesses the highest sensitivity of the commercially available options (Schreiber et al., 2021).

In order to ensure the even loading of samples, generally a control is quantified alongside the peptide of interest. In complex biological samples, this can be a housekeeping protein such as GAPDH (Taylor et al., 2013). As eYFP-tagged versions of hFFA2 and mFFA2 exist, the eYFP tag itself can be targeted with an anti-GFP antibody as a control. Similarly, for HA-tagged receptors an anti-HA antibody can serve as the control for receptor expression. The presence of the tags has a two-fold benefit: in addition to serving as a control, they allow for the purification of the samples through immunoprecipitation or affinity capture (Bonifacino et al., 1999, Cristea et al., 2005). Following the use of GFP- or HA-traps, the resulting samples loaded onto the gels should contain the tagged constructs exclusively.

For initial testing of hFFA2 and mFFA2, C3 was utilised, while for hFFA2-DREADD, SA was used. The characterisation of the phosphosite-specific antisera cannot simply consist of testing agonist-induced activation. Firstly, the use of the hFFA2 antagonist CATPB can reveal the agonist-dependency of phosphorylation.

Importantly, the use of λ PP, which removes all phosphate residues from treated samples, can reveal whether binding of antisera is phosphorylation-dependent (Rusnak et al., 1999, Doll et al., 2011). The use of λ PP does not, however, reveal whether the phosphorylated residues recognised by the phosphosite-specific antisera are identical to the ones they intended to target. To this end, the pairs of stipulated residues were changed to Ala through targeted mutagenesis using primers listed in **Section 2.1.2**, generating a series of phosphodeficient (PD) mutants. Loss of antiserum binding at these mutants would confirm the specificity of the antisera for their phosphorylated targets.

While WB is a useful method for quantification of the target from a homogenised sample, ICC staining can further inform about cellular localisation of antiserum binding, and hence of receptor activation. Phosphosite-specific antisera have been previously utilised in ICC staining, both in transfected cells and in isolated tissues (Butcher et al., 2016). The use of ICC in HA-tagged tissues and cells has been discussed in depth in **Chapter 3**, however experiments presented herein equally utilise Flp-In T-REx 293 cells expressing eYFP-tagged receptors. Importantly, unlike in previous ICC studies, phosphatase inhibitors were employed throughout these experiments in order to preserve receptor phosphorylation. Once the ability of the FFA2 phosphosite-specific antisera to detect agonist activation in ICC was established, the antagonist CATPB and PD mutants of the receptor were employed for further characterisation, as in the case of WB.

As described above, receptor phosphorylation is followed by the recruitment of arrestins to the intracellular surface of the receptor. This interaction can be monitored via BRET-based methods, whereby the eYFP-tag of the receptor acts as an acceptor of photons generated from a β -arrestin tagged with a bioluminescent molecule. While *Renilla* luciferase (RLuc) has been used widely for this purpose (Pfleger and Eidne, 2006), a smaller luciferase derived from *Oplophorus gracilirostris* (NLuc) provides greater signal and was therefore selected for these studies (Hall et al., 2012, Machleidt et al., 2015). The NLuc conjugated to β -arrestin-2 converts the substrate furimazine into furimamide, generating light in the process, which in turn stimulates eYFP. Emission is measured at the wavelength of both the donor and the acceptor, and the ratio

of the two emissions is proportional to the interaction between the two chromophores (Machleidt et al., 2015). Although HTRF-based techniques also exist for the measurement of β -arrestin-2 recruitment, BRET-based assays have been successfully utilised in our lab to examine a range of GPCRs, FFA2 among them (Marsango et al., 2022b, Hudson et al., 2012a, Sergeev et al., 2016).

While for WB and ICC, stably transfected Flp-In T-REx 293 cells were preferred, for BRET assays transiently transfected HEK293T cells were utilised. Although the fact that individual transfections are required for each experiment increases variability due to human error, it also allows for more conditions to be explored. Specifically, PD mutants of FFA2 with 4 or 6 mutated residues (termed “double-site” and “triple-site” PD mutants, respectively) could be utilised while avoiding the fairly lengthy process of generating stably transfected cell lines. These mutants could potentially provide a more comprehensive view of the contribution of phosphorylation at each cluster of residues to β -arrestin-2 recruitment.

Apart from its particular usefulness in BRET-based assays, the eYFP tag should conceptually produce identical results to HA-tagged receptors in both WB and ICC experiments. Exploring cell lines expressing hFFA2-HA and hFFA2-DREADD-HA in these assays is essential in order to be able to translate the results into cells and tissues derived from transgenic mice. In **Chapter 3**, neutrophils were shown by ICC to express HA-tagged receptors, and in **Chapter 4** these receptors were shown to be functional *ex vivo*. The ligand-dependent phosphorylation of hFFA2-HA and hFFA2-DREADD-HA in mouse-derived neutrophils was therefore explored with the use of ICC, following initial experiments in overexpressing cell lines.

The initial aim of this chapter was to validate the novel putative phosphosite-specific antisera for FFA2 through WB and ICC, utilising available antagonists and newly generated mutants of the receptors. In the light of the results, the contribution of specific sets of residues to β -arrestin-2 recruitment was investigated, using additional PD mutants. Finally, the *ex vivo* application of the phosphosite-specific antisera was explored in mouse-derived neutrophils, thus demonstrating hFFA2 and hFFA2-DREADD phosphorylation in primary cells.

5.2 Results

5.2.1 Evaluation of phosphosite-specific antisera for FFA2

For the initial evaluation of phosphosite-specific antisera, a series of WB experiments were performed. To this end, cells were treated with vehicle or an agonist for 5min. This treatment time was selected based on predicted timeframes for receptor phosphorylation using similar antisera (Butcher et al., 2014). Using EC₉₀ concentrations of the agonists (as determined by [³⁵S]GTPγS) ensured that the proportion of activated receptors would be sufficient for detection by the antisera. Following treatment, the eYFP-tag on the receptor constructs was targeted with an anti-GFP agarose trap for immunoprecipitation. Samples were then eluted, run on SDS-PAGE gels, and subsequently transferred to nitrocellulose membranes. Membranes were incubated with either one of the putative phosphosite-specific antisera, or with an anti-GFP control antibody. Fluorescent secondary antibodies were then used to visualise bound primary antisera.

As the antisera were generated using a segment of hFFA2 as the epitope, they were first tested using cells expressing hFFA2-eYFP (*Figure 5.2*). Polypeptides in Flp-In T-REx 293 parental cells were not detected by any of the antisera utilised. After DOX induction of Flp-In T-REx 293 cell harbouring hFFA2-eYFP, the anti-GFP antibody detected various polypeptides in the absence and presence of C3, showing similar fluorescence intensity. In addition to polypeptides between the 50kDa and 70kDa markers (corresponding potentially to the 64kDa expected size for hFFA2-eYFP; black arrow) several additional polypeptides were visible at lower (~30kDa) and higher (~125kDa and ~250kDa) molecular sizes (grey arrows). The anti-pSer²⁹⁶/pSer²⁹⁷ antiserum was found to identify these polypeptides regardless of agonist pre-activation. On the other hand, anti-pThr³⁰⁶/pThr³¹⁰ showed increased binding in C3-treated samples. In both cases, a distinct polypeptide was detected at the anticipated size of hFFA2-eYFP, along with polypeptides with a range of apparently higher molecular masses. Only negligible binding by anti-pSer³²⁴/pSer³²⁵ was observed.

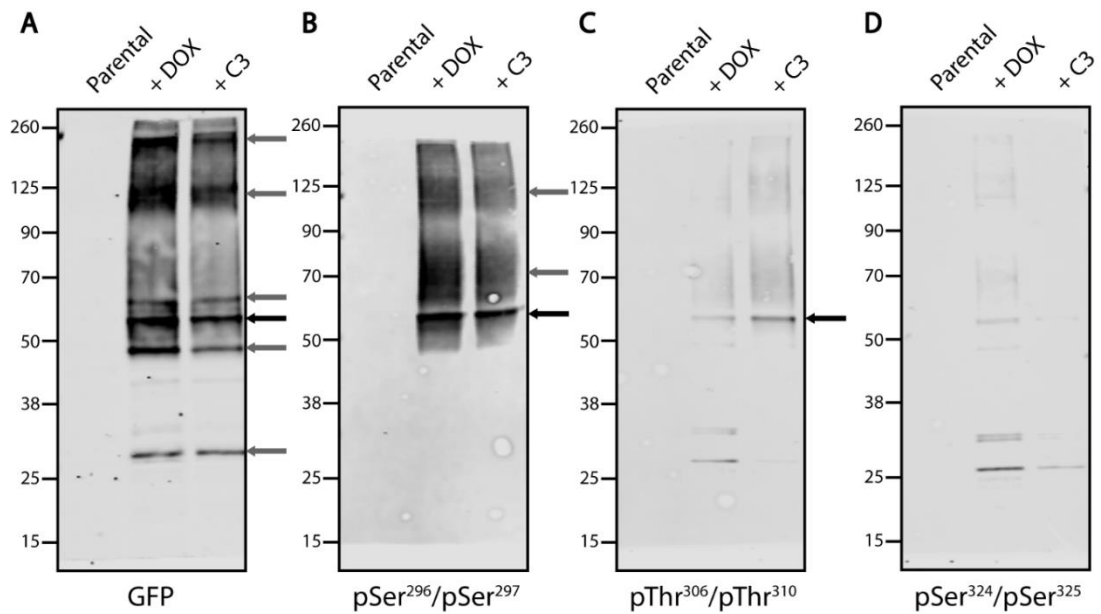


Figure 5.2. Western Blot analysis of hFFA2-eYFP phosphorylation. Serum-starved Flp-In T-REx 293 parental or hFFA2-eYFP-expressing cells were treated with vehicle (+DOX) or 2mM propionate (C3) for 5min prior to lysate preparation in the presence of protease and phosphatase inhibitors. Lysates were immunoprecipitated with GFP-trap agarose and run on NuPAGE 4-12% Bis-Tris SDS-PAGE gels. Proteins were subsequently transferred to nitrocellulose membranes, blocked with TBS supplemented with 5% (w/v) BSA and incubated overnight with A) goat anti-GFP primary antibody (1:10,000), B) rabbit anti-FFA2-pSer²⁹⁶/pSer²⁹⁷ (1:2,000), C) rabbit anti-FFA2-pThr³⁰⁶/pThr³¹⁰ (1:2,000) or D) rabbit anti-FFA2-pSer³²⁴/pSer³²⁵ (1:1,000) antiserum. Membranes were finally incubated with donkey anti-goat IRDye 800CW (1:10,000) or donkey anti-rabbit IRDye 800CW (1:10,000) secondary antibodies, and visualised using the LI-COR Odyssey 9260 gel imaging system. Black arrows represent the expected size of hFFA2-eYFP; grey arrows represent polypeptides detected at other molecular masses. Representative of 3 blots (n=3). GFP - green fluorescent protein.

Although there are considerable differences between the sequences of hFFA2 and mFFA2, the individual residues targeted by the phosphosite-specific antisera are preserved in both species. In order to test the species orthologue-specificity of the antisera, they were employed in an attempt to detect mFFA2-eYFP (Figure 5.3). While eYFP was detected in both vehicle- and C3-treated samples, none of the phosphosite-specific antisera were able to bind the samples.

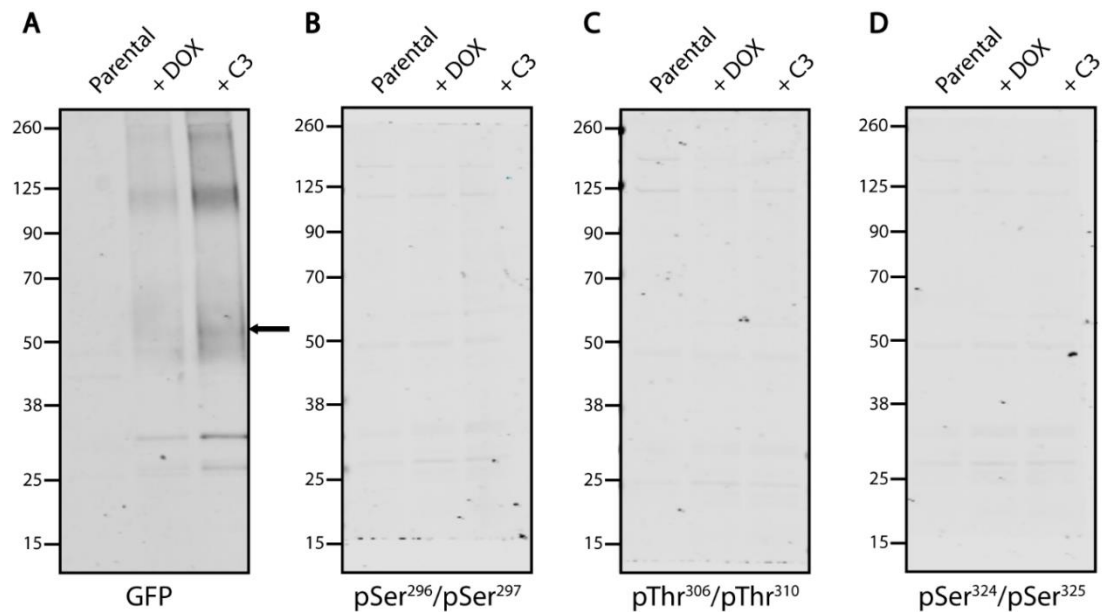


Figure 5.3. Western Blot analysis of mFFA2-eYFP phosphorylation. Serum-starved Flp-In T-REx 293 parental or mFFA2-eYFP-expressing cells were treated with vehicle (+DOX) or 2mM propionate (C3) for 5min prior to lysate preparation in the presence of protease and phosphatase inhibitors. Lysates were immunoprecipitated with GFP-trap agarose and run on NuPAGE 4-12% Bis-Tris SDS-PAGE gels. Proteins were subsequently transferred to nitrocellulose membranes, blocked with TBS supplemented with 5% (w/v) BSA and incubated overnight with A) goat anti-GFP primary antibody (1:10,000), B) rabbit anti-FFA2-pSer²⁹⁶/pSer²⁹⁷ (1:1,000), C) rabbit anti-FFA2-pThr³⁰⁶/pThr³¹⁰ (1:1,000) or D) rabbit anti-FFA2-pSer³²⁴/pSer³²⁵ (1:1,000) antiserum. Membranes were finally incubated with donkey anti-goat IRDye 800CW (1:10,000) or donkey anti-rabbit IRDye 800CW (1:10,000) secondary antibodies, and visualised using the LI-COR Odyssey 9260 gel imaging system. Black arrow represents the expected size of mFFA2-eYFP. Representative of 3 blots (n=3). GFP - green fluorescent protein.

Next, hFFA2-DREADD-eYFP was investigated as its intracellular sequences are identical to that of hFFA2-eYFP (Figure 5.4). As was the case with hFFA2-eYFP, Flp-In T-REx 293 parental cells were not detected by any of the antisera. An immediate observation was that the hFFA2-DREADD-eYFP construct was detected effectively by the anti-GFP antiserum, at similar levels in vehicle- and SA-treated samples. Although polypeptides of various apparent molecular masses were observed, a predominant species of some 75-80kDa was observed (grey arrows), despite the expected size of hFFA2-DREADD-eYFP being 64kDa (black arrows). Also similar to hFFA2-eYFP was the inability of anti-pSer³²⁴/pSer³²⁵ to bind the samples. However, in contrast to hFFA2-eYFP, hFFA2-DREADD-eYFP displayed a strong agonist-dependent response when using both the pSer²⁹⁶/pSer²⁹⁷ and pThr³⁰⁶/pThr³¹⁰ antisera, again with the predominant species being the 75-80kDa form. These results were consistent with the hypothesis that Ser²⁹⁶ and/or Ser²⁹⁷ and Thr³⁰⁶ and/or Thr³¹⁰ became phosphorylated in an agonist-dependent manner. As the anti-pSer³²⁴/pSer³²⁵ antiserum failed to detect signals in any of the cell lines, it was not utilised in further experiments.

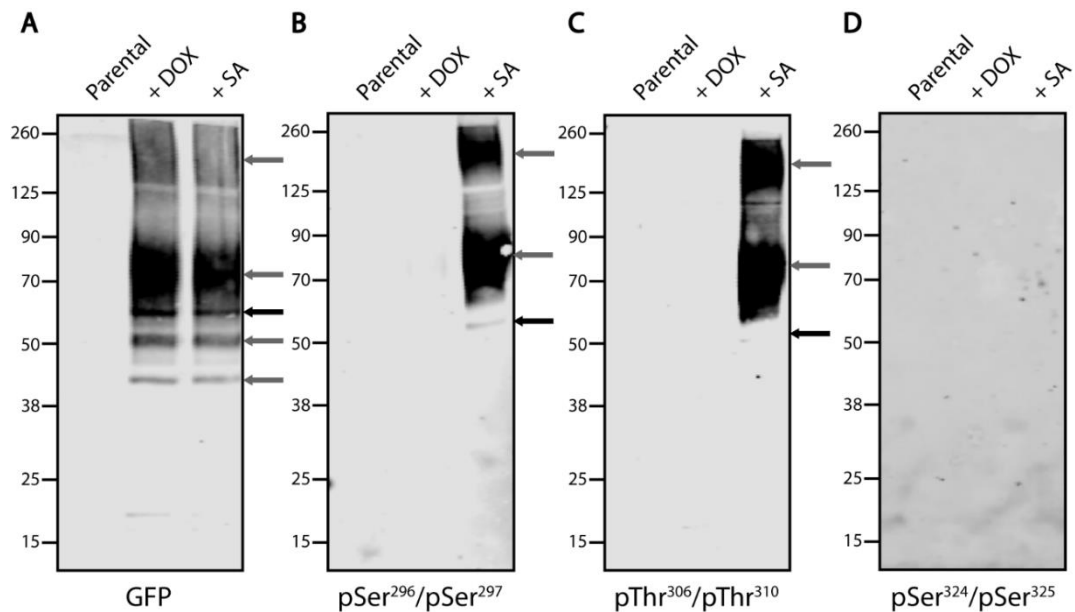


Figure 5.4. Western Blot analysis of hFFA2-DREADD-eYFP phosphorylation. Serum-starved Flp-In T-REx 293 parental or hFFA2-DREADD-eYFP-expressing cells were treated with vehicle (+DOX) or 1.7mM sorbic acid (SA) for 5min prior to lysate preparation in the presence of protease and phosphatase inhibitors. Lysates were immunoprecipitated with GFP-trap agarose and run on NuPAGE 4-12% Bis-Tris SDS-PAGE gels. Proteins were subsequently transferred to nitrocellulose membranes, blocked with TBS supplemented with 5% (w/v) BSA and incubated overnight with A) goat anti-GFP primary antibody (1:10,000), B) rabbit anti-FFA2-pSer²⁹⁶/pSer²⁹⁷ (1:2,000), C) rabbit anti-FFA2-pThr³⁰⁶/pThr³¹⁰ (1:2,000) or D) rabbit anti-FFA2-pSer³²⁴/pSer³²⁵ (1:1,000) antiserum. Membranes were finally incubated with donkey anti-goat IRDye 800CW (1:10,000) or donkey anti-rabbit IRDye 800CW (1:10,000) secondary antibodies, and visualised using the LI-COR Odyssey 9260 gel imaging system. Black arrows represent the expected size of hFFA2-DREADD-eYFP; grey arrows represent polypeptides detected at other molecular masses. Representative of 3 blots (n=3). GFP - green fluorescent protein.

In order to assess whether the purported phosphosite-specific antisera did, in fact, bind phosphorylated residues, the enzyme λ PP was employed. This enzyme catalyses the removal of phosphate groups from phosphorylated amino acids, thus allowing to test whether antiserum binding was eliminated by the absence of phosphorylated residues. In hFFA2-eYFP (*Figure 5.5*), treatment with λ PP abolished both agonist-independent recognition by the purported pSer²⁹⁶/pSer²⁹⁷ and the C3-dependent response of the pThr³⁰⁶/pThr³¹⁰ antisera. Responses in the absence of λ PP corresponded to earlier experiments with C3. This was consistent with recognition of the receptor construct by both antisera, indeed reflecting phosphorylation of potentially these specific residues. Although *Figure 5.5A* displays higher intensity for DOX+ λ PP in the GFP blot, this does not coincide with increased fluorescence intensity in the additional blots, and therefore it was inconsequential.

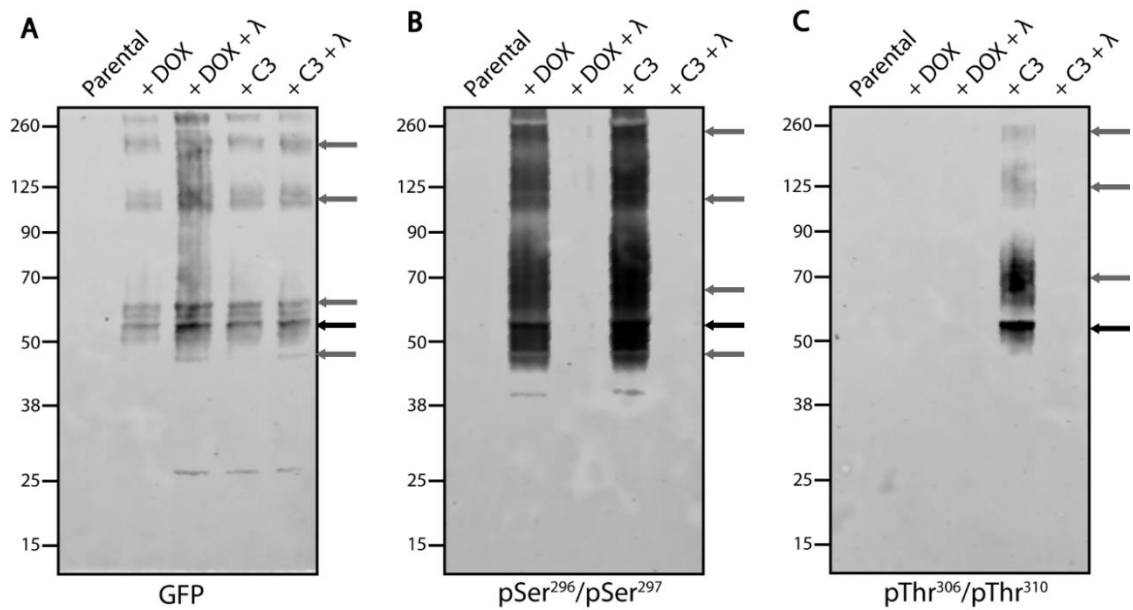


Figure 5.5. Western Blot analysis of hFFA2-eYFP phosphorylation in the presence of λ -protein phosphatase. Serum-starved Flp-In T-REx 293 parental or hFFA2-eYFP-expressing cells were treated with vehicle (+DOX) or 2mM propionate (C3) for 5min prior to lysate preparation in the presence of protease inhibitor. Lysates were treated with λ -protein phosphatase (λ) for 90min at 30°C, immunoprecipitated with GFP-trap agarose and run on NuPAGE 4-12% Bis-Tris SDS-PAGE gels. Proteins were subsequently transferred to nitrocellulose membranes, blocked with TBS supplemented with 5% (w/v) BSA and incubated overnight with A) goat anti-GFP primary antibody (1:10,000), B) rabbit anti-FFA2-pSer²⁹⁶/pSer²⁹⁷ (1:2,000) or C) rabbit anti-FFA2-pThr³⁰⁶/pThr³¹⁰ (1:2,000) antiserum. Membranes were finally incubated with donkey anti-goat IRDye 800CW (1:10,000) or donkey anti-rabbit IRDye 800CW (1:10,000) secondary antibodies, and visualised using the LI-COR Odyssey 9260 gel imaging system. Black arrows represent the expected size of hFFA2-eYFP; grey arrows represent polypeptides detected at other molecular masses. Representative of 2 blots (n=2). GFP - green fluorescent protein.

To further evaluate the agonist-dependent nature of the response in hFFA2-eYFP, the antagonist CATPB was utilised alongside agonists (*Figure 5.6*). In the case of pSer²⁹⁶/pSer²⁹⁷, no inhibition by CATPB was observed. Although there appeared to be some variation in intensities, these corresponded to slight differences in GFP levels. At residues Thr³⁰⁶/Thr³¹⁰, however, the response induced by C3 was blocked fully by CATPB. This could suggest that while the agonist-independent phosphorylation at Ser²⁹⁶/Ser²⁹⁷ was not amenable to CATPB treatment, the agonist-dependent phosphorylation at Thr³⁰⁶/Thr³¹⁰ was.

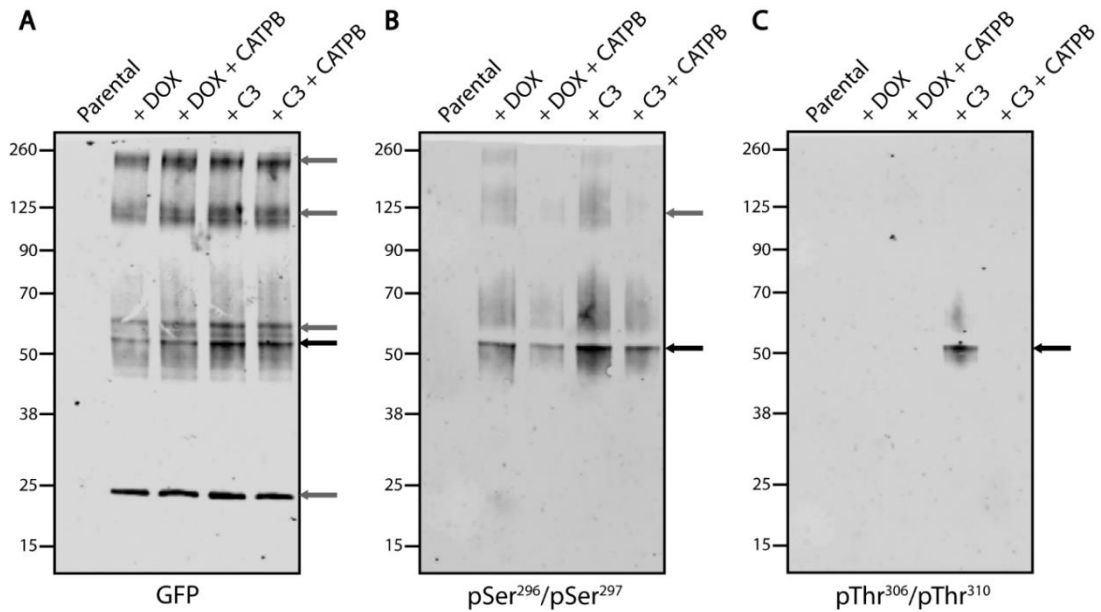


Figure 5.6. Western Blot analysis of CATPB effect on hFFA2-eYFP phosphorylation. Serum-starved Flp-In T-REx 293 parental or hFFA2-eYFP-expressing cells were pre-incubated with $3\mu\text{M}$ CATPB for 15min, then treated with vehicle (+DOX) or 2mM propionate (C3) for 5min prior to lysate preparation in the presence of protease and phosphatase inhibitors. Lysates were immunoprecipitated with GFP-trap agarose and run on NuPAGE 4-12% Bis-Tris SDS-PAGE gels. Proteins were subsequently transferred to nitrocellulose membranes, blocked with TBS supplemented with 5% (w/v) BSA and incubated overnight with A) goat anti-GFP primary antibody (1:10,000), B) rabbit anti-FFA2-pSer²⁹⁶/pSer²⁹⁷ (1:2,000) or rabbit C) anti-FFA2-pThr³⁰⁶/pThr³¹⁰ (1:2,000) antiserum. Membranes were finally incubated with donkey anti-goat IRDye 800CW (1:10,000) or donkey anti-rabbit IRDye 800CW (1:10,000) secondary antibodies, and visualised using the LI-COR Odyssey 9260 gel imaging system. Black arrows represent the expected size of hFFA2-eYFP; grey arrows represent polypeptides detected at other molecular masses. Representative of 3 blots (n=3). GFP - green fluorescent protein.

In the case of hFFA2-DREADD-eYFP (*Figure 5.7*), as previously, response at both sites appeared to be agonist-dependent. CATPB was able to inhibit the effect of SA at residues Ser²⁹⁶/Ser²⁹⁷, albeit not completely. At residues Thr³⁰⁶/Thr³¹⁰, however, pre-treatment with CATPB ablated the SA-induced response. Unlike in hFFA2-eYFP, both sites were previously found to be phosphorylated in an agonist-dependent manner (*Figure 5.4*), therefore it is not unexpected that CATPB would inhibit phosphorylation at these sites in the same manner it did at Thr³⁰⁶/Thr³¹⁰ in hFFA2-eYFP (*Figure 5.6*).

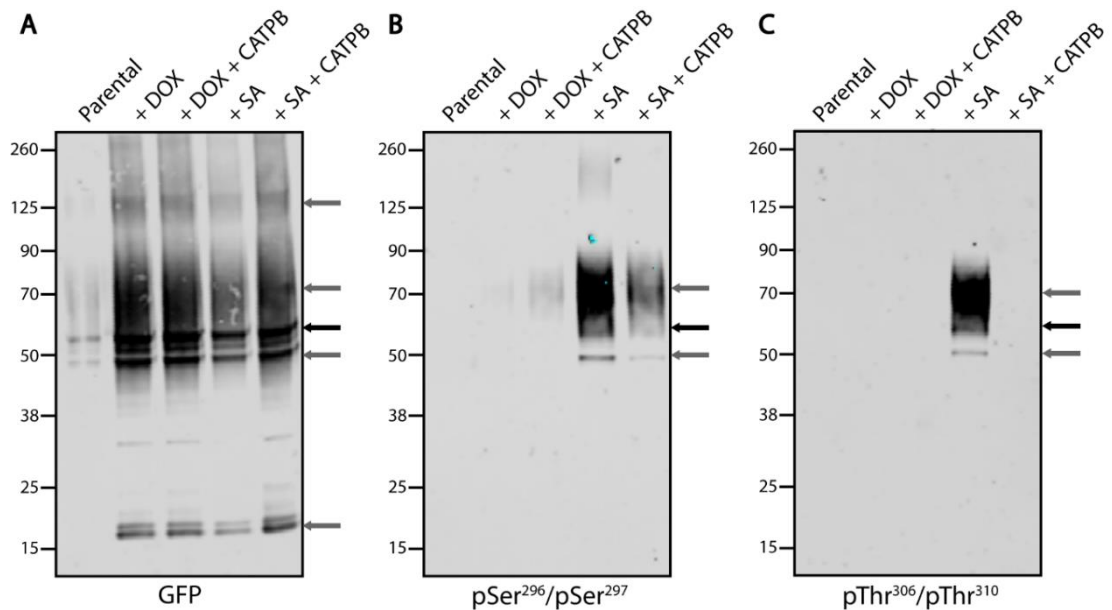


Figure 5.7. Western Blot analysis of CATPB effect on hFFA2-DREADD-eYFP phosphorylation. Serum-starved Flp-In T-REx 293 parental or hFFA2-eYFP-expressing cells were pre-incubated with 3 μ M CATPB for 15min, then treated with vehicle (+DOX) or 1.7mM sorbic acid (SA) for 5min prior to lysate preparation in the presence of protease and phosphatase inhibitors. Lysates were immunoprecipitated with GFP-trap agarose and run on NuPAGE 4-12% Bis-Tris SDS-PAGE gels. Proteins were subsequently transferred to nitrocellulose membranes, blocked with TBS supplemented with 5% (w/v) BSA and incubated overnight with A) goat anti-GFP primary antibody (1:10,000), B) rabbit anti-FFA2-pSer²⁹⁶/pSer²⁹⁷ (1:2,000) or C) rabbit anti-FFA2-pThr³⁰⁶/pThr³¹⁰ (1:2,000) antiserum. Membranes were finally incubated with donkey anti-goat IRDye 800CW (1:10,000) or donkey anti-rabbit IRDye 800CW (1:10,000) secondary antibodies, and visualised using the LI-COR Odyssey 9260 gel imaging system. Black arrows represent the expected size of hFFA2-DREADD-eYFP; grey arrows represent polypeptides detected at other molecular masses. Representative of 2 blots (n=2). GFP - green fluorescent protein.

In order to visualise and further establish the ability of the phosphosite-specific antisera to bind activated receptors, they were tested in a series of ICC experiments. In all cases, Flp-In T-REx 293 cells induced to express eYFP-tagged variants of FFA2 were utilised. For all ICC experiments, agonist treatment was optimised to 2min. This is within the range of predicted timeframes for receptor phosphorylation (Luttrell et al., 2001), and was found to yield better background-to-noise ratio.

Initially, in order to demonstrate non-specific binding patterns, both antisera were employed in Flp-In T-REx 293 parental cells (*Figure 5.8*). In each case, the phosphosite-specific antisera displayed intracellular, DAPI-colocalised binding. As this binding pattern occurred even in the absence of the target receptors, the binding can be regarded as non-specific.

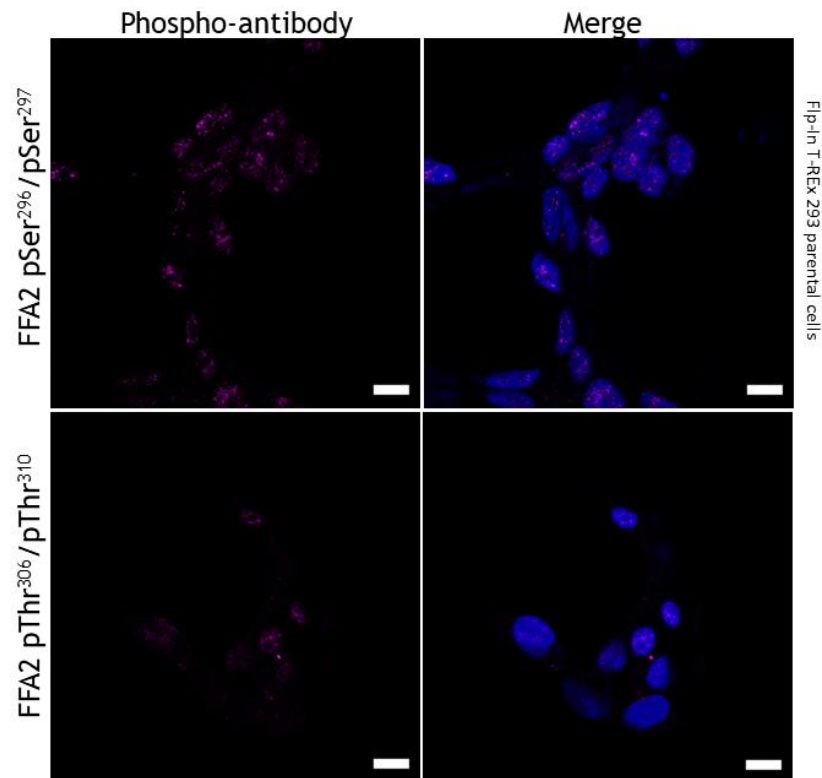


Figure 5.8. Immunocytochemical staining of Flp-In T-REx 293 parental cells. Flp-In T-REx 293 parental cells were treated with 2mM propionate for 2min, then fixed with 4% paraformaldehyde and permeabilised with saponin. Cells were incubated with rabbit anti-FFA2-pSer²⁹⁶/pSer²⁹⁷ or rabbit anti-FFA2-pThr³⁰⁶/pThr³¹⁰ antiserum (1:250) overnight, and with goat anti-rabbit IgG AlexaFluor-546 secondary antibody (1:400; magenta) for 2h. Nuclear DNA was labelled with DAPI (blue). Images were taken with 63× objective of Zeiss 880 Laser Scanning Confocal Microscope. Scale bar represents 10µm. Representative of 3 fields of view each from 3 separate experiments (n=3).

In hFFA2-eYFP cells (*Figure 5.9*), the anti-pSer²⁹⁶/pSer²⁹⁷ antiserum showed strong binding in both vehicle- and C3-treated cells, supporting ligand-independent effects observed in WB. Staining with the antiserum was primarily observed on cell membranes, while eYFP signal was detected in intracellular areas as well. Antiserum staining was colocalised with eYFP on the cell surface in both conditions, and also intracellularly in the C3-treated cells.

Staining with the anti-pThr³⁰⁶/pThr³¹⁰ antiserum (*Figure 5.10*), on the other hand, displayed a C3-dependent response. No discernible signal was detected in vehicle-treated cells, while C3-treated cells displayed strong cell-surface binding, with some intracellular binding present. Again, observations were consistent with the agonist-dependent antibody binding observed in WB.

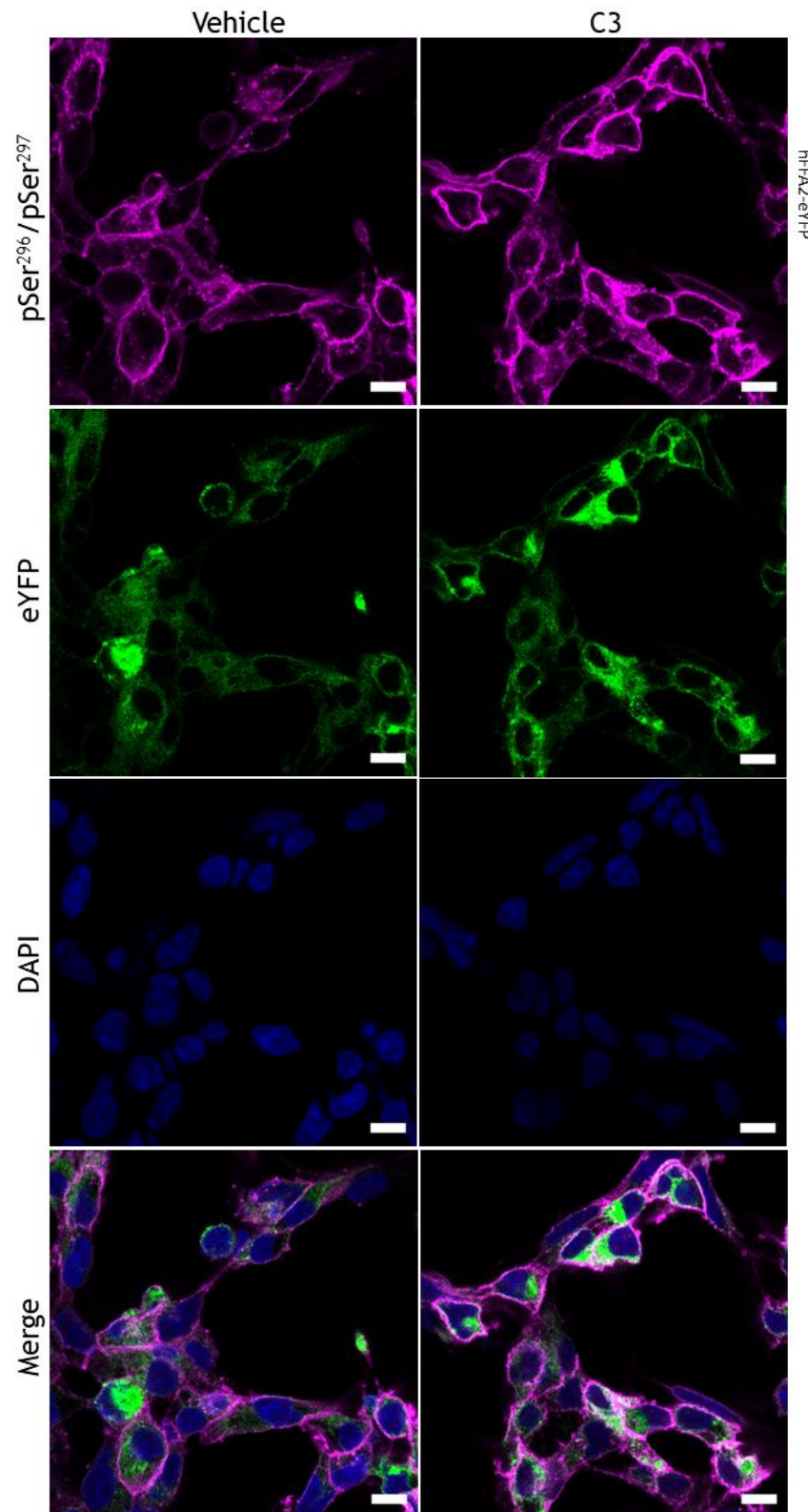


Figure 5.9. Immunocytochemical detection of hFFA2-eYFP phosphorylation in overexpressing cells. Flp-In T-REx 293 cells expressing hFFA2-eYFP were treated with vehicle or 2mM propionate (C3) for 2min, then fixed with 4% paraformaldehyde and permeabilised with saponin. Cells were incubated with rabbit anti-FFA2-pSer²⁹⁶/pSer²⁹⁷ antiserum (1:250) overnight, and with goat anti-rabbit IgG AlexaFluor-546 secondary antibody (1:400; magenta) for 2h. Nuclear DNA was labelled with DAPI (blue). Images were taken with 63× objective of Zeiss 880 Laser Scanning Confocal Microscope. Scale bar represents 10µm. Representative of 3 fields of view each from 3 separate experiments (n=3). eYFP - enhanced yellow fluorescent protein.

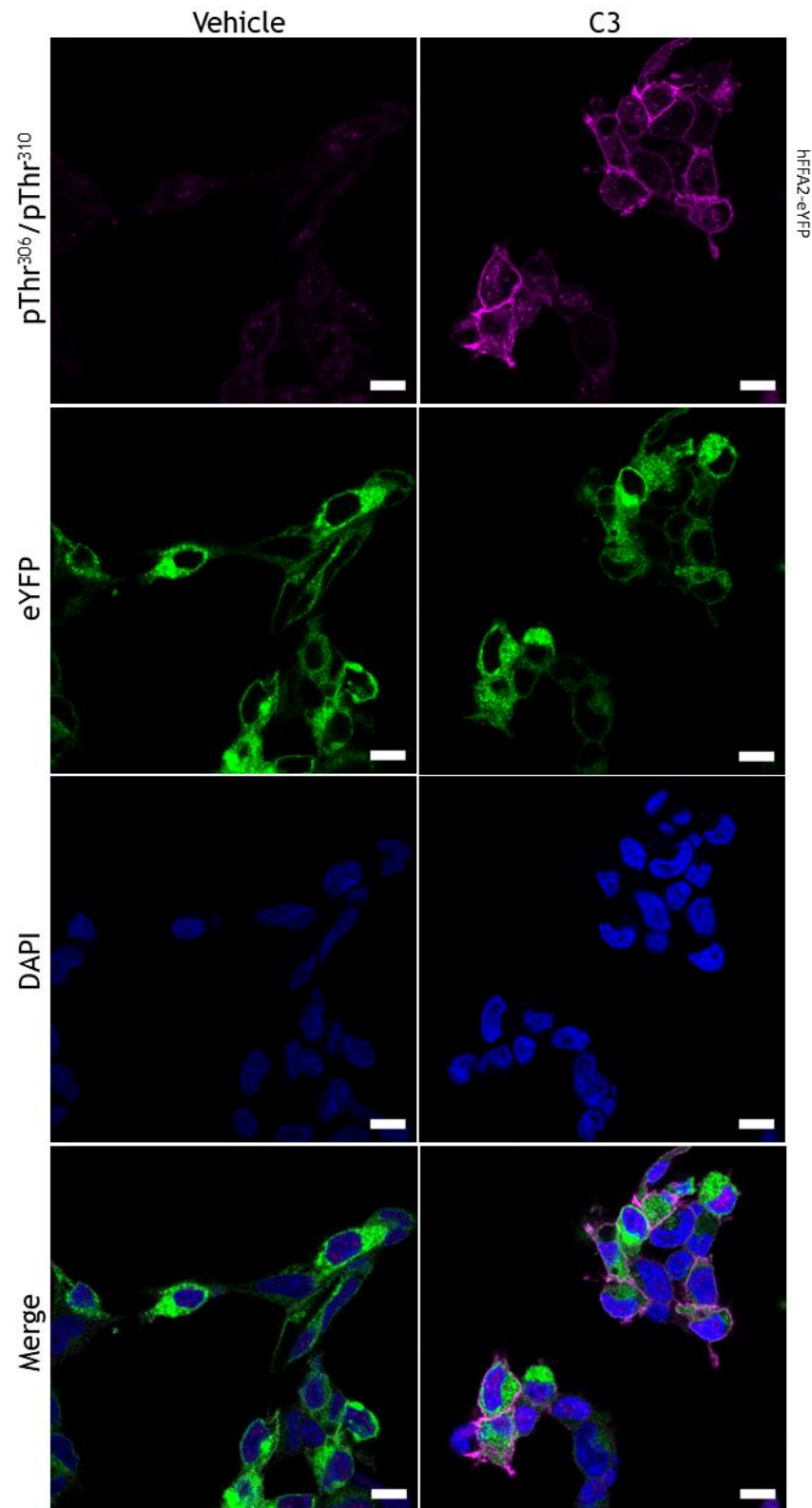


Figure 5.10. Immunocytochemical detection of hFFA2-eYFP phosphorylation in overexpressing cells. Flp-In T-REx 293 cells expressing hFFA2-eYFP were treated with vehicle or 2mM propionate (C3) for 2min, then fixed with 4% paraformaldehyde and permeabilised with saponin. Cells were incubated with rabbit anti-FFA2-pThr³⁰⁶/pThr³¹⁰ antiserum (1:250) overnight, and with goat anti-rabbit IgG AlexaFluor-546 secondary antibody (1:400; magenta) for 2h. Nuclear DNA was labelled with DAPI (blue). Images were taken with 63× objective of Zeiss 880 Laser Scanning Confocal Microscope. Scale bar represents 10µm. Representative of 3 fields of view each from 3 separate experiments (n=3). eYFP - enhanced yellow fluorescent protein.

When investigating the antisera in the hFFA2-DREADD-eYFP mutant, results were distinct from those at the hFFA2-eYFP receptor (*Figure 5.11*). Although a low level of binding by anti-pSer²⁹⁶/pSer²⁹⁷ was observed in the absence of SA, treatment with the agonist produced a discernibly enhanced antiserum binding at the cell surface.

In the case of anti-pThr³⁰⁶/pThr³¹⁰ (*Figure 5.12*), a low level of binding was observed in vehicle-treated cells. The binding was exclusively intracellular and colocalised with DAPI only, therefore it was regarded as non-specific binding. Upon SA-treatment, only a slight increase in intensity was observed, however the binding was now at the cell surface where it colocalised with eYFP. In each case, ICC observations reflected the patterns observed in WBs, describing phosphorylation to be agonist-dependent at both sites on hFFA2-DREADD-eYFP.

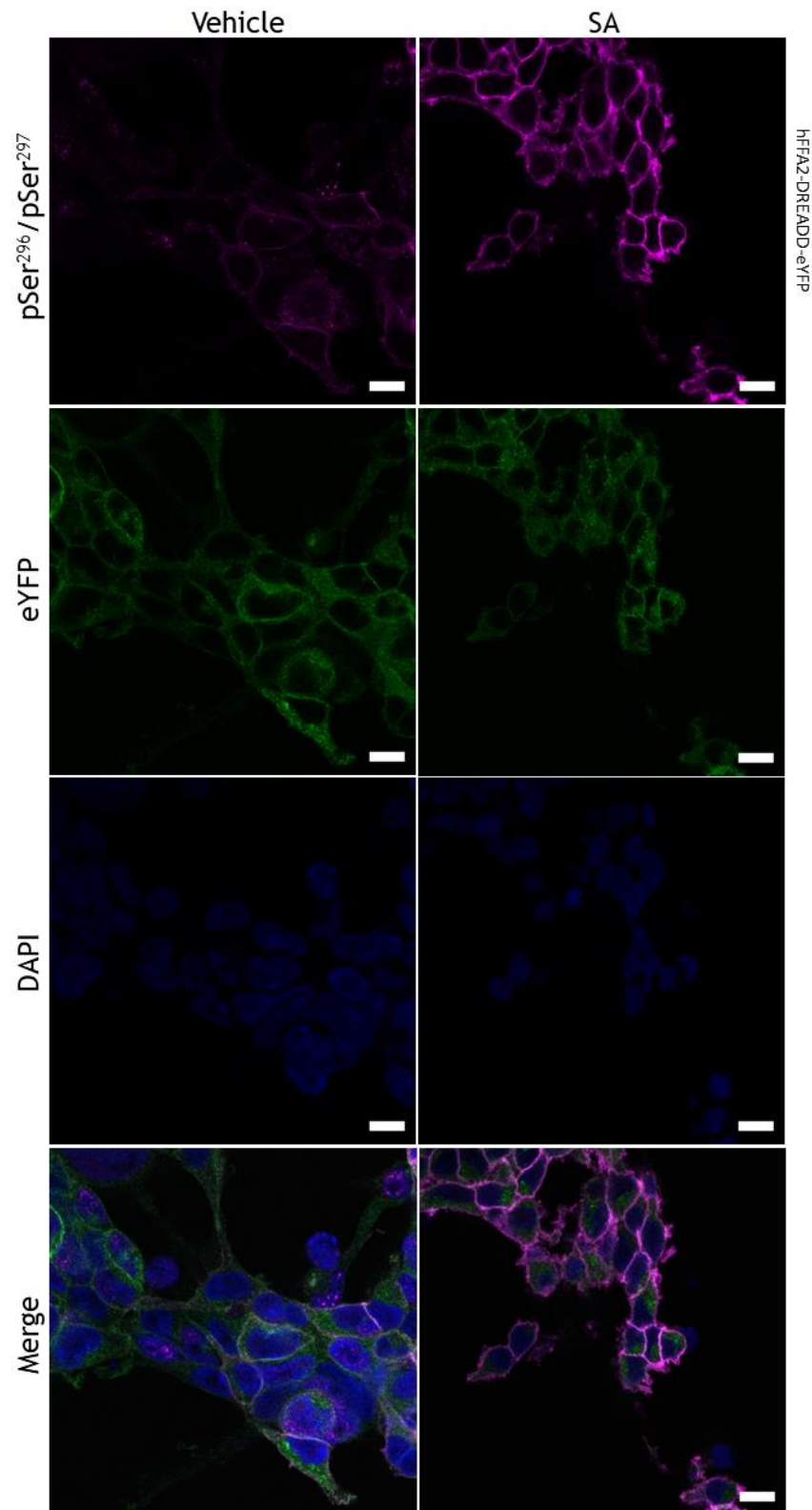


Figure 5.11. Immunocytochemical detection of hFFA2-DREADD-eYFP phosphorylation in overexpressing cells. Flp-In T-Rex 293 cells expressing hFFA2-eYFP were treated with vehicle or 1.7mM sorbic acid (SA) for 2min, then fixed with 4% paraformaldehyde and permeabilised with saponin. Cells were incubated with rabbit anti-FFA2-pSer²⁹⁶/pSer²⁹⁷ antiserum (1:250) overnight, and with goat anti-rabbit IgG AlexaFluor-546 secondary antibody (1:400; magenta) for 2h. Nuclear DNA was labelled with DAPI (blue). Images were taken with 63× objective of Zeiss 880 Laser Scanning Confocal Microscope. Scale bar represents 10µm. Representative of 3 fields of view each from 3 separate experiments (n=3). eYFP - enhanced yellow fluorescent protein.

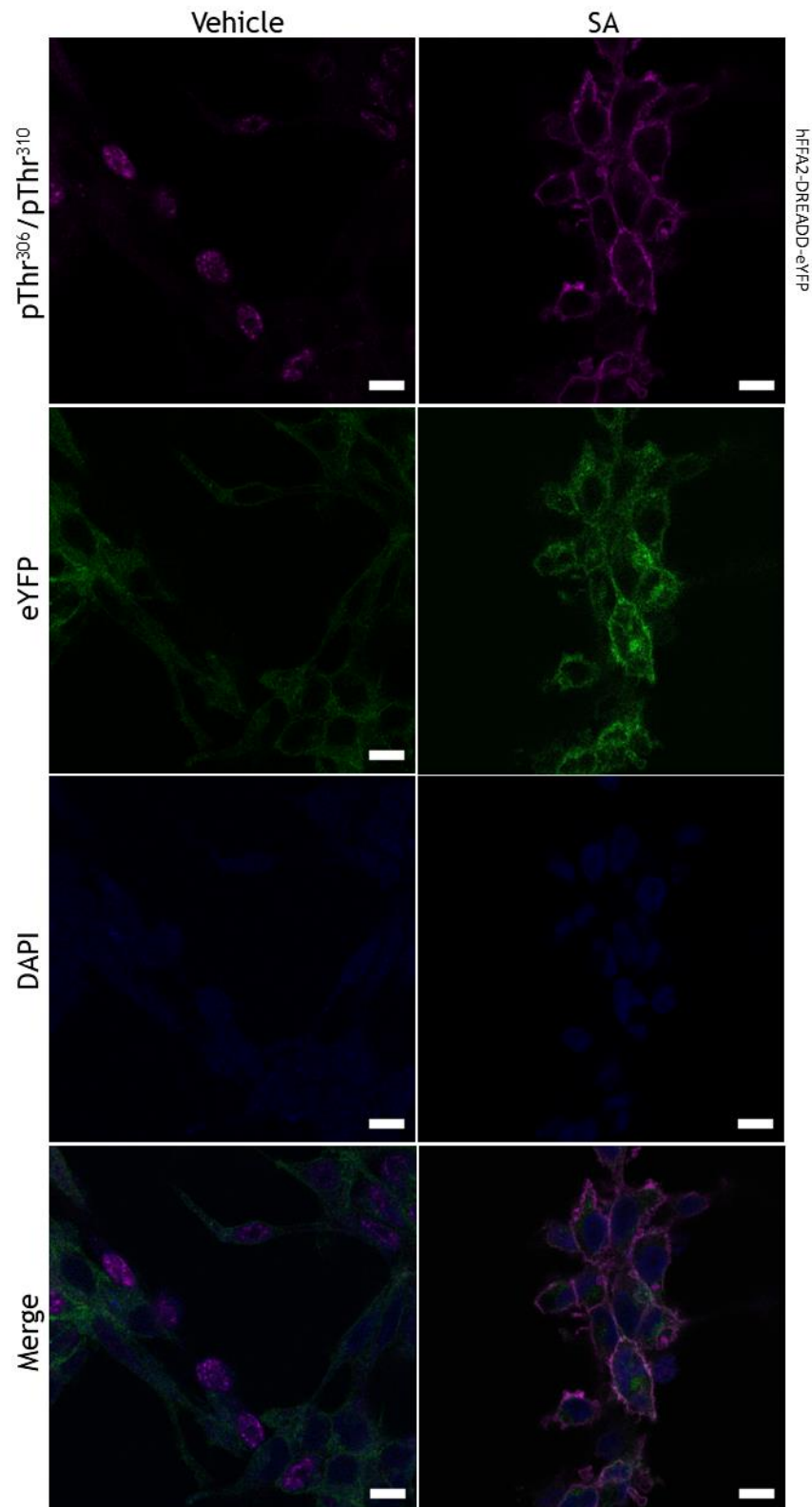


Figure 5.12. Immunocytochemical detection of hFFA2-DREADD-eYFP phosphorylation in overexpressing cells. Flp-In T-REx 293 cells expressing hFFA2-eYFP were treated with vehicle or 1.7mM sorbic acid (SA) for 2min, then fixed with 4% paraformaldehyde and permeabilised with saponin. Cells were incubated with rabbit anti-FFA2-pThr³⁰⁶/pThr³¹⁰ antiserum (1:250) overnight, and with goat anti-rabbit IgG AlexaFluor-546 secondary antibody (1:400; magenta) for 2h. Nuclear DNA was labelled with DAPI (blue). Images were taken with 63× objective of Zeiss 880 Laser Scanning Confocal Microscope. Scale bar represents 10µm. Representative of 3 fields of view each from 3 separate experiments (n=3). eYFP - enhanced yellow fluorescent protein.

As some antisera may display probe-dependency, the antisera which failed to detect phosphorylation of mFFA2-eYFP in WB were also employed in ICC studies (*Figure 5.13 and Figure 5.14*). No specific binding was observed by either of the antisera, as all detected signals were intracellular and colocalised with DAPI only. These results further demonstrated the inability of the antisera to detect phosphorylation of residues on mFFA2-eYFP, corroborating results observed in WBs.

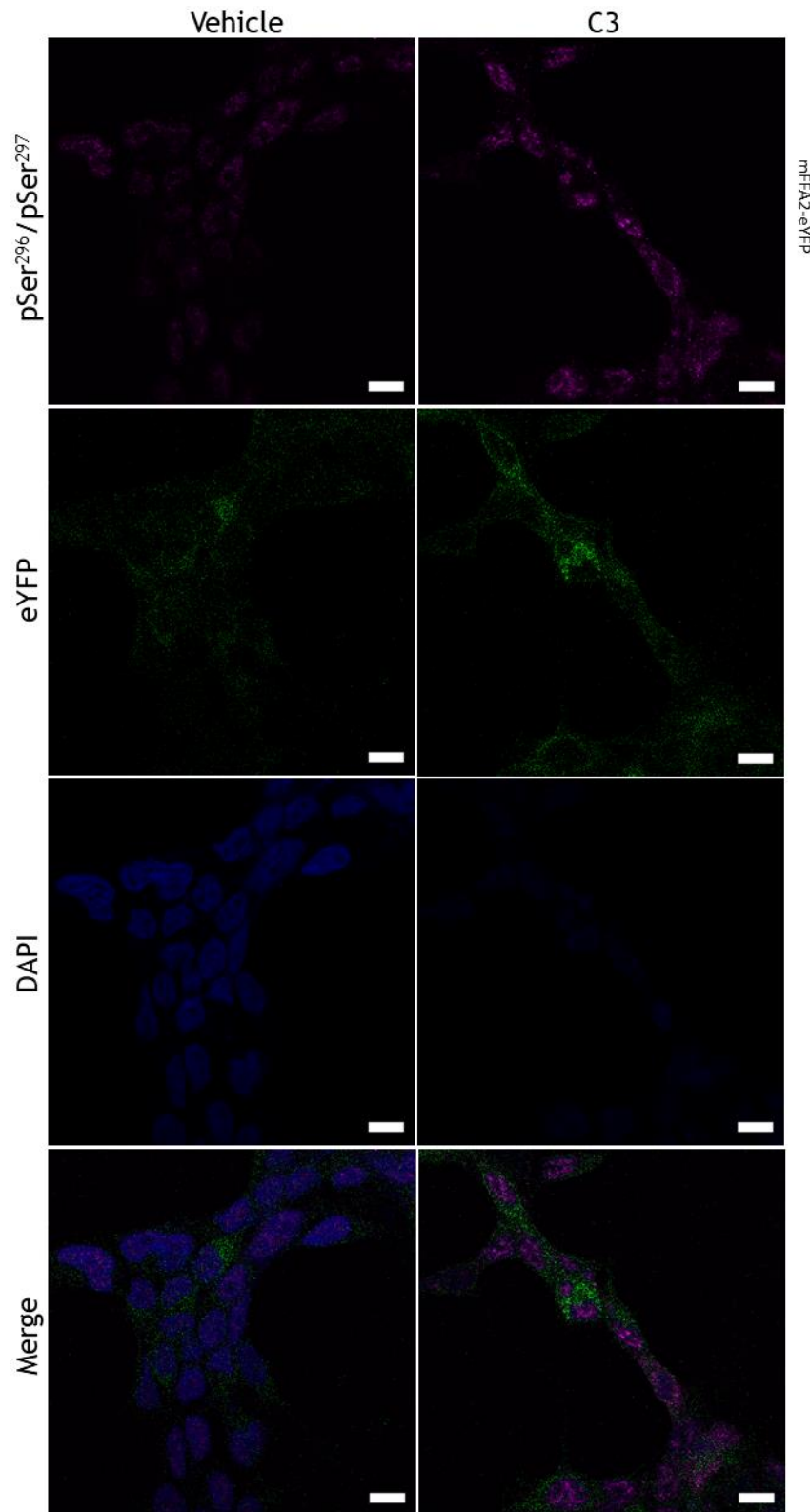


Figure 5.13. Immunocytochemical detection of mFFA2-eYFP phosphorylation in overexpressing cells. Flp-In T-REx 293 cells expressing hFFA2-eYFP were treated with vehicle or 2mM propionate (C3) for 2min, then fixed with 4% paraformaldehyde and permeabilised with saponin. Cells were incubated with rabbit anti-FFA2-pSer²⁹⁶/pSer²⁹⁷ antiserum (1:250) overnight, and with goat anti-rabbit IgG AlexaFluor-546 secondary antibody (1:400; magenta) for 2h. Nuclear DNA was labelled with DAPI (blue). Images were taken with 63× objective of Zeiss 880 Laser Scanning Confocal Microscope. Scale bar represents 10µm. Representative of 3 fields of view each from 3 separate experiments (n=3). eYFP - enhanced yellow fluorescent protein.

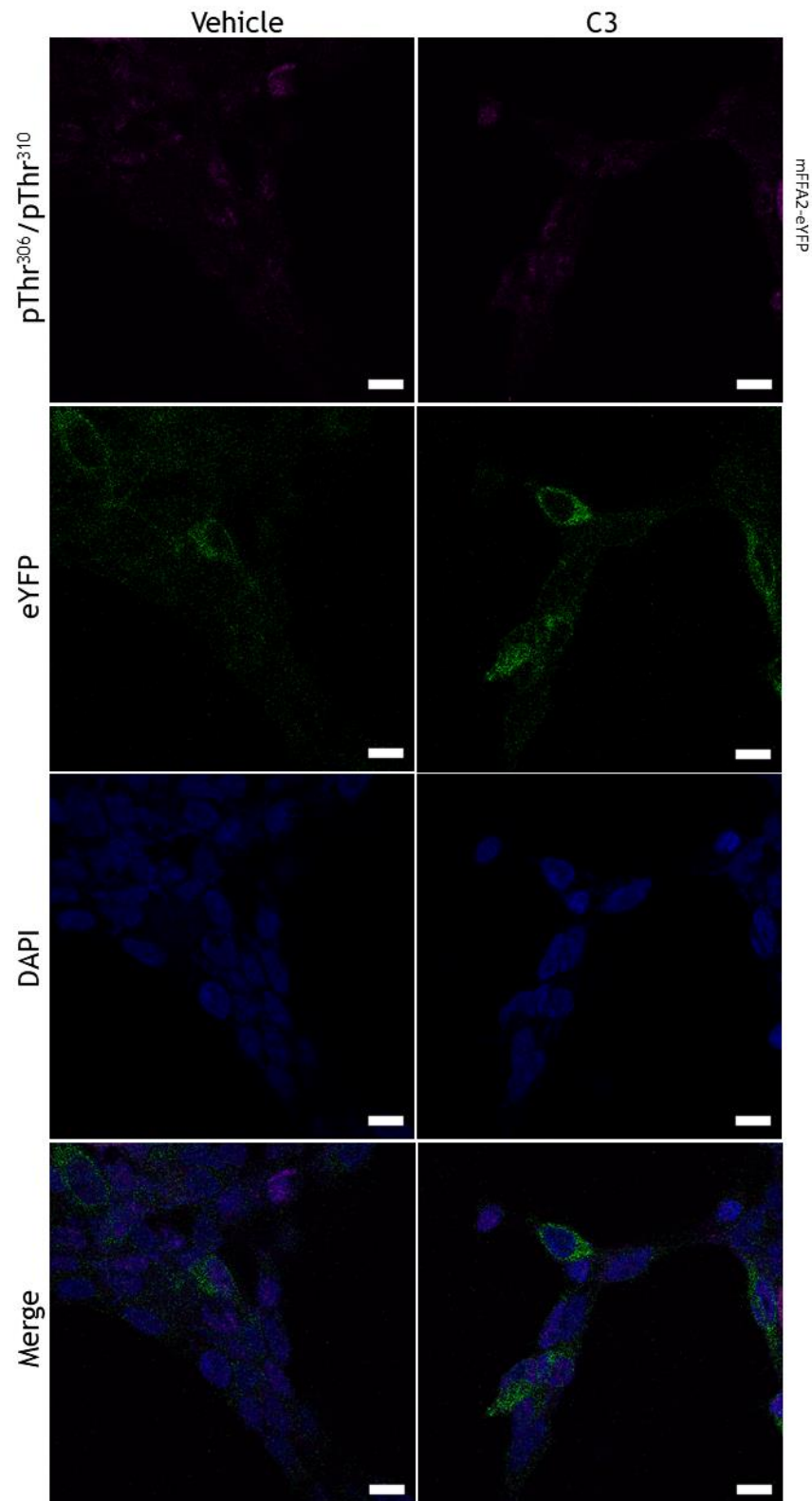


Figure 5.14. Immunocytochemical detection of mFFA2-eYFP phosphorylation in overexpressing cells. Flp-In T-REx 293 cells expressing hFFA2-eYFP were treated with vehicle or 2mM propionate (C3) for 2min, then fixed with 4% paraformaldehyde and permeabilised with saponin. Cells were incubated with rabbit anti-FFA2-pThr³⁰⁶/pThr³¹⁰ antiserum (1:250) overnight, and with goat anti-rabbit IgG AlexaFluor-546 secondary antibody (1:400; magenta) for 2h. Nuclear DNA was labelled with DAPI (blue). Images were taken with 63× objective of Zeiss 880 Laser Scanning Confocal Microscope. Scale bar represents 10µm. Representative of 3 fields of view each from 3 separate experiments (n=3). eYFP - enhanced yellow fluorescent protein.

5.2.2 Characterisation of phosphodeficient mutants of hFFA2

In order to further demonstrate the ability of the phosphosite-specific antisera to bind the phosphorylated residues they were predicted to, a series of PD mutants of hFFA2-eYFP were generated. For each of these, the pairs of residues targeted by the antisera were mutated from Ser or Thr to Ala. Thus, the mutants generated were: hFFA2-Ser²⁹⁶Ala-Ser²⁹⁷Ala-eYFP (hFFA2-PD1), hFFA2-Thr³⁰⁶Ala-Thr³¹⁰Ala-eYFP (hFFA2-PD2) and hFFA2-Ser³²⁴Ala-Ser³²⁵Ala-eYFP (hFFA2-PD3).

In WB experiments (*Figure 5.15*), hFFA2-PD1 and hFFA2-PD2 produced polypeptides detected by an anti-GFP antiserum that were equivalent to hFFA2-WT, suggesting similar expression levels. As evident from the blot with anti-pSer²⁹⁶/pSer²⁹⁷ (*Figure 5.15B*), hFFA2-PD1 lost phosphorylation at this site, while hFFA2-PD2 maintained agonist-independent phosphorylation. In the case of pThr³⁰⁶/pThr³¹⁰, in addition to a loss of detectable signal in the hFFA2-PD2 mutant, phosphorylation was also lost in hFFA2-PD1. Loss of binding by antisera at mutated residues suggests antisera specificity for the phosphorylated residues at those positions. Therefore, the loss of binding by anti-pSer²⁹⁶/pSer²⁹⁷ at hFFA2-PD1 demonstrated the ability of this antiserum to bind pSer²⁹⁶ and/or pSer²⁹⁷. However, the loss of binding by the pThr³⁰⁶/pThr³¹⁰ antiserum at this mutant was unexpected and may suggest issues with antibody specificity or even a phosphorylation hierarchy. These will be discussed further in *Section 5.3*.

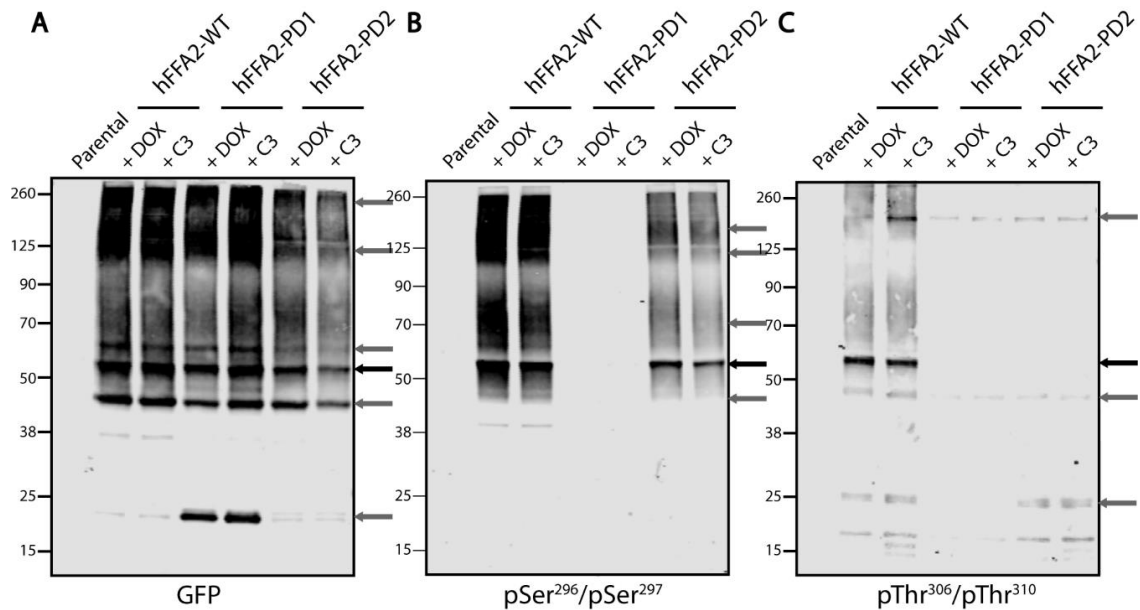


Figure 5.15. Western Blot analysis of phosphorylation in phosphodeficient hFFA2-eYFP mutants. Serum-starved Flp-In T-REx 293 parental cells or cells expressing hFFA2-eYFP (hFFA2-WT), hFFA2-Ser²⁹⁶Ala-Ser²⁹⁷Ala-eYFP (hFFA2-PD1) or hFFA2-Thr³⁰⁶Ala-Thr³¹⁰Ala-eYFP (hFFA2-PD2) were treated with vehicle (+DOX) or 2mM propionate (C3) for 5min prior to lysate preparation in the presence of protease and phosphatase inhibitors. Lysates were immunoprecipitated with GFP-trap agarose and run on NuPAGE 4-12% Bis-Tris SDS-PAGE gels. Proteins were subsequently transferred to nitrocellulose membranes, blocked with TBS supplemented with 5% (w/v) BSA and incubated overnight with A) goat anti-GFP primary antibody (1:10,000), B) rabbit anti-FFA2-pSer²⁹⁶/pSer²⁹⁷ (1:2,000) or C) rabbit anti-FFA2-pThr³⁰⁶/pThr³¹⁰ (1:2,000) antiserum. Membranes were finally incubated with donkey anti-goat IRDye 800CW (1:10,000) or donkey anti-rabbit IRDye 800CW (1:10,000) secondary antibodies, and visualised using the LI-COR Odyssey 9260 gel imaging system. Black arrows represent the expected size of hFFA2-eYFP; grey arrows represent polypeptides detected at other molecular masses. Representative of 2 blots (n=2). GFP - green fluorescent protein.

Next, ICC staining was employed to corroborate the above findings in PD mutants of hFFA2-eYFP. In hFFA2-PD1-expressing cells (*Figure 5.16 and Figure 5.17*), the anti-pSer²⁹⁶/pSer²⁹⁷ antiserum was unable to bind specifically in either of the treatment conditions. Although anti-pThr³⁰⁶/pThr³¹⁰ was found to produce a stronger signal in C3-treated cells, all of the binding was, as with anti-pSer²⁹⁶/pSer²⁹⁷, intracellular and non-specific. These results were consistent with those found in WBs, showing loss of recognition by both antisera, as a result of loss of phosphorylation at mutated residues.

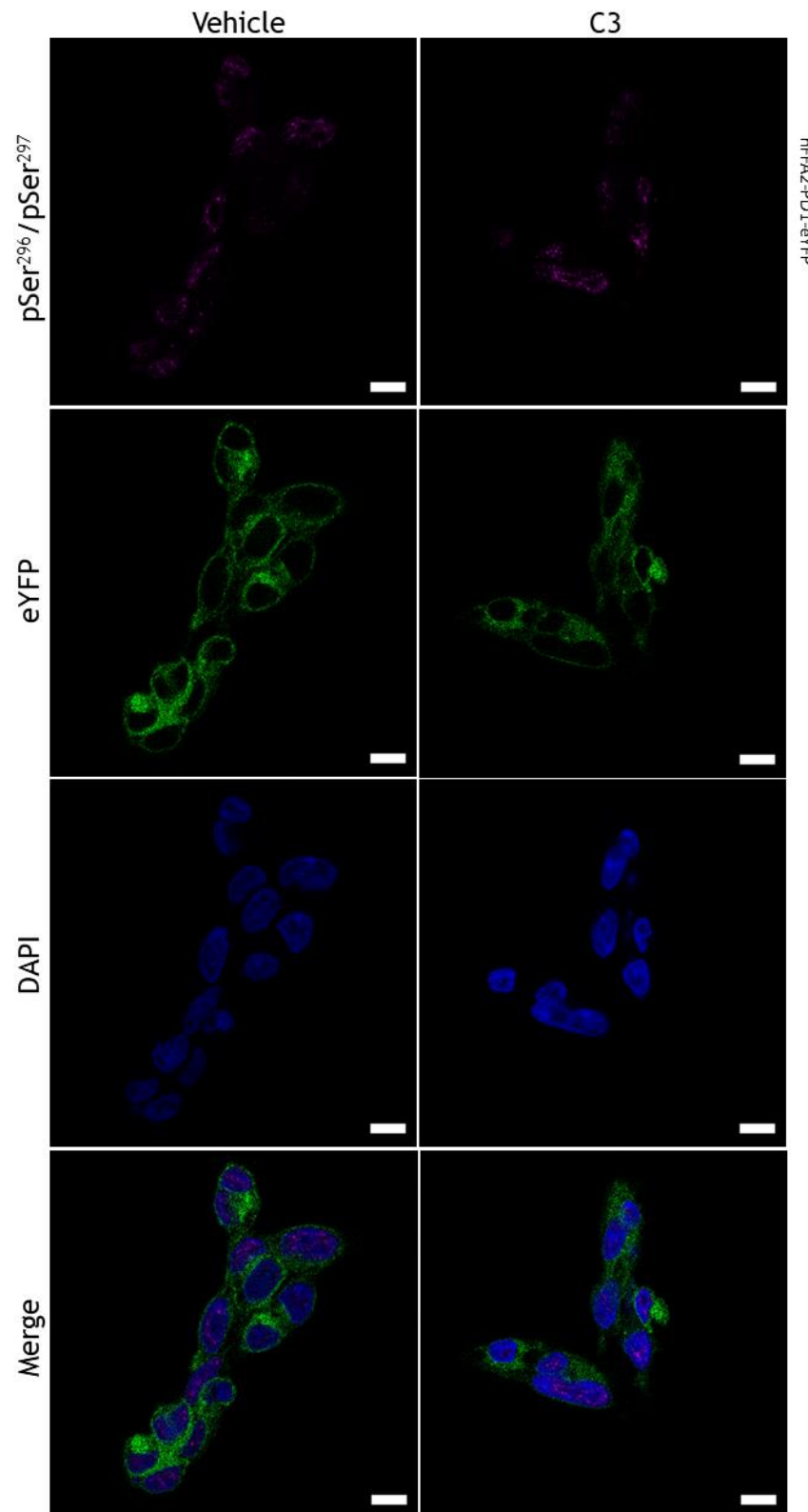


Figure 5.16. Immunocytochemical detection of hFFA2-PD1 phosphorylation in overexpressing cells. Flp-In T-REx 293 cells expressing hFFA2-Ser²⁹⁶Ala-Ser²⁹⁷Ala-eYFP (hFFA2-PD1) were treated with vehicle or 2mM propionate (C3) for 2min, then fixed with 4% paraformaldehyde and permeabilised with saponin. Cells were incubated with rabbit anti-FFA2-pSer²⁹⁶/pSer²⁹⁷ antiserum (1:250) overnight, and with goat anti-rabbit IgG AlexaFluor-546 secondary antibody (1:400; magenta) for 2h. Nuclear DNA was labelled with DAPI (blue). Images were taken with 63× objective of Zeiss 880 Laser Scanning Confocal Microscope. Scale bar represents 10µm. Representative of 3 fields of view each from 3 separate experiments (n=3). eYFP - enhanced yellow fluorescent protein.

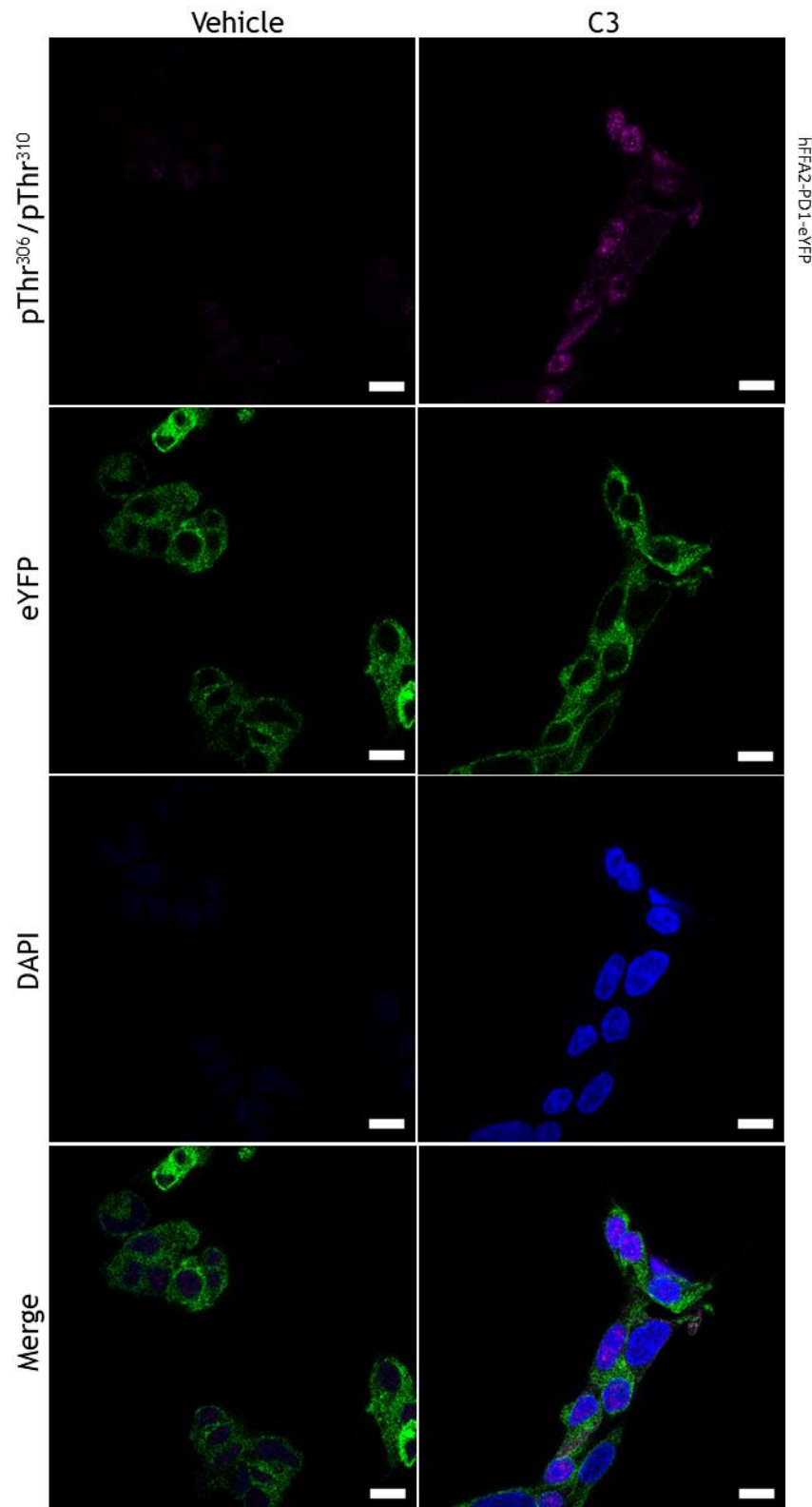


Figure 5.17. Immunocytochemical detection of hFFA2-PD1 phosphorylation in overexpressing cells. Flp-In T-REx 293 cells expressing hFFA2-Ser²⁹⁶Ala-Ser²⁹⁷Ala-eYFP (hFFA2-PD1) were treated with vehicle or 2mM propionate (C3) for 2min, then fixed with 4% paraformaldehyde and permeabilised with saponin. Cells were incubated with rabbit anti-FFA2-pThr³⁰⁶/pThr³¹⁰ antiserum (1:250) overnight, and with goat anti-rabbit IgG AlexaFluor-546 secondary antibody (1:400; magenta) for 2h. Nuclear DNA was labelled with DAPI (blue). Images were taken with 63× objective of Zeiss 880 Laser Scanning Confocal Microscope. Scale bar represents 10µm. Representative of 3 fields of view each from 3 separate experiments (n=3). eYFP - enhanced yellow fluorescent protein.

In hFFA2-PD2-expressing cells (*Figure 5.18 and Figure 5.19*), anti-pSer²⁹⁶/pSer²⁹⁷ displayed strong, specific, ligand-independent binding. The antiserum appeared to colocalise with eYFP both on the cell membrane and intracellularly. This mutation, however, ablated the binding of anti-pThr³⁰⁶/pThr³¹⁰ to C3-treated cells (while maintaining high non-specific binding), similar to observations in WB experiments. Thus, phosphorylation of Thr³⁰⁶ and/or Thr³¹⁰ was shown to be a prerequisite for the binding of anti-pThr³⁰⁶/pThr³¹⁰, but not for the binding of anti-pSer²⁹⁶/pSer²⁹⁷.

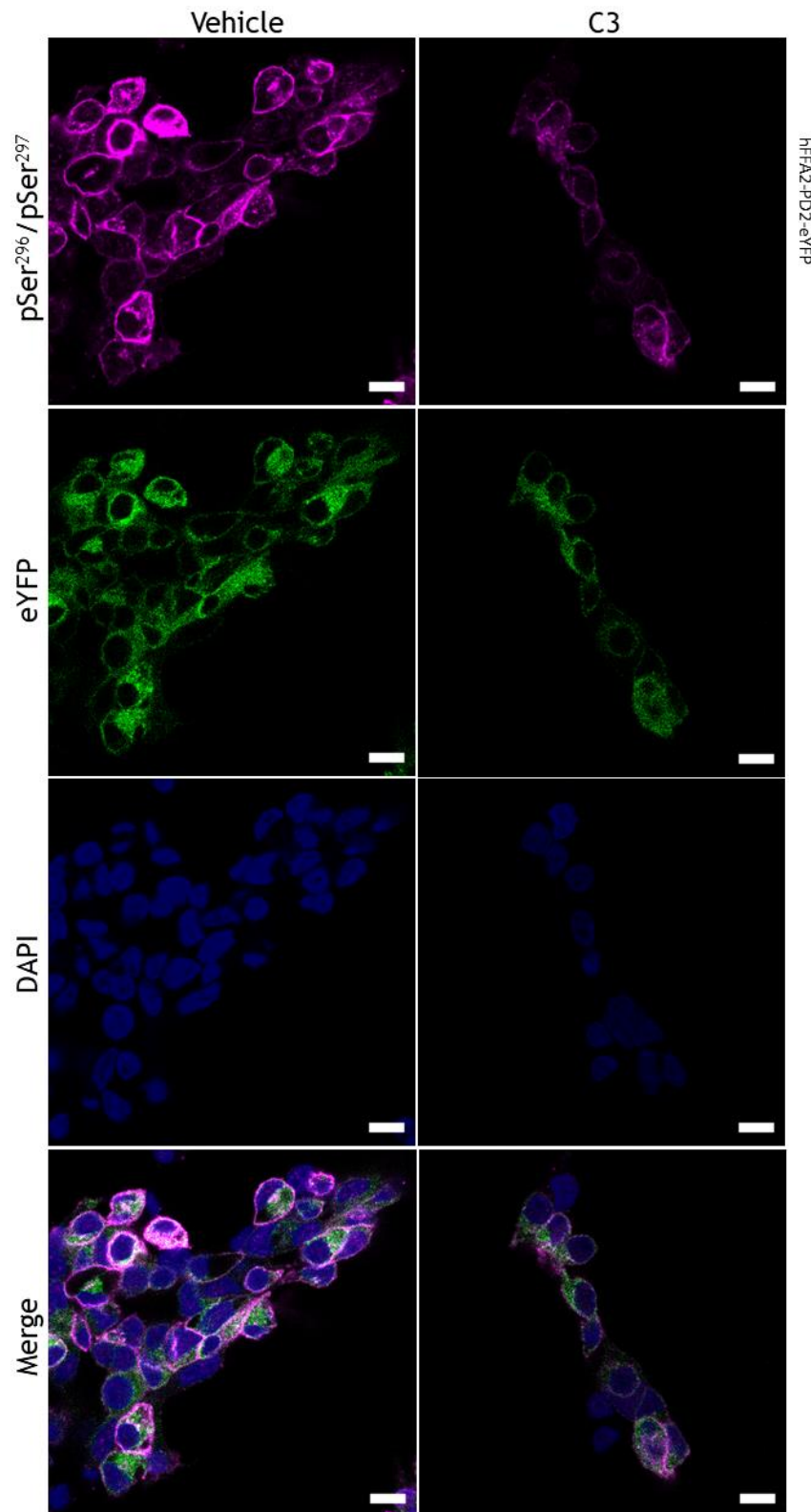


Figure 5.18. Immunocytochemical detection of hFFA2-PD2 phosphorylation in overexpressing cells. Flp-In T-REx 293 cells expressing hFFA2-Thr³⁰⁶Ala-Thr³¹⁰Ala-eYFP (hFFA2-PD2) were treated with vehicle or 2mM propionate (C3) for 2min, then fixed with 4% paraformaldehyde and permeabilised with saponin. Cells were incubated with rabbit anti-FFA2-pSer²⁹⁶/pSer²⁹⁷ antiserum (1:250) overnight, and with goat anti-rabbit IgG AlexaFluor-546 secondary antibody (1:400; magenta) for 2h. Nuclear DNA was labelled with DAPI (blue). Images were taken with 63× objective of Zeiss 880 Laser Scanning Confocal Microscope. Scale bar represents 10µm. Representative of 3 fields of view each from 3 separate experiments (n=3). eYFP - enhanced yellow fluorescent protein.

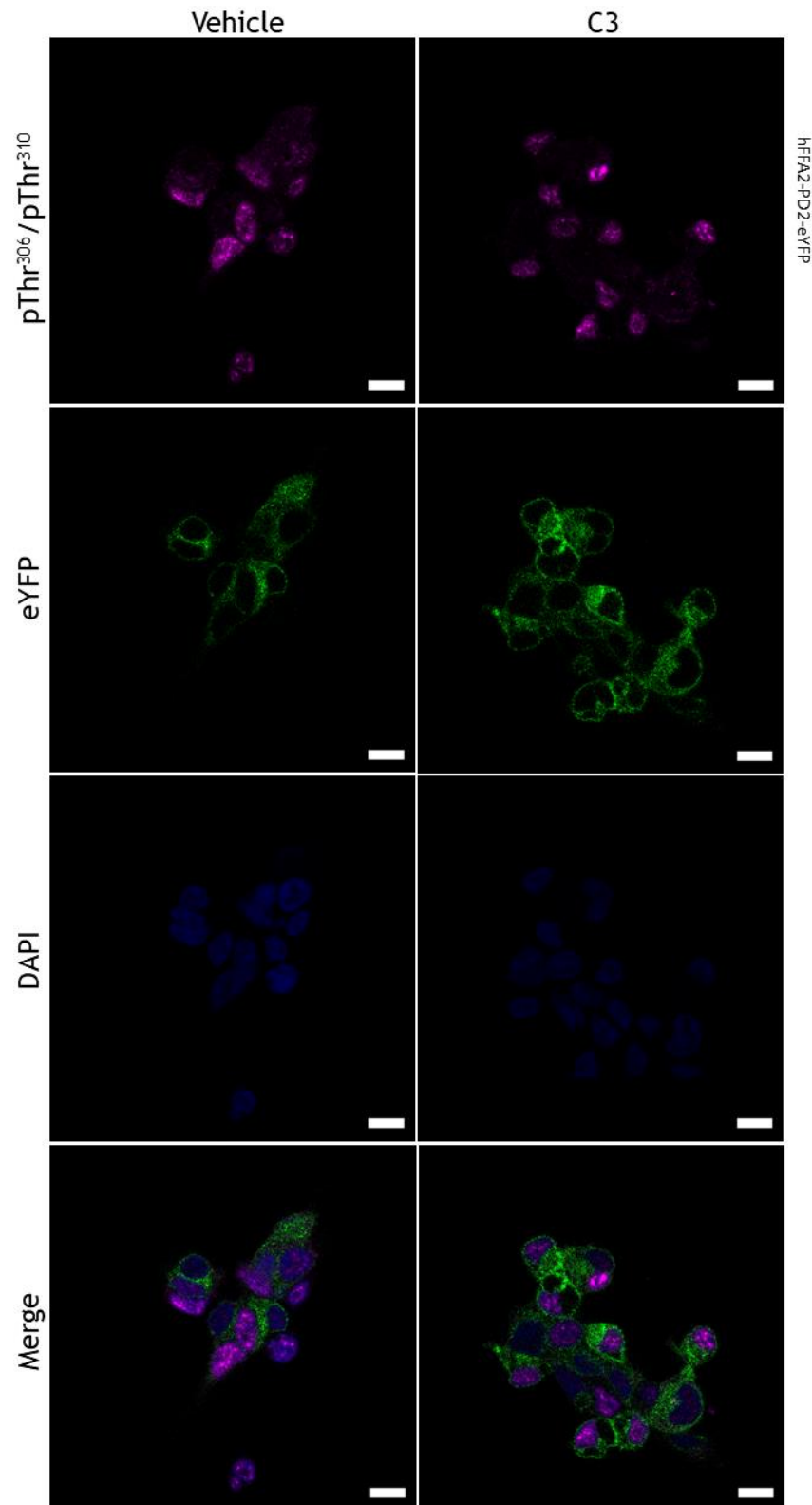


Figure 5.19. Immunocytochemical detection of hFFA2-PD2 phosphorylation in overexpressing cells. Flp-In T-REx 293 cells expressing hFFA2-Thr³⁰⁶Ala-Thr³¹⁰Ala-eYFP (hFFA2-PD2) were treated with vehicle or 2mM propionate (C3) for 2min, then fixed with 4% paraformaldehyde and permeabilised with saponin. Cells were incubated with rabbit anti-FFA2-pThr³⁰⁶/pThr³¹⁰ antiserum (1:250) overnight, and with goat anti-rabbit IgG AlexaFluor-546 secondary antibody (1:400; magenta) for 2h. Nuclear DNA was labelled with DAPI (blue). Images were taken with 63× objective of Zeiss 880 Laser Scanning Confocal Microscope. Scale bar represents 10µm. Representative of 3 fields of view each from 3 separate experiments (n=3). eYFP - enhanced yellow fluorescent protein.

5.2.3 β -arrestin-2 recruitment in phosphodeficient mutants of hFFA2

Receptor phosphorylation constitutes an initial step in non-G protein-mediated downstream signalling. The recruitment of β -arrestin-2 is one such signalling pathway, and as such was explored both in WT and mutant (DREADD and PD) receptors. Endpoint measurements were taken at 5min, as described by Hudson et al. (2013). To calculate mBRET, the following formula was used:

$$mBRET = \left(\frac{\text{sample @535nm}}{\text{sample @475nm}} - \text{mean} \left(\frac{NLuc \text{ control @535nm}}{NLuc \text{ control @475nm}} \right) \right) \times 1,000$$

Initially, agonist-dependent β -arrestin-2 recruitment was measured for each of hFFA2-eYFP, hFFA2-DREADD-eYFP and mFFA2-eYFP (Figure 5.20), and non-linear regression curves were fitted (see Section 2.10.4). The potency of C3 at hFFA2-eYFP ($pEC_{50}=3.53\pm 0.06$) was not significantly different from that of SA at hFFA2-DREADD-eYFP ($pEC_{50}=3.75\pm 0.06$). However, the E_{max} of hFFA2-DREADD-eYFP ($244.7\pm 18.8\%$) was more than double of that of hFFA2-eYFP ($p<0.01$; determined by one-way ANOVA) - an effect consistent with the initial exploration of SA at hFFA2-DREADD (Hudson et al., 2012a). There was no observable response when using C3 to activate mFFA2-eYFP.

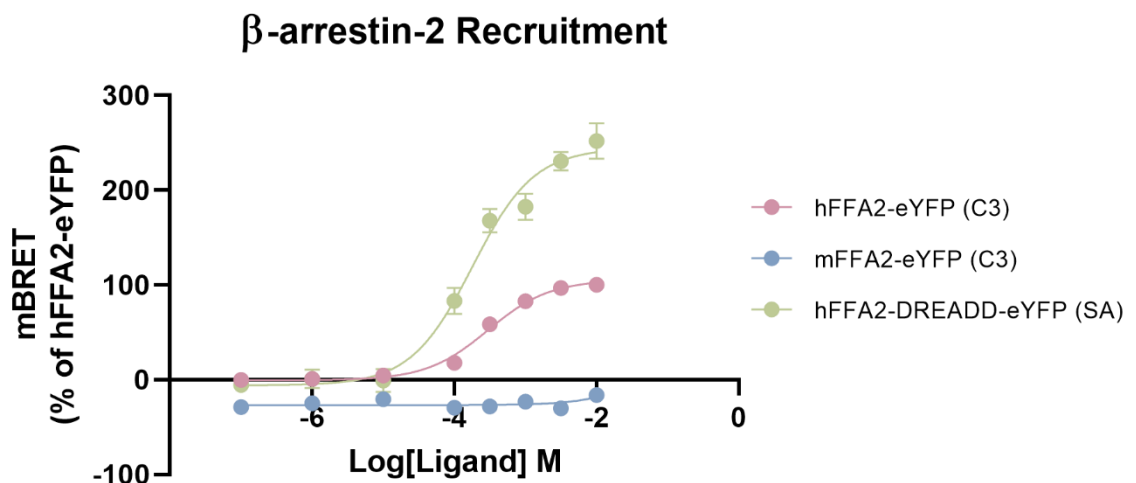


Figure 5.20. Agonist-induced β -arrestin-2 recruitment. HEK293T cells transiently transfected to express hFFA2-eYFP, mFFA2-eYFP and hFFA2-DREADD-eYFP alongside NLuc-tagged β -arrestin-2 were cultured in poly-D-lysine-coated 96-well plates. Cells were pre-incubated with Nano-Glo Luciferase substrate for 10min, followed by 5-min treatment with increasing concentrations of propionate (C3) or sorbic acid (SA). Endpoint BRET luminescence of eYFP and NLuc was measured at 535nm and 475nm, respectively, using the PHERAstar FS plate reader. Raw data baseline adjusted to NLuc- β -arrestin-2 control and normalised to hFFA2-eYFP. Data presented as mean \pm SEM (n=3).

Following these initial experiments, the effect on β -arrestin-2 recruitment of eliminating potential phosphorylation sites from the receptors was explored. To this end, in addition to the previously introduced mutants (hFFA2-PD1, hFFA2-PD2 and hFFA2-PD3; here collectively named “single-site PD mutants”), three additional “double-site” mutants, and one “triple-site” mutant were generated. Namely these were: hFFA2-Ser²⁹⁶Ala-Ser²⁹⁷Ala-Thr³⁰⁶Ala-Thr³¹⁰Ala-eYFP (hFFA2-PD1-2, in short), hFFA2-Ser²⁹⁶Ala-Ser²⁹⁷Ala-Ser³²⁴Ala-Ser³²⁵Ala-eYFP (hFFA2-PD1-3), hFFA2-Thr³⁰⁶Ala-Thr³¹⁰Ala-Ser³²⁴Ala-Ser³²⁵Ala-eYFP (hFFA2-PD2-3) and hFFA2-Ser²⁹⁶Ala-Ser²⁹⁷Ala-Thr³⁰⁶Ala-Thr³¹⁰Ala-Ser³²⁴Ala-Ser³²⁵Ala-eYFP (hFFA2-PD1-2-3).

For this, the endogenous ligand C3 was utilised in these PD mutants of hFFA2-eYFP (*Figure 5.21*). The basal and E_{\max} values of the β -arrestin-2 recruitment curves, as well as the calculated pEC_{50} values are summarised in *Table 5.1*. Although there was some variation in pEC_{50} values between the mutants, none of the differences were found to be significant (determined by one-way ANOVA). While hFFA2-PD1 and hFFA2-PD2 appeared to have higher basal and E_{\max} values than hFFA2-WT, none of these differences were significant. For all the other mutants, both basal and E_{\max} values were lower than hFFA2-WT. Of these, only hFFA2-PD3 had a significantly lower basal ($p < 0.001$), and all mutants containing the Ser³²⁴Ala-Ser³²⁵Ala mutation had a significantly lower E_{\max} ($p < 0.0001$ to $p < 0.05$). The reduced basal efficacy of β -arrestin-2 recruitment in PD mutants could suggest various degrees of baseline phosphorylation of these residues on hFFA2-WT. In addition, removal of phosphate-acceptor residues appeared to limit the maximum extent of β -arrestin-2 recruitment, thus lowering E_{\max} .

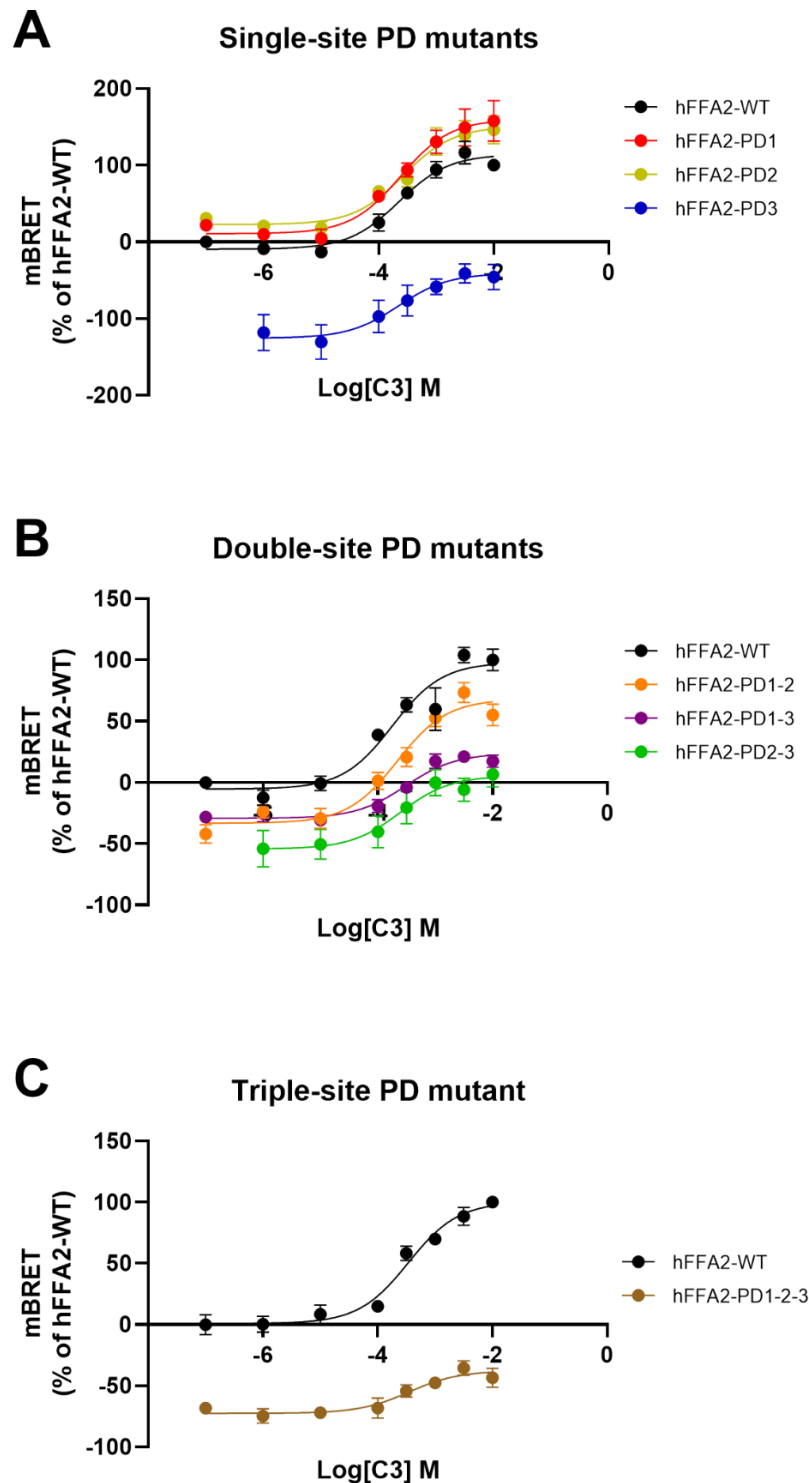


Figure 5.21. Agonist-induced β -arrestin-2 recruitment in phosphodeficient hFFA2-eYFP mutants. HEK293T cells transiently transfected to express hFFA2-eYFP (hFFA2-WT), A) hFFA2-Ser²⁹⁶Ala-Ser²⁹⁷Ala-eYFP (hFFA2-PD1), hFFA2-Thr³⁰⁶Ala-Thr³¹⁰Ala-eYFP (hFFA2-PD2), hFFA2-Ser³²⁴Ala-Ser³²⁵Ala-eYFP (hFFA2-PD3), B) hFFA2-Ser²⁹⁶Ala-Ser²⁹⁷Ala-Thr³⁰⁶Ala-Thr³¹⁰Ala-eYFP (hFFA2-PD1-2), hFFA2-Ser²⁹⁶Ala-Ser²⁹⁷Ala-Ser³²⁴Ala-Ser³²⁵Ala-eYFP (hFFA2-PD1-3), hFFA2-Thr³⁰⁶Ala-Thr³¹⁰Ala-Ser³²⁴Ala-Ser³²⁵Ala (hFFA2-PD2-3) or C) hFFA2-Ser²⁹⁶Ala-Ser²⁹⁷Ala-Thr³⁰⁶Ala-Thr³¹⁰Ala-Ser³²⁴Ala-Ser³²⁵Ala-eYFP (hFFA2-PD1-2-3) alongside NLuc-tagged β -arrestin-2 were cultured in poly-D-lysine-coated 96-well plates. Cells were pre-incubated with Nano-Glo Luciferase substrate for 10min, followed by 5-min treatment with increasing concentrations of propionate (C3). Endpoint BRET luminescence of eYFP and NLuc was measured at 535nm and 475nm, respectively, using the PHERAstar FS plate reader. Raw data baseline adjusted to NLuc- β -arrestin-2 control and normalised to hFFA2-WT. Data presented as mean \pm SEM (n=3).

Receptor	pEC ₅₀	Basal β -arrestin-2 recruitment (%)	β -arrestin-2 recruitment E _{max} (%)
hFFA2-WT	3.55±0.08	-3.91±2.69	106.9±4.13
hFFA2-PD1	3.65±0.13	11.29±6.54	162.7±48.60
hFFA2-PD2	3.47±0.16	23.44±10.38	155.2±24.94
hFFA2-PD3	3.52±0.26	-123.5±47.51 ^{\$\$\$}	-35.95±25.33 ^{****}
hFFA2-PD1-2	3.66±0.01	-33.22±12.26	68.08±11.56
hFFA2-PD1-3	3.52±0.01	-29.29±1.47	23.76±3.67*
hFFA2-PD2-3	3.62±0.15	-54.02±25.51	6.72±14.92**
hFFA2-PD1-2-3	3.48±0.15	-72.9±7.37	-37.87±9.15 ^{****}

Table 5.1. Potency (pEC₅₀), basal and maximum efficacy (E_{max}) of propionate (C3) at hFFA2-eYFP phosphodeficient mutants in BRET-based β -arrestin-2 recruitment assays. Values calculated as percentage of β -arrestin-2 recruitment induced by C3 at hFFA2-WT. Data presented as mean±SEM (n=3). ^{\$\$\$} p<0.001 by one-way ANOVA with Tukey's post-hoc multiple comparisons test against hFFA2-WT basal. ^{****} p<0.0001, ^{**} p<0.01, ^{*} p<0.05 by one-way ANOVA with Tukey's post-hoc multiple comparisons test against hFFA2-WT E_{max}.

In order to examine whether the elimination of phosphorylation sites would influence other signalling, Flp-In T-REx 293 cells expressing the “single-site PD” mutant receptors were employed in [³⁵S]GTP γ S incorporation assays (*Figure 5.22*). Potencies and efficacy values are presented in *Table 5.2*. Neither C3 potencies, nor basal efficacies were significantly different at the mutant receptors in comparison to hFFA2-WT. As in the case of β -arrestin-2 recruitment, the maximum efficacy of C3 was significantly reduced in hFFA2-PD3 (p<0.001 by one-way ANOVA). This could suggest concomitant reduction of [³⁵S]GTP γ S incorporation and β -arrestin-2 recruitment at this mutant. This finding was unexpected and may reflect lower receptor expression at this mutant. ICC studies with hFFA2-PD3 did indeed display lower fluorescence (data not shown).

Receptor	pEC ₅₀	Basal [³⁵ S]GTP γ S incorporation (%)	[³⁵ S]GTP γ S incorporation E _{max} (%)
hFFA2-WT	3.80±0.13	2.83±2.18	108.7±4.72
hFFA2-PD1	3.77±0.15	-14.38±14.76	70.88±7.28
hFFA2-PD2	3.73±0.07	-4.68±11.59	71.47±7.69
hFFA2-PD3	3.9±0.01	-22.38±19.50	14.9±14.28 ^{***}

Table 5.2. Potency (pEC₅₀), basal and maximum efficacy (E_{max}) of propionate (C3) at hFFA2-eYFP phosphodeficient mutants in [³⁵S]GTP γ S incorporation assays. Values calculated as percentage of [³⁵S]GTP γ S incorporation induced by C3 at hFFA2-WT. Data presented as mean±SEM (n=3). ^{***} p<0.001 by one-way ANOVA with Tukey's post-hoc multiple comparisons test against hFFA2-WT E_{max}.

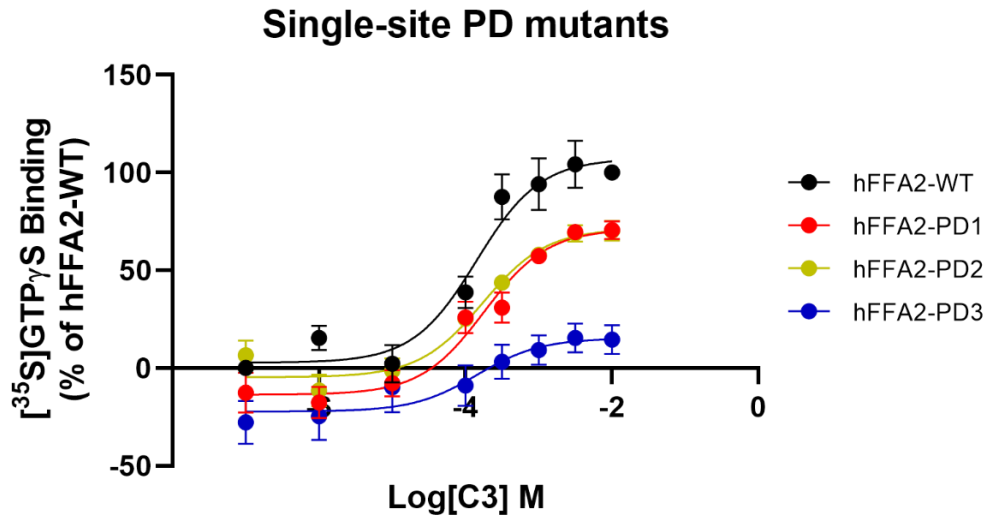


Figure 5.22. Agonist-induced $[^{35}\text{S}]\text{GTP}\gamma\text{S}$ incorporation in phosphodeficient hFFA2-eYFP mutants. Membranes prepared from Flp-In T-REx 293 cells harbouring hFFA2-eYFP (hFFA2-WT), hFFA2-Ser²⁹⁶Ala-Ser²⁹⁷Ala-eYFP (hFFA2-PD1), hFFA2-Thr³⁰⁶Ala-Thr³¹⁰Ala-eYFP (hFFA2-PD2) or hFFA2-Ser³²⁴Ala-Ser³²⁵Ala-eYFP (hFFA2-PD3) were incubated with various concentrations of C3 for 1h at 30°C, and the incorporation of $[^{35}\text{S}]\text{GTP}\gamma\text{S}$ was measured as counts per minute. Response normalised to hFFA2-WT. Data presented as mean \pm SEM (n=3).

5.2.4 Phosphorylation of hFFA2-HA in mouse-derived neutrophils

Although experiments conducted in eYFP-tagged receptors thus far have revealed some features of hFFA2 phosphorylation, in order to translate these findings into the available animal models, the HA-tagged variant of the receptor was also examined in a similar fashion. Initially, WB experiments using hFFA2-HA and hFFA2-DREADD-HA immunoprecipitated with anti-HA antibody agarose were employed (*Figure 5.23*). In control blots with an anti-HA antibody, both receptors showed equivalent levels of HA in the absence and presence of agonist. While distinctly stronger fluorescence was detected at the expected molecular mass of the HA-tagged receptors (~30kDa; black arrows), all lanes displayed a range of polypeptides of various apparent molecular masses (grey arrows). Both antisera were able to bind to HA-tagged receptors in a similar fashion as in the eYFP-tagged versions. In the case of anti-pSer²⁹⁶/pSer²⁹⁷, while hFFA2-HA did display some agonist-independent activity, there appeared to be an agonist-dependent effect. In hFFA2-DREADD-HA, the effect at this site was fully agonist-dependent. At residues Thr³⁰⁶/Thr³¹⁰, agonist treatment had a weak effect on hFFA2-HA phosphorylation. On the other hand, hFFA2-DREADD-HA displayed strong agonist-dependent effects at this site as well.

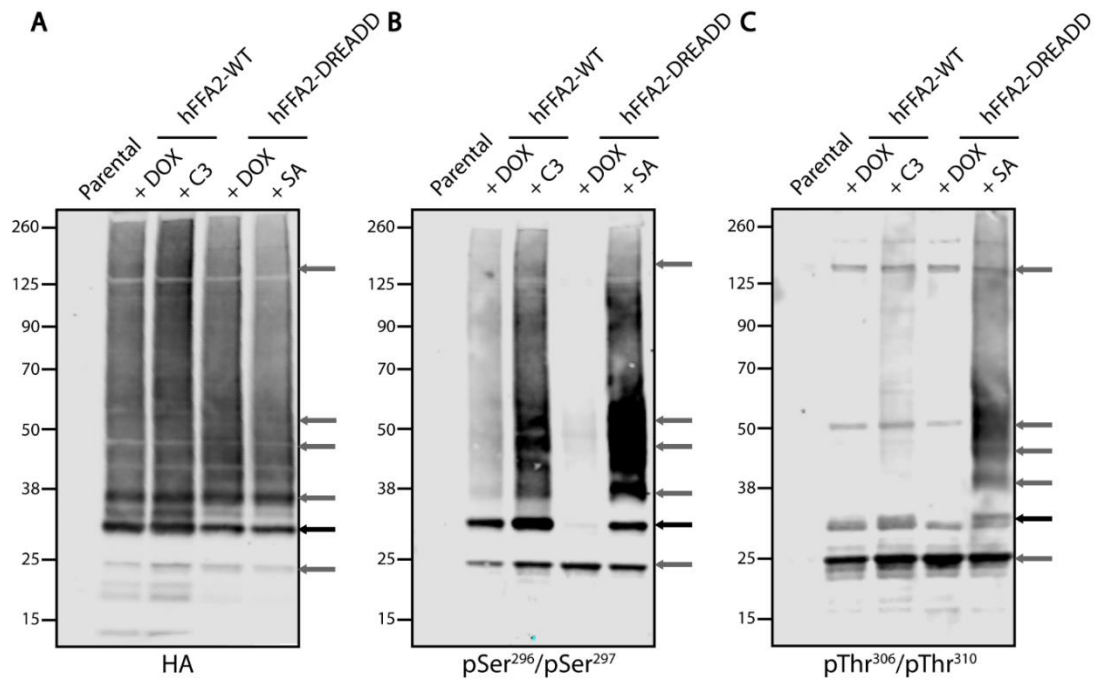


Figure 5.23. Western Blot analysis of hFFA2-HA and hFFA2-DREADD-HA phosphorylation. Serum-starved Flp-In T-REx 293 parental cells or cells expressing hFFA2-HA or hFFA2-DREADD-HA were treated with vehicle (+DOX), 2mM propionate (C3) or 1.7mM sorbic acid (SA) for 5min prior to lysate preparation in the presence of protease and phosphatase inhibitors. Lysates were immunoprecipitated with anti-HA agarose and run on NuPAGE 4-12% Bis-Tris SDS-PAGE gels. Proteins were subsequently transferred to nitrocellulose membranes, blocked with TBS supplemented with 5% (w/v) BSA and incubated overnight with A) rat anti-HA primary antibody (1:10,000), B) rabbit anti-FFA2-pSer²⁹⁶/pSer²⁹⁷ (1:2,000) or C) rabbit anti-FFA2-pThr³⁰⁶/pThr³¹⁰ (1:2,000) antiserum. Membranes were finally incubated with goat anti-rat IRDye 800CW (1:10,000) or donkey anti-rabbit IRDye 800CW (1:10,000) secondary antibodies, and visualised using the LI-COR Odyssey 9260 gel imaging system. Black arrows represent the expected size of hFFA2-HA; grey arrows represent polypeptides detected at other molecular masses. Representative of 3 blots (n=3). HA - haemagglutinin.

Although attempts were made to utilise mouse-derived neutrophil membranes in WB experiments, these samples were not readily detected by the control anti-HA antibody, despite the use of protein concentration equivalent to that of Flp-In T-REx 293 samples (data not shown). As such, an ICC approach was taken in order to demonstrate antiserum binding to hFFA2-HA and hFFA2-DREADD-HA in mouse neutrophils.

Initially, Flp-In T-REx 293 parental cells were utilised (Figure 5.24). As a control for receptor expression, an anti-HA primary antibody was used alongside the phosphosite-specific antisera. No expression of HA was observed in any cells, confirming the lack of receptor expression. Binding of anti-pSer²⁹⁶/pSer²⁹⁷ and anti-pThr³⁰⁶/pThr³¹⁰ was weak and restricted to intracellular compartments, identical of the pattern of non-specific binding in cells expressing eYFP-tagged receptors.

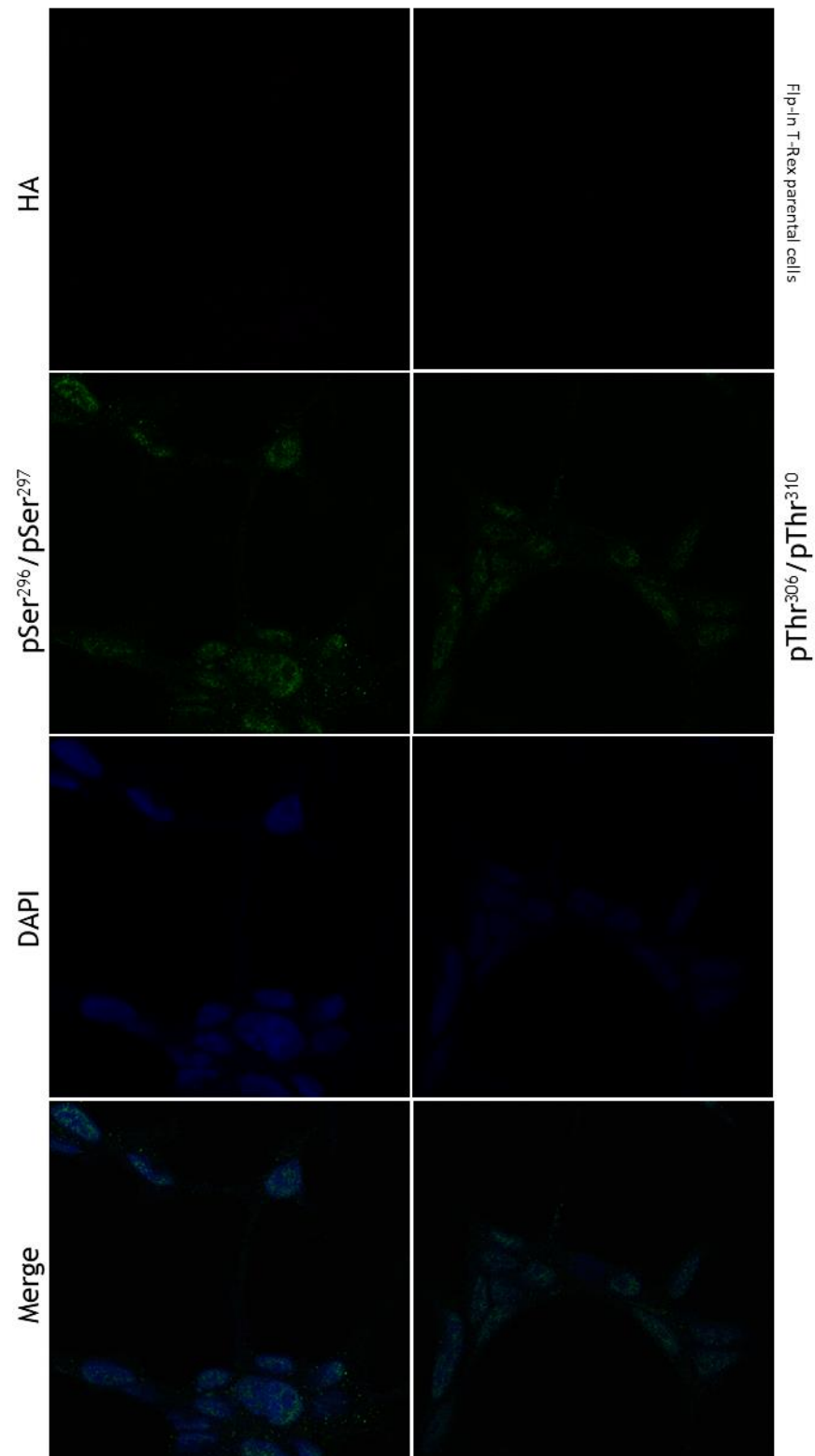


Figure 5.24. Immunocytochemical staining of Flp-In T-REx 293 parental cells. Flp-In T-REx 293 parental cells were treated with 2mM propionate for 2min, then fixed with 4% paraformaldehyde and permeabilised with saponin. Cells were incubated with rat anti-HA, and rabbit anti-FFA2-pSer²⁹⁶/pSer²⁹⁷ or rabbit anti-FFA2-pThr³⁰⁶/pThr³¹⁰ antiserum (1:250) overnight, and with goat anti-rat IgG AlexaFluor-546 (magenta) and goat anti-rabbit IgG AlexaFluor-488 secondary antibody (1:400; green) for 2h. Nuclear DNA was labelled with DAPI (blue). Images were taken with 63× objective of Zeiss 880 Laser Scanning Confocal Microscope. Scale bar represents 10µm. Representative of 3 fields of view each from 3 separate experiments (n=3). HA - haemagglutinin.

In the case of hFFA2-HA (*Figure 5.25 and Figure 5.26*), HA staining was observed both on the cell surface and intracellularly in both conditions. Similar to hFFA2-eYFP, hFFA2-HA displayed agonist-independent activity at residues Ser²⁹⁶/Ser²⁹⁷. The anti-pThr³⁰⁶/pThr³¹⁰ antiserum was found to bind non-specifically in vehicle-treated cells. In C3-induced cells, however, the antiserum bound to the cell surface and colocalised with HA. As such, both antisera reflect binding patterns similar to those previously observed in cells expressing eYFP-tagged receptors.

In the same set of experiments, cells were pre-treated with the antagonist CATPB (*Figure 5.27*). CATPB, while apparently decreasing signal intensity slightly, had no considerable effect at residues Ser²⁹⁶/Ser²⁹⁷. At residues Thr³⁰⁶/Thr³¹⁰, however, pre-treatment with CATPB appeared to reduce antiserum binding at the cell surface while maintaining non-specific intracellular binding. The inability of CATPB to block binding of the anti-pSer²⁹⁶/pSer²⁹⁷ antiserum could reflect constitutive, ligand-independent phosphorylation at these residues. Binding of the anti-pThr³⁰⁶/pThr³¹⁰ antiserum was blocked by CATPB, corroborating agonist-dependent effects observed in WBs in **Section 5.2.1**.

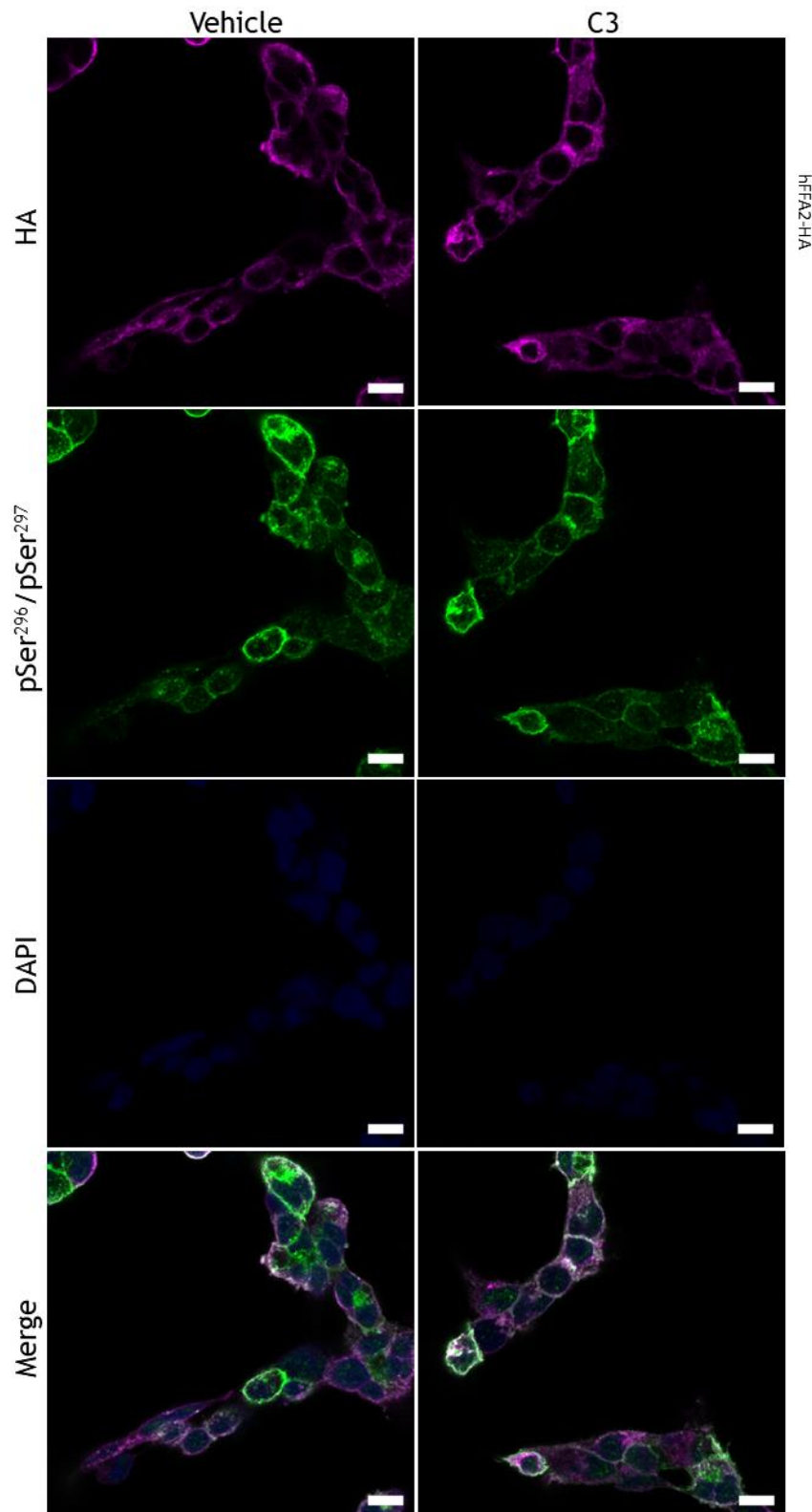


Figure 5.25. Immunocytochemical detection of hFFA2-HA phosphorylation in overexpressing cells. Flp-In T-REx 293 cells expressing hFFA2-HA were treated with vehicle or 2mM propionate (C3) for 2min, then fixed with 4% paraformaldehyde and permeabilised with saponin. Cells were incubated with rat-anti-HA and rabbit anti-FFA2-pSer²⁹⁶/pSer²⁹⁷ antiserum (1:250) overnight, and with goat anti-rat IgG AlexaFluor-546 (magenta) and goat anti-rabbit IgG AlexaFluor-488 secondary antibody (1:400; green) for 2h. Nuclear DNA was labelled with DAPI (blue). Images were taken with 63× objective of Zeiss 880 Laser Scanning Confocal Microscope. Scale bar represents 10µm. Representative of 3 fields of view each from 3 separate experiments (n=3). HA - haemagglutinin.

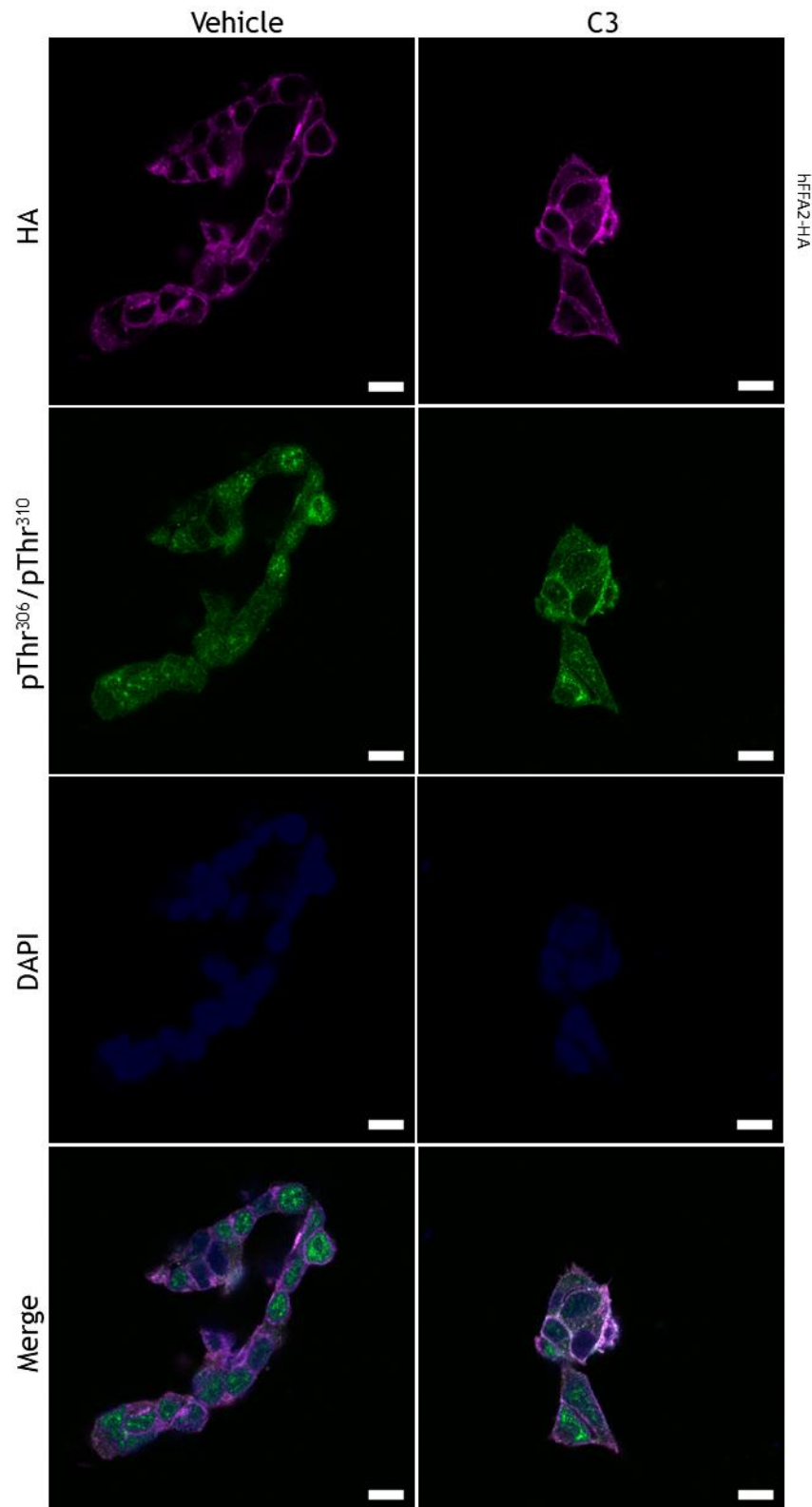


Figure 5.26. Immunocytochemical detection of hFFA2-HA phosphorylation in overexpressing cells. Flp-In T-REx 293 cells expressing hFFA2-HA were treated with vehicle or 2mM propionate (C3) for 2min, then fixed with 4% paraformaldehyde and permeabilised with saponin. Cells were incubated with rat-anti-HA and rabbit anti-FFA2-pThr³⁰⁶/pThr³¹⁰ antiserum (1:250) overnight, and with goat anti-rat IgG AlexaFluor-546 (magenta) and goat anti-rabbit IgG AlexaFluor-488 secondary antibody (1:400; green) for 2h. Nuclear DNA was labelled with DAPI (blue). Images were taken with 63× objective of Zeiss 880 Laser Scanning Confocal Microscope. Scale bar represents 10µm. Representative of 3 fields of view each from 3 separate experiments (n=3). HA - haemagglutinin.

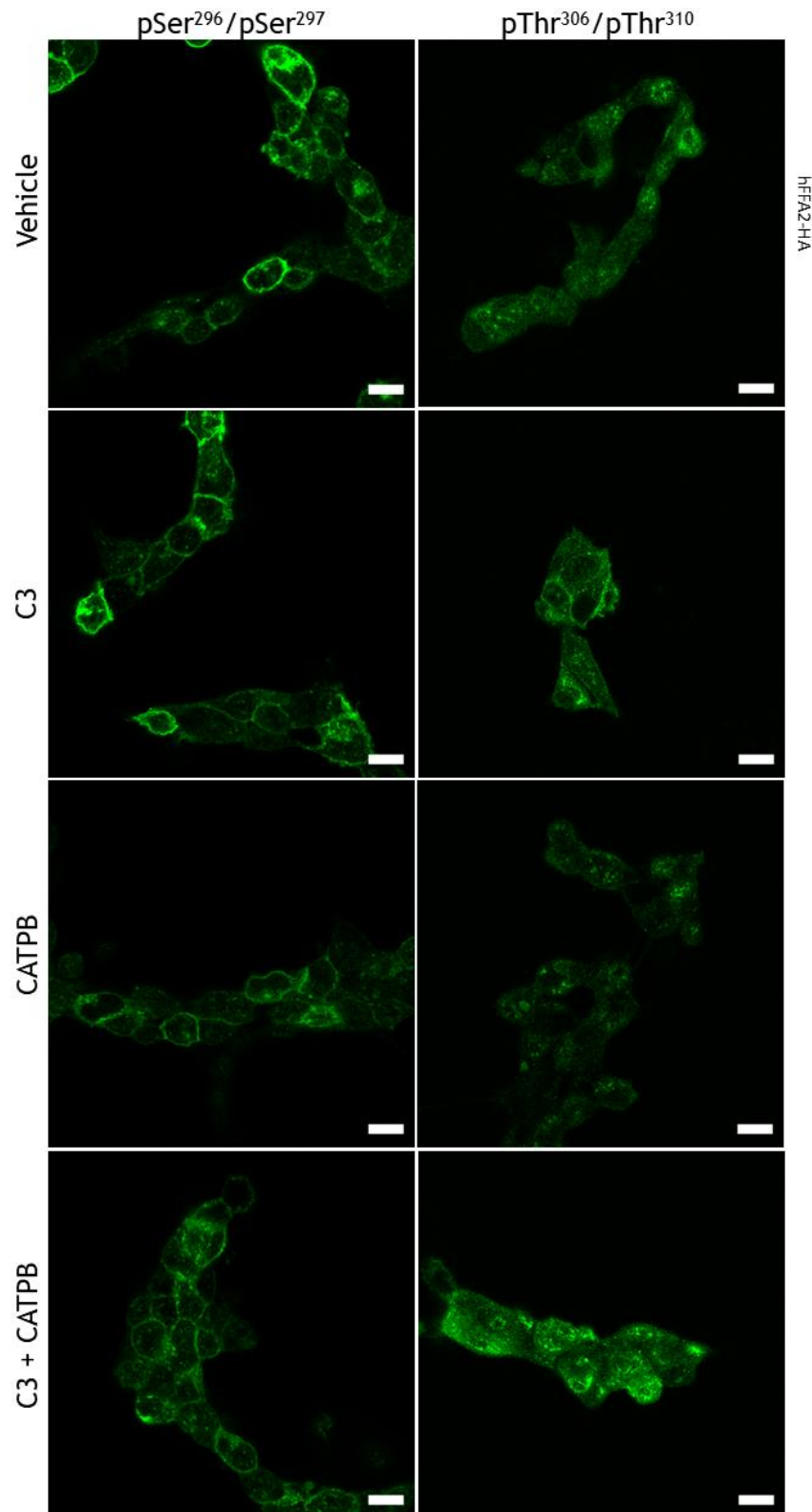


Figure 5.27. Immunocytochemical detection of the effect of CATPB on hFFA2-HA phosphorylation in overexpressing cells. Flp-In T-REx 293 cells expressing hFFA2-HA were pre-incubated with 100 μ M CATPB for 1h, followed by treatment with vehicle or 2mM propionate (C3) for 2min. Samples were then fixed with 4% paraformaldehyde and permeabilised with saponin. Cells were incubated with rabbit anti-FFA2-pSer²⁹⁶/pSer²⁹⁷ or rabbit anti-FFA2-pThr³⁰⁶/pThr³¹⁰ antiserum (1:250) overnight, and with goat anti-rabbit IgG AlexaFluor-488 secondary antibody (1:400; green) for 2h. Nuclear DNA was labelled with DAPI (blue). Images were taken with 63 \times objective of Zeiss 880 Laser Scanning Confocal Microscope. Scale bar represents 10 μ m. Representative of 3 fields of view each from 3 separate experiments (n=3).

In hFFA2-DREADD-HA-expressing cells (*Figure 5.28 and Figure 5.29*), HA expression was similarly unaffected by agonist treatment. While some non-specific binding was observed for the anti-pThr³⁰⁶/pThr³¹⁰ antiserum, there was a discernibly increased binding by both antisera to SA treated cells in comparison untreated cells. These agonist-dependent responses correspond to phosphorylation patterns observed in WBs.

Pre-treatment with CATPB appeared to inhibit agonist-dependent effects at both phosphorylation sites in hFFA2-DREADD-HA (*Figure 5.30*). While fluorescence intensity was maintained by anti-pThr³⁰⁶/pThr³¹⁰, this was restricted to intracellular locations. As binding of both antisera appeared to be blocked by CATPB, the agonist-dependency of phosphorylation at both sites observed in WBs (*Section 5.2.1*) was further corroborated.

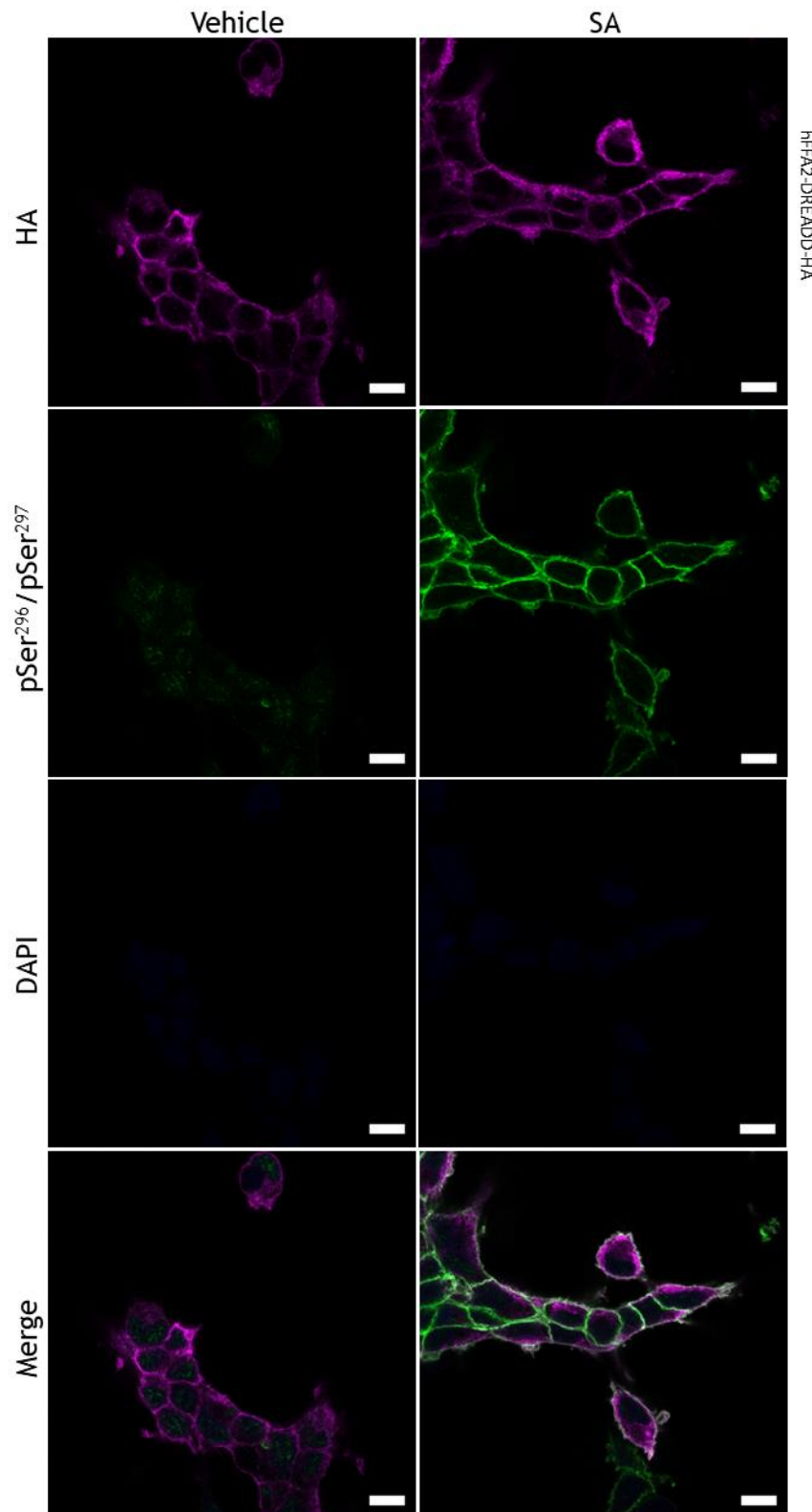


Figure 5.28. Immunocytochemical detection of hFFA2-DREADD-HA phosphorylation in overexpressing cells. Flp-In T-REx 293 cells expressing hFFA2-DREADD-HA were treated with vehicle or 1.7mM sorbic acid (SA) for 2min, then fixed with 4% paraformaldehyde and permeabilised with saponin. Cells were incubated with rat-anti-HA and rabbit anti-FFA2-pSer²⁹⁶/pSer²⁹⁷ antiserum (1:250) overnight, and with goat anti-rat IgG AlexaFluor-546 (magenta) and goat anti-rabbit IgG AlexaFluor-488 secondary antibody (1:400; green) for 2h. Nuclear DNA was labelled with DAPI (blue). Images were taken with 63× objective of Zeiss 880 Laser Scanning Confocal Microscope. Scale bar represents 10µm. Representative of 3 fields of view each from 3 separate experiments (n=3). HA - haemagglutinin.

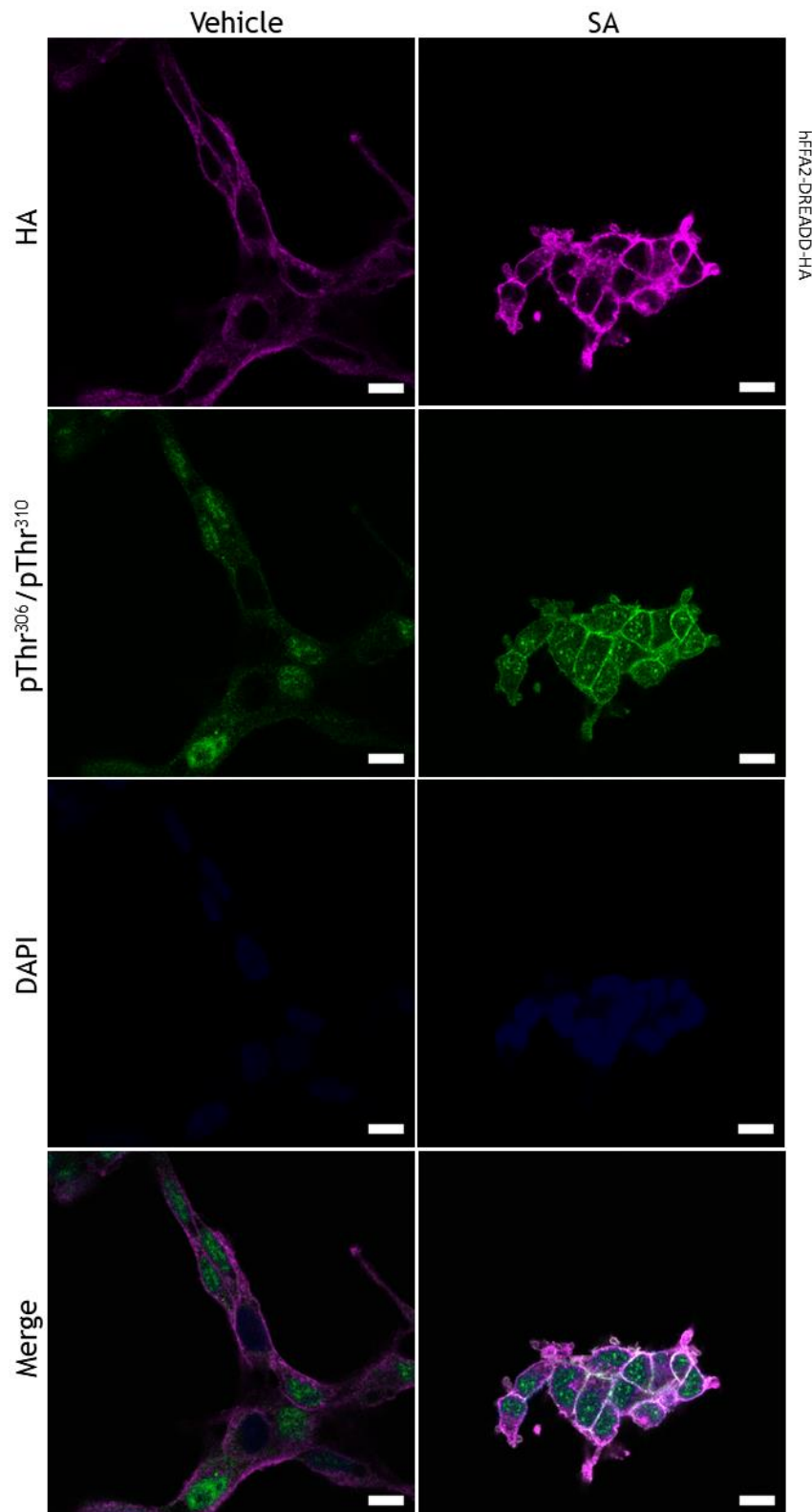


Figure 5.29. Immunocytochemical detection of hFFA2-DREADD-HA phosphorylation in overexpressing cells. Flp-In T-REx 293 cells expressing hFFA2-DREADD-HA were treated with vehicle or 1.7mM sorbic acid (SA) for 2min, then fixed with 4% paraformaldehyde and permeabilised with saponin. Cells were incubated with rat-anti-HA and rabbit anti-FFA2-pThr³⁰⁶/pThr³¹⁰ antiserum (1:250) overnight, and with goat anti-rat IgG AlexaFluor-546 (magenta) and goat anti-rabbit IgG AlexaFluor-488 secondary antibody (1:400; green) for 2h. Nuclear DNA was labelled with DAPI (blue). Images were taken with 63× objective of Zeiss 880 Laser Scanning Confocal Microscope. Scale bar represents 10µm. Representative of 3 fields of view each from 3 separate experiments (n=3). HA - haemagglutinin.

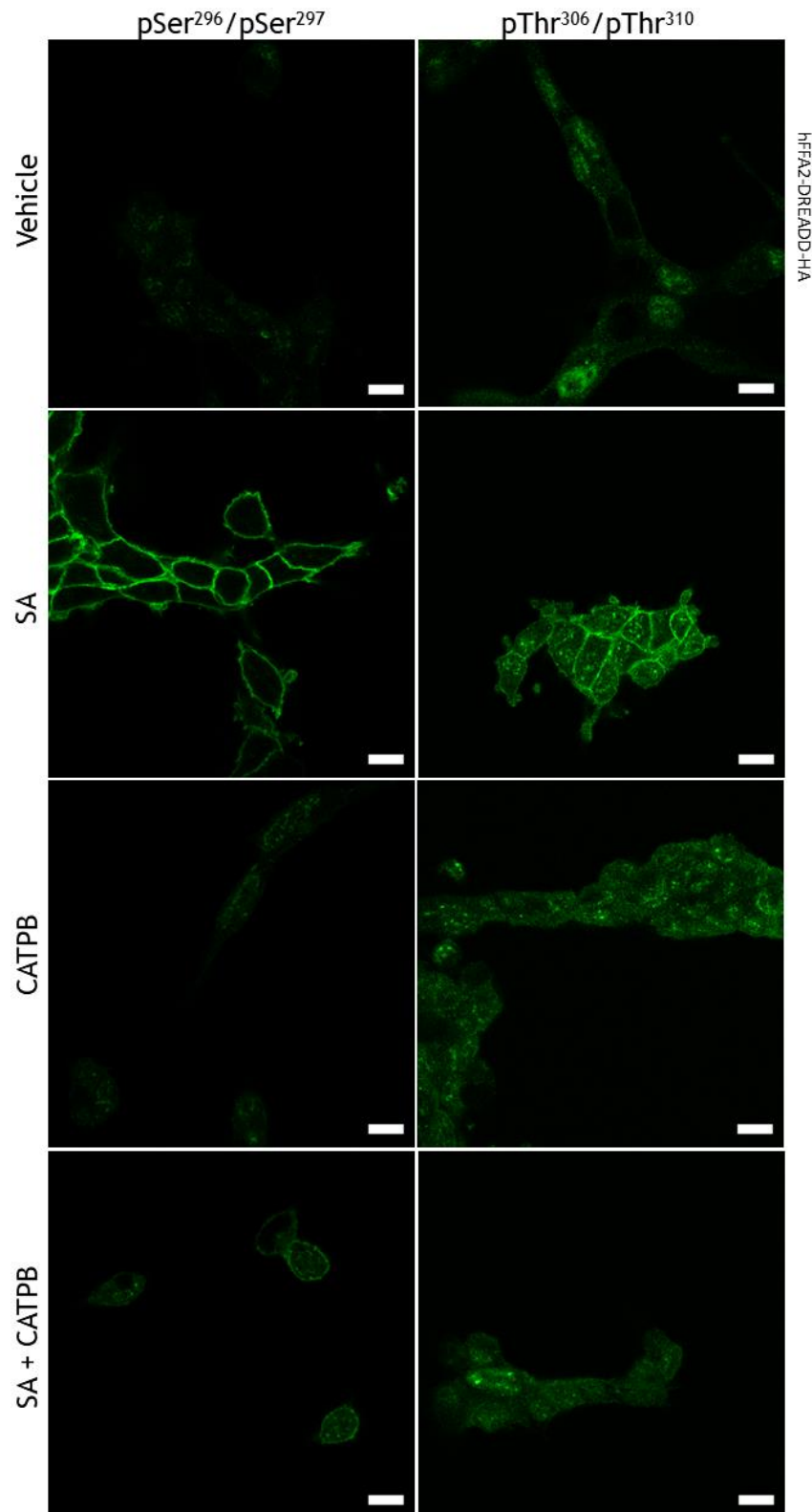


Figure 5.30. Immunocytochemical detection of the effect of CATPB on hFFA2-DREADD-HA phosphorylation in overexpressing cells. Flp-In T-REx 293 cells expressing hFFA2-HA were pre-incubated with 100 μ M CATPB for 1h, followed by treatment with vehicle or 1.7mM sorbic acid (SA) for 2min. Samples were then fixed with 4% paraformaldehyde and permeabilised with saponin. Cells were incubated with rabbit anti-FFA2-pSer²⁹⁶/pSer²⁹⁷ or rabbit anti-FFA2-pThr³⁰⁶/pThr³¹⁰ antiserum (1:250) overnight, and with goat anti-rabbit IgG AlexaFluor-488 secondary antibody (1:400; green) for 2h. Nuclear DNA was labelled with DAPI (blue). Images were taken with 63 \times objective of Zeiss 880 Laser Scanning Confocal Microscope. Scale bar represents 10 μ m. Representative of 3 fields of view each from 3 separate experiments (n=3).

Once the ability of the phosphosite-specific antisera to bind hFFA2-HA and hFFA2-DREADD-HA in ICC was established, they were then employed in neutrophils derived from hFFA2-HA and hFFA2-DREADD-HA mice. As in the overexpressing cell lines, an anti-HA antibody was utilised as a control for receptor expression.

First, antisera were tested in neutrophils isolated from minus-CRE mice as a negative control (*Figure 5.31*). No expression of HA was found in any of these neutrophils, although some non-specific binding was evident. Both phosphosite-specific antisera showed some degree of non-specific binding, with the anti-pSer²⁹⁶/pSer²⁹⁷ antiserum displaying stronger signals. The small dimensions of neutrophils, alongside the relatively low resolution, did not allow for the identification of cellular localisation of signals to the extent it was possible in Flp-In T-REx 293 cells.

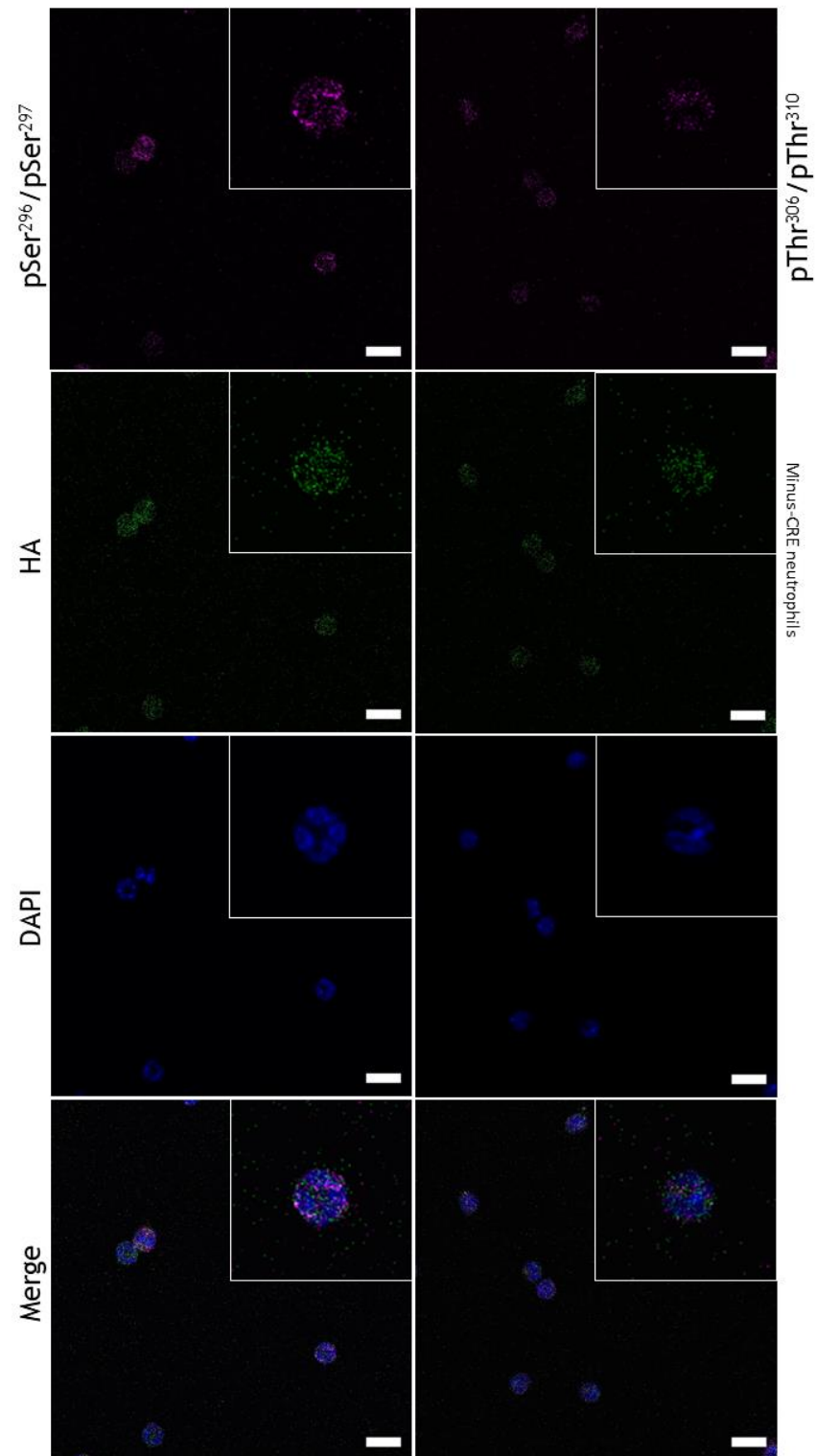


Figure 5.31. Immunocytochemical staining of minus-CRE mouse neutrophils. Bone marrow-derived neutrophils isolated from minus-CRE mice were treated with 2mM propionate (C3) for 2min, then fixed with 4% paraformaldehyde and permeabilised with saponin. Cells were incubated with rabbit anti-FFA2-pSer²⁹⁶/pSer²⁹⁷ or anti-FFA2-pThr³⁰⁶/pThr³¹⁰, and rat-anti-HA antiserum (1:250) overnight, and with goat anti-rabbit IgG AlexaFluor-546 (magenta) and goat anti-rat IgG AlexaFluor-488 secondary antibody (1:400; green) for 2h. Nuclear DNA was labelled with DAPI (blue). Images were taken with 63× objective of Zeiss 880 Laser Scanning Confocal Microscope. Scale bar represents 10µm. Inset shows an enlarged image of a representative neutrophil from the corresponding main image. Representative of 3 fields of view each from 3 experiments (n=3, where each n represents neutrophils pooled from 2-4 mice). HA - haemagglutinin.

In hFFA2-HA neutrophils (*Figure 5.32 and Figure 5.33*), the expression of HA was not apparently influenced by treatment with C3. A strong signal was produced by anti-pSer²⁹⁶/pSer²⁹⁷, which appeared equivalent in vehicle- and C3-treated neutrophils. At residues Thr³⁰⁶/Thr³¹⁰, on the other hand, treatment with C3 lead to an increase in fluorescence intensity. These observations could support the observations on the agonist-independent and -dependent of phosphorylation at each of these sites, respectively, as observed in Flp-In T-REx 293 cells.

Pre-incubation with CATPB (*Figure 5.34*) was found to decrease the binding of anti-pSer²⁹⁶/pSer²⁹⁷, despite the inability of CATPB to inhibit phosphorylation at this site in previous experiments. This discrepancy could reflect the differences in the phosphorylation machinery available in neutrophils in comparison to Flp-In T-REx 293 cells. As for anti-pThr³⁰⁶/pThr³¹⁰, signal was decreased in C3-treated neutrophils when pre-treated with CATPB, resembling observations in Flp-In T-REx 293 cells.

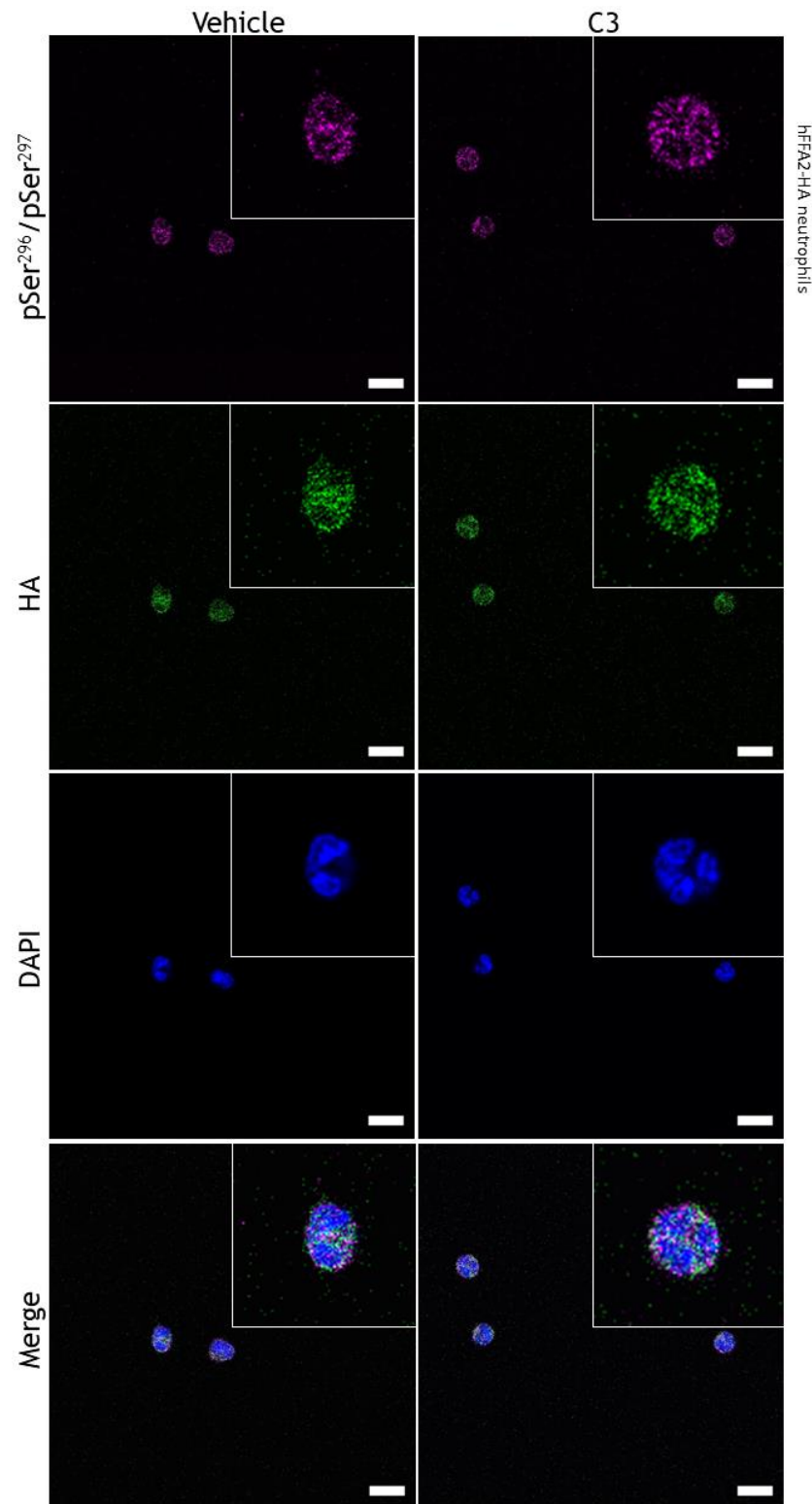


Figure 5.32. Immunocytochemical detection of hFFA2-HA phosphorylation in mouse neutrophils. Bone marrow-derived neutrophils isolated from hFFA2-HA mice were treated with vehicle or 2mM propionate (C3) for 2min, then fixed with 4% paraformaldehyde and permeabilised with saponin. Cells were incubated with rabbit anti-FFA2-pSer²⁹⁶/pSer²⁹⁷ antiserum and rat-anti-HA primary antibody (1:250) overnight, and with goat anti-rabbit IgG AlexaFluor-546 (magenta) and goat anti-rat IgG AlexaFluor-488 secondary antibody (1:400; green) for 2h. Nuclear DNA was labelled with DAPI (blue). Images were taken with 63× objective of Zeiss 880 Laser Scanning Confocal Microscope. Scale bar represents 10µm. Inset shows an enlarged image of a representative neutrophil from the corresponding main image. Representative of 3 fields of view each from 3 experiments (n=3, where each n represents neutrophils pooled from 2-4 mice). HA - haemagglutinin.

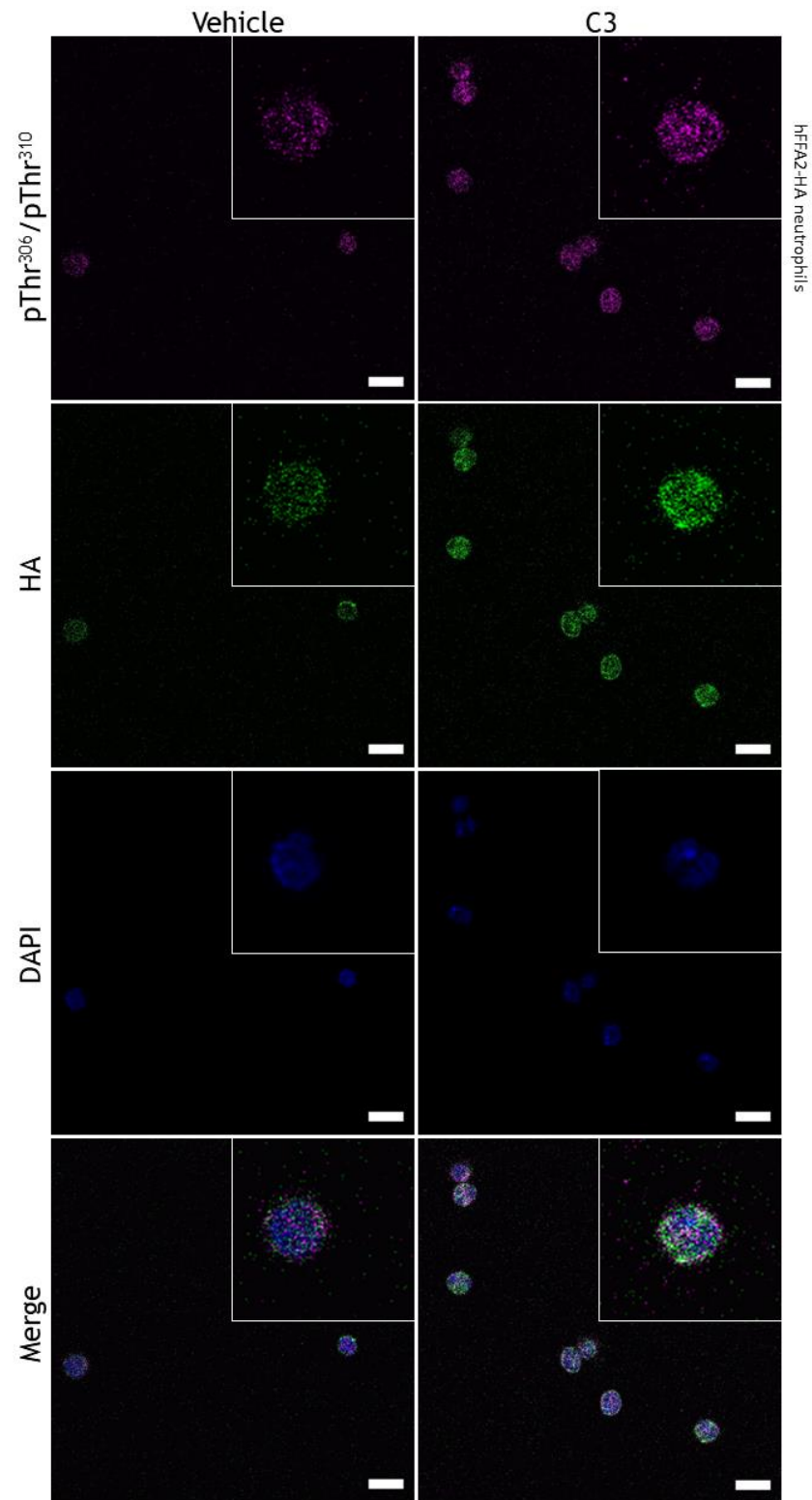


Figure 5.33. Immunocytochemical detection of hFFA2-HA phosphorylation in mouse neutrophils. Bone marrow-derived neutrophils isolated from hFFA2-HA mice were treated with vehicle or 2mM propionate (C3) for 2min, then fixed with 4% paraformaldehyde and permeabilised with saponin. Cells were incubated with rabbit anti-FFA2-pThr³⁰⁶/pThr³¹⁰ antiserum and rat-anti-HA primary antibody (1:250) overnight, and with goat anti-rabbit IgG AlexaFluor-546 (magenta) and goat anti-rat IgG AlexaFluor-488 secondary antibody (1:400; green) for 2h. Nuclear DNA was labelled with DAPI (blue). Images were taken with 63× objective of Zeiss 880 Laser Scanning Confocal Microscope. Scale bar represents 10µm. Inset shows an enlarged image of a representative neutrophil from the corresponding main image. Representative of 3 fields of view each from 3 experiments (n=3, where each n represents neutrophils pooled from 2-4 mice). HA - haemagglutinin.

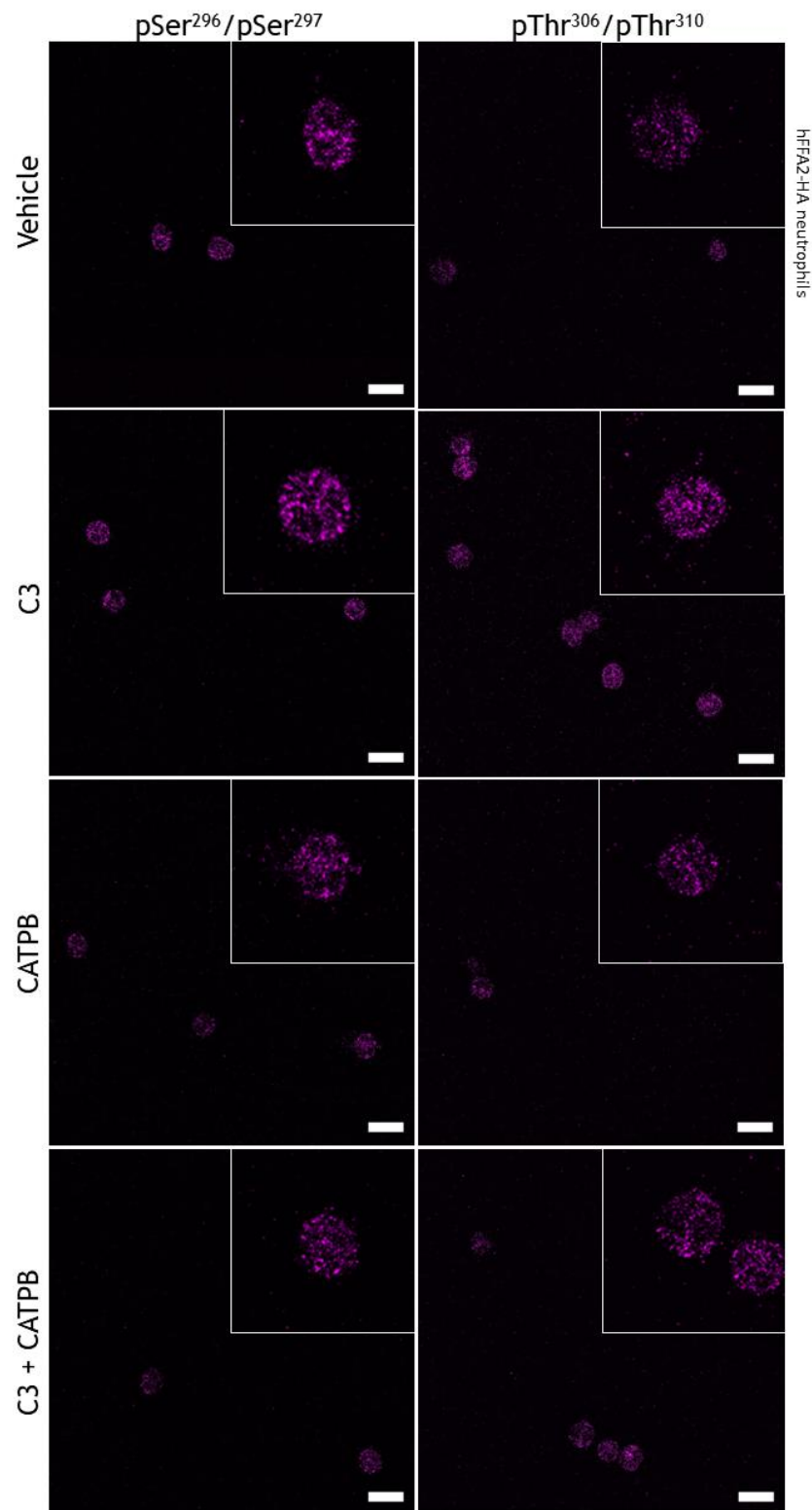


Figure 5.34. Immunocytochemical detection of the effect of CATPB on hFFA2-HA phosphorylation in mouse neutrophils. Bone marrow-derived neutrophils isolated from hFFA2-HA mice were pre-incubated with 100 μ M CATPB for 1h, followed by treatment with vehicle or 2mM propionate (C3) for 2min. Samples were then fixed with 4% paraformaldehyde and permeabilised with saponin. Cells were incubated with rabbit anti-FFA2-pSer²⁹⁶/pSer²⁹⁷ or rabbit anti-FFA2-pThr³⁰⁶/pThr³¹⁰ primary antiserum (1:250) overnight, and with goat anti-rabbit IgG AlexaFluor-546 secondary antibody (1:400; magenta) for 2h. Nuclear DNA was labelled with DAPI (blue). Images were taken with 63 \times objective of Zeiss 880 Laser Scanning Confocal Microscope. Scale bar represents 10 μ m. Inset shows an enlarged image of a representative neutrophil from the corresponding main image. Representative of 3 fields of view each from 3 experiments (n=3, where each n represents neutrophils pooled from 2-4 mice).

In hFFA2-DREADD-HA neutrophils (*Figure 5.35 and Figure 5.36*), SA induced no apparent change in HA expression. SA did, however, induce a moderate increase in the binding of both anti-pSer²⁹⁶/pSer²⁹⁷ and anti-pThr³⁰⁶/pThr³¹⁰. Again, this would reflect the agonist-dependent phosphorylation effects observed both in WBs and ICC in Flp-In T-REx 293 cells.

CATPB pre-treatment in hFFA2-DREADD-HA (*Figure 5.37*) appeared to lead to the inhibition of antiserum binding. This was the case for both antisera, thus supporting the agonist-dependent phosphorylation effects previously observed in hFFA2-DREADD-eYFP, which was amenable to antagonist treatment.

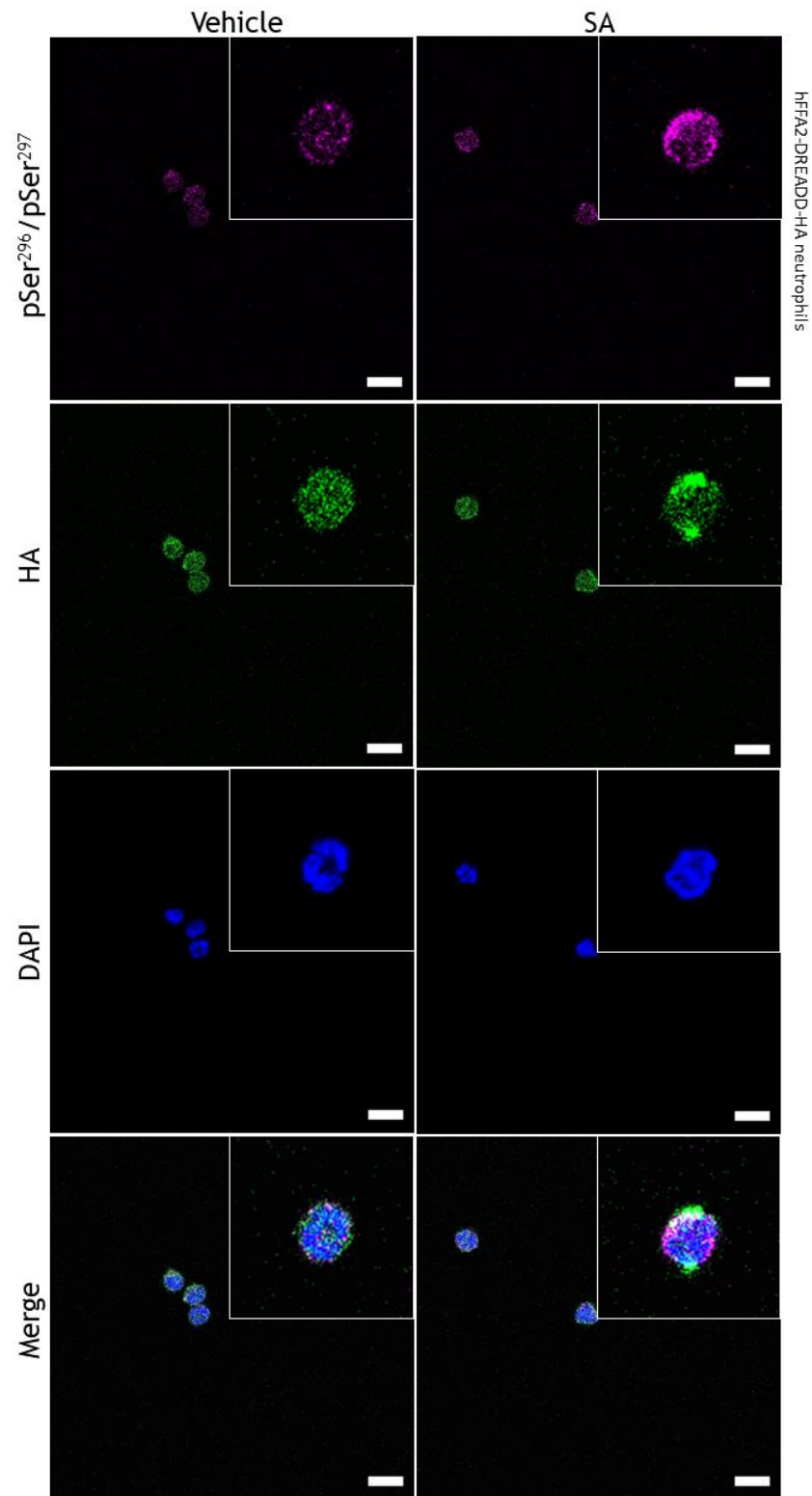


Figure 5.35. Immunocytochemical detection of hFFA2-DREADD-HA phosphorylation in mouse neutrophils. Bone marrow-derived neutrophils isolated from hFFA2-DREADD-HA mice were treated with vehicle or 1.7mM sorbic acid (SA) for 2min, then fixed with 4% paraformaldehyde and permeabilised with saponin. Cells were incubated with rabbit anti-FFA2-pSer²⁹⁶/pSer²⁹⁷ antiserum and rat-anti-HA primary antibody (1:250) overnight, and with goat anti-rabbit IgG AlexaFluor-546 (magenta) and goat anti-rat IgG AlexaFluor-488 secondary antibody (1:400; green) for 2h. Nuclear DNA was labelled with DAPI (blue). Images were taken with 63× objective of Zeiss 880 Laser Scanning Confocal Microscope. Scale bar represents 10µm. Inset shows an enlarged image of a representative neutrophil from the corresponding main image. Representative of 3 fields of view each from 3 experiments (n=3, where each n represents neutrophils pooled from 2-4 mice). HA - haemagglutinin.

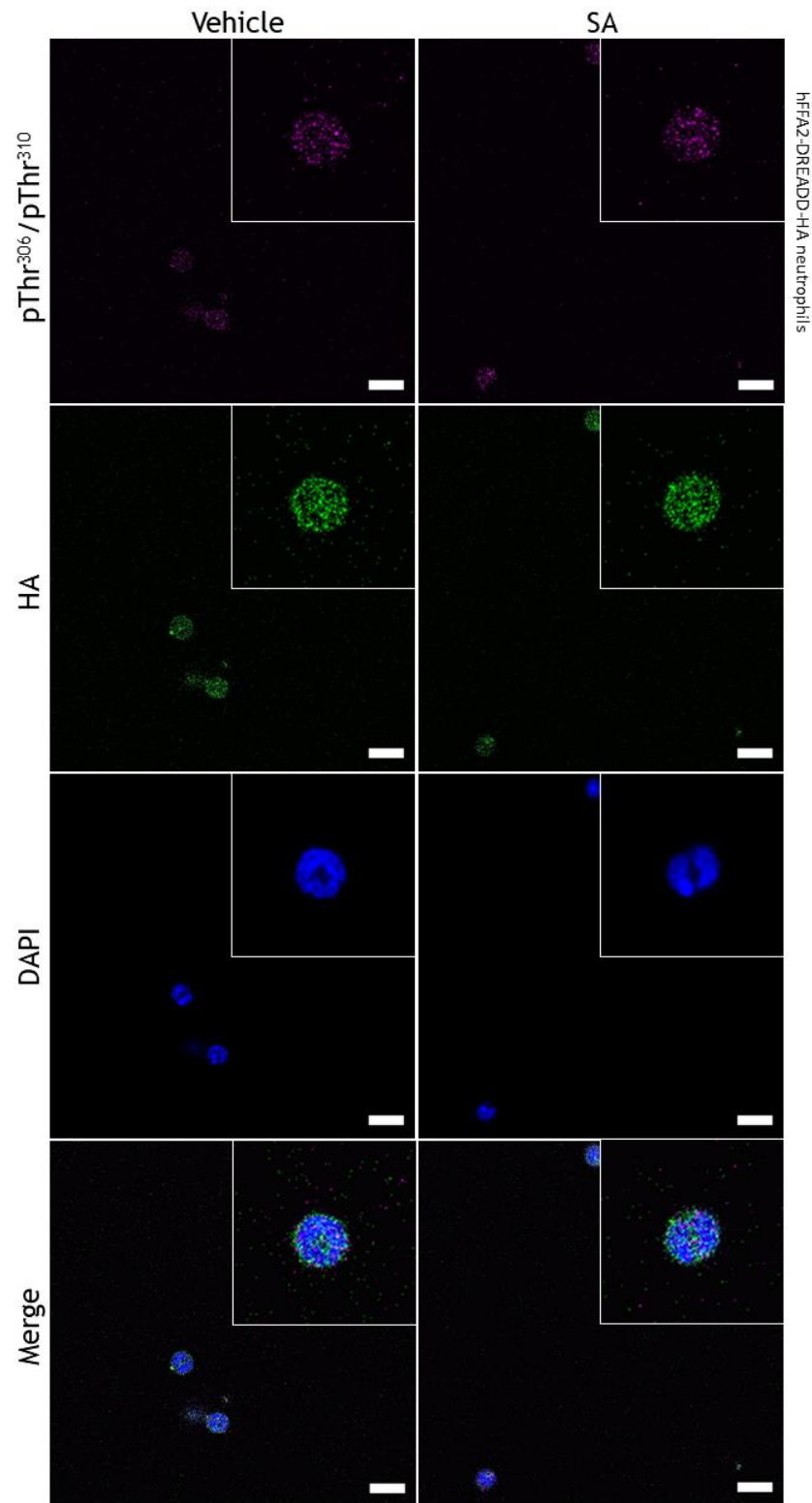


Figure 5.36. Immunocytochemical detection of hFFA2-DREADD-HA phosphorylation in mouse neutrophils. Bone marrow-derived neutrophils isolated from hFFA2-DREADD-HA mice were treated with vehicle or 1.7mM sorbic acid (SA) for 2min, then fixed with 4% paraformaldehyde and permeabilised with saponin. Cells were incubated with rabbit anti-FFA2-pThr³⁰⁶/pThr³¹⁰ antiserum and rat-anti-HA primary antibody (1:250) overnight, and with goat anti-rabbit IgG AlexaFluor-546 (magenta) and goat anti-rat IgG AlexaFluor-488 secondary antibody (1:400; green) for 2h. Nuclear DNA was labelled with DAPI (blue). Images were taken with 63× objective of Zeiss 880 Laser Scanning Confocal Microscope. Scale bar represents 10µm. Inset shows an enlarged image of a representative neutrophil from the corresponding main image. Representative of 3 fields of view each from 3 experiments (n=3, where each n represents neutrophils pooled from 2-4 mice). HA - haemagglutinin.

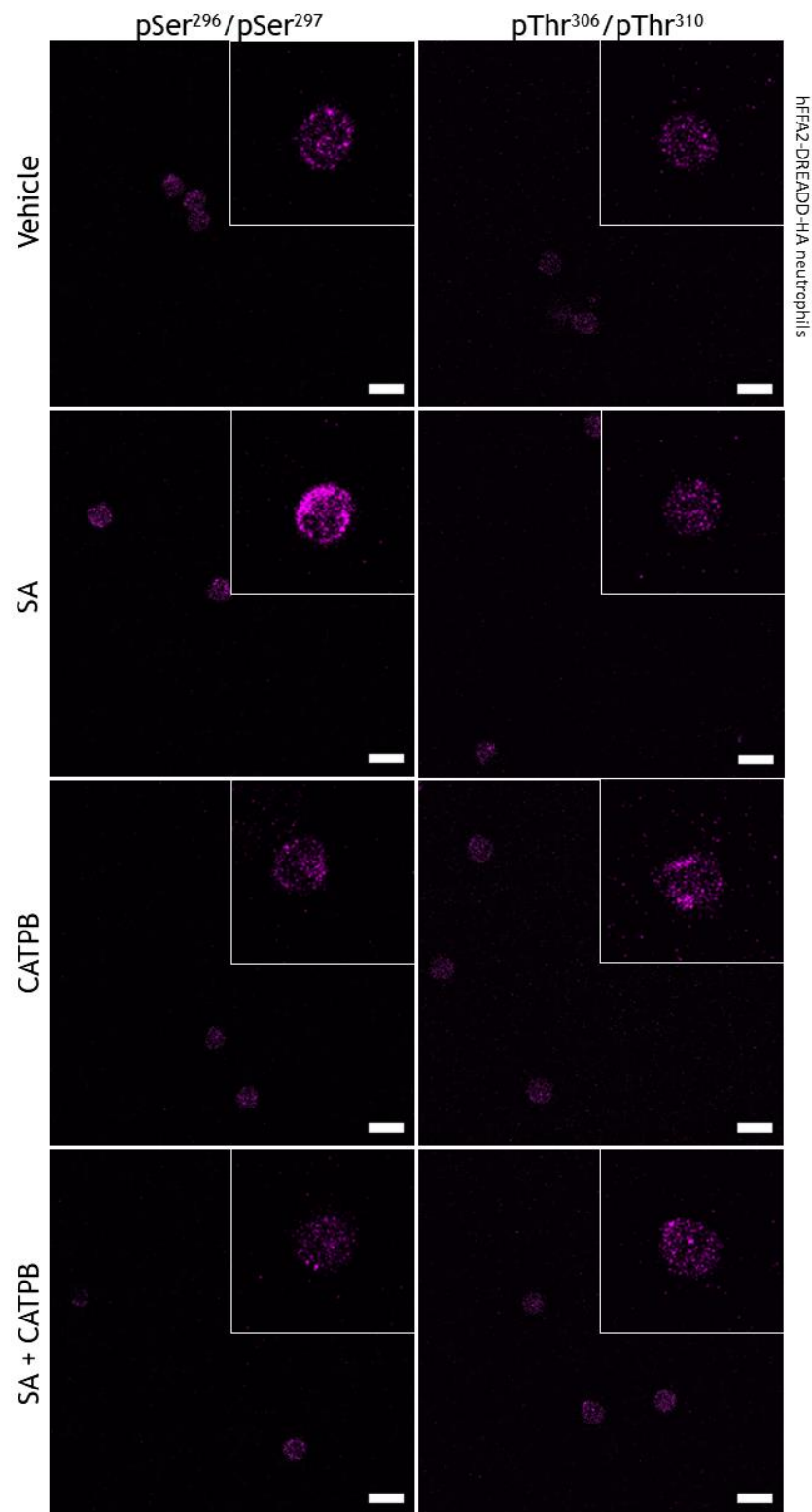


Figure 5.37. Immunocytochemical detection of the effect of CATPB on hFFA2-DREADD-HA phosphorylation in mouse neutrophils. Bone marrow-derived neutrophils isolated from hFFA2-DREADD-HA mice were pre-incubated with 100 μ M CATPB for 1h, followed by treatment with vehicle or 1.7mM sorbic acid (SA) for 2min. Samples were then fixed with 4% paraformaldehyde and permeabilised with saponin. Cells were incubated with rabbit anti-FFA2-pSer²⁹⁶/pSer²⁹⁷ or rabbit anti-FFA2-pThr³⁰⁶/pThr³¹⁰ antiserum (1:250) overnight, and with goat anti-rabbit IgG AlexaFluor-546 secondary antibody (1:400; magenta) for 2h. Nuclear DNA was labelled with DAPI (blue). Images were taken with 63 \times objective of Zeiss 880 Laser Scanning Confocal Microscope. Scale bar represents 10 μ m. Inset shows an enlarged image of a representative neutrophil from the corresponding main image. Representative of 3 fields of view each from 3 experiments (n=3, where each n represents neutrophils pooled from 2-4 mice). HA - haemagglutinin.

The analysis of the above figures has so far been descriptive, relying on distinguishing visually very similar images. Fortunately, the uniform size of neutrophils allows for easy quantification of fluorescence intensities. As in **Section 3.2.4**, fluorescence intensity was quantified in three cells and three zones in the background. Measured intensities were corrected first for area and then for background. Data was then collated from 2-3 individual images (see **Section 2.10.2**).

In hFFA2-HA neutrophils, fluorescence intensity of pSer²⁹⁶/pSer²⁹⁷ (*Figure 5.38A*) was not significantly different between vehicle (4.07 ± 0.40) and C3-treated (3.57 ± 0.22) neutrophils. Although CATPB induced a slight reduction in intensity for both conditions (to 3.19 ± 0.33 and 2.41 ± 0.36 , respectively), this was not found to be significant (determined by one-way ANOVA). Neutrophils treated with vehicle, CATPB or C3 had significantly higher intensity than minus-CRE (1.54 ± 0.24 ; $p < 0.0001$, $p < 0.01$ and $p < 0.001$, respectively), while treatment with a combination of C3 and CATPB resulted in no significantly different intensity. The intensity of HA varied slightly from $4.55 (\pm 0.49)$ up to $5.09 (\pm 0.25)$ but the differences were not found to be significant (*Figure 5.38B*). All of the HA intensities were significantly different from the HA intensity measured in minus-CRE neutrophils (1.83 ± 0.14 ; $p < 0.0001$). These results reflect the trends observed thus far, whereby pSer²⁹⁶ and/or pSer²⁹⁷ was detected by the anti-pSer²⁹⁶/pSer²⁹⁷ antiserum to the same levels in the absence and presence of C3. This ligand-independent phosphorylation did not appear to be amenable to antagonist treatment. For intensities measured for pThr³⁰⁶/pThr³¹⁰ (*Figure 5.38C*), treatment with vehicle (2.00 ± 0.26), CATPB (2.29 ± 0.26), and C3 and CATPB (2.29 ± 0.28) yielded intensities not significantly different from minus-CRE (1.23 ± 0.17). On the other hand, C3-treated cells produced significantly higher signal (4.26 ± 0.35 ; $p < 0.0001$) than minus-CRE neutrophils and vehicle-treated neutrophils. Pre-treatment with CATPB caused a significant decrease in fluorescence intensity in comparison to C3-treated neutrophils ($p < 0.0001$). Increased binding of anti-pThr³⁰⁶/pThr³¹⁰ in C3-treated neutrophils could again reflect the agonist-dependent phosphorylation at this site. Unlike Ser²⁹⁶/Ser²⁹⁷, this site appeared to be amenable to inhibition by CATPB. While HA expression was significantly higher than minus-CRE (1.41 ± 0.08 ; $p < 0.0001$ to $p < 0.05$) in all of the other conditions (*Figure 5.38D*), the pattern of fluorescence intensity of

HA paralleled that of pThr³⁰⁶/pThr³¹⁰, with C3-treated neutrophils (5.82±0.58) displaying a significantly higher intensity than vehicle (3.15±0.26; p<0.0001) or C3 and CATPB-treated (3.39±0.17; p<0.001) neutrophils.

The pattern of activation in hFFA2-DREADD-HA neutrophils was found to be somewhat different. Fluorescence intensity of pSer²⁹⁶/pSer²⁹⁷ (*Figure 5.38E*) was not significantly different from minus-CRE neutrophils (1.54±0.24) in neutrophils treated with vehicle (2.57±0.28), CATPB (2.97±0.42) or SA and CATPB (2.67±0.52). SA-treated neutrophils, on the other hand, displayed significantly higher intensity (4.07±0.45; p<0.001) than minus-CRE, but not vehicle-treated hFFA2-DREADD-HA neutrophils. While causing apparent decrease in SA-induced fluorescence, pre-treatment with CATPB caused no significant changes in fluorescence intensity. This is in contrast to the inhibitory effect of CATPB observed in WB with hFFA2-DREADD-eYFP. The fluorescence intensity of HA was significantly higher in hFFA2-DREADD-HA neutrophils under all conditions than in minus-CRE neutrophils (1.83±0.14) (*Figure 5.38F*). HA intensity was also significantly higher in CATPB-treated neutrophils (9.09±0.90) than in neutrophils treated with both SA and CATPB (6.00±0.65; p<0.05). The intensity of pThr³⁰⁶/pThr³¹⁰ was found to be significantly different from minus-CRE neutrophils in all conditions (p< 0.0001 to p<0.05; *Figure 5.38G*). There was a significant difference between vehicle (2.08±0.13) and CATPB treated neutrophils (2.88±0.24; p<0.05), but not between SA (2.24±0.22), and SA and CATPB-treated neutrophils (2.34±0.16). The fluorescence from HA was found to be significantly higher in all conditions of hFFA2-DREADD-HA than in minus-CRE neutrophils (p<0.0001 to p<0.01; *Figure 5.38H*). However, HA intensity in CATPB-treated neutrophils (7.75±0.73) was significantly higher than in vehicle-treated (4.48±0.43; p<0.01). CATPB pre-treatment also produced higher intensity for HA (6.87±0.82) than SA on its own (4.27±0.43; p<0.05)

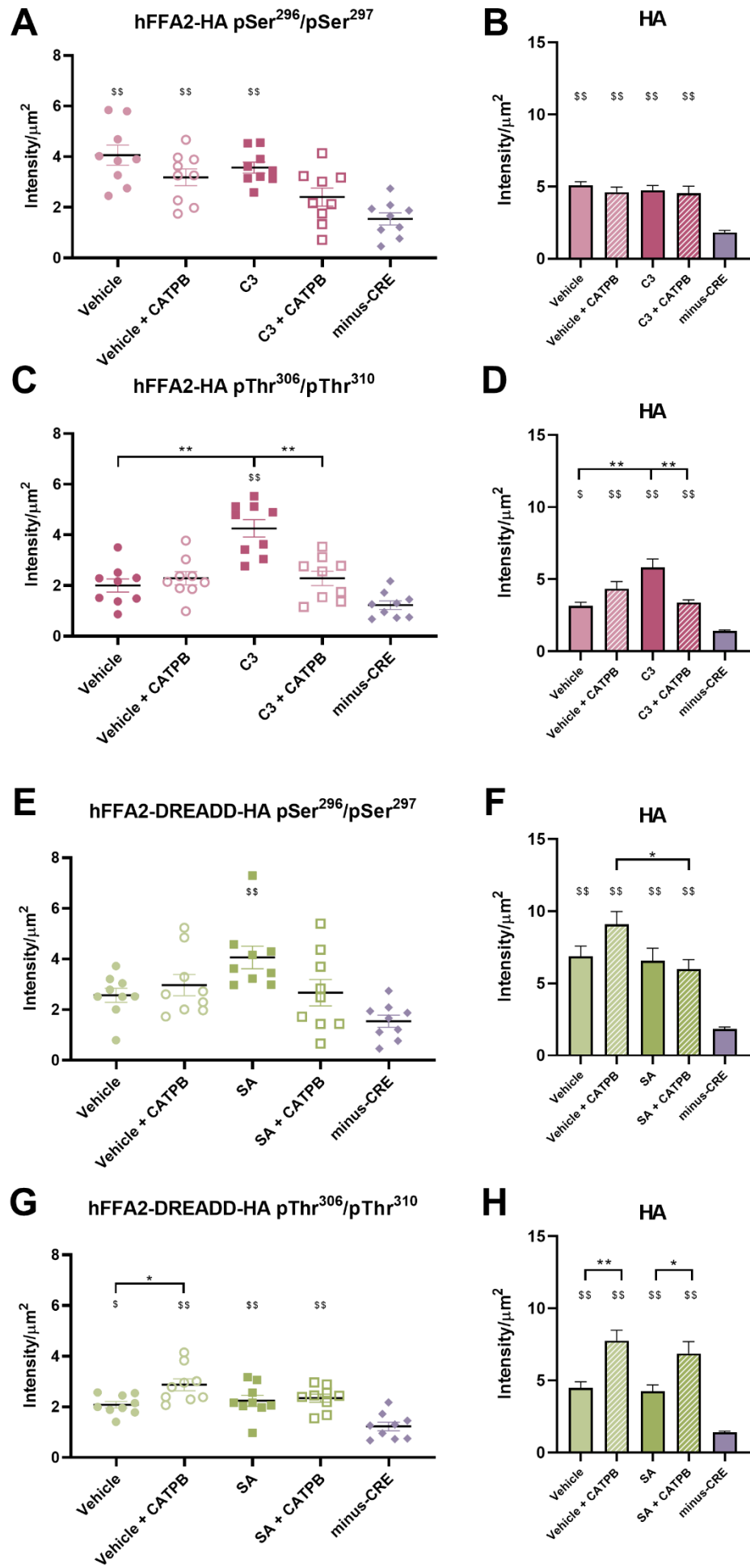


Figure 5.38. Immunocytochemical detection of hFFA2-HA and hFFA2-DREADD-HA phosphorylation in mouse neutrophils. Bone marrow-derived neutrophils isolated from hFFA2-HA (A-D) or hFFA2-DREADD-HA (E-H) mice were pre-incubated with $3\mu\text{M}$ CATPB for 1h, followed by treatment with vehicle, 2mM propionate (C3) or 1.7mM sorbic acid (SA) for 2min. Samples were stained with rat anti-HA primary antibody (B, D, F, H), and rabbit anti-FFA2-pSer²⁹⁶/pSer²⁹⁷ (A, E) or rabbit anti-FFA2-pThr³⁰⁶/pThr³¹⁰ (C, G) antiserum. Fluorescence intensity from goat anti-rabbit AlexaFluor-546 and goat anti-rat AlexaFluor-488 secondary antibodies from individual neutrophils was measured using ZENBlue software and corrected for area and background fluorescence. Data shown as mean \pm SEM (n=3, where each n represents neutrophils pooled from 2-4 mice). \$\$ p<0.01, \$ p<0.05 by one-way ANOVA with Tukey's post-hoc multiple comparisons test against minus-CRE. ** p<0.01, * p<0.05 by one-way ANOVA with Tukey's post-hoc multiple comparisons test. HA - haemagglutinin.

Due to the variation in the fluorescence intensity of HA, and therefore potential variation in receptor expression levels, interpreting the above data can be misleading. In order to compensate for this variation, fluorescence ratios were calculated as the ratio of fluorescence intensity of phosphosite-specific antisera and that of HA (*Figure 5.39*). Thus, in hFFA2-HA, pSer²⁹⁶/pSer²⁹⁷ produced an equivalent value in vehicle (0.79 ± 0.06) and C3-treated neutrophils (0.77 ± 0.04). Although the response produced by both vehicle (0.68 ± 0.04) and C3 (0.54 ± 0.07) appeared to be lower following pre-treatment with CATPB, neither of these were significant reductions (determined by one-way ANOVA). The intensity of pThr³⁰⁶/pThr³¹⁰ increased slightly but insignificantly in C3-treated neutrophils (0.75 ± 0.05) in comparison to vehicle (0.62 ± 0.05). Apparent inhibition by CATPB was modest and also insignificant both for C3-treated (0.67 ± 0.08) and untreated (0.54 ± 0.04) neutrophils. In hFFA2-DREADD-HA neutrophils, pSer²⁹⁶/pSer²⁹⁷ displayed an increase from vehicle (0.37 ± 0.01) and SA-treatment (0.67 ± 0.08), although not a significant one. CATPB pre-treatment caused no apparent change in the response produced by vehicle (0.33 ± 0.03), however it did cause a larger, albeit still insignificant, decrease in SA-induced effects (0.46 ± 0.10). Vehicle (0.54 ± 0.09) and SA-treated neutrophils (0.57 ± 0.09) produced responses of equivalent magnitude in pThr³⁰⁶/pThr³¹⁰ fluorescence. While moderate inhibition was caused by CATPB pre-treatment, this was not significant for either vehicle-treated (0.39 ± 0.05) or SA-treated (0.39 ± 0.06) neutrophils.

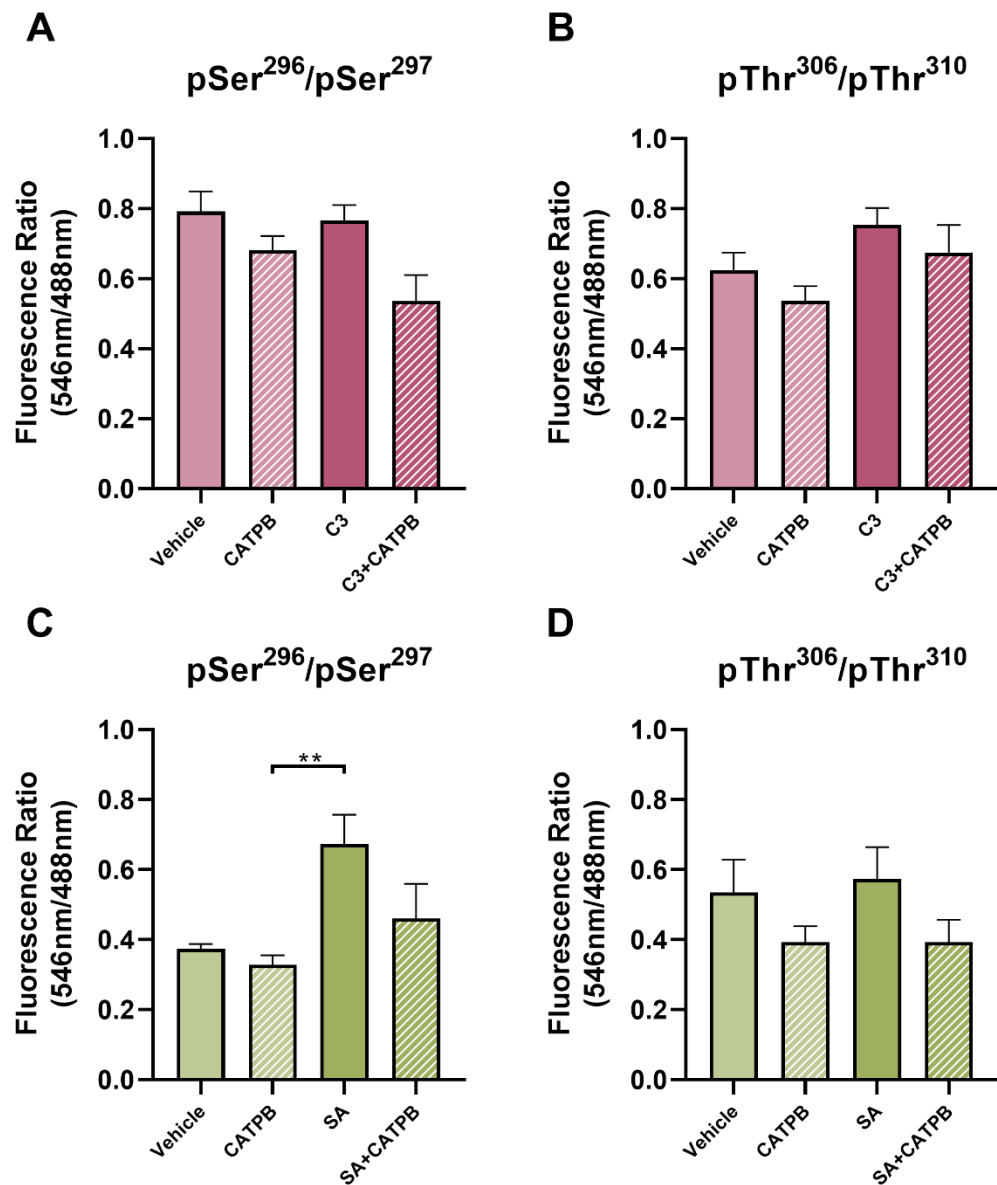


Figure 5.39. Fluorescence ratios of immunocytochemical staining of mouse neutrophils. Bone marrow-derived neutrophils isolated from hFFA2-HA (A, B) or hFFA2-DREADD-HA (C, D) mice were pre-incubated with 3 μ M CATPB for 1h, followed by treatment with vehicle or 2mM propionate (C3) or 1.7mM sorbic acid (SA) for 2min. Samples were stained with rat anti-HA primary antibody, and rabbit anti-FFA2-pSer²⁹⁶/pSer²⁹⁷ (A, C) or rabbit anti-FFA2-pThr³⁰⁶/pThr³¹⁰ (B, D) antiserum. Fluorescence intensity from goat anti-rabbit AlexaFluor-546 and goat anti-rat AlexaFluor-488 secondary antibodies from individual neutrophils was measured using ZENBlue software and corrected for area and background fluorescence. Fluorescence ratio was calculated by dividing fluorescence intensity at 546nm (phosphosite-specific antisera) with fluorescence intensity at 488nm (HA). Data shown as mean \pm SEM (n=3, where each n represents neutrophils pooled from 2-4 mice). ** p<0.01 by one-way ANOVA with Tukey's post-hoc multiple comparisons test.

5.3 Discussion

5.3.1 Phosphosite-specific antisera selectively recognise activated hFFA2 and hFFA2-DREADD

Despite traditionally being considered the end of signalling, in many ways, GPCR phosphorylation constitutes the initial step for numerous downstream cellular processes. The subsequent recruitment of arrestins not only regulates receptor signalling through G proteins, but also generates signalling cascades through interaction with potentially hundreds of other proteins (Xiao et al., 2010). As a result, modulation of these specific pathways independently of G protein-mediated pathways could prove potentially therapeutically useful (Jean-Charles et al., 2017). The development of antisera which are able to bind specific phosphorylated sites on the intracellular surface of GPCRs can both reveal the phosphorylation status of receptor, and subsequently help identify compounds which modulate this in the desired manner.

In the absence of mass spectrometry data for FFA2, there were no preconceived theories as to the phosphorylation patterns that might be observed in either the absence or presence of receptor ligands. Through initial experiments, hFFA2 was found to be phosphorylated in a ligand-independent manner at residues Ser²⁹⁶/Ser²⁹⁷, while residues Thr³⁰⁶/Thr³¹⁰ showed agonist-dependent phosphorylation. No phosphorylation was detected by a potential anti-pSer³²⁴/pSer³²⁵ antiserum which could have two implications: either no phosphorylation occurs at these residues, or the antiserum was unable to detect the phosphorylated residues. Although the Ser and Thr residues assessed are conserved in mFFA2, the differences in the surrounding sequences appeared to be sufficient to ablate antiserum binding. Alternatively, the expression of mFFA2-eYFP might not have been equivalent to that of hFFA2-eYFP, despite using the same concentration of DOX to induce receptor expression. Evaluation of receptor expression in Flp-In T-REx cells would be required if these antisera were to be re-evaluated at mFFA2-eYFP. It is unlikely that these residues in mFFA2 are not phosphorylated at all, considering the necessity of this for receptor desensitisation and internalisation. Perhaps most surprisingly, the phosphorylation pattern in hFFA2-DREADD appeared to be distinct from the WT hFFA2 receptor, in that phosphorylation at residues Ser²⁹⁶/Ser²⁹⁷ appeared to be

agonist-dependent (in contrast to the ligand-independent phosphorylation in the WT). The possibility of WT hFFA2 being activated by contents of the cell culture medium was minimised by serum starving all cells prior to agonist treatment. As a result, the difference between the two receptors must be explained by the two point-mutations present in the DREADD version (Cys¹⁴¹Gly and His²⁴²Gln). This mutant has been shown to have lost affinity for the endogenous SCFA hFFA2 agonists and can only be activated by the synthetic ligands SA (Hudson et al., 2012a) and MOMBA (Barki et al., 2022). In previous studies, the ability of hFFA2-DREADD to induce β -arrestin-2 recruitment was not impaired. Although the mutations have previously been shown to change ligand selectivity but not signalling, the phosphorylation patterns underlying signalling have not been investigated directly. Potentially, the two mutations that give rise to the DREADD receptor could be sufficient to change the receptor conformation in a manner that alters binding of and interaction with GRKs responsible for agonist-independent phosphorylation at residues Ser²⁹⁶/Ser²⁹⁷ (Matthees et al., 2021).

Several blots presented in this chapter displayed some unusual binding patterns. For one, intensities were variable between certain cell lines and treatments. As each figure represents 2 or 3 similar blots, it is unlikely that such differences were the result of random variation. Similarly, since immunoprecipitation of samples for several blots was performed simultaneously, no major differences would be explained by the variability of GFP-trap efficiency. That is, the low intensity signal detected by the anti-GFP antibody in mFFA2-eYFP is probably due to differences in expression, rather than inefficient immunoprecipitation. Another interesting observation was the heightened intensity of samples in experiments involving λ PP (including in blots not presented in this thesis). While no clear explanation exists for this, it should be noted that these samples were incubated in an additional buffer during sample preparation which may have influenced the final detection intensity. Finally, hFFA2-DREADD-eYFP presented consistently more robust signals in comparison to hFFA2-eYFP. This could very well be explained by the concentration of SA utilised in these experiments. Indeed, SA is a more potent agonist than C3 in various assay platforms (Hudson et al., 2012a, Bolognini et al., 2019), yet the concentrations of each agonist used herein were very similar. Although in these experiments both C3 and SA were used at EC₉₀ concentrations, these were calculated based on initial

[³⁵S]GTPγS binding experiments. As G-protein activation may not clearly correlate with receptor phosphorylation, a potentially improved estimate could be calculated based on β-arrestin-2 recruitment (a process associated with phosphorylation).

Although polypeptides were present at the expected size of the eYFP-tagged receptor (~64kDa), additional polypeptides of both higher and lower molecular masses were present on all blots. While polypeptides of lower molecular mass could represent breakdown products, those of apparent higher mass could be the result of a number of processes. Larger polypeptides were present at ~125kDa and ~250kDa, which correspond to approximately double and quadruple predicted receptor molecular mass, respectively. FFA2 and FFA3 have been shown to form heterodimers with each other (Ang et al., 2018), and although homodimers have not been reported, this may simply reflect that the topic has not been addressed. Another possibility is the aggregation of proteins as a result of heating during sample preparation. Samples were incubated for 10min at 60°C, however high temperatures can lead to the formation of aggregates and the loss of detection by antibodies (Tsuji, 2020, McLane et al., 2007). Finally, post-translational modifications such as various states of glycosylation can give rise to polypeptides of numerous molecular masses. In the case of N-glycosylation, commonly present in many GPCRs and other transmembrane polypeptides, the enzyme N-glycosidase F could be employed in order to hydrolyse glycosylamine bonds (Maley et al., 1989), to thus eliminate such post-translational modifications.

Before further studies could be conducted with the anti-pSer²⁹⁶/pSer²⁹⁷ and anti-pThr³⁰⁶/pThr³¹⁰ antisera, their specificity for phosphorylated residues was tested. As the dephosphorylation of all residues on the receptor with the use of λPP resulted in a loss of detection by both antisera in hFFA2, they were confirmed to bind phosphorylated residues. In addition, CATPB was able to inhibit agonist-induced phosphorylation at residues Thr³⁰⁶/Thr³¹⁰ for both receptors, and at residues Ser²⁹⁶/Ser²⁹⁷ in the case of hFFA2-DREADD. Phosphorylation at Ser²⁹⁶/Ser²⁹⁷ was not inhibited in WT hFFA2, further supporting the agonist-independent activity at this site. Although CATPB has been described as an inverse agonist, such effects have only been observed in

[³⁵S]GTPγS incorporation and cAMP inhibition assays (Hudson et al., 2012b), and may not extend to arrestin-mediated signalling. As to how such differences between the sites may be possible could be explained by the identity of GRKs involved in their phosphorylation. Different ligands conceptually stabilise the receptor in distinct conformations, thus influencing GRK binding and phosphorylation. Indeed, GRK2/3 and GRK5/6 have been shown to phosphorylate distinct sites in β₂ adrenergic receptors, thus generating a “site-specific barcode” (Nobles et al., 2011). This, in turn, may have implications on downstream phosphorylation-dependent, or potentially β-arrestin-mediated functions such as internalisation and ERK signalling (Yang et al., 2015). Thus, the conformations stabilised by CATPB may prevent interaction with the GRK responsible for the phosphorylation of Ser²⁹⁶/Ser²⁹⁷ in hFFA2-DREADD but not in WT FFA2.

In this case, manipulation of GRKs could help define their contribution to the potentially differential phosphorylation of the receptors. Perhaps the most straightforward approach would be the use of pharmacological agents: 3-[[[4-methyl-5-(4-pyridyl)-4H-1,2,4-triazole-3-yl]methyl]amino]-N-[2-(trifluoromethyl)-benzyl]benzamidehydrochloride (**Compound 101**) acts as an inhibitor of GRK2/3 (Thal et al., 2011, Lowe et al., 2015), while N2-(4-chloro-2-methoxybenzyl)-N4-(5-ethyl-1H-pyrazol-3-yl)-5-methoxyquinazoline-2,4-diamine (**Compound 18**) is a newly described inhibitor of GRK5/6 (Uehling et al., 2021). The use of antagonists, however, does not account for the relative expression of each GRK subtype being inhibited. Off-target effects at higher concentrations can also be a source of misleading results. Recently, multiple groups have utilised HEK293 cells where individual or multiple GRKs were removed using CRISPR/Cas9 technology. Harnessing this technology has allowed, for example, demonstration of the contribution of GRK2 and GRK3 to β-arrestin-2 recruitment and internalisation of μ opioid receptors (Møller et al., 2020). There is also some evidence for GPCRs being either preferentially GRK2/3-regulated or GRK2/3/5/6-regulated, thus mediating differential responses (Drube et al., 2022). Furthermore, removal of the full complement of GRKs has revealed not only their contribution to internalisation and ERK signalling, but also Gα_{q/11} interactions which lead to GRK subtype selectivity (Kawakami et al., 2022). This latter finding is particularly interesting for the investigation of FFA2, as it has a

promiscuous signalling profile and a $G\alpha_{i/o}$ -biased ligand (AZ1729) available. Whether using antagonists or CRISPR/Cas9-edited cells, elimination of various combinations of GRKs might reveal how a phosphorylation barcode observed in FFA2 and FFA2-DREADD might be generated.

While WB requires denaturation of antigens, paraformaldehyde fixation in ICC can modify antigens by inducing cross-linking. Thus, it is not uncommon for antibodies to show specific binding in one of these assays but not the other (Willingham, 1999, Ramos-Vara and Miller, 2014). However, ICC experiments using cells expressing eYFP-tagged hFFA2, hFFA2-DREADD and mFFA2 corroborated the observations from WB experiments. No activity was observed in mFFA2, however, based on the intensity of eYFP, the expression of the receptor appeared to be low. In hFFA2 and hFFA2-DREADD both antisera sensed phosphorylation. The difference in agonist-dependency between hFFA2 and hFFA2-DREADD at residues Ser²⁹⁶/Ser²⁹⁷ were also observed using this method. Interestingly, phosphorylated receptors were observed both on the cell membrane and intracellularly. Whether the intracellular receptors are simply downregulated or are involved in endosomal signalling warrants further exploration.

5.3.2 Mutational alteration of phosphorylation sites affects antiserum binding and hFFA2 receptor function

Although in *Section 5.3.1* it was demonstrated that the phosphosite-specific antisera do indeed bind phosphorylated residues on the hFFA2 and hFFA2-DREADD, it has not yet been shown whether the binding actually occurs at the residues indicated by the manufacturer. To this end, PD mutants of the receptor were generated, whereby the pairs of residues conceptually targeted by the phosphosite-specific antisera were mutated into Ala.

In the case of hFFA2-PD2 (Thr³⁰⁶Ala-Thr³¹⁰Ala), binding of the anti-pThr³⁰⁶/pThr³¹⁰ antiserum was ablated, while that of anti-pSer²⁹⁶/pSer²⁹⁷ was maintained, which could be expected if anti-pThr³⁰⁶/pThr³¹⁰ did indeed bind pThr³⁰⁶ and/or pThr³¹⁰. Unexpectedly, the hFFA2-PD1 mutant (Ser²⁹⁶Ala-Ser²⁹⁷Ala) lost interaction with both antisera. In ICC staining of Flp-In T-REx 293 cells expressing the PD mutants of hFFA2-eYFP, similar loss of interactions was

observed in hFFA2-PD1 and hFFA2-PD2. On one hand, this could be the result of the anti-pThr³⁰⁶/pThr³¹⁰ antiserum losing affinity to the receptor as a direct result of the change in the amino acid sequence. Importantly, these mutants were generated based on the assumption that the antisera bind to both of the phosphorylated residues they target. To explore whether this is the case, mutants of single residues would be required.

On the other hand, these results could also hint at a temporal hierarchy of phosphorylation. As discussed before, GPCRs may be subject to differential phosphorylation depending on the cellular context (Tobin, 2008). Based on this, there is a possibility that the phosphorylation of Ser²⁹⁶/Ser²⁹⁷ is a prerequisite for the phosphorylation of Thr³⁰⁶/Thr³¹⁰. This would explain why the loss of ligand-independent phosphorylation at Ser²⁹⁶/Ser²⁹⁷ was accompanied by loss of phosphorylation at Thr³⁰⁶/Thr³¹⁰. Such hierarchy has been observed in rhodopsin (Ohguro et al., 1993) and the δ opioid receptor (Kouhen et al., 2000), among others.

It is impossible to draw conclusions based on the experiments performed here alone, however by establishing the phosphorylation barcode of hFFA2 (with the use of either GRK inhibitors or with GRK-KO cells), a more comprehensive picture could be constructed. In addition, it would be of interest to generate PD versions of hFFA2-DREADD, in order to examine the extent to which the constitutively phosphorylated site (which appeared to be agonist-dependent in hFFA2-DREADD) underlies the phosphorylation of other sites in hFFA2.

As effective recruitment of arrestins occurs as a consequence of receptor phosphorylation, β -arrestin-2 recruitment was next examined both in WT and mutant receptor constructs. Initial β -arrestin-2 BRET experiments with hFFA2, mFFA2 and hFFA2-DREADD reflected past findings using RLuc-based probes. That is, no β -arrestin-2 recruitment was observed in mFFA2, while maximum efficacy produced by SA in hFFA2-DREADD was significantly higher than that of C3 in hFFA2 (Hudson et al., 2013, Hudson et al., 2012a). As to why such a difference in β -arrestin-2 recruitment should be produced by hFFA2-DREADD is not clear, however it may very well relate to the differential phosphorylation pattern observed with the use of phosphosite-specific antisera. Even though

phosphorylation and β -arrestin-2 recruitment both occur on the intracellular surface of the receptor, the DREADD mutations on TM4 and TM6 appear to have influenced both of these processes. In fact, even a single mutation may induce conformational changes on the intracellular surface of the active receptor, resulting in variations in effector coupling. Indeed, charge-altering mutants of Lys⁶⁵ display significantly reduced β -arrestin-2 recruitment upon agonist treatment, even though this residue is not involved in agonist binding (Sergeev, 2018). It is thus not inconceivable that signal transduction through conformational changes would affect downstream coupling abilities of the receptor.

The fact that β -arrestin-2 recruitment assays were conducted in transiently transfected cells, rather than in stably transfected cell lines, provided a greater freedom for exploring a wider range of mutants. In addition to the “single-site” PD mutations, where the pairs of residues targeted by the phosphosite-specific antisera were mutated to Ala, “double-site” and “triple-site” PD mutants were generated, with two and three pairs of residues mutated to Ala, respectively. In the absence of residues to accept phosphate groups, the Px(x)PxxP residue pattern believed to interact with the positively charged pockets on β -arrestins is absent, thus causing a reduction in β -arrestin-2 recruitment (Zhou et al., 2017).

None of the PD mutations affected the potency of C3, however there were significant effects on its efficacy. Interestingly, mutations at residues Ser³²⁴/Ser³²⁵ appeared to have the most significant impact on ligand efficacy, both on their own and in combination with other mutations. The removal of this site also produced a significant decrease in baseline mBRET, suggesting that this site is involved in baseline phosphorylation of hFFA2. These observations were surprising for multiple reasons. For one, phosphorylation at this site has not been observed with the use of the phosphosite-specific antiserum. Of course, this could be the result of the antiserum lacking affinity for the phosphorylated residues. The other unexpected finding was the lack of significant impact of Ser²⁹⁶/Ser²⁹⁷ mutations. Considering that both WB and ICC revealed this site of hFFA2 to be constitutively modified, it was anticipated that mutations to alter these residues would have a lower basal or significantly impaired agonist-induced β -arrestin-2 recruitment. Interestingly, mutation of all 6 residues to Ala

did not ablate agonist induced β -arrestin-2 recruitment completely, suggesting that further sites may be involved in the interactions with β -arrestin-2. Indeed, hFFA2 contains two further Thr residues at positions 328 and 329 as well as several Ser residues on the ICLs (see *Figure 5.1*). In addition, in FFA4, acidic residues (glutamic acid and aspartic acid) of the C-terminal tail were found to contribute to the effectiveness of β -arrestin-2 recruitment (Butcher et al., 2014). As several of these residues are also present in hFFA2, it is possible that some of the remaining activity is coordinated by their interaction with β -arrestin-2. An alternative explanation for the observed lower signalling could be due to altered interaction kinetics as a result of the PD mutations. As β -arrestin-2 recruitment was measured at a 5-min endpoint, a shift towards more transient signalling might manifest as a lower BRET signal at the same timepoint measurement (Hoare et al., 2020). Conversely, any apparent increase may reflect a shift to more sustained signalling. Kinetic studies around the PD mutants would therefore be required to fully elucidate the role of these residues in β -arrestin-2 interactions.

In addition, the Ser³²⁴Ala-Ser³²⁵Ala mutation led to an unexpected, significant reduction in [³⁵S]GTP γ S incorporation in response to agonist treatment. Conceptually, the elimination of β -arrestin-2-mediated signalling should not affect other signalling pathways (Bradley et al., 2016b, Marsango et al., 2022b). If phosphorylation at this site and the associated β -arrestin-2 interaction is indeed constitutive, it is unclear how its elimination would lead to diminished signalling through G proteins. As BRET and [³⁵S]GTP γ S incorporation were conducted in transiently and stably transfected cell lines, respectively, it is unlikely that reduction was the result of differences in transfection efficiency. However, the possibility of reduced expression of the receptor cannot be excluded. If this is the case, the role of Ser³²⁴/Ser³²⁵ in receptor trafficking would warrant further exploration.

Generally, β -arrestin binding involves interactions between the phosphorylated residues of the GPCR C-terminal tail or ICL3, and the positively charged residues in the β -arrestin N-domains, as well as between the finger loop region of the β -arrestin and the opened intracellular cavity of the receptor. However, in certain complexes, β -arrestin assumes a “hanging” configuration by binding to the

phosphorylated C-terminal residues exclusively (Thomsen et al., 2016, Nguyen et al., 2019), thus allowing maintained signalling through G proteins. However, to date this configuration has only been demonstrated for β -arrestin-1 interacting with internalised receptors. As [35 S]GTP γ S incorporation assays were performed in membrane preparations rather than whole cells, endosomal receptors might be present, therefore changes at these super-complexes might have influenced the outcomes of this assay. In order to further explore this issue, two outcomes in particular should be investigated: the recruitment of β -arrestin-1 and receptor internalisation. GPCRs interact with β -arrestin-1 and β -arrestin-2 differentially, potentially contributing to distinct downstream signalling (Zurkovsky et al., 2017, Gurevich and Gurevich, 2019). This differential response relies on the conformational signature of β -arrestins, which can be dependent on the nature of the ligand, the identity of the GRKs responsible for the receptor phosphorylation, and the phosphorylation barcode (Lee et al., 2016). In order to gain a comprehensive picture of these interactions, in addition to exploring PD mutants, β -arrestin recruitment should be investigated in concert with experiments using GRK inhibitors described previously. Although β -arrestins can interact with a vast array of downstream effectors (Xiao et al., 2010), internalisation through their interaction with clathrin (Goodman et al., 1996) provides an outcome which can be tracked visually through confocal microscopy. Indeed, the effect of PD mutations on receptor internalisation has been shown in δ -opioid receptors (Mann et al., 2020), FFA4 (Butcher et al., 2014) and GPR84 (Marsango et al., 2022b), among many others. Internalisation of hFFA2 was not successfully demonstrated within the scope of this project, however it would greatly aid our understanding of FFA2-signalling, if completed.

5.3.3 Phosphosite-specific antisera can track receptor phosphorylation *in vitro* and *ex vivo*

Although experiments in overexpressing cell lines can inform our understanding of the complex interactions involved in non-G protein-mediated signalling, they do not necessarily reflect the outcomes in primary cells. For this reason, the same phosphosite-specific antisera were employed in mouse neutrophils. However, due to the difference between the receptor tag utilised in the previous sets of experiments (eYFP) and the one present in the transgenic

animals (HA), the antisera were required to be verified with the latter as well. Throughout these experiments, hFFA2-HA and hFFA2-DREADD-HA were used in parallel, as mice expressing each of these constructs were available. On one hand, this would confirm the differential signalling between the two variants of FFA2 observed the eYFP-tagged receptors. In addition, hFFA2-DREADD-HA would not be affected by potentially circulating SCFAs which could activate hFFA2-HA (Bolognini et al., 2019, Barki et al., 2022).

Initial experiments with HA-tagged receptors in Flp-In T-REx 293 cells were conceptually identical to those conducted with eYFP-tagged receptors. Importantly, for WB, samples were immunoprecipitated with the use of anti-HA-agarose antibody (or HA-trap) and immunoblotted with an anti-HA antibody as a control. An immediate observation with the use of the HA-trap was the presence of smearing which surpassed that of the GFP-trap. This could be the result of the HA-trap containing conjugated IgG (heavy and light chains), while the GFP-trap is based on significantly smaller nanobodies (Fang et al., 2020). For both receptor variants, polypeptides were detected at the expected size of ~40kDa (37.1kDa + ~3kDa for the HA-tag), as well as several higher molecular masses, similar to eYFP-tagged receptors (discussed in **Section 5.3.1**). In these initial blots, hFFA2-HA showed activation at Ser²⁹⁶/Ser²⁹⁷ in the absence of agonists, however this was enhanced by the addition of C3. At the same site in hFFA2-DREADD-HA, activation was entirely SA-dependent. At residues Thr³⁰⁶/Thr³¹⁰, both receptor variants displayed agonist-dependent activation. Unfortunately, attempts to conduct similar experiments in neutrophils were unsuccessful, where no HA was detected despite utilising protein concentrations equivalent to those used for Flp-In T-REx 293 cells. Increasing the amount of neutrophils used further would have required sacrificing a large number of animals, which led to the use of alternative methods to measure neutrophil phosphorylation.

ICC experiments using Flp-In T-REx 293 cells expressing HA-tagged receptors were performed not as a mere repetition of those employing eYFP-tagged receptors, as they were extended to include pre-treatment with the antagonist CATPB. The phosphosite-specific antisera displayed activation patterns corresponding to those observed in the eYFP-tagged receptors for both hFFA2-HA and hFFA2-DREADD-HA. Phosphorylation of Ser²⁹⁶/Ser²⁹⁷ was independent of

agonist treatment in hFFA2-HA, but agonist-dependent in hFFA2-DREADD-HA. By contrast, Thr³⁰⁶/Thr³¹⁰ phosphorylation was agonist-dependent for both receptors. Importantly, relatively high levels of non-specific binding was observed for Thr³⁰⁶/Thr³¹⁰ in the absence of agonists. Pre-treatment with CATPB did not inhibit phosphorylation of Ser²⁹⁶/Ser²⁹⁷ in hFFA2-HA, further corroborating previous observations about the agonist-independent phosphorylation of these residues. Phosphorylation at the same site was, however, inhibited in hFFA2-DREADD-HA, albeit not fully. Treatment with CATPB resulted in the loss of agonist-induced specific antiserum binding at residues Thr³⁰⁶/Thr³¹⁰ for both receptors. Considering that the effects of both agonist and antagonist treatment could be observed using ICC in Flp-In T-REx 293 cells, it was reasonable to infer that receptor phosphorylation might be tracked similarly in mouse-derived neutrophils.

There were two main issues encountered in the experiments investigating hFFA2 phosphorylation in neutrophils. As expected from expression levels of hFFA2-HA (*Chapter 3*), fluorescence intensities were low in every channel. This caused particular challenges when images from several conditions appeared to be highly similar at the level of visual inspection. Fortunately, this issue could be addressed by applying the same quantification method employed in *Section 3.2.4*, whereby fluorescence intensities of individual neutrophils were measured and averaged for each condition. Circumventing the other main difficulty, however, was less straightforward. In comparison to Flp-In T-REx 293 cells, neutrophils are not only significantly smaller, but also have a nucleus which occupies a higher proportion of intracellular space. This, in combination with the relatively low intensity and resolution, made distinguishing non-specific binding of the antisera from any specific binding particularly difficult.

Quantification of fluorescence intensities yielded somewhat contradictory results, confounded by potentially varying levels of receptor expression. As expected, fluorescence intensity corresponding to the HA-tag was significantly higher in all of the conditions for hFFA2-HA and hFFA2-DREADD-HA compared to the cells from the minus-CRE line, thus demonstrating receptor expression. In the case of the phosphosite-specific antisera, no significant difference from minus-CRE would conceptually correspond to non-phosphorylated receptors,

while significant differences would therefore be consistent with receptor phosphorylation. Fluorescence intensity of such phosphosite-specific antisera would, of course, differ if the expression levels of the receptor varied significantly. With the exception of anti-pSer²⁹⁶/pSer²⁹⁷ in hFFA2-HA, each neutrophil strain and antiserum displayed a significant variability in HA fluorescence intensity, and therefore in receptor expression levels. Importantly, in preliminary studies using phosphosite-specific antisera in hFFA2-HA mouse tissues, a lowered HA-signal was observed in some cells displaying agonist-dependent phosphorylation. This may be the result of the proximity of the HA-tag on the C-terminus and the amino acids targeted by the phosphosite-specific antisera. The antisera and the anti-HA antibody may be physically hindered from binding simultaneously, thus manifesting in changes in the HA-signal. By calculating the ratio of fluorescence intensities between the phosphosite-specific antisera and HA, the potential confounding effect of differential receptor expression or differential binding could be normalised. According to this analysis, both vehicle and C3-treatment yielded a high fluorescence at residues Ser²⁹⁶/Ser²⁹⁷ of hFFA2-HA. At residues Thr³⁰⁶/Thr³¹⁰, C3 treatment did moderately increase fluorescence to similar levels observed at Ser²⁹⁶/Ser²⁹⁷, however this was not found to be significant. Importantly, CATPB caused insignificant inhibition at both sites, in the presence and absence of an agonist. In hFFA2-DREADD-HA, relatively low basal fluorescence was observed at pSer²⁹⁶/pSer²⁹⁷ which nearly doubled in the presence of SA. Yet, the difference was not significant. Moderate fluorescence was observed in both vehicle and SA-treated neutrophils at pThr³⁰⁶/pThr³¹⁰. Similar to hFFA2-HA, CATPB treatment caused moderate but insignificant inhibition.

There are obvious differences between the results obtained in overexpressing cell lines and in the mouse-derived neutrophils. There are a number of possibilities that might account for these differences. In the case of hFFA2-HA, constitutive phosphorylation at Ser²⁹⁶/Ser²⁹⁷ has now been demonstrated in a range of experiments, however these tended to be resistant to antagonist treatment. In combination with the high basal phosphorylation at Thr³⁰⁶/Thr³¹⁰, this suggests that the hFFA2-HA may have been stimulated by circulating C3 *in vivo*. This is particularly convincing in relation to basal fluorescence measured in hFFA2-DREADD-HA, where systematic activation cannot be a confounding factor.

The relatively high basal phosphorylation at Thr³⁰⁶/Thr³¹⁰ could, of course, be the result of high non-specific binding by the antiserum, as this has been observed in Flp-In T-REx 293 cells.

Besides factors related to the experimental procedure, there can be fundamental differences in the GRK complement expressed in neutrophils in comparison to Flp-In T-REx 293 cells (Uhlen et al., 2015). In fact, neutrophils and HEK293 cells display similar trends in expression, with high levels of GRK2 and GRK6 mRNA, but comparatively low levels of GRK3 and GRK5. However, the absolute expression of GRK2 in neutrophils is higher, while that of GRK3 and GRK6 is lower than in HEK293 cells. (Matthees et al., 2021, Uhlen et al., 2015). If these differences in mRNA do correlate to varying protein levels, they could account for differential phosphorylation in neutrophils. In addition to the suggested WB experiments with GRK inhibitors, there is also a possibility to use these compounds in ICC experiments with both Flp-In T-REx 293 cells and neutrophils, thus potentially aiding the dissection of the phosphorylation process in each of these cell types.

These approaches could provide an insight into tissue responses under normal conditions, however there are potential approaches to investigate FFA2 activation under inflammatory conditions. Colitis can be induced in mice by the introduction of *Salmonella enterica* serovar Typhimurium, which is one of the primary causes of human enterocolitis (Barthel et al., 2003). Not only does this induce gut inflammation, but it does so with the principal involvement of neutrophils (Harris et al., 1972, Winter et al., 2010). In addition, in model systems infection with *S. enterica* is generally preceded by treatment with streptomycin, which eliminates commensal bacteria, and thus the production of SCFAs and *in vivo* FFA2 activation.

Of course, neutrophils constitute only one of many tissues which express FFA2 at considerable levels. In **Chapter 3**, various cell types were confirmed to express hFFA2-HA in the transgenic mouse line, including EECs, and intestinal and splenic immune cells. It would be reasonable to infer that these phosphosite-specific antisera could detect FFA2 phosphorylation in these tissues. In addition, based on the known differences in GRK expression in various tissues, it would be of

particular interest to explore the tissue-specific phosphorylation. Tissues do not only differ in their expression of various GRK subtypes, but also in the levels of each β -arrestin. In neutrophils, the expression of β -arrestin-2 is five times higher than that of β -arrestin-1, while in the colon the two are expressed at similar levels (Matthees et al., 2021). The various combinations of GRKs and β -arrestins could lead to an array of downstream responses which are specific to each tissue type. Exploring these signalling pathways would be a great challenge, requiring further dissection of the “barcode” hypothesis. The experiments presented here are but the initial steps in the exploration of FFA2 phosphorylation, however the phosphosite-specific antisera examined will hopefully constitute an invaluable tool in this endeavour.

CHAPTER 6 - FINAL DISCUSSION

The GPCR superfamily is a massively diverse group of cell-surface receptors (Fredriksson et al., 2003b), which make up approximately 20% of targets for current small molecule drugs (Yang et al., 2021). As such, they are some of the most successful drug targets. This is not surprising, considering that GPCRs sense a wide range of extracellular stimuli and, in turn, generate signalling cascade-mediated cellular responses (Simon et al., 1991). The discovery of GPCRs which respond to metabolites has opened up novel avenues for therapeutic strategies for a number of metabolic and related disorders. Receptors which sense SCFAs produced by the microbiota are of particular interest, as they highlight the close interactions between the commensal bacteria and physiological processes (Milligan et al., 2017). Indeed, the contribution of SCFA receptors has been demonstrated in gut hormone release (Psichas et al., 2015), immune cell activation (Vinolo et al., 2011), insulin secretion (Priyadarshini et al., 2015), inhibition of lipolysis (Bolognini et al., 2019) and neuronal signalling in the PNS (Barki et al., 2022). The range of these responses implicates SCFA receptors as potential targets for the treatment of metabolic and inflammatory disorders, such as IBD. However, the co-expression of FFA2 and FFA3 in the gut (Nohr et al., 2013) and β -cells (Kebede et al., 2009), in combination with a lack of selective tool compounds, has for a long time hindered understanding the contribution of each receptor to these functions. The development of selective orthosteric agonists (Hudson et al., 2013, Hansen et al., 2018) and antagonists (Hudson et al., 2012b, Pizzonero et al., 2014), alongside various allosteric ligands (Wang et al., 2010, Bolognini et al., 2016) has greatly aided the exploration of FFA2 pharmacology. By contrast, FFA3 tool compounds remain limited to a small number of allosteric ligands (Engelstoft et al., 2013, Ulven et al., 2020) which display complex pharmacology in SAR studies (Hudson et al., 2014). This can, at least in part, be circumvented by employing the DREADD version of FFA2, which allows dissection of FFA2-mediated responses from those mediated by FFA3 *in vivo* (Bolognini et al., 2019). Perhaps one of the most significant hurdles for drug development efforts is posed by the differential ligand interactions between species orthologues (Hudson et al., 2013). Indeed, the fact that available antagonists are selective for hFFA2 with no activity at mFFA2 has made pre-clinical mouse model studies all but impossible.

The overarching theme of this thesis has been the characterisation of novel pharmacological tools which may aid future drug development and general research on SCFA receptors. The recent development of a mouse strain expressing hFFA2-DREADD-HA in place of mFFA2 has greatly aided our understanding of the involvement of both FFA2 and FFA3 in physiological processes (Bolognini et al., 2019, Barki et al., 2022). In a similar vein, a new mouse strain expressing hFFA2-HA was generated, with the desire to create a model which would be amenable to treatment with ligands which are selective for hFFA2 (*Chapter 3*). The overall expression-profile of hFFA2-HA mRNA was shown to mirror that of mFFA2 in WT mice. That is, high expression was observed adipose and colon, and relatively low expression in the spleen and bone marrow-derived neutrophils. Not only are these the tissues where FFA2 is canonically expressed (Nohr et al., 2013, Nilsson et al., 2003, Le Poul et al., 2003) but the equivalent levels of expression suggest that hFFA2-HA expression might be regulated under the same conditions as mFFA2 is in WT mice, and therefore would mediate the effects of SCFA to an extent comparable to mFFA2 in a physiological context. In addition to broad mRNA expression in tissues, an attempt was made to delineate subsets of cells where FFA2-HA was expressed at the protein level. In line with expectations, hFFA2-HA was expressed in subsets of cells which express the generic EEC marker ChgA or the anorexigenic hormone PYY. This was a promising finding, considering that FFA2 activation promotes the release of PYY (Karakı et al., 2006). Using these ICC methods also allowed the separate evaluation of resident immune cells of the small intestine. Thus, ILFs were revealed to contain subsets of CD45⁺ lymphoid cells which express hFFA2-HA, potentially representing a population of CD11c⁺ DCs (Lorenz and Newberry, 2004). Similarly, subsets of myeloid cells of the spleen (mainly in the RP) were found to express hFFA2-HA, however the identity of these cells remains to be resolved. Perhaps most importantly (at least in relation to the work in this thesis), hFFA2-HA was demonstrated to be expressed on isolated bone marrow-derived neutrophils (Le Poul et al., 2003). By employing a larger array of cell marker-specific antibodies, the cell populations in which hFFA2-HA is expressed could be established with certainty. This would confirm the presence of FFA2 in EECs and immune cells, while also suggesting potential functions in the cells of less characterised tissues, such as the spleen.

Although these data hint at what has already been described in literature pertaining to the importance of FFA2 in physiological (and in particular, inflammatory) responses, this receptor is yet to be confirmed as a viable drug target. While an increasing number of selective tool compounds are available, the overlapping expression profiles of the FFA2 and FFA3 still pose an obstacle. The opposing effects of SCFAs on GSIS in the pancreas, for example, are the result of differential signalling through the two receptors (Priyadarshini et al., 2015, Priyadarshini and Layden, 2015). What advances have been made towards this goal, and what further strategies may be employed? As highlighted throughout this thesis, the development of the hFFA2-DREADD-HA mouse line has been an important advance in the dissection of SCFA receptor pharmacology. This model has so far allowed the investigation of the contribution of each receptor to EEC function, gut motility, and the gut-brain axis (Bolognini et al., 2019, Barki et al., 2022). The greatest appeal of the hFFA2-DREADD-HA mouse is the inability of SCFAs to signal through FFA2, yet this characteristic can also be a weakness. By ensuring that FFA2 activation occurs only in response to synthetic ligands (SA and MOMBA), the nuanced signalling established by the different tissue gradients of SCFAs can be lost. Furthermore, in a disease model of colitis, pathophysiological changes resulting in potentially altered levels of SCFAs (Barthel et al., 2003, Raybould et al., 2012) may not display the same overall disease profile in the hFFA2-DREADD-HA, thus diminishing the translatability of the model. In the hFFA2-HA mouse, these differences would be maintained, thus showing a natural response both under physiological and pathophysiological conditions.

Although each of these animal models is a powerful tool, they may be limited for use in conjunction with each other in order to generate a complete picture. The utility of the minus-CRE mouse line has been demonstrated throughout this thesis. This mouse strain, which lacks expression of both the endogenous mFFA2 and the knocked-in hFFA2-HA, was demonstrated to be an indispensable negative control. No agonist-induced activation was observed in minus-CRE neutrophils in any of the assay platforms employed, which could be explained by the lack of expression at both the mRNA and the protein level. Since this mouse strain operates as a functional knockout, there could be a potential for superseding traditional, often imperfect, and genetically non-equivalent KO

strains (Zaibi et al., 2010). In models of disease, the parallel use of such a line would inform about the involvement of the receptors in both establishing the pathophysiology, and in resolving it upon the administration of a compound. The introduction of a further tool into the investigative toolbox, namely a DREADD version of FFA3, would perhaps allow a more comprehensive deconvolution of receptor contributions to physiological functions. Because highly selective FFA3 ligands are still not readily available, and due to the preserved amino acid residues in the orthosteric binding pocket of hFFA3 (Stoddart et al., 2008), taking such a strategy could be viable.

As it was highlighted in the rationale for **Chapter 4**, the mere description of receptor expression cannot serve as complete validation of the transgenic mouse strain. The fact that neutrophils could be isolated as a uniform population of cells, meant that they provided an excellent model for the exploration of immune cell responses. In addition of qRT-PCR and ICC experiments, the expression of hFFA2-HA on neutrophils was further corroborated by radioligand binding assays. Moreover, as both the radioligand and the unlabelled ligands were hFFA2-selective antagonists, their ability to bind these samples further defined the identity of hFFA2-HA. As for receptor activation, the [³⁵S]GTPγS incorporation assay was demonstrated to be a straightforward platform for the investigation of hFFA2-HA function, even in membranes prepared from primary cells. Results with the agonist C3 paralleled those in overexpressing cell lines. By contrast, the PAM AZ1729 displayed diverse cooperativity of efficacy between cell types and species orthologues, contradicting previous descriptions of this ligand (Bolognini et al., 2016). Of paramount importance is the finding that the hFFA2-selective antagonist GLPG0974 was able to fully inhibit C3-induced [³⁵S]GTPγS incorporation in hFFA2-HA, but not in WT neutrophil membranes. This, above all, validates the hFFA2-HA mouse strain as an incredibly important tool, as it would allow the testing of any novel, hFFA2-selective compound in a pre-clinical setting. While this appears to be a promising assay system, allowing the testing of multiple novel ligands simultaneously, it does rely on a limited supply of primary cells. As such, this assay has to complement existing assay platforms using overexpressing cell lines, rather than superseding them. It may also be of interest to adapt these methods for the investigation of other types of

primary cells, or even tissues to understand tissue-dependent signalling of hFFA2-HA.

While [³⁵S]GTPγS incorporation could serve as a useful assay platform in cases where higher throughput is required, the eventual aim would be to utilise the mouse strain for *in vivo* exploration of such compounds. Bridging the gap between the two, the *ex vivo* experiments conducted as part of this thesis were also revealing. In neutrophil chemotaxis experiments, the antagonist CATPB blocked C3-induced chemotaxis in hFFA2-HA neutrophils, but not in WT. While not statistically significant, both GLPG0974 and CATPB caused modest reductions in C3-induced NET formation in hFFA2-HA neutrophils. Both the *in vitro* and *ex vivo* experiments using neutrophils were able to demonstrate not only agonist-induced activation but also PAM and antagonist effects. Therefore, while there were certainly challenges with these assays, with further optimisation they may constitute an important part of the toolbox for exploring new compounds with a variety of pharmacological characteristics to target hFFA2 for the treatment of inflammatory diseases.

While utilising a uniform population of cells, such as neutrophils, is attractive due to the simplicity of such assays, there is a risk of losing insight into the important tissue level communication between the various cell types. Having established the functionality of the hFFA2-HA in this mouse line, the use of whole tissue preparations for the investigation of tissue-wide functions would be warranted. In line with the investigation of inflammatory conditions, intestinal Peyer's patches would be an ideal target for such investigation in the first instance (Shreedhar et al., 2003). Due to their morphology, these provide a simple target for isolation, yet they contain immune cells from a multitude of lineages (Iwasaki and Kelsall, 2000, Iwasaki and Kelsall, 2001). As such, the interactions between the various cell types, and the role of hFFA2-HA therein, could be investigated. A similar approach is then required in each tissue where expression has been observed. The next logical step in this timeline would be *in vivo* investigation of well-characterised tool compounds (antagonists and PAMs in particular), in order to establish their effects on a whole organism level. Only after crossing all of these additional hurdles is there a possibility of validating FFA2 as a target for the treatment of colitis or other inflammatory diseases. If

this is achieved, the hFFA2-HA mouse model will constitute an essential step in the pre-clinical validation of new compounds.

In addition to the advances in drug discovery and pre-clinical models, there have been developments in basic research around FFA2 signalling. Until now, the β -arrestin-mediated signalling of FFA2 has received limited attention, perhaps due to the shortcomings of the available assay formats. However, the development of the novel phosphosite-specific antibodies has rekindled interest in the non-G protein-mediated signalling of FFA2 and their use as post-activation sensors of the receptor (*Chapter 5*). Of the three antisera employed that were designed to target phosphorylated residues on hFFA2, only two were shown to actually do so. In particular, the antiserum targeting pThr³⁰⁶/pThr³¹⁰ displayed increased binding upon stimulation by agonists in both hFFA2 and hFFA2-DREADD, and this was prevented by co-incubation with CATPB. By contrast, anti-pSer²⁹⁶/pSer²⁹⁷ appeared to bind hFFA2-DREADD in a ligand-dependent manner, but WT hFFA2 in a ligand-independent manner. This could demonstrate that mutants of the receptor may have altered conformational states which could influence interactions with effectors. This is the first observation that the hFFA2-DREADD receptor construct may not be entirely equivalent to the WT receptor. In order to understand such differences in conformational changes and coupling to downstream effectors, deciphering the crystal structure of FFA2 would be of particular importance. Specifically, the differences between hFFA2 and hFFA2-DREADD would be important to explore, in complex with both G-proteins and β -arrestins. Considering the complex pharmacology of FFA2 - the promiscuous signalling, the variety of ligands and their probe dependency (Milligan et al., 2017, Bolognini et al., 2016) - access to such a powerful tool could inform our understanding, as well as allow more rational drug design in the future.

In addition to the differences between FFA2 variants, exploration of the hFFA2 PD mutants also revealed additional complexity of signalling. The PD mutant of Ser²⁹⁶/Ser²⁹⁷ lost affinity for both the anti-pSer²⁹⁶/pSer²⁹⁷ and the anti-pThr³⁰⁶/pThr³¹⁰ antisera, while the PD mutant of Thr³⁰⁶/Thr³¹⁰ only lost interaction with the corresponding anti-pThr³⁰⁶/pThr³¹⁰ antiserum. This could be the first hint at a potential hierarchy of phosphorylation at hFFA2 (Ohguro et al., 1993, Kouhen et al., 2000), where phosphorylation of Ser²⁹⁶ and/or Ser²⁹⁷ may be

a prerequisite for the phosphorylation of Thr³⁰⁶/Thr³¹⁰. Importantly, all of these trends were observed in both WB and ICC experiments. Exploration of β -arrestin-2 recruitment in PD mutants, by contrast, revealed a different rank order of importance for the pairs of residues involved, with mutants of Ser³²⁴/Ser³²⁵ displaying the most significant reduction in response. To fully explore these discrepancies, it would be pertinent to conduct a series of time-course and kinetic experiments in each assay, utilising all available PD mutants and GRK KO cell lines (Møller et al., 2020) or inhibitors (Lowe et al., 2015, Uehling et al., 2021). In addition to PD mutants presented here, additional varieties are possible through single residue mutations, replacement of all Ser, Thr and acidic residues, and the generation of PD version of hFFA2-DREADD. The use of the full complement of available tool compounds could also reveal any additional ligand-dependent effects. This comprehensive approach would allow us to fully decipher the phosphorylation landscape of FFA2.

An important first step was made towards demonstrating receptor phosphorylation in mouse-derived primary cells. Although in neutrophils the signal-to-noise ratio of the phosphosite-specific antibodies confounded the production of clear data and conclusions, some trends of agonist-dependent phosphorylation could be observed. This was an essential finding, as it opens the doors for future exploration of receptor phosphorylation at the tissue level. Whether using tissue samples from the hFFA2-HA mouse or from clinical patients, the use of the antibodies described herein may expand our understanding of tissue-specific phosphorylation patterns and the barcode hypothesis as it pertains to FFA2. Since non-G protein-mediated signalling in FFA2 is not well-characterised, the physiological effects of such signalling are also poorly understood. To advance our understanding, there is a need for the development of either β -arrestin-biased ligands for use in primary cell and tissues, or receptor mutants biased towards signalling through β -arrestins. The latter could then be expressed in immortalised cell lines of relevant tissues, such as RAW264.7 (Taciak et al., 2018) or MIN6 (Ishihara et al., 1993), representing macrophages and pancreatic β -cells, respectively. If these, in combination with the experiments with FFA2-PD variants, point toward important β -arrestin-mediated physiological roles of FFA2, there could be a potential for the development of yet another transgenic mouse model: one expressing hFFA2-PD.

A similar model expressing the PD variant of M_1 mAChR has been successfully used to determine physiological effects of phosphorylation-dependent signalling *in vivo* (Bradley et al., 2020).

Overall, the novel tools characterised herein have the potential to make significant contributions to the field of research around FFA2. By establishing a hFFA2-HA-expressing mouse strain, one of the most significant hurdles in FFA2 drug development can be overcome. This would allow more focused efforts in finding effective drugs to target ulcerative colitis, IBD, and other chronic inflammatory diseases if FFA2 can indeed be validated as a therapeutic target in these and potentially other conditions. In addition, a deeper understanding of non-G protein-mediated signalling at FFA2 might warrant future efforts to target these pathways specifically, through the further development of biased ligands.

REFERENCES

- Abbott, R. M., Levy, A. D., Aguilera, N. S., Gorospe, L. & Thompson, W. M. 2004. Primary vascular neoplasms of the spleen: Radiologic-pathologic correlation. *Radiographics*, 24, 1137-1163.
- Albillos, A., De Gottardi, A. & Rescigno, M. 2020. The gut-liver axis in liver disease: Pathophysiological basis for therapy. *Journal of Hepatology*, 72, 558-577.
- Alfonso-Prieto, M., Giorgetti, A. & Carloni, P. 2019. Multiscale simulations on human Frizzled and Taste2 GPCRs. *Current Opinion in Structural Biology*, 55, 8-16.
- Ang, Z., Xiong, D., Wu, M. & Ding, J. L. 2018. FFAR2-FFAR3 receptor heteromerization modulates short-chain fatty acid sensing. *FASEB Journal*, 32, 289-303.
- Antunes, K. H., Fachi, J. L., De Paula, R., Da Silva, E. F., Pral, L. P., Dos Santos, A. A., Malaquias Dias, G. B., Vargas, J. E., Puga, R., Mayer, F. Q., Maito, F., Zarate-Blades, C. R., Ajami, N. J., St Ana, M. R., Candreva, T., Rodrigues, H. G., Schmiele, M., Pedrosa Silva Clerici, M. T., Proenca-Modena, J. L., Vieira, A. T., Mackay, C. R., Mansur, D., Caballero, M. T., Marzec, J., Li, J., Wang, X., Bell, D., Polack, F. P., Kleeberger, S. R., Stein, R. T., Ramirez Vinolo, M. A. & Duarte De Souza, A. P. 2019. Microbiota-derived acetate protects against respiratory syncytial virus infection through a GPR43-type 1 interferon response. *Nature Communications*, 10, 3273.
- Armbruster, B. N., Li, X., Pausch, M. H., Herlitze, S. & Roth, B. L. 2007. Evolving the lock to fit the key to create a family of G protein-coupled receptors potently activated by an inert ligand. *Proceedings of the National Academy of Sciences of the United States of America*, 104, 5163-5168.
- Arnaout, M. A. 2016. Biology and structure of leukocyte B2 integrins and their role in inflammation. *F1000Research*, 5, 2433.
- Barker, G., Davenport, R., Downham, R., Farnaby, W., Goldby, A., Hannah, D., Harrison, D. & Willems, H. 2015. 3-substituted 2-amino-indole derivatives. *International Patent*. WO 2015/198045 A1.

- Barki, N., Bolognini, D., Börjesson, U., Jenkins, L., Riddell, J., Hughes, D. I., Ulven, T., Hudson, B. D., Ulven, E. R., Dekker, N., Tobin, A. B. & Milligan, G. 2022. Chemogenetics defines a short-chain fatty acid receptor gut-brain axis. *eLife*, 11, e73777.
- Barthel, M., Hapfelmeier, S., Quintanilla-Martinez, L., Kremer, M., Rohde, M., Hogardt, M., Pfeffer, K., Russmann, H. & Hardt, W. D. 2003. Pretreatment of mice with streptomycin provides a *Salmonella enterica* serovar typhimurium colitis model that allows analysis of both pathogen and host. *Infection and Immunity*, 71, 2839-2858.
- Berg, S. & Kolmodin, K. 2007. Thiazol-guanidine derivatives useful as a β -related pathologies. *International Patent*. WO 2007/120096 A1.
- Bhatt, J. M., Styers, M. L. & Sztul, E. 2016. Expression of Epitope-Tagged Proteins in Mammalian Cells in Culture. *Methods in Molecular Biology*. Springer New York.
- Bjursell, M., Admyre, T., Goransson, M., Marley, A. E., Smith, D. M., Oscarsson, J. & Bohlooly-Y, M. 2011. Improved glucose control and reduced body fat mass in free fatty acid receptor 2-deficient mice fed a high-fat diet. *American Journal of Physiology-Endocrinology and Metabolism*, 300, E211-E220.
- Bolognini, D., Barki, N., Butcher, A. J., Hudson, B. D., Sergeev, E., Molloy, C., Moss, C. E., Bradley, S. J., Le Gouill, C., Bouvier, M., Tobin, A. B. & Milligan, G. 2019. Chemogenetics defines receptor-mediated functions of short chain free fatty acids. *Nature Chemical Biology*, 15, 489-498.
- Bolognini, D., Dedeo, D. & Milligan, G. 2021. Metabolic and inflammatory functions of short-chain fatty acid receptors. *Current opinion in endocrine and metabolic research*, 16, 1-9.
- Bolognini, D., Moss, C. E., Nilsson, K., Petersson, A. U., Donnelly, I., Sergeev, E., Koenig, G. M., Kostenis, E., Kurowska-Stolarska, M., Miller, A., Dekker, N., Tobin, A. B. & Milligan, G. 2016. A Novel Allosteric Activator of Free Fatty Acid 2 Receptor Displays Unique G_i-functional Bias. *Journal of Biological Chemistry*, 291, 18915-18931.

- Bonifacino, J. S., Dell'angelica, E. C. & Springer, T. A. 1999. Immunoprecipitation. *Current Protocols in Molecular Biology*, 48.
- Bradley, S. J., Bourgognon, J.-M., Sanger, H. E., Verity, N., Mogg, A. J., White, D. J., Butcher, A. J., Moreno, J. A., Molloy, C., Macedo-Hatch, T., Edwards, J. M., Wess, J., Pawlak, R., Read, D. J., Sexton, P. M., Broad, L. M., Steinert, J. R., Mallucci, G. R., Christopoulos, A., Felder, C. C. & Tobin, A. B. 2016a. M1 muscarinic allosteric modulators slow prion neurodegeneration and restore memory loss. *Journal of Clinical Investigation*, 127, 487-499.
- Bradley, S. J., Molloy, C., Valuskova, P., Dwomoh, L., Scarpa, M., Rossi, M., Finlayson, L., Svensson, K. A., Chernet, E., Barth, V. N., Gherbi, K., Sykes, D. A., Wilson, C. A., Mistry, R., Sexton, P. M., Christopoulos, A., Mogg, A. J., Rosethorne, E. M., Sakata, S., John Challiss, R. A., Broad, L. M. & Tobin, A. B. 2020. Biased M1-muscarinic-receptor-mutant mice inform the design of next-generation drugs. *Nature Chemical Biology*, 16, 240-249.
- Bradley, S. J., Tobin, A. B. & Prihandoko, R. 2018. The use of chemogenetic approaches to study the physiological roles of muscarinic acetylcholine receptors in the central nervous system. *Neuropharmacology*, 136, 421-426.
- Bradley, S. J., Wiegman, C. H., Iglesias, M. M., Kong, K. C., Butcher, A. J., Plouffe, B., Goupil, E., Bourgognon, J.-M., Macedo-Hatch, T., Legouill, C., Russell, K., Laporte, S. A., Koenig, G. M., Kostenis, E., Bouvier, M., Chung, K. F., Amrani, Y. & Tobin, A. B. 2016b. Mapping physiological G protein-coupled receptor signaling pathways reveals a role for receptor phosphorylation in airway contraction. *Proceedings of the National Academy of Sciences of the United States of America*, 113, 4524-4529.
- Brantis, C. E., Ooms, F. & Bernard, J. 2011. Novel amino acid derivatives and their use as GPR43 receptor modulators. *International Patent*. WO 2011/092284 A1.
- Breivogel, C. S., Walker, J. M., Huang, S. M., Roy, M. B. & Childers, S. R. 2004. Cannabinoid signaling in rat cerebellar granule cells: G-protein activation, inhibition of glutamate release and endogenous cannabinoids. *Neuropharmacology*, 47, 81-91.

- Brinkmann, V., Reichard, U., Goosmann, C., Fauler, B., Uhlemann, Y., Weiss, D. S., Weinrauch, Y. & Zychlinsky, A. 2004. Neutrophil extracellular traps kill bacteria. *Science*, 303, 1532-1535.
- Briscoe, C. P., Tadayyon, M., Andrews, J. L., Benson, W. G., Chambers, J. K., Eilert, M. M., Ellis, C., Elshourbagy, N. A., Goetz, A. S., Minnick, D. T., Murdock, P. R., Sauls, H. R., Shabon, U., Spinage, L. D., Strum, J. C., Szekeres, P. G., Tan, K. B., Way, J. M., Ignar, D. M., Wilson, S. & Muir, A. I. 2003. The Orphan G Protein-coupled Receptor GPR40 Is Activated by Medium and Long Chain Fatty Acids. *Journal of Biological Chemistry*, 278, 11303-11311.
- Brooks, L., Viardot, A., Tsakmaki, A., Stolarczyk, E., Howard, J. K., Cani, P. D., Everard, A., Sleeth, M. L., Psichas, A., Anastasovskaj, J., Bell, J. D., Bell-Anderson, K., Mackay, C. R., Ghatei, M. A., Bloom, S. R., Frost, G. & Bewick, G. A. 2017. Fermentable carbohydrate stimulates FFAR2-dependent colonic PYY cell expansion to increase satiety. *Molecular Metabolism*, 6, 48-60.
- Brown, A. J., Goldsworthy, S. M., Barnes, A. A., Eilert, M. M., Tcheang, L., Daniels, D., Muir, A. I., Wigglesworth, M. J., Kinghorn, I., Fraser, N. J., Pike, N. B., Strum, J. C., Steplewski, K. M., Murdock, P. R., Holder, J. C., Marshall, F. H., Szekeres, P. G., Wilson, S., Ignar, D. M., Foord, S. M., Wise, A. & Dowell, S. J. 2003. The orphan G protein-coupled receptors GPR41 and GPR43 are activated by propionate and other short chain carboxylic acids. *Journal of Biological Chemistry*, 278, 11312-11319.
- Brown, A. J., Tsoulou, C., Ward, E., Gower, E., Bhudia, N., Chowdhury, F., Dean, T. W., Faucher, N., Gangar, A. & Dowell, S. J. 2015. Pharmacological properties of acid N-thiazolylamide FFA2 agonists. *Pharmacology Research & Perspectives*, 3, e00141.
- Bustin, S. A., Benes, V., Garson, J. A., Hellems, J., Huggett, J., Kubista, M., Mueller, R., Nolan, T., Pfaffl, M. W., Shipley, G. L., Vandesompele, J. & Wittwer, C. T. 2009. The MIQE Guidelines: Minimum Information for Publication of Quantitative Real-Time PCR Experiments. *Clinical Chemistry*, 55, 611-622.

- Butcher, A. J., Bradley, S. J., Prihandoko, R., Brooke, S. M., Mogg, A., Bourgognon, J.-M., Macedo-Hatch, T., Edwards, J. M., Bottrill, A. R., Challiss, R. A. J., Broad, L. M., Felder, C. C. & Tobin, A. B. 2016. An Antibody Biosensor Establishes the Activation of the M1 Muscarinic Acetylcholine Receptor during Learning and Memory. *Journal of Biological Chemistry*, 291, 8862-8875.
- Butcher, A. J., Hudson, B. D., Shimpukade, B., Alvarez-Curto, E., Prihandoko, R., Ulven, T., Milligan, G. & Tobin, A. B. 2014. Concomitant Action of Structural Elements and Receptor Phosphorylation Determines Arrestin-3 Interaction with the Free Fatty Acid Receptor FFA4. *Journal of Biological Chemistry*, 289, 18451-18465.
- Caengprasath, N., Gonzalez-Abuin, N., Shchepinova, M., Ma, Y., Inoue, A., Tate, E. W., Frost, G. & Hanyaloglu, A. C. 2020. Internalization-Dependent Free Fatty Acid Receptor 2 Signaling Is Essential for Propionate-Induced Anorectic Gut Hormone Release. *iScience*, 23, 101449.
- Canfora, E. E., Van Der Beek, C. M., Jocken, J. W. E., Goossens, G. H., Holst, J. J., Damink, S. W. M. O., Lenaerts, K., Dejong, C. H. C. & Blaak, E. E. 2017. Colonic infusions of short-chain fatty acid mixtures promote energy metabolism in overweight/obese men: a randomized crossover trial. *Scientific Reports*, 7, 2360.
- Cani, P. D., Bibiloni, R., Knauf, C., Neyrinck, A. M., Delzenne, N. M. & Burcelin, R. 2008. Changes in gut microbiota control metabolic endotoxemia-induced inflammation in high-fat diet-induced obesity and diabetes in mice. *Diabetes*, 57, 1470-1481.
- Cani, P. D., Neyrinck, A. M., Fava, F., Knauf, C., Burcelin, R. G., Tuohy, K. M., Gibson, G. R. & Delzenne, N. M. 2007. Selective increases of bifidobacteria in gut microflora improve high-fat-diet-induced diabetes in mice through a mechanism associated with endotoxaemia. *Diabetologia*, 50, 2374-2383.
- Carretta, M. D., Barría, Y., Borquez, K., Urra, B., Rivera, A., Alarcón, P., Hidalgo, M. A. & Burgos, R. A. 2020. β -hydroxybutyrate and hydroxycarboxylic acid receptor 2 agonists activate the AKT, ERK and AMPK pathways, which are involved in bovine neutrophil chemotaxis. *Scientific Reports*, 10, 12491.

- Carretta, M. D., Hidalgo, A. I., Burgos, J., Opazo, L., Castro, L., Hidalgo, M. A., Figueroa, C. D., Taubert, A., Hermosilla, C. & Burgos, R. A. 2016. Butyric acid stimulates bovine neutrophil functions and potentiates the effect of platelet activating factor. *Veterinary Immunology and Immunopathology*, 176, 18-27.
- Carretta, M. D., Quiroga, J., Lopez, R., Hidalgo, M. A. & Burgos, R. A. 2021. Participation of Short-Chain Fatty Acids and Their Receptors in Gut Inflammation and Colon Cancer. *Frontiers in Physiology*, 12, 662739.
- Chambers, E. S., Byrne, C. S., Aspey, K., Chen, Y., Khan, S., Morrison, D. J. & Frost, G. 2018. Acute oral sodium propionate supplementation raises resting energy expenditure and lipid oxidation in fasted humans. *Diabetes Obesity & Metabolism*, 20, 1034-1039.
- Chambers, E. S., Byrne, C. S., Morrison, D. J., Murphy, K. G., Preston, T., Tedford, C., Garcia-Perez, I., Fountana, S., Serrano-Contreras, J. I., Holmes, E., Reynolds, C. J., Roberts, J. F., Boyton, R. J., Altmann, D. M., McDonald, J. A. K., Marchesi, J. R., Akbar, A. N., Riddell, N. E., Wallis, G. A. & Frost, G. S. 2019. Dietary supplementation with inulin-propionate ester or inulin improves insulin sensitivity in adults with overweight and obesity with distinct effects on the gut microbiota, plasma metabolome and systemic inflammatory responses: a randomised cross-over t. *Gut*, 68, 1430-1438.
- Chambers, E. S., Viardot, A., Psichas, A., Morrison, D. J., Murphy, K. G., Zaccarelli, S. E. K., MacDougall, K., Preston, T., Tedford, C., Finlayson, G. S., Blundell, J. E., Bell, J. D., Thomas, E. L., Mt-Isa, S., Ashby, D., Gibson, G. R., Kolida, S., Dhillo, W. S., Bloom, S. R., Morley, W., Clegg, S. & Frost, G. 2015. Effects of targeted delivery of propionate to the human colon on appetite regulation, body weight maintenance and adiposity in overweight adults. *Gut*, 64, 1744-1754.
- Chen, H., Zhang, S., Zhang, X. & Liu, H. 2022. QR code model: a new possibility for GPCR phosphorylation recognition. *Cell Communication and Signaling*, 20, 23.

- Christiansen, E., Hudson, B. D., Hansen, A. H., Milligan, G. & Ulven, T. 2016. Development and Characterization of a Potent Free Fatty Acid Receptor 1 (FFA1) Fluorescent Tracer. *Journal of Medicinal Chemistry*, 59, 4849-4858.
- Christiansen, E., Watterson, K. R., Stocker, C. J., Sokol, E., Jenkins, L., Simon, K., Grundmann, M., Petersen, R. K., Wargent, E. T., Hudson, B. D., Kostenis, E., Ejsing, C. S., Cawthorne, M. A., Milligan, G. & Ulven, T. 2015. Activity of dietary fatty acids on FFA1 and FFA4 and characterisation of pinolenic acid as a dual FFA1/FFA4 agonist with potential effect against metabolic diseases. *British Journal of Nutrition*, 113, 1677-1688.
- Chun, E., Lavoie, S., Fonseca-Pereira, D., Bae, S., Michaud, M., Hoveyda, H. R., Fraser, G. L., Comeau, C. A. G., Glickman, J. N., Fuller, M. H., Layden, B. T. & Garrett, W. S. 2019. Metabolite-Sensing Receptor Ffar2 Regulates Colonic Group 3 Innate Lymphoid Cells and Gut Immunity. *Immunity*, 51, 871-884.
- Colina, C., Puhl, H. L., III & Ikeda, S. R. 2018. Selective tracking of FFAR3-expressing neurons supports receptor coupling to N-type calcium channels in mouse sympathetic neurons. *Scientific Reports*, 8, 17379.
- Cook, S. I. & Sellin, J. H. 1998. Review article: short chain fatty acids in health and disease. *Alimentary Pharmacology & Therapeutics*, 12, 499-507.
- Cristea, I. M., Williams, R., Chait, B. T. & Rout, M. P. 2005. Fluorescent Proteins as Proteomic Probes. *Molecular & Cellular Proteomics*, 4, 1933-1941.
- Cummings, J. H., Pomare, E. W., Branch, W. J., Naylor, C. P. & MacFarlane, G. T. 1987. Short chain fatty acids in human large intestine, portal, hepatic and venous blood. *Gut*, 28, 1221-1227.
- Dahlgren, C., Holdfeldt, A., Lind, S., Martensson, J., Gabl, M., Bjorkman, L., Sundqvist, M. & Forsman, H. 2020. Neutrophil Signaling That Challenges Dogmata of G Protein-Coupled Receptor Regulated Functions. *ACS Pharmacology & Translational Science*, 3, 203-220.
- Dann, C. E., Hsieh, J.-C., Rattner, A., Sharma, D., Nathans, J. & Leahy, D. J. 2001. Insights into Wnt binding and signalling from the structures of two Frizzled cysteine-rich domains. *Nature*, 412, 86-90.

- Davenport, A. P., Alexander, S. P. H., Sharman, J. L., Pawson, A. J., Benson, H. E., Monaghan, A. E., Liew, W. C., Mpamhanga, C. P., Bonner, T. I., Neubig, R. R., Pin, J. P., Spedding, M. & Harmar, A. J. 2013. International Union of Basic and Clinical Pharmacology. LXXXVIII. G Protein-Coupled Receptor List: Recommendations for New Pairings with Cognate Ligands. *Pharmacological Reviews*, 65, 967-986.
- Devkota, S., Wang, Y., Musch, M. W., Leone, V., Fehlner-Peach, H., Nadimpalli, A., Antonopoulos, D. A., Jabri, B. & Chang, E. B. 2012. Dietary-fat-induced taurocholic acid promotes pathobiont expansion and colitis in *Il10^{-/-}* mice. *Nature*, 487, 104-108.
- Dewulf, E. M., Ge, Q., Bindels, L. B., Sohet, F. M., Cani, P. D., Brichard, S. M. & Delzenne, N. M. 2013. Evaluation of the relationship between GPR43 and adiposity in human. *Nutrition & Metabolism*, 10, 11.
- Doll, C., Konietzko, J., Poell, F., Koch, T., Hoell, V. & Schulz, S. 2011. Agonist-selective patterns of μ -opioid receptor phosphorylation revealed by phosphosite-specific antibodies. *British Journal of Pharmacology*, 164, 298-307.
- Dragan, A. I., Casas-Finet, J. R., Bishop, E. S., Strouse, R. J., Schenerman, M. A. & Geddes, C. D. 2010. Characterization of PicoGreen Interaction with dsDNA and the Origin of Its Fluorescence Enhancement upon Binding. *Biophysical Journal*, 99, 3010-3019.
- Drube, J., Haider, R. S., Matthees, E. S. F., Reichel, M., Zeiner, J., Fritzwanker, S., Ziegler, C., Barz, S., Klement, L., Filor, J., Weitzel, V., Kliewer, A., Miess-Tanneberg, E., Kostenis, E., Schulz, S. & Hoffmann, C. 2022. GPCR kinase knockout cells reveal the impact of individual GRKs on arrestin binding and GPCR regulation. *Nature Communications*, 13, 540.
- Eaton, S. L., Hurtado, M. L., Oldknow, K. J., Graham, L. C., Marchant, T. W., Gillingwater, T. H., Farquharson, C. & Wishart, T. M. 2014. A Guide to Modern Quantitative Fluorescent Western Blotting with Troubleshooting Strategies. *Journal of Visualized Experiments*, 93, e52099.
- El Hage, R., Hernandez-Sanabria, E., Arroyo, M. C., Props, R. & Van De Wiele, T. 2019. Propionate-Producing Consortium Restores Antibiotic-Induced

- Dysbiosis in a Dynamic in vitro Model of the Human Intestinal Microbial Ecosystem. *Frontiers in Microbiology*, 10, 1206.
- Engelstoft, M. S., Lund, M. L., Grunddal, K. V., Egerod, K. L., Osborne-Lawrence, S., Poulsen, S. S., Zigman, J. M. & Schwartz, T. W. 2015. Research Resource: A Chromogranin A Reporter for Serotonin and Histamine Secreting Enteroendocrine Cells. *Molecular Endocrinology*, 29, 1658-1671.
- Engelstoft, M. S., Park, W.-M., Sakata, I., Kristensen, L. V., Husted, A. S., Osborne-Lawrence, S., Piper, P. K., Walker, A. K., Pedersen, M. H., Nohr, M. K., Pan, J., Sinz, C. J., Carrington, P. E., Akiyama, T. E., Jones, R. M., Tang, C., Ahmed, K., Offermanns, S., Egerod, K. L., Zigman, J. M. & Schwartz, T. W. 2013. Seven transmembrane G protein-coupled receptor repertoire of gastric ghrelin cells. *Molecular Metabolism*, 2, 376-392.
- Everard, A., Belzer, C., Geurts, L., Ouwerkerk, J. P., Druart, C., Bindels, L. B., Guiot, Y., Derrien, M., Muccioli, G. G., Delzenne, N. M., De Vos, W. M. & Cani, P. D. 2013. Cross-talk between *Akkermansia muciniphila* and intestinal epithelium controls diet-induced obesity. *Proceedings of the National Academy of Sciences of the United States of America*, 110, 9066-9071.
- Fachi, J. L., Secca, C., Rodrigues, P. B., Mato, F. C. P. D., Di Luccia, B., Felipe, J. D. S., Pral, L. P., Rungue, M., Rocha, V. D. M., Sato, F. T., Sampaio, U., Clerici, M. T. P. S., Rodrigues, H. G., Camara, N. O. S., Consonni, S. R., Vieira, A. T., Oliveira, S. C., Mackay, C. R., Layden, B. T., Bortoluci, K. R., Colonna, M. & Vinolo, M. A. R. 2020. Acetate coordinates neutrophil and ILC3 responses against *C. difficile* through FFAR2. *The Journal of experimental medicine*, 217, e20190489.
- Fang, Z., Cao, D. & Qiu, J. 2020. Development and production of nanobodies specifically against green fluorescence protein. *Applied Microbiology and Biotechnology*, 104, 4837-4848.
- Fells, J. I., Ai, X., Weinglass, A., Feng, W., Lei, Y., Finley, M., Hoveyda, H. R., Fraser, G. L. & Machacek, M. 2020. Identification of free fatty acid receptor 2 agonists using virtual screening. *Bioorganic & Medicinal Chemistry Letters*, 30, 127460.

- Feng, Z., Jensen, S. M., Messenheimer, D. J., Farhad, M., Neuberger, M., Bifulco, C. B. & Fox, B. A. 2016. Multispectral Imaging of T and B Cells in Murine Spleen and Tumor. *The Journal of Immunology*, 196, 3943-3950.
- Flanagan, C. A. 2016. GPCR-radioligand binding assays. *Methods in Cell Biology*. Elsevier.
- Fleischer, J., Bumbalo, R., Bautze, V., Strotmann, J. & Breer, H. 2015. Expression of odorant receptor Olfr78 in enteroendocrine cells of the colon. *Cell and Tissue Research*, 361, 697-710.
- Flø, R. W., Næss, A., Lund-Johansen, F., Mæhle, B. O., Sjørusen, H., Lehmann, V. & Solberg, C. O. 1991. Negative selection of human monocytes using magnetic particles covered by anti-lymphocyte antibodies. *Journal of Immunological Methods*, 137, 89-94.
- Forbes, S., Stafford, S., Coope, G., Heffron, H., Real, K., Newman, R., Davenport, R., Barnes, M., Grosse, J. & Cox, H. 2015. Selective FFA2 Agonism Appears to Act via Intestinal PYY to Reduce Transit and Food Intake but Does Not Improve Glucose Tolerance in Mouse Models. *Diabetes*, 64, 3763-3771.
- Ford, C. E., Skiba, N. P., Bae, H. S., Daaka, Y. H., Reuveny, E., Shekter, L. R., Rosal, R., Weng, G. Z., Yang, C. S., Iyengar, R., Miller, R. J., Jan, L. Y., Lefkowitz, R. J. & Hamm, H. E. 1998. Molecular basis for interactions of G protein β subunits with effectors. *Science*, 280, 1271-1274.
- Fredriksson, R., Hoglund, P. J., Gloriam, D. E. I., Lagerstrom, M. C. & Schiöth, H. B. 2003a. Seven evolutionarily conserved human rhodopsin G protein-coupled receptors lacking close relatives. *FEBS Letters*, 554, 381-388.
- Fredriksson, R., Lagerström, M. C., Lundin, L.-G. & Schiöth, H. B. 2003b. The G-Protein-Coupled Receptors in the Human Genome Form Five Main Families. Phylogenetic Analysis, Paralogon Groups, and Fingerprints. *Molecular Pharmacology*, 63, 1256-1272.
- Fuchs, T. A., Abed, U., Goosmann, C., Hurwitz, R., Schulze, I., Wahn, V., Weinrauch, Y., Brinkmann, V. & Zychlinsky, A. 2007. Novel cell death program leads to neutrophil extracellular traps. *Journal of Cell Biology*, 176, 231-241.
- Galvao, I., Tavares, L. P., Correa, R. O., Fachi, J. L., Rocha, V. M., Rungue, M., Garcia, C. C., Cassali, G., Ferreira, C. M., Martins, F. S., Oliveira, S. C.,

- Mackay, C. R., Teixeira, M. M., Vinolo, M. A. R. & Vieira, A. T. 2018. The Metabolic Sensor GPR43 Receptor Plays a Role in the Control of *Klebsiella pneumoniae* Infection in the Lung. *Frontiers in Immunology*, 9, 142.
- Ge, H. F., Li, X. F., Weiszmann, J., Wang, P., Baribault, H., Chen, J. L., Tian, H. & Li, Y. 2008. Activation of G protein-coupled receptor 43 in adipocytes leads to inhibition of lipolysis and suppression of plasma free fatty acids. *Endocrinology*, 149, 4519-4526.
- Generoso, J. S., Giridharan, V. V., Lee, J., Macedo, D. & Barichello, T. 2021. The role of the microbiota-gut-brain axis in neuropsychiatric disorders. *Brazilian Journal of Psychiatry*, 43, 293-305.
- Gesty-Palmer, D., Flannery, P., Yuan, L., Corsino, L., Spurney, R., Lefkowitz, R. J. & Luttrell, L. M. 2009. A β -Arrestin-Biased Agonist of the Parathyroid Hormone Receptor (PTH1R) Promotes Bone Formation Independent of G Protein Activation. *Science Translational Medicine*, 1.
- Goodman, O. B., Krupnick, J. G., Santini, F., Gurevich, V. V., Penn, R. B., Gagnon, A. W., Keen, J. H. & Benovic, J. L. 1996. β -Arrestin acts as a clathrin adaptor in endocytosis of the β_2 -adrenergic receptor. *Nature*, 383, 447-450.
- Graff, E. C., Fang, H., Wanders, D. & Judd, R. L. 2016. Anti-inflammatory effects of the hydroxycarboxylic acid receptor 2. *Metabolism-Clinical and Experimental*, 65, 102-113.
- Grundmann, M., Merten, N., Malfacini, D., Inoue, A., Preis, P., Simon, K., Ruettiger, N., Ziegler, N., Benkel, T., Schmitt, N. K., Ishida, S., Mueller, I., Reher, R., Kawakami, K., Inoue, A., Rick, U., Kuehl, T., Imhof, D., Aoki, J., Koenig, G. M., Hoffmann, C., Gomeza, J., Wess, J. & Kostenis, E. 2018. Lack of β -arrestin signaling in the absence of active G proteins. *Nature Communications*, 9.
- Guo, D., Van Dorp, E. J. H., Mulder-Krieger, T., Van Veldhoven, J. P. D., Brussee, J., Ijzerman, A. P. & Heitman, L. H. 2013. Dual-Point Competition Association Assay: A Fast and High-Throughput Kinetic Screening Method for Assessing Ligand-Receptor Binding Kinetics. *SLAS Discovery*, 18, 309-320.
- Gupta, A. K., Giaglis, S., Hasler, P. & Hahn, S. 2014. Efficient Neutrophil Extracellular Trap Induction Requires Mobilization of Both Intracellular and

- Extracellular Calcium Pools and Is Modulated by Cyclosporine A. *PLOS One*, 9, e97088.
- Gurevich, V. V. & Gurevich, E. V. 2003. The New Face of Active Receptor Bound Arrestin Attracts New Partners. *Structure*, 11, 1037-1042.
- Gurevich, V. V. & Gurevich, E. V. 2019. GPCR Signaling Regulation: The Role of GRKs and Arrestins. *Frontiers in Pharmacology*, 10, 125.
- Haddad, L., Francis, J., Rizk, T., Akoka, S., Remaud, G. S. & Bejjani, J. 2022. Cheese characterization and authentication through lipid biomarkers obtained by high-resolution ¹H NMR profiling. *Food Chemistry*, 383.
- Hakkim, A., Fuchs, T. A., Martinez, N. E., Hess, S., Prinz, H., Zychlinsky, A. & Waldmann, H. 2011. Activation of the Raf-MEK-ERK pathway is required for neutrophil extracellular trap formation. *Nature Chemical Biology*, 7, 75-77.
- Hall, M. P., Unch, J., Binkowski, B. F., Valley, M. P., Butler, B. L., Wood, M. G., Otto, P., Zimmerman, K., Vidugiris, G., Machleidt, T., Robers, M. B., Benink, H. A., Eggers, C. T., Slater, M. R., Meisenheimer, P. L., Klaubert, D. H., Fan, F., Encell, L. P. & Wood, K. V. 2012. Engineered Luciferase Reporter from a Deep Sea Shrimp Utilizing a Novel Imidazopyrazinone Substrate. *ACS Chemical Biology*, 7, 1848-1857.
- Hamada, H., Hiroi, T., Nishiyama, Y., Takahashi, H., Masunaga, Y., Hachimura, S., Kaminogawa, S., Takahashi-Iwanaga, H., Iwanaga, T., Kiyono, H., Yamamoto, H. & Ishikawa, H. 2002. Identification of Multiple Isolated Lymphoid Follicles on the Antimesenteric Wall of the Mouse Small Intestine. *The Journal of Immunology*, 168, 57-64.
- Hamann, J., Aust, G., Araç, D., Engel, F. B., Formstone, C., Fredriksson, R., Hall, R. A., Harty, B. L., Kirchhoff, C., Knapp, B., Krishnan, A., Liebscher, I., Lin, H.-H., Martinelli, D. C., Monk, K. R., Peeters, M. C., Piao, X., Prömel, S., Schöneberg, T., Schwartz, T. W., Singer, K., Stacey, M., Ushkaryov, Y. A., Vallon, M., Wolfrum, U., Wright, M. W., Xu, L., Langenhan, T. & Schiöth, H. B. 2015. International Union of Basic and Clinical Pharmacology. XCIV. Adhesion G Protein-Coupled Receptors. *Pharmacological Reviews*, 67, 338-367.
- Han, J.-H., Kim, I.-S., Jung, S.-H., Lee, S.-G., Son, H.-Y. & Myung, C.-S. 2014. The Effects of Propionate and Valerate on Insulin Responsiveness for Glucose

- Uptake in 3T3-L1 Adipocytes and C2C12 Myotubes via G Protein-Coupled Receptor 41. *PLoS One*, 9, e95268.
- Hansen, A. H., Christensen, H. B., Pandey, S. K., Sergeev, E., Valentini, A., Dunlop, J., Dedeo, D., Fratta, S., Hudson, B. D., Milligan, G., Ulven, T. & Rexen Ulven, E. 2021. Structure-Activity Relationship Explorations and Discovery of a Potent Antagonist for the Free Fatty Acid Receptor 2. *ChemMedChem*, 16, 3326-3341.
- Hansen, A. H., Sergeev, E., Bolognini, D., Sprenger, R. R., Ekberg, J. H., Ejsing, C. S., McKenzie, C. J., Ulven, E. R., Milligan, G. & Ulven, T. 2018. Discovery of a Potent Thiazolidine Free Fatty Acid Receptor 2 Agonist with Favorable Pharmacokinetic Properties. *Journal of Medicinal Chemistry*, 61, 9534-9550.
- Hansen, A. H., Sergeev, E., Pandey, S. K., Hudson, B. D., Christiansen, E., Milligan, G. & Ulven, T. 2017. Development and Characterization of a Fluorescent Tracer for the Free Fatty Acid Receptor 2 (FFA2/GPR43). *Journal of Medicinal Chemistry*, 60, 5638-5645.
- Harris, J. C., Dupont, H. L. & Hornick, R. B. 1972. Fecal leukocytes in diarrheal illness. *Annals of Internal Medicine*, 76, 697-703.
- Hashiguchi, M., Kashiwakura, Y., Kojima, H., Kobayashi, A., Kanno, Y. & Kobata, T. 2015. Peyer's patch innate lymphoid cells regulate commensal bacteria expansion. *Immunology Letters*, 165, 1-9.
- Heid, C. A., Stevens, J., Livak, K. J. & Williams, P. M. 1996. Real time quantitative PCR. *Genome Research*, 6, 986-994.
- Hermiston, M. L., Xu, Z. & Weiss, A. 2003. CD45: A Critical Regulator of Signaling Thresholds in Immune Cells. *Annual Review of Immunology*, 21, 107-137.
- Hii, C. S., Anson, D. S., Costabile, M., Mukaro, V., Dunning, K. & Ferrante, A. 2004. Characterization of the MEK5-ERK5 Module in Human Neutrophils and Its Relationship to ERK1/ERK2 in the Chemotactic Response. *Journal of Biological Chemistry*, 279, 49825-49834.
- Hirasawa, A., Tsumaya, K., Awaji, T., Katsuma, S., Adachi, T., Yamada, M., Sugimoto, Y., Miyazaki, S. & Tsujimoto, G. 2005. Free fatty acids regulate gut incretin glucagon-like peptide-1 secretion through GPR120. *Nature Medicine*, 11, 90-94.

- Hoare, S. R. J., Tewson, P. H., Quinn, A. M., Hughes, T. E. & Bridge, L. J. 2020. Analyzing kinetic signaling data for G-protein-coupled receptors. *Scientific Reports*, 10, 12263.
- Hollands, A., Corriden, R., Gysler, G., Dahesh, S., Olson, J., Ali, S. R., Kunkel, M. T., Lin, A. E., Forli, S., Newton, A. C., Kumar, G. B., Nair, B. G., Perry, J. J. P. & Nizet, V. 2016. Natural Product Anacardic Acid from Cashew Nut Shells Stimulates Neutrophil Extracellular Trap Production and Bactericidal Activity. *Journal of Biological Chemistry*, 291, 13964-13973.
- Hong, Y. H., Nishimura, Y., Hishikawa, D., Tsuzuki, H., Miyahara, H., Gotoh, C., Choi, K. C., Feng, D. D., Chen, C., Lee, H. G., Katoh, K., Roh, S. G. & Sasaki, S. 2005. Acetate and propionate short chain fatty acids stimulate adipogenesis via GPCR43. *Endocrinology*, 146, 5092-5099.
- Horiuchi, H., Kamikado, K., Aoki, R., Suganuma, N., Nishijima, T., Nakatani, A. & Kimura, I. 2020. Bifidobacterium animalis subsp. lactis GCL2505 modulates host energy metabolism via the short-chain fatty acid receptor GPR43. *Scientific reports*, 10, 4158-4158.
- Hoveyda, H., Brantis, C. E., Dutheil, G., Zoute, L., Schils, D. & Bernard, J. 2010. Compounds, pharmaceutical composition and methods for use in treating metabolic disorders. *International Patent*. WO 2010/066682 A1.
- Hoveyda, H., Brantis, C. E., Dutheil, G., Zoute, L., Schils, D. & Fraser, G. 2011a. Compounds, pharmaceutical composition and methods for use in treating gastrointestinal disorders. *International Patent*. WO 2011/076732 A1.
- Hoveyda, H., Schils, D., Zoute, L. & Parcq, J. 2011b. Pyrrolidine or thiazolidine carboxylic acid derivatives, pharmaceutical composition and methods for use in treating metabolic disorders as agonists of G-protein coupled receptor 43 (GPR43). *International Patent*. WO 2011/073376 A1.
- Hoveyda, H., Schils, D., Zoute, L., Parcq, J., Bernard, J. & Fraser, G. 2015. Compounds, pharmaceutical composition and methods for use in treating inflammatory diseases. *International Patent*. WO 2015/078949 A1.
- Hoveyda, H. R., Fraser, G. L., Zoute, L., Dutheil, G., Schils, D., Brantis, C., Lapin, A., Parcq, J., Guitard, S., Lenoir, F., El Bousmaqui, M., Rorive, S., Hospied, S., Blanc, S., Bernard, J., Ooms, F., McNelis, J. C. & Olefsky, J. M.

2018. N-Thiazolylamide-based free fatty-acid 2 receptor agonists: Discovery, lead optimization and demonstration of off-target effect in a diabetes model. *Bioorganic & Medicinal Chemistry*, 26, 5169-5180.
- Hudson, B. D., Christiansen, E., Murdoch, H., Jenkins, L., Hansen, A. H., Madsen, O., Ulven, T. & Milligan, G. 2014. Complex Pharmacology of Novel Allosteric Free Fatty Acid 3 Receptor Ligands. *Molecular Pharmacology*, 86, 200-210.
- Hudson, B. D., Christiansen, E., Tikhonova, I. G., Grundmann, M., Kostenis, E., Adams, D. R., Ulven, T. & Milligan, G. 2012a. Chemically engineering ligand selectivity at the free fatty acid receptor 2 based on pharmacological variation between species orthologs. *FASEB Journal*, 26, 4951-4965.
- Hudson, B. D., Due-Hansen, M. E., Christiansen, E., Hansen, A. M., Mackenzie, A. E., Murdoch, H., Pandey, S. K., Ward, R. J., Marquez, R., Tikhonova, I. G., Ulven, T. & Milligan, G. 2013. Defining the Molecular Basis for the First Potent and Selective Orthosteric Agonists of the FFA2 Free Fatty Acid Receptor. *Journal of Biological Chemistry*, 288, 17296-17312.
- Hudson, B. D., Tikhonova, I. G., Pandey, S. K., Ulven, T. & Milligan, G. 2012b. Extracellular Ionic Locks Determine Variation in Constitutive Activity and Ligand Potency between Species Orthologs of the Free Fatty Acid Receptors FFA2 and FFA3. *Journal of Biological Chemistry*, 287, 41195-41209.
- Hulme, E. C. & Trevethick, M. A. 2010. Ligand binding assays at equilibrium: validation and interpretation. *British Journal of Pharmacology*, 161, 1219-1237.
- Husted, A. S., Trauelsen, M., Rudenko, O., Hjorth, S. A. & Schwartz, T. W. 2017. GPCR-Mediated Signaling of Metabolites. *Cell Metabolism*, 25, 777-796.
- Inoue, D., Kimura, I., Wakabayashi, M., Tsumoto, H., Ozawa, K., Hara, T., Takei, Y., Hirasawa, A., Ishihama, Y. & Tsujimoto, G. 2012. Short-chain fatty acid receptor GPR41-mediated activation of sympathetic neurons involves synapsin 2b phosphorylation. *FEBS Letters*, 586, 1547-1554.
- Inoue, A., Raimondi, F., Kadji, F. M. N., Singh, G., Kishi, T., Uwamizu, A., Ono, Y., Shinjo, Y., Ishida, S., Arang, N., Kawakami, K., Gutkind, J. S., Aoki, J. & Russell, R. B. 2019. Illuminating G-Protein-Coupling Selectivity of GPCRs. *Cell*, 177, 1933-1947.

- Irannejad, R., Tomshine, J. C., Tomshine, J. R., Chevalier, M., Mahoney, J. P., Steyaert, J., Rasmussen, S. G. F., Sunahara, R. K., El-Samad, H., Huang, B. & Von Zastrow, M. 2013. Conformational biosensors reveal GPCR signalling from endosomes. *Nature*, 495, 534-538.
- Ishihara, H., Asano, T., Tsukuda, K., Katagiri, H., Inukai, K., Anai, M., Kikuchi, M., Yazaki, Y., Miyazaki, J. I. & Oka, Y. 1993. Pancreatic β -cell line MIN6 exhibits characteristics of glucose-metabolism and glucose-stimulated insulin-secretion similar to those of normal islets. *Diabetologia*, 36, 1139-1145.
- Isobe, J., Maeda, S., Obata, Y., Iizuka, K., Nakamura, Y., Fujimura, Y., Kimizuka, T., Hattori, K., Kim, Y.-G., Morita, T., Kimura, I., Offermanns, S., Adachi, T., Nakao, A., Kiyono, H., Takahashi, D. & Hase, K. 2020. Commensal-bacteria-derived butyrate promotes the T cell-independent IgA response in the colon. *International immunology*, 32, 243-258.
- Itoh, Y., Kawamata, Y., Harada, M., Kobayashi, M., Fujii, R., Fukusumi, S., Ogi, K., Hosoya, M., Tanaka, Y., Uejima, H., Tanaka, H., Maruyama, M., Satoh, R., Okubo, S., Kizawa, H., Komatsu, H., Matsumura, F., Noguchi, Y., Shinohara, T., Hinuma, S., Fujisawa, Y. & Fujino, M. 2003. Free fatty acids regulate insulin secretion from pancreatic β cells through GPR40. *Nature*, 422, 173-176.
- Iwasaki, A. & Kelsall, B. L. 2000. Localization of Distinct Peyer's Patch Dendritic Cell Subsets and Their Recruitment by Chemokines Macrophage Inflammatory Protein (Mip)-3 α , Mip-3 β , and Secondary Lymphoid Organ Chemokine. *Journal of Experimental Medicine*, 191, 1381-1394.
- Iwasaki, A. & Kelsall, B. L. 2001. Unique Functions of CD11b⁺, CD8 α ⁺, and Double-Negative Peyer's Patch Dendritic Cells. *The Journal of Immunology*, 166, 4884-4890.
- Jazayeri, A., Doré, A. S., Lamb, D., Krishnamurthy, H., Southall, S. M., Baig, A. H., Bortolato, A., Koglin, M., Robertson, N. J., Errey, J. C., Andrews, S. P., Teobald, I., Brown, A. J. H., Cooke, R. M., Weir, M. & Marshall, F. H. 2016. Extra-helical binding site of a glucagon receptor antagonist. *Nature*, 533, 274-277.

- Jean-Charles, P.-Y., Kaur, S. & Shenoy, S. K. 2017. G Protein-Coupled Receptor Signaling Through β -Arrestin-Dependent Mechanisms. *Journal of Cardiovascular Pharmacology*, 70, 142-158.
- Jenkins, L., Marsango, S., Mancini, S., Mahmud, Z. A., Morrison, A., McElroy, S. P., Bennett, K. A., Barnes, M., Tobin, A. B., Tikhonova, I. G. & Milligan, G. 2021. Discovery and Characterization of Novel Antagonists of the Proinflammatory Orphan Receptor GPR84. *ACS Pharmacology & Translational Science*, 4, 1598-1613.
- Jia, W., Li, H., Zhao, L. & Nicholson, J. K. 2008. Gut microbiota: a potential new territory for drug targeting. *Nature Reviews Drug Discovery*, 7, 123-129.
- Kaji, I., Akiba, Y., Furuyama, T., Adelson, D. W., Iwamoto, K., Watanabe, M., Kuwahara, A. & Kaunitz, J. D. 2018. Free fatty acid receptor 3 activation suppresses neurogenic motility in rat proximal colon. *Neurogastroenterology and Motility*, 30, e13157.
- Kaji, I., Akiba, Y., Konno, K., Watanabe, M., Kimura, S., Iwanaga, T., Kuri, A., Iwamoto, K.-I., Kuwahara, A. & Kaunitz, J. D. 2016. Neural FFA3 activation inversely regulates anion secretion evoked by nicotinic ACh receptor activation in rat proximal colon. *Journal of Physiology*, 594, 3339-3352.
- Kaji, I., Karaki, S.-I., Tanaka, R. & Kuwahara, A. 2011. Density distribution of free fatty acid receptor 2 (FFA2)-expressing and GLP-1-producing enteroendocrine L cells in human and rat lower intestine, and increased cell numbers after ingestion of fructo-oligosaccharide. *Journal of Molecular Histology*, 42, 27-38.
- Kamp, M. E., Shim, R., Nicholls, A. J., Oliveira, A. C., Mason, L. J., Binge, L., Mackay, C. R. & Wong, C. H. Y. 2016. G Protein-Coupled Receptor 43 Modulates Neutrophil Recruitment during Acute Inflammation. *PLOS One*, 11, e0163750.
- Karaki, S.-I., Mitsui, R., Hayashi, H., Kato, I., Sugiya, H., Iwanaga, T., Furness, J. B. & Kuwahara, A. 2006. Short-chain fatty acid receptor, GPR43, is expressed by enteroendocrine cells and mucosal mast cells in rat intestine. *Cell and Tissue Research*, 324, 353-360.

- Karaki, S.-I., Tazoe, H., Hayashi, H., Kashiwabara, H., Tooyama, K., Suzuki, Y. & Kuwahara, A. 2008. Expression of the short-chain fatty acid receptor, GPR43, in the human colon. *Journal of Molecular Histology*, 39, 135-142.
- Kawakami, K., Yanagawa, M., Hiratsuka, S., Yoshida, M., Ono, Y., Hiroshima, M., Ueda, M., Aoki, J., Sako, Y. & Inoue, A. 2022. Heterotrimeric G_q proteins act as a switch for GRK5/6 selectivity underlying β -arrestin transducer bias. *Nature Communications*, 13, 487.
- Kebede, M. A., Alquier, T., Latour, M. G. & Poitout, V. 2009. Lipid receptors and islet function: therapeutic implications? *Diabetes, Obesity and Metabolism*, 11, 10-20.
- Kenakin, T. 2001. Inverse, protean, and ligand-selective agonism: matters of receptor conformation. *The FASEB Journal*, 15, 598-611.
- Kenakin, T. 2002. Efficacy at g-protein-coupled receptors. *Nature Reviews Drug Discovery*, 1, 103-110.
- Kenakin, T. 2007. Allosteric theory: Taking therapeutic advantage of the malleable nature of GPCRs. *Current Neuropharmacology*, 5, 149-156.
- Kenakin, T. 2019a. Biased Receptor Signaling in Drug Discovery. *Pharmacological Reviews*, 71, 267-315.
- Kenakin, T. 2019b. Emergent Concepts of Receptor Pharmacology. *Concepts and Principles of Pharmacology*. Springer International Publishing.
- Kenakin, T., Jenkinson, S. & Watson, C. 2006. Determining the potency and molecular mechanism of action of insurmountable antagonists. *Journal of Pharmacology and Experimental Therapeutics*, 319, 710-723.
- Kenakin, T. & Miller, L. J. 2010. Seven Transmembrane Receptors as Shapeshifting Proteins: The Impact of Allosteric Modulation and Functional Selectivity on New Drug Discovery. *Pharmacological Reviews*, 62, 265-304.
- Kenakin, T. & Strachan, R. T. 2018. PAM-Antagonists: A Better Way to Block Pathological Receptor Signaling? *Trends in Pharmacological Sciences*, 39, 748-765.

- Keov, P., Sexton, P. M. & Christopoulos, A. 2011. Allosteric modulation of G protein-coupled receptors: A pharmacological perspective. *Neuropharmacology*, 60, 24-35.
- Kim, M. H., Kang, S. G., Park, J. H., Yanagisawa, M. & Kim, C. H. 2013. Short-Chain Fatty Acids Activate GPR41 and GPR43 on Intestinal Epithelial Cells to Promote Inflammatory Responses in Mice. *Gastroenterology*, 145, 396-406.
- Kimura, I., Inoue, D., Maeda, T., Hara, T., Ichimura, A., Miyauchi, S., Kobayashi, M., Hirasawa, A. & Tsujimoto, G. 2011. Short-chain fatty acids and ketones directly regulate sympathetic nervous system via G protein-coupled receptor 41 (GPR41). *Proceedings of the National Academy of Sciences of the United States of America*, 108, 8030-8035.
- Kimura, I., Miyamoto, J., Ohue-Kitano, R., Watanabe, K., Yamada, T., Onuki, M., Aoki, R., Isobe, Y., Kashihara, D., Inoue, D., Inaba, A., Takamura, Y., Taira, S., Kumaki, S., Watanabe, M., Ito, M., Nakagawa, F., Irie, J., Kakuta, H., Shinohara, M., Iwatsuki, K., Tsujimoto, G., Ohno, H., Arita, M., Itoh, H. & Hase, K. 2020. Maternal gut microbiota in pregnancy influences offspring metabolic phenotype in mice. *Science*, 367, eaaw8429.
- Kimura, I., Ozawa, K., Inoue, D., Imamura, T., Kimura, K., Maeda, T., Terasawa, K., Kashihara, D., Hirano, K., Tani, T., Takahashi, T., Miyauchi, S., Shioi, G., Inoue, H. & Tsujimoto, G. 2013. The gut microbiota suppresses insulin-mediated fat accumulation via the short-chain fatty acid receptor GPR43. *Nature Communications*, 4, 1829.
- Kootte, R. S., Vrieze, A., Holleman, F., Dallinga-Thie, G. M., Zoetendal, E. G., De Vos, W. M., Groen, A. K., Hoekstra, J. B. L., Stoes, E. S. & Nieuwdorp, M. 2012. The therapeutic potential of manipulating gut microbiota in obesity and type 2 diabetes mellitus. *Diabetes, Obesity and Metabolism*, 14, 112-120.
- Kotarsky, K., Nilsson, N. E., Flodgren, E., Owman, C. & Olde, B. 2003. A human cell surface receptor activated by free fatty acids and thiazolidinedione drugs. *Biochemical and Biophysical Research Communications*, 301, 406-410.
- Kotlo, K., Anbazhagan, A. N., Priyamvada, S., Jayawardena, D., Kumar, A., Chen, Y., Xia, Y., Finn, P. W., Perkins, D. L., Dudeja, P. K. & Layden, B. T. 2020. The olfactory G protein-coupled receptor (Olfr-78/OR51E2) modulates

the intestinal response to colitis. *American Journal of Physiology-Cell Physiology*, 318, C502-C513.

- Kouhen, O. M.-E., Wang, G., Solberg, J., Erickson, L. J., Law, P.-Y. & Loh, H. H. 2000. Hierarchical Phosphorylation of δ -Opioid Receptor Regulates Agonist-induced Receptor Desensitization and Internalization. *Journal of Biological Chemistry*, 275, 36659-36664.
- Kunishima, N., Shimada, Y., Tsuji, Y., Sato, T., Yamamoto, M., Kumasaka, T., Nakanishi, S., Jingami, H. & Morikawa, K. 2000. Structural basis of glutamate recognition by a dimeric metabotropic glutamate receptor. *Nature*, 407, 971-977.
- Lagerström, M. C. & Schiöth, H. B. 2008. Structural diversity of G protein-coupled receptors and significance for drug discovery. *Nature Reviews Drug Discovery*, 7, 339-357.
- Lakso, M., Sauer, B., Mosinger, B., Lee, E. J., Manning, R. W., Yu, S. H., Mulder, K. L. & Westphal, H. 1992. Targeted oncogene activation by site-specific recombination in transgenic mice. *Proceedings of the National Academy of Sciences*, 89, 6232-6236.
- Lambright, D. G., Sondek, J., Böhm, A., Skiba, N. P., Hamm, H. E. & Sigler, P. B. 1996. The 2.0 Å crystal structure of a heterotrimeric G protein. *Nature*, 379, 311-319.
- Laporte, S. A., Oakley, R. H., Zhang, J., Holt, J. A., Ferguson, S. S. G., Caron, M. G. & Barak, L. S. 1999. The β_2 -adrenergic receptor/Barrestin complex recruits the clathrin adaptor AP-2 during endocytosis. *Proceedings of the National Academy of Sciences of the United States of America*, 96, 3712-3717.
- Latorraca, N. R., Masureel, M., Hollingsworth, S. A., Heydenreich, F. M., Suomivuori, C.-M., Brinton, C., Townshend, R. J. L., Bouvier, M., Kobilka, B. K. & Dror, R. O. 2020. How GPCR Phosphorylation Patterns Orchestrate Arrestin-Mediated Signaling. *Cell*, 183, 1813-1825.
- Latorraca, N. R., Venkatakrisnan, A. J. & Dror, R. O. 2017. GPCR Dynamics: Structures in Motion. *Chemical Reviews*, 117, 139-155.

- Le Poul, E., Loison, C., Struyf, S., Springael, J. Y., Lannoy, V., Decobecq, M. E., Brezillon, S., Dupriez, V., Vassart, G., Van Damme, J., Parmentier, M. & Detheux, M. 2003. Functional characterization of human receptors for short chain fatty acids and their role in polymorphonuclear cell activation. *Journal of Biological Chemistry*, 278, 25481-25489.
- Lee, M.-H., Appleton, K. M., Strungs, E. G., Kwon, J. Y., Morinelli, T. A., Peterson, Y. K., Laporte, S. A. & Luttrell, L. M. 2016. The conformational signature of β -arrestin2 predicts its trafficking and signalling functions. *Nature*, 531, 665-668.
- Lee, T., Schwandner, R., Swaminath, G., Weiszmann, J., Cardozo, M., Greenberg, J., Jaeckel, P., Ge, H., Wang, Y., Jiao, X., Liu, J., Kayser, F., Tian, H. & Li, Y. 2008. Identification and Functional Characterization of Allosteric Agonists for the G Protein-Coupled Receptor FFA2. *Molecular Pharmacology*, 74, 1599-1609.
- Lehmann, A., Kliewer, A., Schuetz, D., Nagel, F., Stumm, R. & Schulz, S. 2014. Carboxyl-terminal multi-site phosphorylation regulates internalization and desensitization of the human $ss2$ somatostatin receptor. *Molecular and Cellular Endocrinology*, 387, 44-51.
- Leonard, J. N., Chu, Z. L., Bruce, M. A. & Boatman, P. D. 2006. GPR41 and modulators thereof for the treatment of insulin-related disorders. *International Patent*. WO 2006/052566 A2.
- Li, M., Van Esch, B. C. A. M., Wagenaar, G. T. M., Garssen, J., Folkerts, G. & Henricks, P. A. J. 2018. Pro- and anti-inflammatory effects of short chain fatty acids on immune and endothelial cells. *European Journal of Pharmacology*, 831, 52-59.
- Li, Y., Kokrashvili, Z., Mosinger, B. & Margolskee, R. F. 2013. Gustducin couples fatty acid receptors to GLP-1 release in colon. *American Journal of Physiology-Endocrinology and Metabolism*, 304, E651-E660.
- Liang, Y.-L., Khoshouei, M., Radjainia, M., Zhang, Y., Glukhova, A., Tarrasch, J., Thal, D. M., Furness, S. G. B., Christopoulos, G., Coudrat, T., Danev, R., Baumeister, W., Miller, L. J., Christopoulos, A., Kobilka, B. K., Wootten, D., Skiniotis, G. & Sexton, P. M. 2017. Phase-plate cryo-EM structure of a class B GPCR-G-protein complex. *Nature*, 546, 118-123.

- Lim, H. K. & O'Neill, H. C. 2019. Identification of Stromal Cells in Spleen Which Support Myelopoiesis. *Frontiers in Cell and Developmental Biology*, 7, 1.
- Lind, S., Hoffmann, D. O., Forsman, H. & Dahlgren, C. 2022. Allosteric receptor modulation uncovers an FFA2R antagonist as a positive orthosteric modulator/agonist in disguise. *Cellular Signalling*, 90, 110208.
- Lind, S., Holdfeldt, A., Martensson, J., Sundqvist, M., Bjorkman, L., Forsman, H. & Dahlgren, C. 2019. Functional selective ATP receptor signaling controlled by the free fatty acid receptor 2 through a novel allosteric modulation mechanism. *FASEB Journal*, 33, 6887-6903.
- Lind, S., Holdfeldt, A., Martensson, J., Sundqvist, M., Kenakin, T. P., Bjorkman, L., Forsman, H. & Dahlgren, C. 2020. Interdependent allosteric free fatty acid receptor 2 modulators synergistically induce functional selective activation and desensitization in neutrophils. *Biochimica Et Biophysica Acta-Molecular Cell Research*, 1867, 118689.
- Lind, S., Holdfeldt, A., Mårtensson, J., Granberg, K. L., Forsman, H. & Dahlgren, C. 2021. Multiple ligand recognition sites in free fatty acid receptor 2 (FFA2R) direct distinct neutrophil activation patterns. *Biochemical Pharmacology*, 193, 114762.
- Livak, K. J. & Schmittgen, T. D. 2001. Analysis of Relative Gene Expression Data Using Real-Time Quantitative PCR and the $2^{-\Delta\Delta CT}$ Method. *Methods*, 25, 402-408.
- Lobbestael, E., Reumers, V., Ibrahimi, A., Paesen, K., Thiry, I., Gijssbers, R., Van Den Haute, C., Debyser, Z., Baekelandt, V. & Taymans, J.-M. 2010. Immunohistochemical detection of transgene expression in the brain using small epitope tags. *BMC Biotechnology*, 10, 16.
- Lorenz, R. G. & Newberry, R. D. 2004. Isolated Lymphoid Follicles Can Function as Sites for Induction of Mucosal Immune Responses. *Annals of the New York Academy of Sciences*, 1029, 44-57.
- Lorza-Gil, E., Kaiser, G., Rexen Ulven, E., König, G. M., Gerst, F., Oquendo, M. B., Birkenfeld, A. L., Häring, H.-U., Kostenis, E., Ulven, T. & Ullrich, S. 2020. FFA2, but not FFA3-agonists inhibit GSIS of human pseudoislets: a

- comparative study with mouse islets and rat INS-1E cells. *Scientific Reports*, 10, 16497.
- Lowe, J. D., Sanderson, H. S., Cooke, A. E., Ostovar, M., Tsisanova, E., Withey, S. L., Chavkin, C., Husbands, S. M., Kelly, E., Henderson, G. & Bailey, C. P. 2015. Role of G Protein-Coupled Receptor Kinases 2 and 3 in μ -Opioid Receptor Desensitization and Internalization. *Molecular Pharmacology*, 88, 347-356.
- Lundquist, F., Winkler, K., Munckpet.S, Tygstrup, N. & Mellempgaard, K. 1962. Ethanol metabolism and production of free acetate in human liver. *Journal of Clinical Investigation*, 41, 955-961.
- Luttrell, L. M., Roudabush, F. L., Choy, E. W., Miller, W. E., Field, M. E., Pierce, K. L. & Lefkowitz, R. J. 2001. Activation and targeting of extracellular signal-regulated kinases by β -arrestin scaffolds. *Proceedings of the National Academy of Sciences of the United States of America*, 98, 2449-2454.
- MacDonald, B. T. & He, X. 2012. Frizzled and LRP5/6 Receptors for Wnt/ β -Catenin Signaling. *Cold Spring Harbor Perspectives in Biology*, 4, a007880-a007880.
- Machleidt, T., Woodrooffe, C. C., Schwinn, M. K., Méndez, J., Robers, M. B., Zimmerman, K., Otto, P., Daniels, D. L., Kirkland, T. A. & Wood, K. V. 2015. NanoBRET—A Novel BRET Platform for the Analysis of Protein-Protein Interactions. *ACS Chemical Biology*, 10, 1797-1804.
- Magnani, F., Serrano-Vega, M. J., Shibata, Y., Abdul-Hussein, S., Lebon, G., Miller-Gallacher, J., Singhal, A., Strege, A., Thomas, J. A. & Tate, C. G. 2016. A mutagenesis and screening strategy to generate optimally thermostabilized membrane proteins for structural studies. *Nature Protocols*, 11, 1554-1571.
- Mahindra, A., Jenkins, L., Marsango, S., Huggett, M., Huggett, M., Robinson, L., Gillespie, J., Rajamanickam, M., Morrison, A., Mcelroy, S., Tikhonova, I. G., Milligan, G. & Jamieson, A. G. 2022. Investigating the Structure-Activity Relationship of 1,2,4-Triazine G-Protein-Coupled Receptor 84 (GPR84) Antagonists. *Journal of Medicinal Chemistry*, 65, 11270-11290.

- Maley, F., Trimble, R. B., Tarentino, A. L. & Plummer, T. H. 1989. Characterization of glycoproteins and their associated oligosaccharides through the use of endoglycosidases. *Analytical Biochemistry*, 180, 195-204.
- Mann, A., Keen, A. C., Mark, H., Dasgupta, P., Javitch, J. A., Canals, M., Schulz, S. & Lane, J. R. 2021. New phosphosite-specific antibodies to unravel the role of GRK phosphorylation in dopamine D₂ receptor regulation and signaling. *Scientific Reports*, 11, 8288.
- Mann, A., Liebetrau, S., Klima, M., Dasgupta, P., Massotte, D. & Schulz, S. 2020. Agonist-induced phosphorylation bar code and differential post-activation signaling of the δ opioid receptor revealed by phosphosite-specific antibodies. *Scientific Reports*, 10, 8585.
- Mann, A., Mouldous, L., Froment, C., O'Neill, P. R., Dasgupta, P., Guenther, T., Brunori, G., Kieffer, B. L., Toll, L., Bruchas, M. R., Zaveri, N. T. & Schulz, S. 2019. Agonist-selective NOP receptor phosphorylation correlates in vitro and in vivo and reveals differential post-activation signaling by chemically diverse agonists. *Science Signaling*, 12, eaau8072.
- Marsango, S., Barki, N., Jenkins, L., Tobin, A. B. & Milligan, G. 2022a. Therapeutic validation of an orphan G protein-coupled receptor: The case of GPR84. *British Journal of Pharmacology*, 179, 3529-3541.
- Marsango, S., Ward, R. J., Jenkins, L., Butcher, A. J., Al Mahmud, Z., Dwomoh, L., Nagel, F., Schulz, S., Tikhonova, I. G., Tobin, A. B. & Milligan, G. 2022b. Selective phosphorylation of threonine residues defines GPR84-arrestin interactions of biased ligands. *The Journal of Biological Chemistry*, 298, 101932-101932.
- Martensson, J., Holdfeldt, A., Sundqvist, M., Gabl, M., Kenakin, T. P., Bjorkman, L., Forsman, H. & Dahlgren, C. 2018. Neutrophil priming that turns natural FFA2R agonists into potent activators of the superoxide generating NADPH-oxidase. *Journal of Leukocyte Biology*, 104, 1117-1132.
- Maslowski, K. M., Vieira, A. T., Ng, A., Kranich, J., Sierro, F., Yu, D., Schilter, H. C., Rolph, M. S., Mackay, F., Artis, D., Xavier, R. J., Teixeira, M. M. & Mackay, C. R. 2009. Regulation of inflammatory responses by gut microbiota and chemoattractant receptor GPR43. *Nature*, 461, 1282-1286.

- Masui, R., Sasaki, M., Funaki, Y., Ogasawara, N., Mizuno, M., Iida, A., Izawa, S., Kondo, Y., Ito, Y., Tamura, Y., Yanamoto, K., Noda, H., Tanabe, A., Okaniwa, N., Yamaguchi, Y., Iwamoto, T. & Kasugai, K. 2013. G Protein-Coupled Receptor 43 Moderates Gut Inflammation Through Cytokine Regulation from Mononuclear Cells. *Inflammatory Bowel Diseases*, 19, 2848-2856.
- Matthees, E. S. F., Haider, R. S., Hoffmann, C. & Drube, J. 2021. Differential Regulation of GPCRs-Are GRK Expression Levels the Key? *Frontiers in Cell and Developmental Biology*, 9, 687489.
- McDonald, K. G., McDonough, J. S., Dieckgraefe, B. K. & Newberry, R. D. 2010. Dendritic Cells Produce CXCL13 and Participate in the Development of Murine Small Intestine Lymphoid Tissues. *The American Journal of Pathology*, 176, 2367-2377.
- McLane, M. W., Hatzidimitriou, G., Yuan, J., McCann, U. & Ricaurte, G. 2007. Heating induces aggregation and decreases detection of serotonin transporter protein on western blots. *Synapse*, 61, 875-876.
- McNelis, J. C., Lee, Y. S., Mayoral, R., Van Der Kant, R., Johnson, A. M. F., Wollam, J. & Olefsky, J. M. 2015. GPR43 Potentiates B-Cell Function in Obesity. *Diabetes*, 64, 3203-3217.
- Miller, L. J., Dong, M. & Harikumar, K. G. 2012. Ligand binding and activation of the secretin receptor, a prototypic family B G protein-coupled receptor. *British Journal of Pharmacology*, 166, 18-26.
- Milligan, G. 2003. Principles: Extending the utility of [³⁵S]GTPγS binding assays. *Trends in Pharmacological Sciences*, 24, 87-90.
- Milligan, G., Shimpukade, B., Ulven, T. & Hudson, B. D. 2017. Complex Pharmacology of Free Fatty Acid Receptors. *Chemical Reviews*, 117, 67-110.
- Miyamoto, J., Ohue-Kitano, R., Mukouyama, H., Nishida, A., Watanabe, K., Igarashi, M., Irie, J., Tsujimoto, G., Satoh-Asahara, N., Itoh, H. & Kimura, I. 2019. Ketone body receptor GPR43 regulates lipid metabolism under ketogenic conditions. *Proceedings of the National Academy of Sciences of the United States of America*, 116, 23813-23821.

- Møller, T. C., Pedersen, M. F., Van Senten, J. R., Seiersen, S. D., Mathiesen, J. M., Bouvier, M. & Bräuner-Osborne, H. 2020. Dissecting the roles of GRK2 and GRK3 in μ -opioid receptor internalization and β -arrestin2 recruitment using CRISPR/Cas9-edited HEK293 cells. *Scientific Reports*, 10, 17395.
- Morrison, D. J. & Preston, T. 2016. Formation of short chain fatty acids by the gut microbiota and their impact on human metabolism. *Gut Microbes*, 7, 189-200.
- Nagasaki, H., Kondo, T., Fuchigami, M., Hashimoto, H., Sugimura, Y., Ozaki, N., Arima, H., Ota, A., Oiso, Y. & Hamada, Y. 2012. Inflammatory changes in adipose tissue enhance expression of GPR84, a medium-chain fatty acid receptor TNF α enhances GPR84 expression in adipocytes. *FEBS Letters*, 586, 368-372.
- Nakajima, A., Nakatani, A., Hasegawa, S., Irie, J., Ozawa, K., Tsujimoto, G., Suganami, T., Itoh, H. & Kimura, I. 2017. The short chain fatty acid receptor GPR43 regulates inflammatory signals in adipose tissue M2-type macrophages. *PLOS One*, 12, e0179696.
- Namour, F., Galien, R., Van Kaem, T., Van Der Aa, A., Vanhoutte, F., Beetens, J. & Klooster, G. 2016. Safety, pharmacokinetics and pharmacodynamics of GLPG0974, a potent and selective FFA2 antagonist, in healthy male subjects. *British Journal of Clinical Pharmacology*, 82, 139-148.
- Nguyen, A. H., Thomsen, A. R. B., Cahill, T. J., Huang, R., Huang, L.-Y., Marcink, T., Clarke, O. B., Heissel, S., Masoudi, A., Ben-Hail, D., Samaan, F., Dandey, V. P., Tan, Y. Z., Hong, C., Mahoney, J. P., Triest, S., Little, J., Chen, X., Sunahara, R., Steyaert, J., Molina, H., Yu, Z., Des Georges, A. & Lefkowitz, R. J. 2019. Structure of an endosomal signaling GPCR-G protein- β -arrestin megacomplex. *Nature Structural & Molecular Biology*, 26, 1123-1131.
- Nilsson, N. E., Kotarsky, K., Owman, C. & Olde, B. 2003. Identification of a free fatty acid receptor, FFA2R, expressed on leukocytes and activated by short-chain fatty acids. *Biochemical and Biophysical Research Communications*, 303, 1047-1052.
- Nobles, K. N., Xiao, K., Ahn, S., Shukla, A. K., Lam, C. M., Rajagopal, S., Strachan, R. T., Huang, T.-Y., Bressler, E. A., Hara, M. R., Shenoy, S. K.,

- Gygi, S. P. & Lefkowitz, R. J. 2011. Distinct Phosphorylation Sites on the β_2 -Adrenergic Receptor Establish a Barcode That Encodes Differential Functions of β -Arrestin. *Science Signaling*, 4, ra51.
- Nohr, M. K., Egerod, K. L., Christiansen, S. H., Gille, A., Offermanns, S., Schwartz, T. W. & Moller, M. 2015. Expression of the short chain fatty acid receptor GPR41/FFAR3 in autonomic and somatic sensory ganglia. *Neuroscience*, 290, 126-137.
- Nohr, M. K., Pedersen, M. H., Gille, A., Egerod, K. L., Engelstoft, M. S., Husted, A. S., Sichlau, R. M., Grunddal, K. V., Poulsen, S. S., Han, S., Jones, R. M., Offermanns, S. & Schwartz, T. W. 2013. GPR41/FFAR3 and GPR43/FFAR2 as Cosensors for Short-Chain Fatty Acids in Enteroendocrine Cells vs FFAR3 in Enteric Neurons and FFAR2 in Enteric Leukocytes. *Endocrinology*, 154, 3552-3564.
- Offermanns, S., Colletti, S. L., Lovenberg, T. W., Semple, G., Wise, A. & Ijzerman, A. P. 2011. International Union of Basic and Clinical Pharmacology. LXXXII: Nomenclature and Classification of Hydroxycarboxylic Acid Receptors (GPR81, GPR109A, and GPR109B). *Pharmacological Reviews*, 63, 269-290.
- Oh, D. Y. & Olefsky, J. M. 2012. Omega 3 Fatty Acids and GPR120. *Cell Metabolism*, 15, 564-565.
- Oh, D. Y., Talukdar, S., Bae, E. J., Imamura, T., Morinaga, H., Fan, W., Li, P., Lu, W. J., Watkins, S. M. & Olefsky, J. M. 2010. GPR120 Is an Omega-3 Fatty Acid Receptor Mediating Potent Anti-inflammatory and Insulin-Sensitizing Effects. *Cell*, 142, 687-698.
- Ohguro, H., Palczewski, K., Ericsson, L. H., Walsh, K. A. & Johnson, R. S. 1993. Sequential phosphorylation of rhodopsin at multiple sites. *Biochemistry*, 32, 5718-5724.
- Olaniru, O. E. & Persaud, S. J. 2019. Adhesion G-protein coupled receptors: Implications for metabolic function. *Pharmacology & Therapeutics*, 198, 123-134.

- Orban, P. C., Chui, D. & Marth, J. D. 1992. Tissue- and site-specific DNA recombination in transgenic mice. *Proceedings of the National Academy of Sciences*, 89, 6861-6865.
- Orgaard, A., Jepsen, S. L. & Holst, J. J. 2019. Short-chain fatty acids and regulation of pancreatic endocrine secretion in mice. *Islets*, 11, 103-111.
- Osmond, R. I. W., Sheehan, A., Borowicz, R., Barnett, E., Harvey, G., Turner, C., Brown, A., Crouch, M. F. & Dyer, A. R. 2005. GPCR Screening via ERK 1/2: A Novel Platform for Screening G Protein-Coupled Receptors. *Journal of Biomolecular Screening*, 10, 730-737.
- Pabst, O., Herbrand, H., Friedrichsen, M., Velaga, S., Dorsch, M., Berhardt, G., Worbs, T., Macpherson, A. J. & Förster, R. 2006. Adaptation of Solitary Intestinal Lymphoid Tissue in Response to Microbiota and Chemokine Receptor CCR7 Signaling. *The Journal of Immunology*, 177, 6824-6832.
- Paddock, S. W. & Eliceiri, K. W. 2014. Laser Scanning Confocal Microscopy: History, Applications, and Related Optical Sectioning Techniques. *Confocal Microscopy*. Springer New York.
- Park, B.-O., Kang, J. S., Paudel, S., Park, S. G., Park, B. C., Han, S.-B., Kwak, Y.-S., Kim, J.-H. & Kim, S. 2022. Novel GPR43 Agonists Exert an Anti-Inflammatory Effect in a Colitis Model. *Biomolecules & Therapeutics*, 30, 48-54.
- Park, B.-O., Kim, S. H., Kong, G. Y., Kim, D. H., Kwon, M. S., Lee, S. U., Kim, M.-O., Cho, S., Lee, S., Lee, H.-J., Han, S.-B., Kwak, Y. S., Lee, S. B. & Kim, S. 2016. Selective novel inverse agonists for human GPR43 augment GLP-1 secretion. *European Journal of Pharmacology*, 771, 1-9.
- Parker, H., Dragunow, M., Hampton, M. B., Kettle, A. J. & Winterbourn, C. C. 2012. Requirements for NADPH oxidase and myeloperoxidase in neutrophil extracellular trap formation differ depending on the stimulus. *Journal of Leukocyte Biology*, 92, 841-849.
- Patel, M., Kawano, T., Suzuki, N., Hamakubo, T., Karginov, A. V. & Kozasa, T. 2014. $G\alpha_{13}$ /PDZ-RhoGEF/RhoA Signaling Is Essential for Gastrin-Releasing Peptide Receptor-Mediated Colon Cancer Cell Migration. *Molecular Pharmacology*, 86, 252-262.

- Pfleger, K. D. G. & Eidne, K. A. 2006. Illuminating insights into protein-protein interactions using bioluminescence resonance energy transfer (BRET). *Nature Methods*, 3, 165-174.
- Pillai-Kastoori, L., Schutz-Geschwender, A. R. & Harford, J. A. 2020. A systematic approach to quantitative Western blot analysis. *Analytical Biochemistry*, 593, 113608.
- Pillaiyar, T., Koese, M., Sylvester, K., Weighardt, H., Thimm, D., Borges, G., Foerster, I., Von Kuegelgen, I. & Mueller, C. E. 2017. Diindolylmethane Derivatives: Potent Agonists of the Immunostimulatory Orphan G Protein-Coupled Receptor GPR84. *Journal of Medicinal Chemistry*, 60, 3636-3655.
- Pingitore, A., Gonzalez-Abuin, N., Ruz-Maldonado, I., Huang, G. C., Frost, G. & Persaud, S. J. 2019. Short chain fatty acids stimulate insulin secretion and reduce apoptosis in mouse and human islets in vitro: Role of free fatty acid receptor 2. *Diabetes Obesity & Metabolism*, 21, 330-339.
- Pizzonero, M., Dupont, S., Babel, M., Beaumont, S., Bienvenu, N., Blaque, R., Cherel, L., Christophe, T., Crescenzi, B., De Lemos, E., Delerive, P., Deprez, P., De Vos, S., Djata, F., Fletcher, S., Kopiejewski, S., L'ebaly, C., Lefrancois, J.-M., Lavazais, S., Manioc, M., Nelles, L., Oste, L., Polancec, D., Quenehen, V., Soulas, F., Triballeau, N., Van Der Aar, E. M., Vandeghinste, N., Wakselman, E., Brys, R. & Saniere, L. 2014. Discovery and Optimization of an Azetidine Chemical Series As a Free Fatty Acid Receptor 2 (FFA2) Antagonist: From Hit to Clinic. *Journal of Medicinal Chemistry*, 57, 10044-10057.
- Pluznick, J. 2014. A novel SCFA receptor, the microbiota, and blood pressure regulation. *Gut Microbes*, 5, 202-207.
- Pluznick, J. L., Zou, D.-J., Zhang, X., Yan, Q., Rodriguez-Gil, D. J., Eisner, C., Wells, E., Greer, C. A., Wang, T., Firestein, S., Schnermann, J. & Caplan, M. J. 2009. Functional expression of the olfactory signaling system in the kidney. *Proceedings of the National Academy of Sciences*, 106, 2059-2064.
- Portela-Gomes, G. M., Stridsberg, M., Johansson, H. & Grimelius, L. 1997. Complex Co-localization of Chromogranins and Neurohormones in the Human Gastrointestinal Tract. *Journal of Histochemistry & Cytochemistry*, 45, 815-822.

- Priyadarshini, M., Cole, C., Oroskar, G., Ludvik, A. E., Wicksteed, B., He, C. & Layden, B. T. 2020. Free fatty acid receptor 3 differentially contributes to β -cell compensation under high-fat diet and streptozotocin stress. *American Journal of Physiology-Regulatory Integrative and Comparative Physiology*, 318, R691-R700.
- Priyadarshini, M. & Layden, B. T. 2015. FFAR3 modulates insulin secretion and global gene expression in mouse islets. *Islets*, 7, e1045182.
- Priyadarshini, M., Villa, S. R., Fuller, M., Wicksteed, B., Mackay, C. R., Alquier, T., Poitout, V., Mancebo, H., Mirmira, R. G., Gilchrist, A. & Layden, B. T. 2015. An Acetate-Specific GPCR, FFAR2, Regulates Insulin Secretion. *Molecular Endocrinology*, 29, 1055-1066.
- Psichas, A., Sleeth, M. L., Murphy, K. G., Brooks, L., Bewick, G. A., Hanyaloglu, A. C., Ghatei, M. A., Bloom, S. R. & Frost, G. 2015. The short chain fatty acid propionate stimulates GLP-1 and PYY secretion via free fatty acid receptor 2 in rodents. *International Journal of Obesity*, 39, 424-429.
- Puhl III, H. L., Won, Y.-J., Lu, V. B. & Ikeda, S. R. 2015. Human GPR42 is a transcribed multisite variant that exhibits copy number polymorphism and is functional when heterologously expressed. *Scientific Reports*, 5, 12880.
- Qiao, Y., Zhang, K., Zhang, Z., Zhang, C., Sun, Y. & Feng, Z. 2022. Fermented soybean foods: A review of their functional components, mechanism of action and factors influencing their health benefits. *Food Research International*, 158.
- Ramos-Vara, J. A. & Miller, M. A. 2014. When Tissue Antigens and Antibodies Get Along. *Veterinary Pathology*, 51, 42-87.
- Rask-Andersen, M., Masuram, S. & Schioth, H. B. 2014. The Druggable Genome: Evaluation of Drug Targets in Clinical Trials Suggests Major Shifts in Molecular Class and Indication. In: Insel, P. A. (ed.) *Annual Review of Pharmacology and Toxicology*, Vol 54. Palo Alto: Annual Reviews.
- Rasmussen, S. G. F., Devree, B. T., Zou, Y., Kruse, A. C., Chung, K. Y., Kobilka, T. S., Thian, F. S., Chae, P. S., Pardon, E., Calinski, D., Mathiesen, J. M., Shah, S. T. A., Lyons, J. A., Caffrey, M., Gellman, S. H., Steyaert, J., Skiniotis, G., Weis, W. I., Sunahara, R. K. & Kobilka, B. K. 2011. Crystal

- structure of the β_2 adrenergic receptor-Gs protein complex. *Nature*, 477, 549-555.
- Raybould, H. E. 2012. Gut microbiota, epithelial function and derangements in obesity. *The Journal of Physiology*, 590, 441-446.
- Rochereau, N., Verrier, B., Pin, J.-J., Genin, C. & Paul, S. 2011. Phenotypic localization of distinct DC subsets in mouse Peyer Patch. *Vaccine*, 29, 3655-3661.
- Rogers-Broadway, K.-R. & Karteris, E. 2015. Amplification efficiency and thermal stability of qPCR instrumentation: Current landscape and future perspectives. *Experimental and Therapeutic Medicine*, 10, 1261-1264.
- Rovati, G. E., Capra, V. & Neubig, R. R. 2007. The Highly Conserved DRY Motif of Class A G Protein-Coupled Receptors: Beyond the Ground State. *Molecular Pharmacology*, 71, 959-964.
- Rusnak, F., Yu, L., Todorovic, S. & Mertz, P. 1999. Interaction of Bacteriophage λ Protein Phosphatase with Mn(II): Evidence for the Formation of a $[\text{Mn(II)}]_2$ Cluster. *Biochemistry*, 38, 6943-6952.
- Samuel, B. S., Shaito, A., Motoike, T., Rey, F. E., Backhed, F., Manchester, J. K., Hammer, R. E., Williams, S. C., Crowley, J., Yanagisawa, M. & Gordon, J. I. 2008. Effects of the gut microbiota on host adiposity are modulated by the short-chain fatty-acid binding G protein-coupled receptor, Gpr41. *Proceedings of the National Academy of Sciences*, 105, 16767-16772.
- Sawzdargo, M., George, S. R., Nguyen, T., Xu, S. J., Kolakowski, L. F. & Odowd, B. F. 1997. A cluster of four novel human G protein-coupled receptor genes occurring in close proximity to CD22 gene on chromosome 19q13.1. *Biochemical and Biophysical Research Communications*, 239, 543-547.
- Schioth, H. B. & Fredriksson, R. 2005. The GRAFS classification system of G-protein coupled receptors in comparative perspective. *General and Comparative Endocrinology*, 142, 94-101.
- Schmidt, J., Smith, N. J., Christiansen, E., Tikhonova, I. G., Grundmann, M., Hudson, B. D., Ward, R. J., Drewke, C., Milligan, G., Kostenis, E. & Ulven, T. 2011. Selective Orthosteric Free Fatty Acid Receptor 2 (FFA2) Agonists: Identification of the structural and chemical requirements for selective

activations of FFA2 versus FFA3. *Journal of Biological Chemistry*, 286, 10628-10640.

- Schofield, Z. V., Croker, D., Robertson, A. A. B., Massey, N. L., Donovan, C., Tee, E., Edwards, D., Woodruff, T. M., Halai, R., Hansbro, P. M. & Cooper, M. A. 2018. Characterisation of small molecule ligands 4CMTB and 2CTAP as modulators of human FFA2 receptor signalling. *Scientific reports*, 8, 17819-17819.
- Schreiber, C. L., Li, D.-H. & Smith, B. D. 2021. High-Performance Near-Infrared Fluorescent Secondary Antibodies for Immunofluorescence. *Analytical Chemistry*, 93, 3643-3651.
- Sencio, V., Barthelemy, A., Tavares, L. P., Machado, M. G., Soulard, D., Cuinat, C., Queiroz-Junior, C. M., Noordine, M.-L., Salome-Desnoulez, S., Deryuter, L., Foligne, B., Wahl, C., Frisch, B., Vieira, A. T., Paget, C., Milligan, G., Ulven, T., Wolowczuk, I., Faveeuw, C., Le Goffic, R., Thomas, M., Ferreira, S., Teixeira, M. M. & Trottein, F. 2020. Gut Dysbiosis during Influenza Contributes to Pulmonary Pneumococcal Superinfection through Altered Short-Chain Fatty Acid Production. *Cell Reports*, 30, 2934-2947.
- Sergeev, E. 2018. Investigating the molecular pharmacology of the short chain fatty acid receptor FFA2. PhD thesis. University of Glasgow. Available at: <http://theses.gla.ac.uk/8963/>
- Sergeev, E., Hansen, A. H., Bolognini, D., Kawakami, K., Kishi, T., Aoki, J., Ulven, T., Inoue, A., Hudson, B. D. & Milligan, G. 2017. A single extracellular amino acid in Free Fatty Acid Receptor 2 defines antagonist species selectivity and G protein selection bias. *Scientific Reports*, 7, 13741.
- Sergeev, E., Hansen, A. H., Pandey, S. K., Mackenzie, A. E., Hudson, B. D., Ulven, T. & Milligan, G. 2016. Non-equivalence of Key Positively Charged Residues of the Free Fatty Acid 2 Receptor in the Recognition and Function of Agonist Versus Antagonist Ligands. *Journal of Biological Chemistry*, 291, 303-317.
- Shreedhar, V. K., Kelsall, B. L. & Neutra, M. R. 2003. Cholera Toxin Induces Migration of Dendritic Cells from the Subepithelial Dome Region to T- and B-Cell Areas of Peyer's Patches. *Infection and Immunity*, 71, 504-509.

- Simon, M. I., Strathmann, M. P. & Gautam, N. 1991. Diversity of G-proteins in signal transduction. *Science*, 252, 802-808.
- Sina, C., Gavrilova, O., Foerster, M., Till, A., Derer, S., Hildebrand, F., Raabe, B., Chalaris, A., Scheller, J., Rehmann, A., Franke, A., Ott, S., Haesler, R., Nikolaus, S., Foelsch, U. R., Rose-John, S., Jiang, H.-P., Li, J., Schreiber, S. & Rosenstiel, P. 2009. G Protein-Coupled Receptor 43 Is Essential for Neutrophil Recruitment during Intestinal Inflammation. *Journal of Immunology*, 183, 7514-7522.
- Smith, N. J., Ward, R. J., Stoddart, L. A., Hudson, B. D., Kostenis, E., Ulven, T., Morris, J. C., Traenkle, C., Tikhonova, I. G., Adams, D. R. & Milligan, G. 2011. Extracellular Loop 2 of the Free Fatty Acid Receptor 2 Mediates Allosterism of a Phenylacetamide Ago-Allosteric Modulator. *Molecular Pharmacology*, 80, 163-173.
- Smith, P. M., Howitt, M. R., Panikov, N., Michaud, M., Gallini, C. A., Bohlooly-Y, M., Glickman, J. N. & Garrett, W. S. 2013. The Microbial Metabolites, Short-Chain Fatty Acids, Regulate Colonic Treg Cell Homeostasis. *Science*, 341, 569-573.
- Smith-Garvin, J. E., Koretzky, G. A. & Jordan, M. S. 2009. T Cell Activation. *Annual Review of Immunology*, 27, 591-619.
- Smits, L. P., Bouter, K. E. C., De Vos, W. M., Borody, T. J. & Nieuwdorp, M. 2013. Therapeutic Potential of Fecal Microbiota Transplantation. *Gastroenterology*, 145, 946-953.
- Smrcka, A. V. & Fisher, I. 2019. G-protein $\beta\gamma$ subunits as multi-functional scaffolds and transducers in G-protein-coupled receptor signaling. *Cellular and Molecular Life Sciences*, 76, 4447-4459.
- Soehnlein, O., Steffens, S., Hidalgo, A. & Weber, C. 2017. Neutrophils as protagonists and targets in chronic inflammation. *Nature Reviews Immunology*, 17, 248-261.
- Soergel, K. H. 1994. Colonic fermentation: metabolic and clinical implications. *The Clinical Investigator*, 72, 742-748.
- Sriram, K., Wiley, S. Z., Moyung, K., Gorr, M. W., Salmerón, C., Marucut, J., French, R. P., Lowy, A. M. & Insel, P. A. 2019. Detection and Quantification

- of GPCR mRNA: An Assessment and Implications of Data from High-Content Methods. *ACS Omega*, 4, 17048-17059.
- Stanley, P. E. 1989. A review of bioluminescent ATP techniques in rapid microbiology. *Journal of Bioluminescence and Chemiluminescence*, 4, 375-380.
- Stenman, L. K. 2012. High-fat-induced intestinal permeability dysfunction associated with altered fecal bile acids. *World Journal of Gastroenterology*, 18, 923-929.
- Stoddart, L. A., Smith, N. J., Jenkins, L., Brown, A. J. & Milligan, G. 2008. Conserved Polar Residues in Transmembrane Domains V, VI, and VII of Free Fatty Acid Receptor 2 and Free Fatty Acid Receptor 3 Are Required for the Binding and Function of Short Chain Fatty Acids. *Journal of Biological Chemistry*, 283, 32913-32924.
- Strange, P. G. 2010. Use of the GTP γ S ([³⁵S]GTP γ S and Eu-GTP γ S) binding assay for analysis of ligand potency and efficacy at G protein-coupled receptors. *British Journal of Pharmacology*, 161, 1238-1249.
- Sun, W., Dong, H., Balaz, M., Slyper, M., Drokhlyansky, E., Colleluori, G., Giordano, A., Kovanicova, Z., Stefanicka, P., Balazova, L., Ding, L., Husted, A. S., Rudofsky, G., Ukropec, J., Cinti, S., Schwartz, T. W., Regev, A. & Wolfrum, C. 2020. snRNA-seq reveals a subpopulation of adipocytes that regulates thermogenesis. *Nature*, 587, 98-102.
- Sun, Y., Ip, P. & Chakrabarty, A. 2017. Simple Elimination of Background Fluorescence in Formalin-Fixed Human Brain Tissue for Immunofluorescence Microscopy. *Jove-Journal of Visualized Experiments*, 127, 56188.
- Sundqvist, M., Christenson, K., Holdfeldt, A., Gabl, M., Martensson, J., Bjorkman, L., Dieckmann, R., Dahlgren, C. & Forsman, H. 2018. Similarities and differences between the responses induced in human phagocytes through activation of the medium chain fatty acid receptor GPR84 and the short chain fatty acid receptor FFA2R. *Biochimica Et Biophysica Acta-Molecular Cell Research*, 1865, 695-708.
- Swirski, F. K., Nahrendorf, M., Etzrodt, M., Wildgruber, M., Cortez-Retamozo, V., Panizzi, P., Figueiredo, J.-L., Kohler, R. H., Chudnovskiy, A., Waterman,

- P., Aikawa, E., Mempel, T. R., Libby, P., Weissleder, R. & Pittet, M. J. 2009. Identification of Splenic Reservoir Monocytes and Their Deployment to Inflammatory Sites. *Science*, 325, 612-616.
- Taciak, B., Bialasek, M., Braniewska, A., Sas, Z., Sawicka, P., Kiraga, L., Rygiel, T. & Krol, M. 2018. Evaluation of phenotypic and functional stability of RAW 264.7 cell line through serial passages. *Plos One*, 13.
- Taggart, A. K. P., Kero, J., Gan, X., Cai, T.-Q., Cheng, K., Ippolito, M., Ren, N., Kaplan, R., Wu, K., Wu, T.-J., Jin, L., Liaw, C., Chen, R., Richman, J., Connolly, D., Offermanns, S., Wright, S. D. & Waters, M. G. 2005. (d)-B-Hydroxybutyrate Inhibits Adipocyte Lipolysis via the Nicotinic Acid Receptor PUMA-G. *Journal of Biological Chemistry*, 280, 26649-26652.
- Tang, C., Ahmed, K., Gille, A., Lu, S., Groene, H.-J., Tunaru, S. & Offermanns, S. 2015. Loss of FFA2 and FFA3 increases insulin secretion and improves glucose tolerance in type 2 diabetes. *Nature Medicine*, 21, 173-177.
- Taylor, S. C., Berkelman, T., Yadav, G. & Hammond, M. 2013. A Defined Methodology for Reliable Quantification of Western Blot Data. *Molecular Biotechnology*, 55, 217-226.
- Tazoe, H., Otomo, Y., Karaki, S.-I., Kato, I., Fukami, Y., Terasaki, M. & Kuwahara, A. 2009. Expression of short-chain fatty acid receptor GPR41 in the human colon. *Biomedical Research*, 30, 149-156.
- Thal, D. M., Yeow, R. Y., Schoenau, C., Huber, J. & Tesmer, J. J. G. 2011. Molecular Mechanism of Selectivity among G Protein-Coupled Receptor Kinase 2 Inhibitors. *Molecular Pharmacology*, 80, 294-303.
- Thangaraju, M., Cresci, G. A., Liu, K., Ananth, S., Gnanaprakasam, J. P., Browning, D. D., Mellinger, J. D., Smith, S. B., Digby, G. J., Lambert, N. A., Prasad, P. D. & Ganapathy, V. 2009. GPR109A Is a G-protein-Coupled Receptor for the Bacterial Fermentation Product Butyrate and Functions as a Tumor Suppressor in Colon. *Cancer Research*, 69, 2826-2832.
- Thomsen, A. R. B., Plouffe, B., Cahill, T. J., Shukla, A. K., Tarrasch, J. T., Dosey, A. M., Khsai, A. W., Strachan, R. T., Pani, B., Mahoney, J. P., Huang, L., Breton, B., Heydenreich, F. M., Sunahara, R. K., Skiniotis, G.,

- Bouvier, M. & Lefkowitz, R. J. 2016. GPCR-G Protein-β-Arrestin Super-Complex Mediates Sustained G Protein Signaling. *Cell*, 166, 907-919.
- Tobin, A. B. 2008. G-protein-coupled receptor phosphorylation: where, when and by whom. *British Journal of Pharmacology*, 153, S167-S176.
- Tolhurst, G., Heffron, H., Lam, Y. S., Parker, H. E., Habib, A. M., Diakogiannaki, E., Cameron, J., Grosse, J., Reimann, F. & Gribble, F. M. 2012. Short-Chain Fatty Acids Stimulate Glucagon-Like Peptide-1 Secretion via the G-Protein-Coupled Receptor FFAR2. *Diabetes*, 61, 364-371.
- Tough, I. R., Forbes, S. & Cox, H. M. 2018. Signaling of free fatty acid receptors 2 and 3 differs in colonic mucosa following selective agonism or coagonism by luminal propionate. *Neurogastroenterology and Motility*, 30, e13454.
- Trinquet, E., Bouhelal, R. & Dietz, M. 2011. Monitoring Gq-coupled receptor response through inositol phosphate quantification with the IP-One assay. *Expert Opinion on Drug Discovery*, 6, 981-994.
- Trompette, A., Gollwitzer, E. S., Yadava, K., Sichelstiel, A. K., Sprenger, N., Ngom-Bru, C., Blanchard, C., Junt, T., Nicod, L. P., Harris, N. L. & Marsland, B. J. 2014. Gut microbiota metabolism of dietary fiber influences allergic airway disease and hematopoiesis. *Nature Medicine*, 20, 159-166.
- Tsuji, M., Suzuki, K., Kitamura, H., Maruya, M., Kinoshita, K., Ivanov, I. I., Itoh, K., Littman, D. R. & Fagarasan, S. 2008. Requirement for Lymphoid Tissue-Inducer Cells in Isolated Follicle Formation and T Cell-Independent Immunoglobulin A Generation in the Gut. *Immunity*, 29, 261-271.
- Tsuji, Y. 2020. Transmembrane protein western blotting: Impact of sample preparation on detection of SLC11A2 (DMT1) and SLC40A1 (ferroportin). *PLOS One*, 15, e0235563.
- Uehling, D. E., Joseph, B., Chung, K. C., Zhang, A. X., Ler, S., Prakesch, M. A., Poda, G., Grouleff, J., Aman, A., Kiyota, T., Leung-Hagesteijn, C., Konda, J. D., Marcellus, R., Griffin, C., Subramaniam, R., Abibi, A., Strathdee, C. A., Isaac, M. B., Al-Awar, R. & Tiedemann, R. E. 2021. Design, Synthesis, and Characterization of 4-Aminoquinazolines as Potent Inhibitors of the G Protein-Coupled Receptor Kinase 6 (GRK6) for the Treatment of Multiple Myeloma. *Journal of Medicinal Chemistry*, 64, 11129-11147.

- Uhlen, M., Fagerberg, L., Hallstroem, B. M., Lindskog, C., Oksvold, P., Mardinoglu, A., Sivertsson, A., Kampf, C., Sjoestedt, E., Asplund, A., Olsson, I., Edlund, K., Lundberg, E., Navani, S., Szgyarto, C. A.-K., Odeberg, J., Djureinovic, D., Takanen, J. O., Hober, S., Alm, T., Edqvist, P.-H., Berling, H., Tegel, H., Mulder, J., Rockberg, J., Nilsson, P., Schwenk, J. M., Hamsten, M., Von Feilitzen, K., Forsberg, M., Persson, L., Johansson, F., Zwahlen, M., Von Heijne, G., Nielsen, J. & Ponten, F. 2015. Tissue-based map of the human proteome. *Science*, 347, 1260419.
- Ulven, E. R., Quon, T., Sergeev, E., Barki, N., Brvar, M., Hudson, B. D., Dutta, P., Hansen, A. H., Bielefeldt, L. Ø., Tobin, A. B., McKenzie, C. J., Milligan, G. & Ulven, T. 2020. Structure-Activity Relationship Studies of Tetrahydroquinolone Free Fatty Acid Receptor 3 Modulators. *Journal of Medicinal Chemistry*, 63, 3577-3595.
- Urban, C. F., Ermert, D., Schmid, M., Abu-Abed, U., Goosmann, C., Nacken, W., Brinkmann, V., Jungblut, P. R. & Zychlinsky, A. 2009. Neutrophil Extracellular Traps Contain Calprotectin, a Cytosolic Protein Complex Involved in Host Defense against *Candida albicans*. *PLOS Pathogens*, 5, e1000639.
- Urizar, E., Claeysen, S., Deupí, X., Govaerts, C., Costagliola, S., Vassart, G. & Pardo, L. 2005. An Activation Switch in the Rhodopsin Family of G Protein-coupled Receptors. *Journal of Biological Chemistry*, 280, 17135-17141.
- Varani, K., Gessi, S., Dionisotti, S., Ongini, E. & Andrea Borea, P. 1998. [³H]SCH58261 labelling of functional A₂A adenosine receptors in human neutrophil membranes. *British Journal of Pharmacology*, 123, 1723-1731.
- Veprík, A., Laufer, D., Weiss, S., Rubins, N. & Walker, M. D. 2016. GPR41 modulates insulin secretion and gene expression in pancreatic β-cells and modifies metabolic homeostasis in fed and fasting states. *FASEB Journal*, 30, 3860-3869.
- Vermeire, S., Kojecky, V., Knoflicek, V., Reinisch, W., Van Kaem, T., Namour, F., Beetens, J. & Vanhoutte, F. 2015. GLPG0974, an FFA2 antagonist, in ulcerative colitis: efficacy and safety in a multicenter proof-of-concept study. *Journal of Crohns & Colitis*, 9, S39-S39.

- Vermeire, S., Reinisch, W., Wasko-Czopnik, D., Van Kaem, T., Desrivot, J., Vanhoutte, F. & Beets, J. 2017. Efficacy and safety of GLPG1205, a GPR84 antagonist, in ulcerative colitis: multi-centre proof-of-concept study. *Journal of Crohns & Colitis*, 11, S390-S391.
- Vieira, A. T., Macia, L., Galvão, I., Martins, F. S., Canesso, M. C. C., Amaral, F. A., Garcia, C. C., Maslowski, K. M., De Leon, E., Shim, D., Nicoli, J. R., Harper, J. L., Teixeira, M. M. & Mackay, C. R. 2015. A Role for Gut Microbiota and the Metabolite-Sensing Receptor GPR43 in a Murine Model of Gout. *Arthritis & Rheumatology*, 67, 1646-1656.
- Villa, S. R., Mishra, R. K., Zapater, J. L., Priyadarshini, M., Gilchrist, A., Mancebo, H., Schiltz, G. E. & Layden, B. T. 2017. Homology modeling of FFA2 identifies novel agonists that potentiate insulin secretion. *Journal of Investigative Medicine*, 65, 1116-1124.
- Vinolo, M. A. R., Ferguson, G. J., Kulkarni, S., Damoulakis, G., Anderson, K., Bohlooly-Y, M., Stephens, L., Hawkins, P. T. & Curi, R. 2011. SCFAs Induce Mouse Neutrophil Chemotaxis through the GPR43 Receptor. *PLOS One*, 6, e21205.
- Wang, C., McDonald, K. G., McDonough, J. S. & Newberry, R. D. 2006a. Murine isolated lymphoid follicles contain follicular B lymphocytes with a mucosal phenotype. *American Journal of Physiology-Gastrointestinal and Liver Physiology*, 291, G595-G604.
- Wang, D. D. & Hu, F. B. 2017. Dietary Fat and Risk of Cardiovascular Disease: Recent Controversies and Advances. *Annual Review of Nutrition*, 37, 423-446.
- Wang, G., Jiang, L., Wang, J., Zhang, J., Kong, F., Li, Q., Yan, Y., Huang, S., Zhao, Y., Liang, L., Li, J., Sun, N., Hu, Y., Shi, W., Deng, G., Chen, P., Liu, L., Zeng, X., Tian, G., Bu, Z., Chen, H. & Li, C. 2020. The G Protein-Coupled Receptor FFAR2 Promotes Internalization during Influenza A Virus Entry. *Journal of Virology*, 94, e01707-19.
- Wang, J., Wu, X., Simonavicius, N., Tian, H. & Ling, L. 2006b. Medium-chain fatty acids as ligands for orphan G protein-coupled receptor GPR84. *Journal of Biological Chemistry*, 281, 34457-34464.

- Wang, Y., Jiao, X., Kayser, F., Liu, J., Wang, Z., Wanska, M., Greenberg, J., Weiszmann, J., Ge, H., Tian, H., Wong, S., Schwandner, R., Lee, T. & Li, Y. 2010. The first synthetic agonists of FFA2: Discovery and SAR of phenylacetamides as allosteric modulators. *Bioorganic & Medicinal Chemistry Letters*, 20, 493-498.
- Ward, R. J., Alvarez-Curto, E. & Milligan, G. 2011. Using the Flp-In™ T-Rex™ System to Regulate GPCR Expression. *Methods in Molecular Biology*, 746, 21-37.
- Willingham, M. C. 1999. Conditional Epitopes: Is Your Antibody Always Specific? *Journal of Histochemistry & Cytochemistry*, 47, 1233-1235.
- Winer, J., Jung, C. K. S., Shackel, I. & Williams, P. M. 1999. Development and Validation of Real-Time Quantitative Reverse Transcriptase-Polymerase Chain Reaction for Monitoring Gene Expression in Cardiac Myocytes in Vitro. *Analytical Biochemistry*, 270, 41-49.
- Winter, S. E., Thiennimitr, P., Winter, M. G., Butler, B. P., Huseby, D. L., Crawford, R. W., Russell, J. M., Bevins, C. L., Adams, L. G., Tsohis, R. M., Roth, J. R. & Bäumlner, A. J. 2010. Gut inflammation provides a respiratory electron acceptor for Salmonella. *Nature*, 467, 426-429.
- Witkowski, M., Weeks, T. L. & Hazen, S. L. 2020. Gut Microbiota and Cardiovascular Disease. *Circulation Research*, 127, 553-570.
- Wittenberger, T., Schaller, H. C. & Hellebrand, S. 2001. An expressed sequence tag (EST) data mining strategy succeeding in the discovery of new G-protein coupled receptors. *Journal of Molecular Biology*, 307, 799-813.
- Wittwer, C. T., Herrmann, M. G., Moss, A. A. & Rasmussen, R. P. 1997. Continuous fluorescence monitoring of rapid cycle DNA amplification. *Biotechniques*, 22, 130-138.
- Won, Y.-J., Lu, V. B., Puhl, H. L. & Ikeda, S. R. 2013. β -Hydroxybutyrate Modulates N-Type Calcium Channels in Rat Sympathetic Neurons by Acting as an Agonist for the G-Protein-Coupled Receptor FFA3. *Journal of Neuroscience*, 33, 19314-19325.
- Wu, W., Sun, M., Chen, F., Cao, A. T., Liu, H., Zhao, Y., Huang, X., Xiao, Y., Yao, S., Zhao, Q., Liu, Z. & Cong, Y. 2017. Microbiota metabolite short-chain

fatty acid acetate promotes intestinal IgA response to microbiota which is mediated by GPR43. *Mucosal Immunology*, 10, 946-956.

- Xiao, K., McClatchy, D. B., Shukla, A. K., Zhao, Y., Chen, M., Shenoy, S. K., Yates, J. R., III & Lefkowitz, R. J. 2007. Functional specialization of β -arrestin interactions revealed by proteomic analysis. *Proceedings of the National Academy of Sciences of the United States of America*, 104, 12011-12016.
- Xiao, K., Sun, J., Kim, J., Rajagopal, S., Zhai, B., Villen, J., Haas, W., Kovacs, J. J., Shukla, A. K., Hara, M. R., Hernandez, M., Lachmann, A., Zhao, S., Lin, Y., Cheng, Y., Mizuno, K., Ma'ayan, A., Gygi, S. P. & Lefkowitz, R. J. 2010. Global phosphorylation analysis of β -arrestin-mediated signaling downstream of a seven transmembrane receptor (7TMR). *Proceedings of the National Academy of Sciences of the United States of America*, 107, 15299-15304.
- Xiong, Y. M., Miyamoto, N., Shibata, K., Valasek, M. A., Motoike, T., Kedzierski, R. M. & Yanagisawa, M. 2004. Short-chain fatty acids stimulate leptin production in adipocytes through the G protein-coupled receptor GPR41. *Proceedings of the National Academy of Sciences of the United States of America*, 101, 1045-1050.
- Yamashita, H., Kaneyuki, T. & Tagawa, K. 2001. Production of acetate in the liver and its utilization in peripheral tissues. *Biochimica Et Biophysica Acta-Molecular and Cell Biology of Lipids*, 1532, 79-87.
- Yang, D., Zhou, Q., Labroska, V., Qin, S., Darbalaei, S., Wu, Y., Yuliantie, E., Xie, L., Tao, H., Cheng, J., Liu, Q., Zhao, S., Shui, W., Jiang, Y. & Wang, M.-W. 2021. G protein-coupled receptors: structure- and function-based drug discovery. *Signal Transduction and Targeted Therapy*, 6, 7.
- Yang, F., Yu, X., Liu, C., Qu, C.-X., Gong, Z., Liu, H.-D., Li, F.-H., Wang, H.-M., He, D.-F., Yi, F., Song, C., Tian, C.-L., Xiao, K.-H., Wang, J.-Y. & Sun, J.-P. 2015. Phospho-selective mechanisms of arrestin conformations and functions revealed by unnatural amino acid incorporation and ^{19}F -NMR. *Nature Communications*, 6, 8202.
- Yang, W., Xiao, Y., Huang, X., Chen, F., Sun, M., Bilotta, A. J., Xu, L., Lu, Y., Yao, S., Zhao, Q., Liu, Z. & Cong, Y. 2019. Microbiota Metabolite Short-

- Chain Fatty Acids Facilitate Mucosal Adjuvant Activity of Cholera Toxin through GPR43. *Journal of Immunology*, 203, 282-292.
- Yang, Z., Yang, F., Zhang, D., Liu, Z., Lin, A., Liu, C., Xiao, P., Yu, X. & Sun, J.-P. 2017. Phosphorylation of G Protein-Coupled Receptors: From the Barcode Hypothesis to the Flute Model. *Molecular Pharmacology*, 92, 201-210.
- Yao, Y., Cai, X., Zheng, Y., Zhang, M., Fei, W., Sun, D., Zhao, M., Ye, Y. & Zheng, C. 2022. Short-chain fatty acids regulate B cells differentiation via the FFA2 receptor to alleviate rheumatoid arthritis. *British Journal of Pharmacology*, 179, 4315-4329.
- Zaibi, M. S., Stocker, C. J., O'dowd, J., Davies, A., Bellahcene, M., Cawthorne, M. A., Brown, A. J. H., Smith, D. M. & Arch, J. R. S. 2010. Roles of GPR41 and GPR43 in leptin secretory responses of murine adipocytes to short chain fatty acids. *FEBS Letters*, 584, 2381-2386.
- Zhang, C., Jang, S., Amadi, O. C., Shimizu, K., Lee, R. T. & Mitchell, R. N. 2013. A Sensitive Chemotaxis Assay Using a Novel Microfluidic Device. *BioMed Research International*, 2013, 373569.
- Zhang, Y., Sun, B., Feng, D., Hu, H., Chu, M., Qu, Q., Tarrasch, J. T., Li, S., Kobilka, T. S., Kobilka, B. K. & Skiniotis, G. 2017. Cryo-EM structure of the activated GLP-1 receptor in complex with a G protein. *Nature*, 546, 248-253.
- Zhao, L., Liu, L., Guo, B. & Zhu, B. 2015. Regulation of adaptive immune responses by guiding cell movements in the spleen. *Frontiers in Microbiology*, 6, 645.
- Zhou, X. E., He, Y., De Waal, P. W., Gao, X., Kang, Y., Van Eps, N., Yin, Y., Pal, K., Goswami, D., White, T. A., Barty, A., Latorraca, N. R., Chapman, H. N., Hubbell, W. L., Dror, R. O., Stevens, R. C., Cherezov, V., Gurevich, V. V., Griffin, P. R., Ernst, O. P., Melcher, K. & Xu, H. E. 2017. Identification of Phosphorylation Codes for Arrestin Recruitment by G Protein-Coupled Receptors. *Cell*, 170, 457-469.
- Zigmond, S. H., Slonczewski, J. L., Wilde, M. W. & Carson, M. 1988. Polymorphonuclear leukocyte locomotion is insensitive to lowered cytoplasmic calcium levels. *Cell Motility and the Cytoskeleton*, 9, 184-189.

Zurkovsky, L., Sedaghat, K., Ahmed, M. R., Gurevich, V. V. & Gurevich, E. V.
2017. Arrestin-2 and arrestin-3 differentially modulate locomotor responses
and sensitization to amphetamine. *Neuropharmacology*, 121, 20-29.